The Blood-Brain Barrier in Neuropsychiatric Disorders

A thesis submitted to the University of Dublin for the Degree of Doctor of Philosophy

By

Chris Greene
2018

Under the supervision of Doctor Matthew Campbell

Department of Genetics
Trinity College Dublin

Declaration

I declare that this thesis has not been submitted as an exercise for a degree at this or any other university and it is entirely my own work. I agree to deposit this thesis in the University's open access institutional repository or allow the library to do so on my behalf, subject to Irish Copyright Legislation and Trinity College Library conditions of use and acknowledgement.

_____

Chris Greene
March 2018

Summary

The vasculature of the central nervous system (CNS) forms a tight barrier that regulates the movement of molecules and ions between the blood and brain. This blood-brain barrier (BBB) is critical for proper function of the CNS as well as protecting neural tissue from potentially damaging blood-borne agents. To maintain CNS homeostasis, brain endothelial cells strictly regulate entry and exit with specific transporter and receptor proteins for metabolite movement across the endothelium (transcellular). In addition, brain endothelial cells are linked by tight junction (TJ) protein complexes that effectively seal the space between adjacent endothelial cells (paracellular). The importance of the BBB is highlighted by the severe pathologies of diseases in which it is broken down. Many of the symptoms of stroke, brain trauma and oedema are due to a breakdown of the BBB following the primary insult. This has direct relevance to schizophrenia where cerebral microvascular anomalies are being recognised as pathological hallmarks of the condition. The presence of elevated serum levels of albumin and S100β, markers of BBB dysfunction, is a common finding in individuals with schizophrenia. Additionally, gene expression studies have identified several endothelial-specific genes dysregulated in schizophrenia. While changes in BBB permeability have been detected in schizophrenia patients, the consequences of alterations of TJ components in schizophrenia progression and symptomatology has not been explored.

In this study, the association of a single nucleotide polymorphism (SNP) in the 3' untranslated region (UTR) of the transmembrane protein-coding claudin-5 gene with schizophrenia was investigated. These results revealed a significant association between the rs10314 SNP and schizophrenia in 22q11.2 deletion syndrome patients (22q11DS), a high-risk population estimated to be 25 times more likely to develop schizophrenia. The effect of the SNP on levels of claudin-5 was investigated in *in vitro* models of the BBB. These studies showed that the rs10314 SNP lead to reduced levels of claudin-5 protein. Furthermore, claudin-5 was reduced in post-mortem schizophrenia brain samples in patients that harboured the claudin-5 risk allele. In *in vitro* BBB models, up-regulation of claudin-5 was observed following exposure of brain endothelial cells to anti-psychotic drugs while *in vivo* administration of anti-psychotic drugs increased levels of claudin-5, tricellulin and ZO-1 proteins. To assess how claudin-5 down-regulation affects BBB permeability and schizophrenia symptomatology, a behavioural dataset was generated

following targeted suppression of claudin-5 *in vivo* in specific brain regions. Utilising adeno-associated viral vectors containing a doxycycline-inducible shRNA targeting claudin-5 transcripts, claudin-5 was knocked down in the hippocampus and medial prefrontal cortex of mice. Using a behavioural battery of tests, it was demonstrated that targeted suppression of claudin-5 resulted in localised permeability of the BBB and impairments in learning and memory and social interaction and increased depressive-like behaviours. Next, a novel doxycycline-inducible claudin-5 knockdown mouse was generated to allow for brain-wide knockdown of claudin-5. This model revealed that knockdown of claudin-5 in the entire brain produced permeability of the BBB that resulted in impairments in learning and memory and increased anxiety. Additionally, knockdown of claudin-5 impaired prepulse inhibition (PPI), a sensorimotor gating deficit consistently observed in schizophrenia patients. Finally, chronic knockdown of claudin-5 was lethal with mice developing seizures and hyperactivity that resulted gliosis, macromolecule leakage and premature death. In chapter 5, the role of the circadian clock in regulating the integrity of the BBB was explored. It has recently been reported that up to one third of the genome is controlled by the circadian clock. Given the extensive pattern of sleep disruption in schizophrenic individuals, the role of the circadian clock in regulating BBB integrity was investigated. Transcription factors that regulate circadian rhythms were expressed in brain endothelial cells. Furthermore, claudin-5 expression cycled in mice dependent on the time of day and permeability of the BBB was regulated in a time-dependent manner with elevated permeability of tracer molecules in the morning. Silencing of the clock transcription factor BMAL-1, a key activator of circadian rhythms, *in vitro,* attenuated the cycling of TJ components and impaired barrier integrity. These results suggest that targeting therapies at distinct times associated with increased BBB permeability may improve brain penetration and therapeutic outcome.

The results obtained here from human schizophrenia brain samples, 22q11DS patient samples, knockdown studies in C57BL/6 mice and claudin-5 knockdown mice and *in vitro* and *in vivo* BBB permeability studies indicate that depletion of claudin-5 can size-selectively increase BBB permeability and impair behaviour. In this respect, changes in TJ protein levels may represent a mechanism behind impaired CNS homeostasis and induction of symptoms associated with schizophrenia. To conclude, these observations suggest claudin-5 may represent a novel therapeutic target to modulate schizophrenia progression.

Acknowledgements

Firstly, I would like to share my appreciations with my supervisor, Dr Matthew Campbell for providing a fascinating concept which I have been able to explore over the past four years and for the help and guidance that has culminated in this thesis. Many thanks to Dr. John Kealy, for all his help and expertise with the behavioural studies. Special thanks to Dr. Natalie Hudson for her help with genotyping and ordering supplies and managing the lab. My deepest gratitude to my colleagues Dr. Marian Humphries, Dr. Ema Ozaki, Lucia Celkova, Eoin O'Keeffe and Conor Delaney for their advice and friendship. Thanks also to everyone else in the Farrar and Humphries labs for creating such a great environment to work in. Special thanks to those working in the animal unit past and present, Charlie, Caroline, Dave and Monica for taking care of my animals and Rustam for his help with the MRI work. In the prep room, thanks to Brenda, Rachel, Dave and Paul. To the Stanley Medical Research Institute for supplying human brain tissue. I would also like to thank Science Foundation Ireland for their financial support over the last four years.

To my parents, Margaret and Gerry, for their love and support and words of encouragement and advice, thank you.

Finally, I'm forever grateful to and inspired by Emma and Leo. Thank you for making the past few years the most joyous and exciting of my life, I love you very much.

Table of Contents ..... **Page No.**

Figures and Tables ..... **Page No.**

Abbreviations

AJ	Adherens junction
ANOVA	Analysis of variance
APS	Ammonium persulfate
AQP	Aquaporin
Aβ	Amyloid beta
BBB	Blood-brain barrier
BCA	Bicinchoninic acid
BCSFB	Blood-cerebrospinal fluid barrier
bEnd.3	Brain endothelial cell line
BM	Basement membrane
BMVEC	Brain microvascular endothelial cell
BRB	Blood-retina barrier
BSA	Bovine serum albumin
C4	Complement component 4
CBF	Cerebral blood flow
CNS	Central nervous system
CNV	Copy number variation
CO_2	Carbon dioxide
CPZ	Chlorpromazine
CRY	Cryptochrome
CSF	Cerebrospinal fluid
CVD	Cardiovascular disease
CZP	Clozapine
Da	Dalton
DAPI	4', 6-diamidino-2-phenylindole
DCE-MRI	Dynamic contrast-enhanced magnetic resonance imaging
DEPC	Diethyl-pyrocarbonate
DMEM	Dulbecco's modified Eagle medium
DMSO	Dimethyl sulfoxide
DNA	Deoxyribonucleic acid
DTT	Dithiothreitol
EC	Endothelial cell

ECD	Extracellular domain
ECL	Enhanced chemiluminescence
ECM	Extracellular matrix
EDTA	Ethylenediaminetetraacetic acid
ERG	Electroretinogram
EV	Empty vector
FBS	Foetal bovine serum
FDA	Food and drug administration
FGF	Fibroblast growth factor
Gd-DTPA	Gadolinium diethylenetriaminepentaacetic acid
GLUT	Glucose transporter
HAL	Haloperidol
HBSS	Hank's balanced salt solution
HCl	Hydrochloric acid
HEK	Human embryonic kidney cell
HEPES	N-2-hydroxyethylpiperazine-N-2-ethane Sulfonic acid
HRP	Horseradish peroxidase
ICAM	Intracellular adhesion molecule
IF	Interstitial fluid
Ig	Immunoglobulin
IL-1β	Interleukin-1 beta
IP	Intra-peritoneal
IPL	Inferior parietal lobe
IV	Intra-venous
JAM	Junction adhesion molecule
K	Potassium
KD	Knockdown
LCR	Low copy repeat
LiCl	Lithium chloride
MAGUK	Membrane associated guanylkinase
MDCK	Madin darby canine kidney cells
Mfsd2a	Major facilitator super family domain

	containing 2a
MgCl2	Magnesium chloride
MMP	Matrix metalloproteinase
MRI	Magnetic resonance imaging
mTOR	Mammalian target of rapamycin
MW	Molecular weight
Na	Sodium
Na^+/K^+-ATPase	Sodium/potassium adenosine triphosphate
NaCl	Sodium chloride
NADH	Nicotinamide adenine dinucleotide
NADPH	Nicotinamide adenine dinucleotide phosphate
NaOH	Sodium hydroxide
NF	Nuclease-free
NGS	Normal goat serum
NT	Non-targeting
NVU	Neurovascular unit
OAT3	Organic ion transporter 3
OCT	Optimal cutting temperature
OLZ	Olanzapine
P/S	Penicillin-streptomycin
P_{app}	Apparent permeability coefficient
PBS	Phosphate buffered saline
PCR	Polymerase chain reaction
PDGF	Platelet-derived growth factor
PDGFRβ	PDGF receptor beta
PER	Period
PFA	Paraformaldehyde
PPI	Prepulse inhibition
PVDF	Polyvinyl difluoride
RAGE	Receptor for advanced glycation end product
RFU	Relative fluorescence unit
RNA	Ribonucleic acid

ROS	Reactive oxygen species
RPM	Revolutions per minute
RT-PCR	Reverse transcription polymerase chain reaction
rtTA	Reverse tetracycline controlled transactivator
SCN	Suprachiasmatic nucleus
SD	Standard deviation
SDS	Sodium dodecyl sulphate
SEM	Standard error of the mean
Shh	Sonic hedgehog
siRNA	Small interfering ribonucleic acid
SNP	Single nucleotide polymorphism
TBI	Traumatic brain injury
TBS	Tris buffered saline
TBX	T-box transcription factor
TEER	Transendothelial electrical resistance
TEMED	N, N, N', N'-tetramethylethylenediamine
TGFRβ	Transforming growth factor receptor-beta
TGFβ	Transforming growth factor-beta
TIMP	Tissue inhibitor of metalloproteinases
TJ	Tight junction
TLCK	Tosyl-L-lysyl-chlormethane hydrochloride
TNF-α	Tumor necrosis factor-alpha
TRE	Tetracycline response element
Tris-HCl	Trizma Hydrochloride
UNT	Untransfected
UTR	Untranslated region
VCAM-1	Vascular cell adhesion molecule-1
VCFS	Velocardiofacial syndrome
VEGF	Vascular endothelial growth factor
VEGFR	VEGF receptor
VPA	Valproic acid

WT	Wildtype
ZO	Zonula occludens
22q11DS	22q11.2 deletion syndrome

Chapter 1:

General Introduction

1. General Introduction

1.1 The Blood-Brain Barrier (BBB)

The central nervous system (CNS) consists of the brain and spinal cord and functions to regulate the body's response to internal and external stimuli. Central to this function is the neuron, a terminally differentiated electrically excitable cell, which requires a fine control of both electrophysiological and chemical signals to function efficiently. Given the lack of regenerative capacities of neurons, maintaining a constant state of homeostasis in the CNS is essential for the health and integrity of neurons. To maintain optimal synaptic signalling, a tight control of the microenvironment is required to efficiently process the vast array of information received by the CNS. Indeed, while the brain accounts for just 2% of bodily mass, it expends 20% of the body's energy production (Raichle and Gusnard, 2002). To this end, three cellular barriers exist in the brain to form an interface between the blood and neural tissue: the blood-cerebrospinal fluid barrier (BCSFB), the blood-brain barrier (BBB) and the arachnoid barrier. The BCSFB is formed by epithelial cells of the choroid plexus (Abbott et al., 2006) (Figure 1.1B). The choroid plexus epithelium secretes cerebrospinal fluid (CSF) which fills the cerebral and spinal subarachnoid spaces and ventricles and functions as a buffer to protect the brain from injury as well as regulating cerebral blood flow (CBF) and molecular exchange with the brain. A second barrier is formed by the arachnoid epithelium, an avascular membrane underlying the dura and completely enclosing the CNS. This forms a seal between the CSF and the extracellular fluids of the rest of the body (Abbott et al., 2010). The blood-brain barrier (BBB) positioned along blood vessels of the CNS is a third selective and tightly regulated barrier (Figure 1.1A), reflecting the brain's critical roles in cognitive function, maintaining homeostasis and strictly coordinating the functions of peripheral organs. The BBB is important in regulating the exchange of ions and nutrients between the blood and brain but also to protect delicate neural tissue from potentially damaging blood-borne agents such as pathogens, immune cells and anaphylatoxins (Abbott et al., 2010). Additionally, the brain endothelium secretes ~200 ml of fresh interstitial fluid (IF) per day to create an ideal ionic environment for neural function (Hladky and Barrand, 2016). In fact, as the CNS has no local energy reserves, it requires a constant supply of glucose delivered from the blood and is sensitive to changes in blood flow. This energy need is met by the cerebral microvasculature. The combined surface area of microvessels in the brain is 150-200 cm^2/g of tissue, equating to ~15-20 m^2 per adult human brain

resulting in a dense mesh-like network of vessels providing blood flow to all brain regions (Abbott et al., 2006). Such is the extent of the cerebral vasculature, no neuron is further than ~25 µm from a blood vessel (Schlageter et al., 1999).

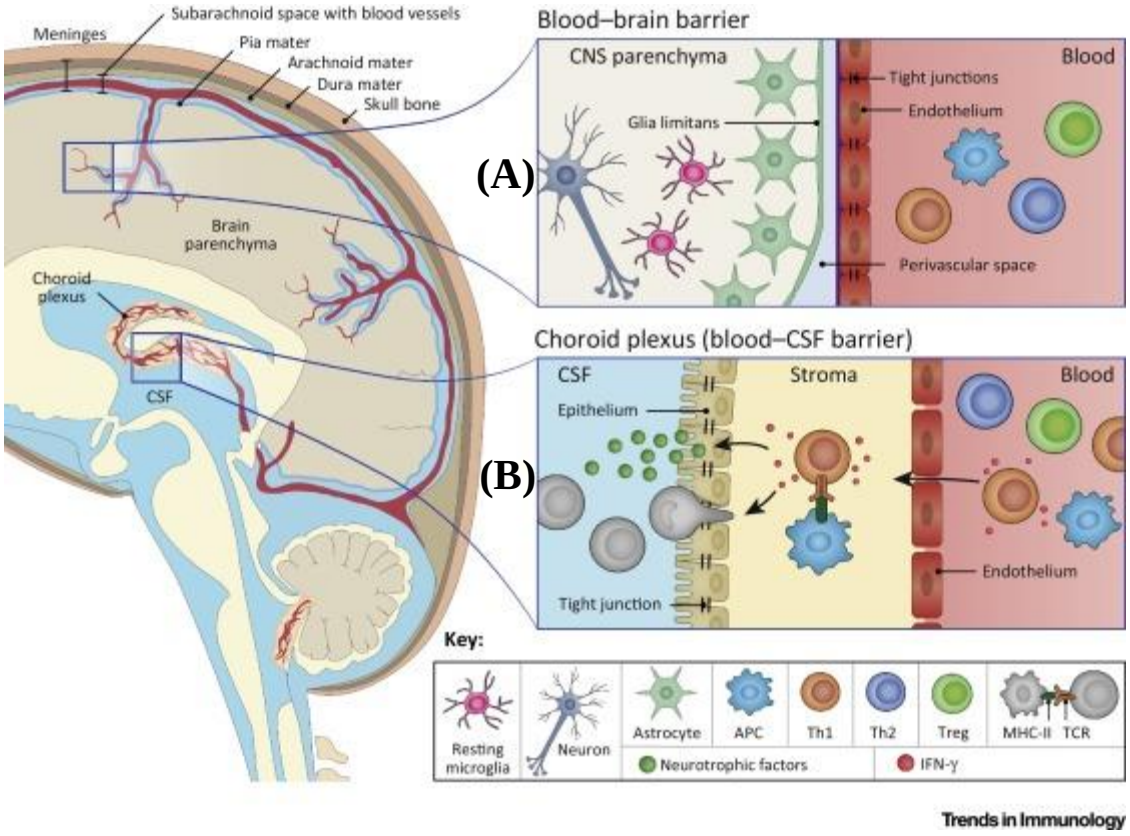

Figure 1.1: Barriers of the CNS. **(A)** The BBB is located at the endothelium lining the cerebral microvessels and is the major site of molecular blood-brain exchange owing to the proximity of neurons to capillaries. **(B)** The blood-cerebrospinal fluid barrier (BCSFB) is found along the epithelium of the choroid plexus. The BCSFB helps to separate the CSF secreted by the choroid plexus epithelium from the brain vasculature and neural tissue. Not highlighted is the arachnoid barrier formed by the epithelium of the arachnoid layer of the meninges that completely surrounds the brain. At each cellular barrier, tight junction (TJ) complexes help to limit the paracellular (intercellular cleft) permeability with the highly electrical resistant TJs of the BBB forming the tightest barrier. Source: (Deczkowska et al., 2016).

To maintain homeostasis within the CNS, the BBB evolved at the level of the cerebral microvasculature. Lining blood vessels of the CNS are endothelial cells (EC) which separate the peripheral blood from brain tissue. Owing to their specialised function, CNS ECs are distinct from ECs of the periphery in several ways (Figure 1.2) and possess numerous specialisations including:

i) BBB-specific proteins to control the entry and exit of metabolites across cells (transcellular pathway).

ii) Enrichment of highly electrical resistant tight junction (TJ) proteins to limit the flow of material between adjacent ECs (paracellular pathway).

iii) Absence of fenestrations which are pores to allow the rapid exchange of molecules between blood and tissue in peripheral ECs.

iv) Low rate of vesicular transport (absorptive transcytosis) to prevent transport of large hydrophilic molecules to the CNS (Saunders et al., 2012, Abbott et al., 2010).

v) Increased mitochondrial numbers to facilitate higher energy expenditure.

Additionally, in contrast to peripheral ECs where TJ strands associate with the extracellular fraction face (E-face) of the membrane bilayer, TJ particles of CNS ECs associate with the protoplasmic membrane leaflets (P-face) (Liebner et al., 2000). It is thought that the association of the TJ with the P- or E-face reflects the degree of permeability and resistance of the barrier (Lippoldt et al., 2000).

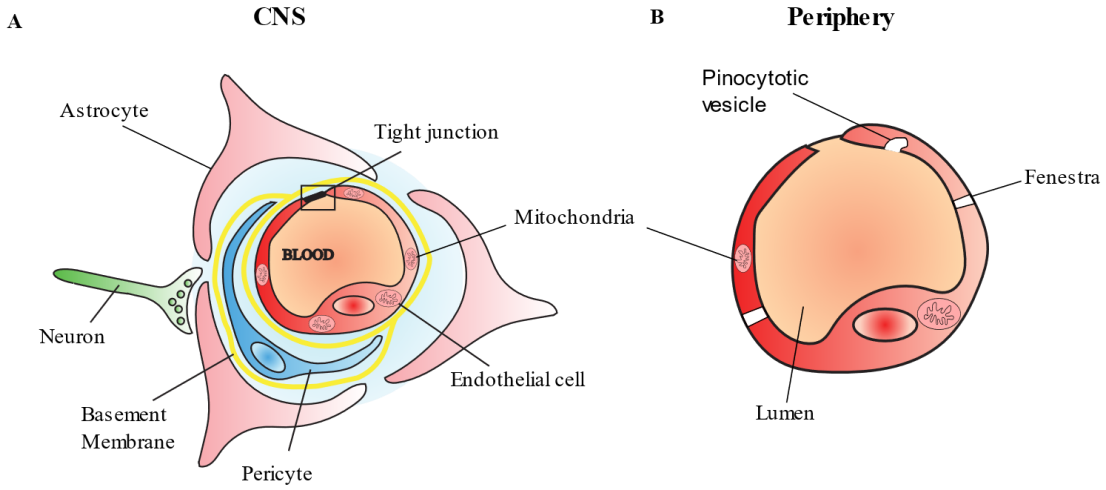

Figure 1.2: CNS vs peripheral ECs. **(A)** CNS ECs are enveloped by pericytes, astrocytes and basement membrane where bidirectional signalling of various signalling components enhances barrier integrity. In addition, CNS ECs contain higher numbers of mitochondria for greater energy consumption and restrict the movement of material from blood to brain and vice versa due to the presence of highly electrical resistant TJ components located between adjacent ECs. **(B)** ECs of the peripheral vasculature are noted by an absence of TJs, fewer mitochondria, increased pinocytotic vesicles and the presence of fenestra to allow the rapid exchange of material between the blood and parenchyma.

Over a century has passed since Paul Ehrlich and Edwin Goldmann's seminal staining experiments in which they noted a clear compartmentalisation of the blood and brain. Initially these observations were attributed to nervous tissue lacking a chemical affinity for the non-staining dyes, however subsequent investigations revealed that intravenous

injections (I.V) of ferrocyanide or bile acids induced no central pharmacological effects, but direct injections to CNS parenchyma induced strong pharmacological changes. While these experiments suggested a barrier between substances in the blood and brain and led Lewandowsky to coin the term "blood-brain barrier", it wasn't until several years later when Ehrlich's student Edwin Goldmann identified a distinct barrier between the CNS and peripheral tissue. Following I.V injection of trypan blue (960 Da), the entire body stained except for the brain and spinal cord. However, direct injection into CSF heavily stained the CNS (reviewed in (Liddelow, 2011)). Future work began to hypothesise on a size-selective permeability of the BBB to certain compounds. Ehrlich noted several dyes injected I.V could stain the CNS. It wasn't until the advent of electron microscopy that a visualisation of the size-selective nature of the BBB could be determined. Pioneering experiments by Reese and Karnovsky showed, for the first time, that in mouse cerebral capillaries, horseradish peroxidase (HRP) could enter the interendothelial space up to but not past the first TJ between adjacent ECs (Reese and Karnovsky, 1967). This work was then repeated with smaller molecules such as microperoxidase (1900 Da) and lanthanum (139 Da) (Brightman and Reese, 1969, Feder, 1971). Concurrently, Reese and Brightman confirmed that the barrier properties of the BBB were established by the endothelium and not the astrocytic end-feet or basement membrane (BM) (Brightman and Reese, 1969). While the physical barrier function of the BBB provided by TJs is the main obstacle to the brain penetrance of blood-borne substances, the BBB also has transport capacities due to the presence of transendothelial transporters such as glucose transporter (GLUT-1) for transporting glucose. The BBB also functions as a metabolic and immune barrier and possesses drug metabolising enzymes on the plasma membrane such as several P450 enzymes, monoamine oxidase, alkaline phosphatase and specific peptidases that modify substances as they enter and exit the brain (Cecchelli et al., 2007).

1.1.1 The Neurovascular Unit

Much of the early research on the BBB focussed on the unique barrier properties of cerebral ECs and whether these properties were unique to this cell type or whether signals from the surrounding microenvironment induced BBB formation. However, significant advancements pointed to a melange of cells types that form the so called "neurovascular unit" (NVU) that interact and communicate with an intricate degree of cross-talk to create a dynamic microenvironment (Figure 1.3). In early transplantation experiments by Stewart and Wiley it was found that following grafting of immature avascular brain tissue

from embryonic quails into the coelom of chick embryos, the abdominal vessels vascularising the grafted brain tissue formed structural and functional properties of the BBB such as TJs and few pinocytotic vesicles. In contrast, when mesodermal tissue was transplanted into the brain, the capillaries in the grafts lacked barrier properties (Stewart and Wiley, 1981). This pointed to yet undefined cues from the neural microenvironment that were involved in developing barrier properties.

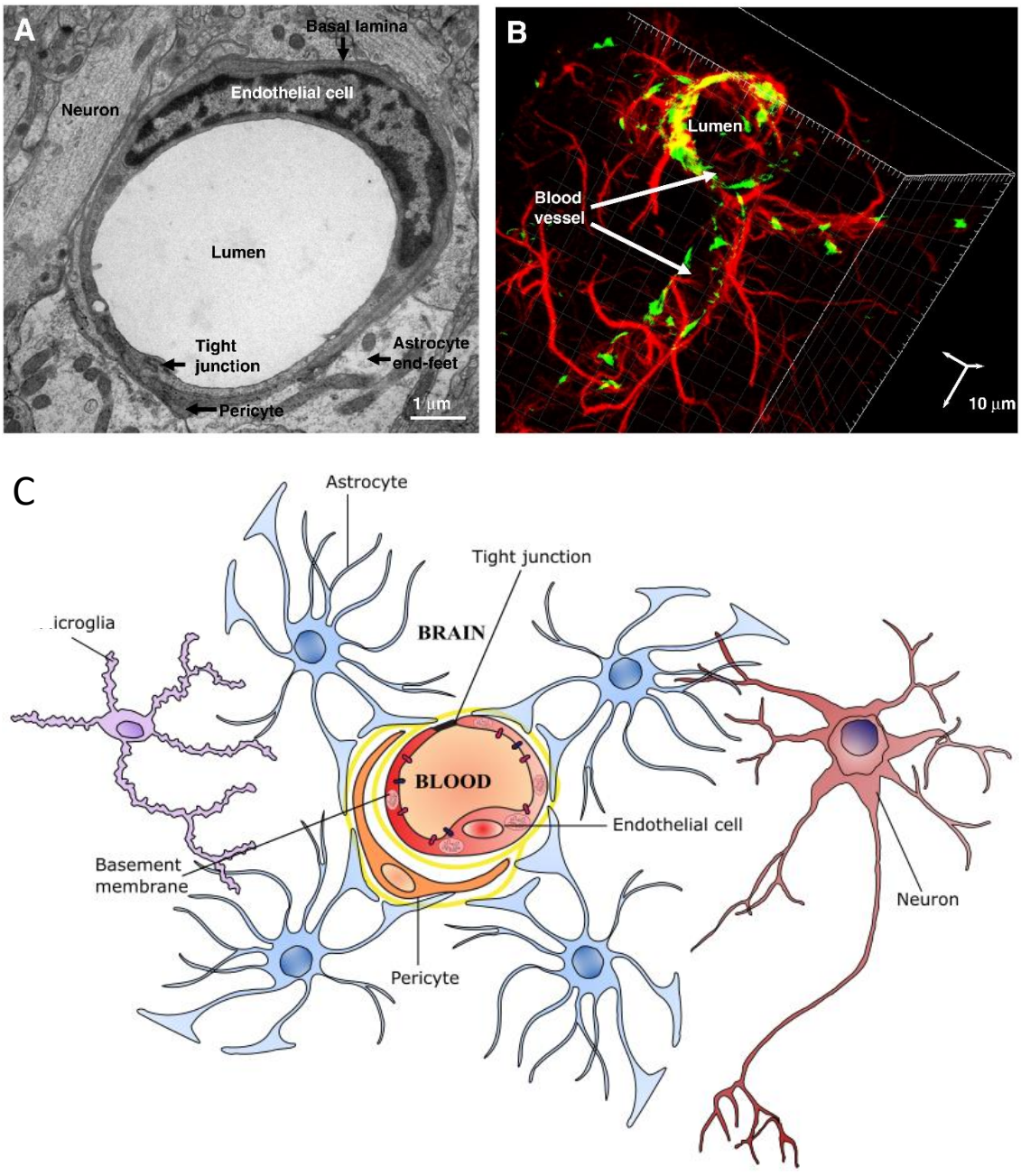

Figure 1.3: The BBB and NVU. **(A)** Electron microscopy of a rat brain section reveals the proximity of neurons, pericytes and astrocytes to the ECs lining the blood vessels in the CNS. Arrows point to the presence of tight junctions between ECs, the basal lamina surrounding the endothelial cells and astrocyte end-feed in contact with the endothelium.

(B) 3D reconstruction of a rat brain section showing part of the cerebral vasculature. Source: (Weiss et al., 2009) **(C)** The NVU is an intricately developed milieu of ECs, astrocytes and pericytes that interact with neurons, microglia and other brain components to impart specific properties on the BBB. Pericytes partially surround the microvessel endothelium while astrocyte end-feet also surround the capillaries.

1.1.1.1 Pericytes

Pericytes are specialised perivascular cells of mesoderm origin embedded in the BM that envelop blood capillaries. First described in the late 19th century, pericytes contain a cell body with a prominent nucleus and long cytoplasmic processes that can contact numerous ECs and extend to more than one capillary. Pericytes are a diverse and multifaceted cell type and are morphologically, biochemically and physiologically heterogeneous depending on vascular bed location, tissue type and differentiation state. As a result, finding a pan-pericyte marker is extremely difficult.

Functionally, pericytes are key components of the BBB and blood-retina barrier (BRB) and have an important role in regulating CBF and capillary diameter (Peppiatt et al., 2006), microvessel stabilisation and extracellular matrix (ECM) protein secretion (Winkler et al., 2011). During early angiogenesis (driven primarily by vascular endothelial growth factor and Wnt/β-catenin signalling) (Liebner et al., 2008) (Obermeier et al., 2013) (Daneman et al., 2009), pericyte recruitment to cerebral blood vessels is key to BBB formation. Loss of pericyte coverage in platelet derived growth factor (PDGFβ) or platelet derived growth factor receptor (PDGFRβ) null mice has been shown to result in capillary microhaemorrhages, TJ dysfunction, increased vascular permeability, failure to recruit pericyte precursor cells and embryonic lethality (Daneman et al., 2010b) (Lindahl et al., 1997). It is thought that recruitment and attachment of pericytes is mediated by PDGFβ secretion from ECs and binding the PDGFRβ receptor on pericytes (Hellstrom et al., 1999). The barrier promoting function of pericytes results from inhibition of molecules such as angiopoietin-2, plvap and leukocyte adhesion molecules that promote vascular permeability and immune cell infiltration (Daneman et al., 2010b). Pericytes are also critical to the integrity of the BBB during adulthood because pericyte deficient mice have been reported with less capillary coverage, reduced cerebral microcirculation as well as TJ dysfunction and increased paracellular leakage of small molecules and transcytosis of serum proteins (Bell et al., 2010, Armulik et al., 2010). Armulik *et al* also noted that pericytes guide astrocytic foot processes to the vessel wall via polarization of astrocyte end-feet and expression of cues that mediate attachment of

astrocyte end-feet to the vessel wall (Armulik et al., 2010). Additionally, pericytes express the contractile proteins α-smooth muscle actin, tropomyosin and myosin (Bandopadhyay et al., 2001) and loss of pericyte coverage results in reduced CBF (Bell et al., 2010). A recent study has highlighted the crucial role of pericytes in regulating CBF in which the neurotransmitter glutamate evokes the release of messengers including prostaglandin E_2 and nitric oxide that help dilate capillaries by actively relaxing pericytes (Hall et al., 2014).

Interestingly, CNS pericytes can perform macrophage-like activities. They express scavenger receptors and pericytes in culture can ingest macromolecules including polystyrene beads (Balabanov et al., 1996). Further evidence for the macrophage activity of pericytes was detailed through the discovery of Fc receptors as well as the macrophage markers CR3 complement receptor, CD4 and major histocompatibility complexes. Additionally, systemic injection of protein tracers in immature mice accumulate in pericytes (Kristensson and Olsson, 1973).

1.1.1.2 Astrocytes

Astrocytes are specialised glial cells derived from the ependymoglia of the developing neural tube. Astrocytes function to protect neurons by regulating neurotransmitter levels and water and ion concentrations to maintain homeostasis of the neural microenvironment. Astrocytic end-feet envelop the abluminal surface of cerebral ECs (Abbott et al., 2006). These interactions are key to regulating brain water volume and synchronising metabolite and ion levels with CBF and vasodilation in the adult brain. The most abundant water channel protein, aquaporin 4 (AQP4), is predominantly expressed in the end-feet surrounding cerebral vessels as well as the ATP-sensitive potassium channel $K_{ir}4.1$ (Abbott et al., 2006). Astrocytes express several factors proposed to be involved in maintenance of the BBB as opposed to induction of BBB integrity. One such factor is sonic hedgehog (Shh), which is known to upregulate claudin-5 and occludin levels *in vitro* (Alvarez et al., 2011). Shh knockout mice are embryonic lethal between E11 and E13.5. While mice have normal numbers of blood vessels, Shh knockout mouse embryos have reduced levels of TJ proteins such as claudin-5 and occludin (Alvarez et al., 2011). Additionally, conditional knockout of smoothened, a downstream signalling component of the Shh pathway, from ECs results in reduced TJ expression and increased extravasation of plasma proteins. Along with pericytes, astrocytes express angiotensin-1

(Milsted et al., 1990) following expression of Src-suppressed C-kinase substrate (SSeCKs) (rodent homolog of human AKAP12), which signals to Tie-2 receptors on ECs leading to the development of more advanced TJs, inhibition of transcytosis and downregulation of leukocyte adhesion molecules (Lee et al., 2003). AKAPs are important scaffolding proteins that control the activity of protein kinase A, the main cAMP effector protein. Maintenance of cAMP levels is vital for the barrier function of ECs (Wolburg and Lippoldt, 2002). Taken together, this data suggests that astrocytes have key functions in maintaining cerebrovascular integrity. Furthermore, the finding that astrocytes are present at the BBB postnatally adds further weight to this argument (Daneman et al., 2010b). Indeed, the cholesterol and phospholipid transporter molecule Apolipoprotein E (ApoE), produced by astrocytes, signals through low density lipoprotein receptor-related protein 1 on ECs to regulate TJ levels. More recently however, production and release of retinoic acid from radial glial cells (precursor astrocytes) has been shown to interact with RA receptor-β on developing ECs to induce barrier properties (Mizee et al., 2013).

1.1.1.3 Microglia

Microglia are the resident immune cell of the CNS. They are derived from haematopoietic precursor cells that migrate from the embryonic yolk sac into the CNS (Ginhoux et al., 2010). In the developing brain, microglia are involved in engulfing and eliminating synapses. This is thought to be mediated by the chemokine receptor CX3CR1 as CX3CR1 null mice have impaired synaptic pruning and increased dendritic spine densities in the hippocampus compared to controls. (Paolicelli et al., 2011). Despite their proximity, little is known about the interaction of microglial cells and ECs. One study shows that microglia are involved in tip cell fusion following vascular endothelial growth factor (VEGF)-induced tip cell induction (Fantin et al., 2010). Microglia are present in the embryonic CNS prior to endothelial sprouting and appear to be involved in cerebrovascular growth indicating that microglial-EC interactions may be a possible mechanism in BBB formation and regulation. It was thought that microglia remain in a resting, dormant state in the healthy brain however, *in vivo* two-photon imaging in the neocortex of adult mice found that highly motile microglial processes and protrusions constantly survey the neural microenvironment and dynamically interact with other cortical components (Davalos et al., 2005, Nimmerjahn et al., 2005). Additionally, microglia were shown to directly monitor neuronal function as application of the ionotropic γ-aminobutyric acid receptor blocker bicuculline significantly increases

microglia volume sampling (Nimmerjahn et al., 2005). Much more is known about the involvement of microglia in CNS disorders and following brain trauma. Microglia actively migrate towards the site of damage, such as ischemia and neurodegeneration, and engulf and eliminate neuronal cellular debris following cell death. To do this, microglia can shift between two activated morphological states. In the M1 activated state, microglia release proinflammatory cytokines such as interlukin-1β and tumour necrosis factor-α, while M2 activated microglia can dampen inflammation and promote tissue repair (Aguzzi et al., 2013).

1.1.1.4 Basement membrane

The often-overlooked component of the NVU is the noncellular BM, yet it has a pivotal role in establishing and maintaining BBB properties such as supporting pericytes and astrocytes. Structurally, BMs are a specialised layer of ECM proteins found basolateral to the endothelium and epithelium in all body tissues. Cells of the NVU synthesise and secrete proteins extracellularly that form the BM. BMs are a heterogeneous mix of proteins, the principal constituents of which are type IV collagen, laminin, nidogen/entactin and perlecan (LeBleu et al., 2007) that form a layer approximately 20-200 nm in thickness. The BM has an intricate role in crosstalk between NVU components. Astrocyte-specific deletion of laminin induces spontaneous haemorrhages in mice with impaired smooth muscle cell differentiation and loss of AQP4 and TJ proteins (Chen et al., 2013). In a follow-up study, a subset of mice with a pericyte-specific deletion of laminin develop hydrocephalus and BBB breakdown and loss of AQP4 (Gautam et al., 2016). Today, BM components are routinely used *in vitro* in the culture of primary BMVEC as well as immortalised brain endothelial cell lines. Collagen IV and fibronectin are two such components that are routinely used for the culture of primary and immortalised BMVEC.

It is now clear that communication between cellular and noncellular components of the NVU is critical for the health and integrity of the BBB from embryogenesis into adulthood. Breakdown of this communication may contribute directly or indirectly to CNS disease pathogenesis. As will be discussed in the following sections, these cellular components of the NVU have critical roles in the development of the BBB as well as in forming transport routes across and between brain ECs. Disruption of these processes can result in impaired homeostasis and BBB permeability.

1.1.2 Development of the BBB

BBB development is a multi-step process that begins at embryonic day 9.5 (E9.5) when sprouting endothelial progenitor cells from newly formed blood vessels invade the embryonic neuroectoderm. These early endothelial sprouts exhibit many properties of the BBB including the expression of TJ proteins and nutrient transporters. They also contain large numbers of transcytotic vesicles and display high expression levels of leukocyte adhesion molecules. Key mediators of angiogenesis are VEGF and Wnt. VEGF, a mitogen secreted by cells in the sub ventricular neuroectoderm of the embryonic brain, drives vessel expansion along a VEGF concentration gradient (Raab et al., 2004). VEGF binds to Flk1 receptor (VEGFR-2) on ECs to initiate vessel expansion. It has been shown that Flk1 knockout mice fail to develop vessels throughout the body and die between E8.5 and E9.5 (Shalaby et al., 1995) while $VEGF^{-/-}$ and $VEGF^{+/-}$ mice have severely compromised, but not abolished, vessel formation and suffer from early embryonic lethality at mid gestation (Carmeliet et al., 1996).

A key signalling pathway involved in angiogenesis during embryonic development is the Wnt signalling pathway. It has been shown that Wnt/β-catenin induced angiogenesis is unique to the CNS. During embryogenesis, the Wnt ligands Wnt7a and Wnt7b are expressed by neural progenitor cells in the developing forebrain and ventral regions of the neural tube, while Wnt1, Wnt3 and Wnt3b are expressed in the dorsal spinal cord and hindbrain (Daneman et al., 2009). In the canonical Wnt signalling pathway, Wnt ligands bind to frizzled receptors on the vascular endothelium, preventing β-catenin degradation by the proteasome. As a result, β-catenin accumulates in the cytoplasm and translocates to the nucleus where it induces the transcription of target genes including axin-2, Lef1, Apcdd1, Stra6 and Slc2a1 by binding to lymphoid enhancer-binding factor 1/T cell-specific transcription factor DNA-binding proteins (MacDonald et al., 2009). Knockout of Wnt7b results in embryonic lethality owing to severe brain haemorrhage and abnormal vessel morphology (Stenman et al., 2008, Daneman et al., 2009). When downstream signalling by β-catenin is absent, normal vascularisation is apparent throughout the body except for the CNS. As well as its intrinsic role in angiogenesis, Wnt signalling also has a crucial role in BBB formation. One of the downstream targets of Wnt signalling, slc2a1 codes for the BBB enriched glucose transporter (GLUT-1).

The next major step in BBB formation stems from the recruitment of pericytes and astrocytes to envelop the endothelium. Sprouting ECs from nascent blood vessels release PDGFβ which attracts pericytes that express PDGFRβ resulting in pericyte proliferation and migration with sprouting ECs (Hellstrom et al., 1999). EC-pericyte interaction is mediated by bidirectional transforming growth factor-β (TGFβ)/transforming growth factor receptor-β (TGFRβ) signalling. This signalling event leads to upregulation of the cell adhesion molecule N-cadherin on ECs resulting in firm adhesion between ECs and pericytes. Recent work has shown that CD146 is a receptor that is critical to EC-pericyte interactions. Initially specifically expressed by ECs in early BBB development, the subsequent recruitment of pericytes shifts CD146 expression specifically to pericytes via downregulation of EC CD146 by pericyte secreted TGFβ1. Mice deficient for CD146 were found to have reduced pericyte coverage and impaired BBB integrity (Chen et al., 2017). Following pericyte recruitment, the next step in BBB development involves the deposition of ECM proteins, such as collagen type IV, laminin and fibronectin by pericytes to promote formation of the BM. The crosstalk between ECs and pericytes results in TJ formation, barrier tightness, decreased transcytosis and decreased expression of leukocyte adhesion molecules. The precise role of astrocytes in BBB development has not been as well characterised but *in vitro* co-culture experiments revealed that ECs co-cultured with astrocytes have improved barrier characteristics with elevated expression levels of transporters, increased metabolic activity and increased TJ formation, compared to EC monocultures.

Finally, interendothelial TJs are sealed and maintained via pericyte-EC crosstalk (Lee et al., 2003). Astrocytes are key to sustained BBB integrity with angiotensin II-angiotensin II receptor type 1 signalling promoting the formation and maintenance of interendothelial TJs. Additionally, Shh secretion by astrocytes upregulates TJ protein expression.

1.1.3 Crossing the BBB

While oxygen and carbon dioxide can rapidly diffuse across the brain endothelium; as a result of the BBB, only the smallest (<400 da) lipophilic molecules containing fewer than 8-10 hydrogen bonds can passively diffuse across the BBB (Figure 1.4B) (Pardridge, 2009). However, as the energy needs of the brain are met by the cerebral circulation, numerous protein transport systems are present on the luminal and abluminal surface of brain ECs to regulate the CNS entry and exit of molecules (Figure 1.4).

1.1.3.1 Paracellular pathway

The paracellular pathway comprises the interendothelial space between adjacent ECs positioned along cerebral blood vessels (Figure 1.4A). The presence of highly electrical resistant TJ proteins in this space limits the flow of material to all but the smallest solutes and ions and lipid soluble molecules. Many lipid soluble molecules with molecular weights less than 400 Da can cross the BBB via diffusion through the endothelial lipid membranes (Figure 1.4 B). It has been estimated that all large molecule neurotherapeutics and up to 95 % of small molecule drugs cannot circumvent the BBB (Pardridge, 2005). Some substances can enter the brain through the paracellular pathway by deploying specific mechanisms. For example, leukocytes can gain passage to the brain in inflammatory situations. Leukocyte migration across the BBB is a multistep process that begins when leukocytes bind to P- and E-selectin on brain ECs to slow and bind to vascular cell adhesion molecule 1 (VCAM-1) and intercellular adhesion molecule 1 (ICAM-1) to attach to the ECs for subsequent transmigration (Figure 1.4E) (Takeshita and Ransohoff, 2012). Leukocyte adhesion molecules are typically expressed at low levels in the healthy brain microvasculature however they may become upregulated in inflammatory conditions (Takeshita and Ransohoff, 2012).

1.1.3.2 Transcellular pathway

The transcellular pathway is the predominant pathway for the delivery of proteins, peptides, amino acids, ions and carbohydrates to the brain. In addition, various therapeutic drugs have been delivered across the BBB by taking advantage of the molecular composition of various receptors expressed on the apical surface of brain ECs such as the transferrin receptor. Ions and other small solutes can enter the brain via solute carriers on the apical and basal membrane together with intracellular and extracellular enzymes. Ion regulation which is critical for optimal synaptic signaling between neurons is maintained by proteins such as the Na^+/K^+-ATPase pump on the abluminal membrane (Hawkins and Davis, 2005) and potassium channels (Figure 1.4C). Carrier-mediated transport is the major route for the entry of essential nutrients such as glucose and amino acids. GLUT-1 encoded for by the SLC2A1 gene is enriched in CNS ECs compared to peripheral tissues. GLUT-1 facilitates the transport of glucose and has a profound impact on BBB and NVU integrity (Figure 1.4 C). Indeed, slc2a1$^{+/-}$ mice show extensive microvascular leakage to serum proteins as well as reduced TJ protein levels (Winkler et al., 2015). The major facilitator super family domain containing 2a (mfsd2a) is specifically expressed in

cerebral blood vessels. Mfsd2a is expressed during BBB formation and is critical for BBB integrity as evidenced by mfsd2a ablated mice which have increased extravasation of injected tracer molecules. Importantly, BBB permeability was not a result of reduced TJ protein expression. Additionally, a potential role for msfd2a was identified whereby msfd2a$^{-/-}$ mice had increased levels of CNS-EC vesicular transcytosis (Ben-Zvi et al., 2014). A follow-up study confirmed that mfsd2a inhibits transcytosis and proposed that this happens by preventing caveolae formation through the enrichment of docosahexaenoic acid in the plasma membrane, creating a CNS plasma membrane microenvironment that is unfavourable for the assembly of caveolae domains and subsequent vesicle formation (Andreone et al., 2017). Numerous transporters are also present to facilitate amino acid entry to the CNS. For example, LAT1 (large neutral amino acid transporter) is highly expressed in brain capillaries relative to peripheral tissues and is responsible for transporting essential amino acids into the brain (Verrey et al., 2004). Receptor-mediated transcytosis enables bidirectional transendothelial transport of proteins and peptides such as transferrin and insulin (blood to brain) and apolipoproteins (brain to blood) (Figure 1.4G). Additionally, some plasma proteins such as albumin can cross the brain endothelium through adsorptive transcytosis (Figure 1.4F) which results from the binding of the positively charged protein to the negatively charged phospholipid membrane.

ATP-binding cassette transporters expressed on the luminal side of brain ECs prevent the brain accumulation of drugs, drug conjugates and xenobiotics via active efflux from the endothelium into blood. P-glycoprotein (PGP) is a particularly important efflux transporter that protects the brain from many neurotoxic compounds by substantially reducing their CNS entry (Figure 1.4D) (Lin and Yamazaki, 2003). The functional importance of PGP at the BBB was investigated in mice deficient for Mdr1a and Mdr1b. Mdr1a knockout mice were found to have 10-fold increases in brain concentrations of PGP substrates (Schinkel et al., 1994).

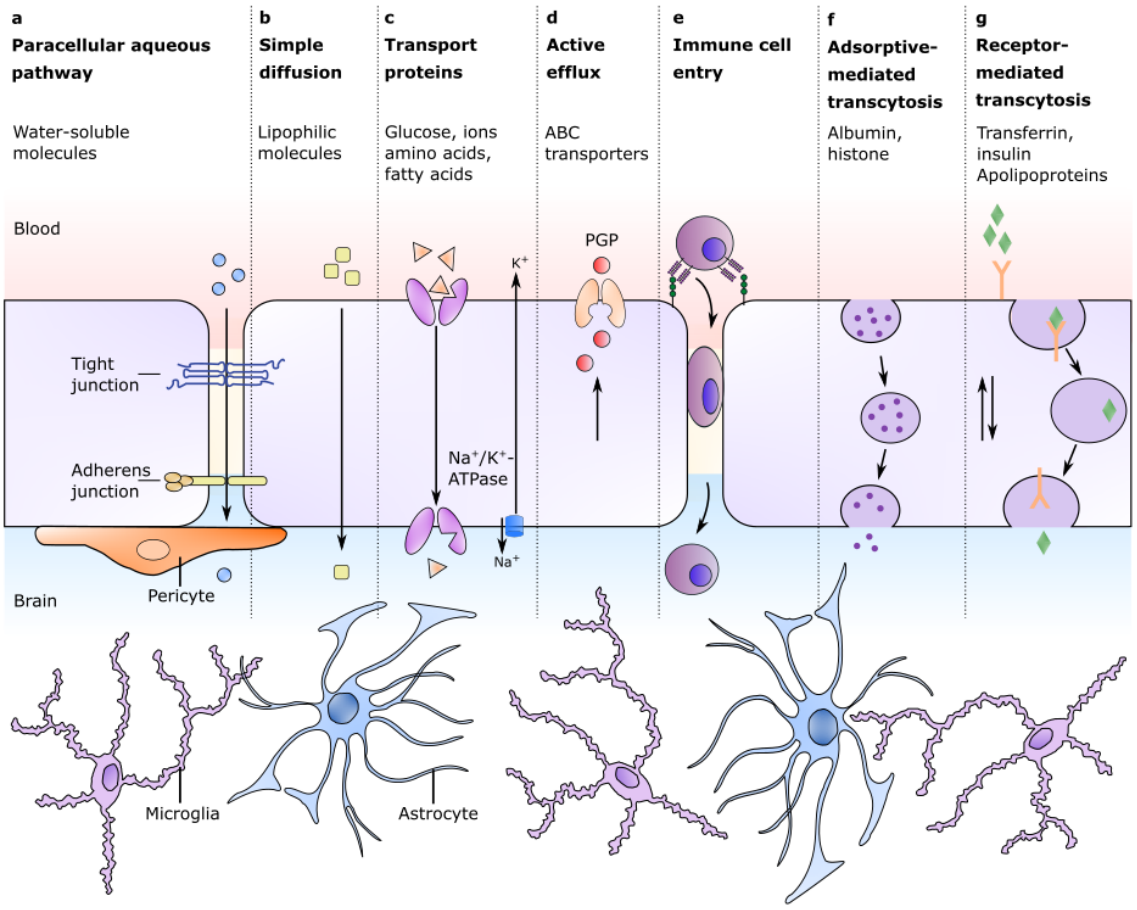

Figure 1.4: Transport properties of the capillary endothelium. **(A)** TJ protein complexes seal the interendothelial space between neighbouring ECs and restrict the free movement of solutes. **(B)** O_2 and CO_2 cross the BBB by diffusion as do lipophilic molecules with a molecular weight <400 Da and containing fewer than 8 hydrogen bonds. **(C)** Protein transporters on the luminal surface of the endothelium facilitate the entry of glucose, amino acids and nucleosides into the CNS. **(D)** ATP-binding cassette (ABC) active efflux transporters limit entry of drugs and xenobiotics. **(E)** Immune cells bind to cell adhesion molecules such as P-/E-selectin to infiltrate the brain parenchyma via the paracellular or transcellular route. **(F)** Adsorptive-mediated transcytosis involves the cationization of plasma proteins such as albumin and subsequent binding of the positively charged protein to sites along the negatively charged plasma membrane. This induces internalisation and transcytosis of the ligand across the cell within a vesicle. **(G)** Receptor-mediated transcytosis is used to transfer a variety of macromolecules such as insulin, IgG and transferrin across the BBB. This process involves binding of a ligand to a receptor, endocytosis and transport of the receptor-macromolecule complex within a vesicle followed by dissociation of the complex and exocytosis of the ligand.

1.1.4 Junctional complexes of the BBB

Two major junctional complexes are present at the BBB: adherens junctions (AJs) and TJs. AJs are composed primarily of cadherin proteins that span the intercellular cleft and provide stability by linking to the cell cytoplasm by α/β/γ catenin proteins (Wolburg and Lippoldt, 2002). The precise role of AJ has yet to be resolved, however it is thought that

the molecular components play a key role in maintaining cellular polarity, providing stability, promoting endothelial cell survival and responding to stimuli via interactions with cadherin proteins and the actin cytoskeleton. Evidence suggests that AJs are also essential for the formation of TJs. Unlike AJs which are present in all vascular beds, TJs are enriched in the endothelium of the brain microvasculature. TJs appear as continuous, anastomosing, intramembranous networks of strands that interact with TJ proteins on the same cell or on adjacent endothelial cells at so called "kissing points" to eliminate the paracellular space (Tsukita et al., 2001) (Figure 1.5). This fusion of TJs is responsible for impeding the flow of solutes and ions from the blood to brain and vice-versa, in turn creating a dynamic and highly regulatable barrier system.

Barrier properties at the BBB are conferred by highly electrical-resistant TJ proteins that limit the flux of all but the smallest molecules. TJs interact with TJs on adjacent endothelial cells as well as interacting with intracellular scaffolding proteins which tether the TJs to cytoskeletal proteins. TJ's have two main functions. The first is to significantly reduce the permeation of polar solutes and ions from the blood to the brain and vice-versa. This impediment to the flow of ions across the BBB leads to a high electrical resistance *in vivo* of ~1800 $\Omega.cm^2$ (Butt et al., 1990). Early studies with electron microscopy showed that ionic lanthanum introduced into the cerebral capillary lumen could penetrate the intercellular cleft as far as the TJ where its movement was subsequently impeded (Bouldin and Krigman, 1975). A second function of TJ proteins is to help maintain polarity of cells. This is achieved by restricting the lateral diffusion of membrane lipids and proteins between the apical and basolateral compartments of endothelial cells (van Meer and Simons, 1986). While certain substances can cross the barrier via the paracellular route, these are usually extremely small or employ specific mechanisms to move between TJs. For example, T-cell migration is initiated by leukocytes binding to ICAM-1 and -2 expressed on endothelial cell surfaces leading to migration across the transcellular pathway (Steiner et al., 2010b). Indeed, the major route of transport across the BBB is via the transcellular pathway. Neurons require energy to maintain synaptic signalling and this energy need is met by proteins such as GLUT-1 which controls the entry of glucose into the brain. Ion regulation which is critical for optimal synaptic signalling between neurons is maintained by protein pumps such as the Na^+/K^+-ATPase pump. Brain ECs also possess specific receptors to control the entry and exit of essential peptides, such as hormones.

The predominant TJ proteins are the claudins and occludin. Claudins and occludin also interact with cytoskeletal scaffolding proteins called zonula occludens on the intercellular domain of the plasma membrane to "tether" the TJs to the actin cytoskeleton (Fanning et al., 1998, Fanning et al., 2007, Hartsock and Nelson, 2008). At three cell contacts, tricellulin and lipolysis-stimulated lipoprotein receptor have been identified as potentially regulating paracellular permeability (Ikenouchi et al., 2005). Other proteins present within the TJ system are the junctional adhesion molecules (JAM) of which several isoforms have been discovered.

The following TJs have been described in detail:

1.1.4.1 Occludin

Occludin was identified as the first integral membrane protein within the TJ of endothelial cells (Furuse et al., 1993). Occludin is a tetraspan integral membrane protein that has four membrane spanning domains and two extracellular loops and is enriched at the TJ of epithelial and endothelial cells. The role of occludin was first elucidated following ectopic expression of chicken occludin in Sf9 insect cells, whereupon it induced the formation of TJ-like structures (Furuse et al., 1996). Following this it was found that a mutated occludin protein, introduced into Madin Darby Canine Kidney cells (MDCK), increased the paracellular leakage of MDCK cells to small tracers, implying a role in the barrier properties of TJs (Balda et al., 1996). Subsequent investigations in embryonic stem cells deficient in occludin could still form intact TJs indicating that occludin is dispensable to barrier formation (Saitou et al., 1998). Additionally, there were no overt morphological differences between TJs of normal and occludin deficient embryonic stem cells as well as normal localization and expression of the TJ-associated protein ZO-1. Further to this, occludin knockout mice have been reported with a complex phenotype and postnatal growth retardation and brain calcification. However, occludin null mice still formed intact TJs and displayed no size-selective loosening of the intestinal epithelia as recorded electrophysiologically. The complex array of abnormalities indicates a potential physiological role of occludin secondary to TJ formation (Saitou et al., 2000). In fact, numerous studies have now shown that occludin undergoes extensive modifications at the post-transcriptional and post-translational level (Cummins, 2012). Prior to development of disease symptoms in experimental autoimmune encephalomyelitis (EAE), an animal model of brain inflammation, dephosphorylation of occludin occurs

suggesting that occludin could be a target for signalling events in EAE (Morgan et al., 2007). It is also known that occludin plays a key role in redox regulation of TJs. Normoxia (normal oxygen levels) conditions promote occludin oligomerization and TJ assembly while oxidative stress associated with inflammation promotes TJ disruption (Blasig et al., 2011). It is evident that occludin has a role beyond that of a barrier forming TJ and that dysfunctional occludin expression is involved in numerous neuropathologies. For example, phosphorylation of occludin at Ser-490 in response to VEGF leads to its ubiquitination and subsequent internalisation. This process results in increased permeability to macromolecules and ions (Murakami et al., 2009). Furthermore, in a mouse model of neovascularisation, occludin phosphorylation is required for VEGF-induced neovascularisation and subsequent loss of BRB integrity (Liu et al., 2016).

1.1.4.2 Claudins

Claudins are a multigene family of 20-24 kDa integral membrane proteins consisting of four membrane spanning domains with a short N terminus, two extracellular loops and a cytoplasmic tail. 24 claudin proteins have been identified in humans (Morita et al., 1999) with sequence analysis separating the family into two groups based on their sequence similarity and proposed function: Group one contains the classic claudins (1-10, 14, 15, 17, 19) and group two contains the non-classic claudins (11-13, 16, 18, 20-24). Claudins are similar in structure to occludin, tricellulin and connexins as they contain four transmembrane domains, despite having minimal sequence homology. The claudins are expressed in numerous tissues with claudins 3, 5 and 12 being expressed by brain ECs with claudin-5 being the most enriched (Daneman et al., 2010a). They are the major component of the TJ and a general role of the claudins is the paracellular sealing function to limit the paracellular movement of material. The first extracellular domain (ECD) of claudins is known to be vital for the barrier properties of the TJs. Mutations to conserved cysteine residues in ECD1 of claudin-5 in MDCK cells results in increased paracellular permeability to mannitol and monosaccharides (Wen et al., 2004). The second ECD has been less intensively studied however, for claudin-5, it has been proposed to be involved in strand formation via trans interactions (Piontek et al., 2008). Claudins associate with claudin species on adjacent cells as well as forming cis interactions on the same cell (Blasig et al., 2006, Furuse et al., 1999). Claudins are a major structural component of the TJ and form the backbone of TJs through homotypic and heterotypic interactions via their extracellular domains (Krause et al., 2008, Krause et al., 2009). The spatial organisation

of claudin TJ strands is determined by the ZO scaffolding proteins with most claudin species containing a C terminus PDZ-binding motif which can bind to PDZ motifs on the ZO proteins (Itoh et al., 1999) linking them to the actin cytoskeleton. *In vitro* models of the BBB as well as genetic mouse models have improved our understanding of the physiological roles of the claudin proteins. Claudin-1 deficient mice die within 1 day of birth from excessive skin dehydration and were shown to have impaired barrier functions at the epidermis with increased permeation of a 600 Da tracer compared to controls (Furuse et al., 2002). Claudin-5 was identified to form stable TJ networks upon transfection into TJ free MDCK cells concurrent with a selective decrease in permeability to ions (Wen et al., 2004). Claudin-5 deficient mice have an impaired BBB with electron microscopy revealing intact TJs at cell-cell contacts. Tracer molecule experiments revealed increased permeation of molecules up to ~800 Da in size. These mice also die within hours of birth from undefined causes. Interestingly, the BBB of claudin-5 deficient mice remained intact to molecules greater than 1 kDa indicating other unidentified TJ components may be involved in regulating barrier integrity towards different sized molecules (Nitta et al., 2003). Claudin-11 is expressed in CNS myelin and the testis and mice deficient for claudin-11 have CNS myelin defects that manifest behaviourally as hindlimb weakness and impaired movement on the rotarod. Claudin-11 deficient mice also display male sterility (Gow et al., 1999) and deafness (Gow et al., 2004). The claudin proteins are expressed abundantly in numerous tissues and are central to the barrier function of tissues such as the intestinal epithelia, inner ear, BBB, blood-retinal barrier and blood-testis barrier. It is apparent that the claudins have an intrinsic role in regulating permeability and manipulation of TJ components is a promising approach to improved drug delivery to the CNS to offer novel therapeutic strategies for several CNS disorders (Greene and Campbell, 2016)**.**

1.1.4.3 Junctional adhesion molecules (JAM)

JAMs, like TJ proteins, are integral membrane proteins belonging to the immunoglobulin superfamily. They consist of a single membrane-spanning domain, an extracellular domain with an N terminus and a short cytoplasmic C terminus (Martin-Padura et al., 1998). The cytoplasmic C terminus contains a PDZ motif that interacts with scaffolding proteins including ZO-1, AF-6, ASIP/Par3 and cingulin (Bazzoni et al., 2000, Ebnet et al., 2000). JAMs can form homotypic interactions with JAMs on opposing endothelial cells and form heterotypic interactions with different JAM family members as well as

other adhesion molecules (Weber et al., 2007). Through binding to Par3, JAMs promote cell polarity and the localization of ZO-1 and occludin at points of cell contact (Itoh et al., 2001). Mounting evidence has implicated a role for JAM family members in leukocyte migration across endothelial cell layers (Aurrand-Lions et al., 2005, Bradfield et al., 2007).

1.1.4.4 Scaffolding proteins

The membrane-associated guanylate-kinase (MAGUK) protein family are accessory elements for the transmembranous components of TJs. The ZO (ZO-1, ZO-2, and ZO-3) proteins are members of the MAGUK protein family. They are the prominent scaffolding proteins linking TJs to the actin cytoskeleton. ZO-1 is a 220 kDa protein essential for endothelial barrier formation, VE-cadherin-mediated cell tension and actomyosin organization through its interaction with F-actin (Tornavaca et al., 2015). Mice deficient in ZO-1 are embryonic lethal by E10.5 with embryonic and extraembryonic defects including impaired angiogenesis and increased apoptosis in the neural tube and notochord (Katsuno et al., 2008). ZO-2 is a 160 kDa protein that is also critical for embryonic development with mice deficient for ZO-2 being embryonic lethal due to a loss of cell proliferation and induction of apoptosis between E6.5 and E7.5 (Xu et al., 2008). In contrast, ZO-3, a 130 kDa protein, deficient mice developed normally and had no apparent phenotype (Adachi et al., 2006, Xu et al., 2008). The ZO proteins contain a PDZ motif on the C terminus to link ZO proteins with transmembrane proteins or with PDZ motifs on other proteins. ZO-1 binds to the claudins, occludin and JAM via PDZ motifs as well as with various components of the cytoskeleton (Bazzoni et al., 2000, Ebnet et al., 2000, Tornavaca et al., 2015). Knockdown of ZO-1 in MDCK cells delays TJ assembly while knockout of ZO-1 in MDCK cells by TALEN-mediated gene targeting results in alterations in myosin organization at cell-cell contacts and disruption of the localization of TJ proteins (Tokuda et al., 2014, McNeil et al., 2006).

Cingulin is a cytoplasmic protein localized on the cytoplasmic face of TJs (Citi et al., 1991). It is a 140 kDa protein that interacts with several TJ species. *In vitro* studies have identified ZO-1, ZO-2, ZO-3, myosin and AF-6 interacting with the N terminus of cingulin (Cordenonsi et al., 1999). Investigations in MDCK cells have shown that cingulin is not involved in the basic structure and function of TJs (Guillemot and Citi,

2006). Subsequent work demonstrated that cingulin is involved in the regulation of cell proliferation and gene expression through RhoA signalling (Citi et al., 2009)

1.1.4.5 Adherens junctions

Like TJs, adherens junctions associate with the actin cytoskeleton and are involved in the initiation and stabilisation of cell-cell adhesion, regulation of the actin cytoskeleton, intracellular signalling and transcriptional regulation. AJs are composed primarily of cadherin proteins, such as E-cadherin, that span the intercellular cleft and provide stability by initiating intercellular contacts through trans-pairing between cadherins on adjacent cells. Cadherins can also link directly to cell cytoplasm proteins and the interactions between cadherins and catenins has a crucial role in the formation and function of AJs (Takeichi, 2014). Catenin family members including p120 catenin and β-catenin can bind to classical cadherins to form a cadherin-catenin core complex which can subsequently bind to the F-actin cytoskeleton through α-catenin which is crucial for firm cell adhesion (Hansen et al., 2013). The molecular components of AJs play a key role in maintaining cellular polarity, providing stability, promoting endothelial cell survival and responding to stimuli via interactions with cadherin proteins and the actin cytoskeleton. AJ are involved in the regulation of endothelial permeability through dynamic opening and closing of cell-cell adherens junctions as a result of the phosphorylation of VE-cadherin and subsequent internalisation (Dejana et al., 2008). Evidence also suggests that AJs are essential for the formation of TJs. VE-cadherin is an endothelial cell-specific AJ component that mediates the upregulation of claudin-5 through Akt-dependent phosphorylation of the forkhead box factor Fox01 which inhibits β-catenin translocation to the nucleus and repression of claudin-5 transcription (Taddei et al., 2008).

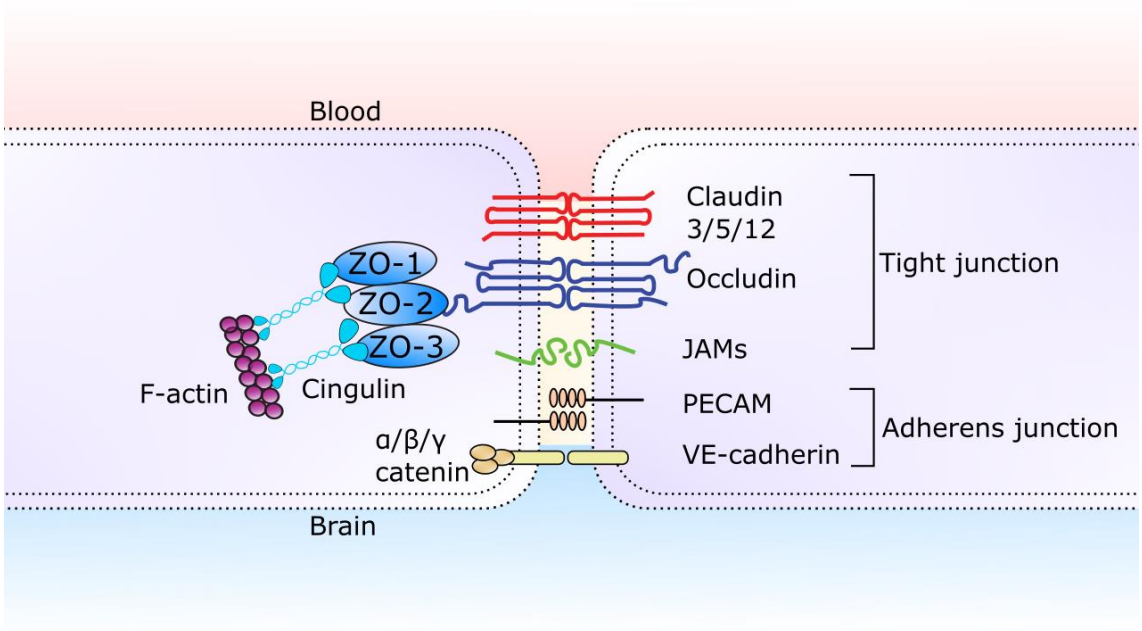

Figure 1.5: Junctional complexes of the BBB. Claudin-5 and occludin are the major TJ components at the BBB and are linked to the actin cytoskeleton via the ZO family of scaffolding proteins and other intracellular proteins such as cingulin. Other TJs such as tricellulin and LSR are enriched at three cell contacts (not pictured here). VE-cadherin is a component of the adherens junction and is linked to the actin cytoskeleton by α/β/γ catenin proteins.

1.2 Schizophrenia

1.2.1 Overview

Schizophrenia is a chronic mental disorder with a complex, heterogeneous mix of symptoms. It affects approximately 1% of the population and affects more than 21 million people worldwide. The most comprehensive study on the lifetime risk of schizophrenia according to DSM-IV criteria was carried out in Finland and estimated at 0.87% for schizophrenia and 0.32% for schizoaffective disorder. In total, there was a 3.06% lifetime prevalence of all psychotic disorders (Perala et al., 2007). The characteristic symptoms of schizophrenia can be divided into two groups, positive symptoms and negative symptoms. Positive symptoms are defined by behaviours and thoughts not normally present such as psychosis which involves disorganised thinking and speech, hallucinations and a failure to recognise what is real. Negative symptoms refer to affective behaviours and include anhedonia (loss of ability to feel pleasure), social withdrawal,

diminished energy and motivation. A third characteristic symptom of schizophrenia involves a broad group of cognitive dysfunctions. Symptoms can lead to abnormal social behaviours, depression and anxiety disorders as well as depression, self-harm, drug and alcohol abuse. These disabling symptoms may account for the high prevalence of suicide observed compared to the general population. The prodromal phase is defined as the initial onset of the disorder prior to the first psychotic episode and typically begins in early adolescent years. The prodromal phase consists of a decline in cognitive and social functioning. A diagnosis of schizophrenia rarely occurs during the prodromal phase with clinical diagnosis usually following the manifestation of psychotic episodes.

Individuals with schizophrenia have a shorter life expectancy than the general population with a standardised mortality ratio of 2.6 which has continued to rise in recent decades (McGrath et al., 2008). Suicide is the main contributor to early mortality in early years with cardiovascular diseases being the primary contributor later in life (McGrath et al., 2008). Individuals with schizophrenia are up to 12 times more likely to commit suicide compared to the general population (Caldwell and Gottesman, 1990). Contributing factors to the shorter life expectancy include the high rate of cigarette smoking and unhealthy lifestyle as well as the obesity promoting effects of anti-psychotic drugs. These factors contribute to the metabolic syndrome, diabetes and elevated cardiovascular and respiratory deaths observed among patients (Hoang et al., 2011). The aetiologies of schizophrenia are not clear, however research points to a combination of genetics and environment being major contributors to the development of the disorder. Owing to its heterogeneous clinical presentation and complex aetiology, in the absence of a biological marker, clinical diagnosis of schizophrenia relies on an examination of mental state and observation of the patient's behaviour. Pharmacological treatments are available to control the psychotic symptoms of schizophrenia however they have no overall benefit in social and cognitive functioning. Psychosocial interventions such as cognitive behavioural therapy have proven beneficial but are inconsistently applied (Kahn et al., 2015).

1.2.2 Risk factors

Risk factors for schizophrenia can be grouped into 3 categories:

- Sociodemographic characteristics;
- Predisposing factors;

- Precipitating factors;

People who are exposed to complications in foetal life and at birth have an increased risk of developing schizophrenia. Pre-natal risk factors in the development of schizophrenia have been proposed, such as birth trauma, which includes: complications of pregnancy (bleeding, pre-eclampsia, diabetes, rhesus incompatibility and infection), abnormal foetal growth and development (low birth weight, congenital malformations) and complications of delivery (emergency caesarean section, asphyxia, uterine atony) (Cannon et al., 2002a). Presumably, these risk factors affect neural connectivity in the developing brain. Peculiarly, there is a slight but significant excess number (7-10%) of individuals with schizophrenia born in late winter to spring (Stilo and Murray, 2010). Schizophrenia is more common in men than women as well as the disorder being more severe in men. Additionally, men develop schizophrenia earlier in life than women and are more likely to have a history of pre or perinatal complications and to show brain malformations (Castle and Murray, 1991).

In developed countries, there is an association between the prevalence of schizophrenia in urban areas compared to rural areas (Freeman, 1994). A Danish study found that there was a greater risk of schizophrenia in individuals who were not just born, but raised exclusively in large cities compared to individuals who lived in less urbanized environments (Pedersen and Mortensen, 2001). Densely populated, disadvantaged areas of inner cities are most common for schizophrenia. This was initially noted in Chicago in 1939 (1960) but was more recently replicated in Ireland (Kelly et al., 2010) and the UK where it was found that the smaller cities of Nottingham and Bristol had an incidence of schizophrenia that was less than half that of London (Kirkbride et al., 2006). Migration is another commonly linked factor with a significantly increased risk of schizophrenia among migrants and ethnic minority groups and especially black migrants to European countries (Cantor-Graae and Selten, 2005). In England, it was found that all ethnic minorities were at an increased risk for schizophrenia but especially so with African-Caribbean's and black Africans at nine-fold and six-fold respectively (Fearon et al., 2006).

Drug abuse has been an extensively covered risk factor with an increased risk of psychosis associated with early and excessive use of methamphetamine (Chen et al., 2003). Recent

evidence has also implicated cannabis use and later psychosis (Fergusson et al., 2003, van Os et al., 2002, Weiser et al., 2002).

1.2.3 Genetics of schizophrenia

Genetics is recognised as one of the most significant risk factors for schizophrenia. While incidence in the general population is ~1%, in first degree relatives (e.g., parents, siblings or children) the incidence is 6%-17%. Twin studies suggest approximately 17% incidence in dizygotic twins and up to 50% incidence in monozygotic twins (Figure 1.6) (Vogel, 1991). Indeed, meta-analysis of association studies has identified a large number of candidate gene variants highly associated to schizophrenia phenotype (Allen et al., 2008). Further analysis revealed a number of these high candidate variants are involved in the metabolism of key neurotransmitters as well as genes related to DNA methylation, apoptosis and neurodevelopment (Shi et al., 2008). Over 100 loci in the human genome contain single nucleotide polymorphism (SNP) haplotypes that associate with the risk of schizophrenia (2014). Most genes from this study are enriched in the brain and several are involved in glutamatergic neurotransmission as well as many genes involved in the immune response, providing support for the link between the immune system and schizophrenia. Further weight to this speculative link between the immune system and schizophrenia was discovered in a recent study of 65,000 individuals that revealed a significant risk of schizophrenia associated with inheritance of specific variants of the complement component 4 (C4) protein, a key member of the immune system complement cascade. Post-mortem analysis of human brains revealed structural forms of C4 associated with increased C4 transcript and increased elimination of synapses in schizophrenia subjects (Sekar et al., 2016).

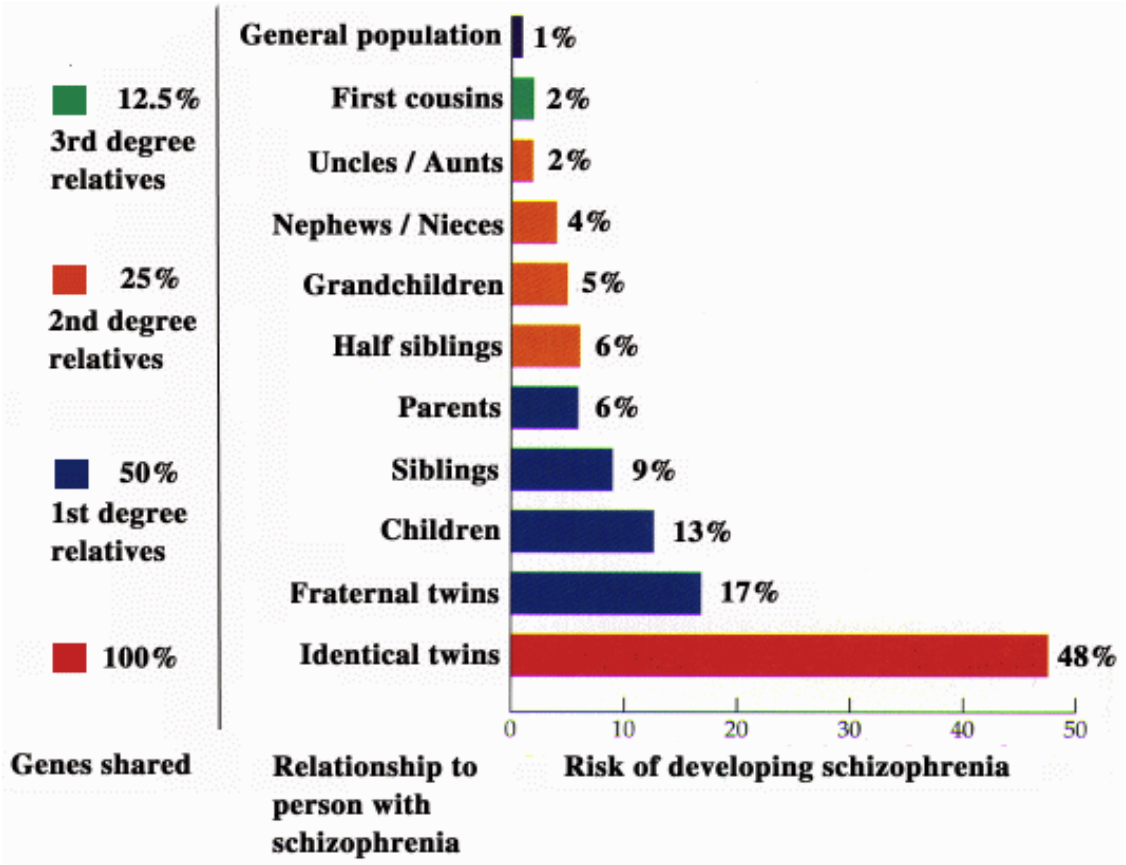

Figure 1.6: Rates of schizophrenia. The incidence of schizophrenia in the general population is ~1 % while in first-degree relatives, this increases to 6-17 %. The incidence in dizygotic twins is 17 % and in monozygotic twins is 48 %. Source: (Gottesman, 1991).

Many genetic studies have identified linkage to chromosome 22, suggesting this region harbours major susceptible loci for schizophrenia (Liu et al., 2002, Pulver, 2000, Rees et al., 2014). Individuals with the chromosomal abnormality 22q11 Deletion Syndrome (22q11DS) have a 25-fold increased lifetime risk of developing schizophrenia and other neuropsychiatric related conditions compared to the general population due to microdeletions at the chromosomal region 22q11.21 (Kao et al., 2004, Murphy, 2002, Williams, 2011).

1.2.4 Microvascular dysfunction in schizophrenia

There is accumulating evidence suggesting that anomalies of the microvasculature are involved in the pathogenesis of schizophrenia (Najjar et al., 2017, Najjar et al., 2013). Up to 50% of deaths of individuals with schizophrenia are accounted for by cardiovascular disease (CVD). Indeed, schizophrenic patients have a significantly increased burden of CVD compared to the general population and as such, measurements of endothelial dysfunction may prove useful in identifying high risk individuals. Identifying markers of

vascular endothelial dysfunction may offer alternative approaches to identifying at risk individuals.

1.2.4.1 Post-mortem studies

Much of the early research on the role of the microvasculature in schizophrenia focussed on microscopic analysis of capillary vessels in post-mortem control and schizophrenic brains. Post-mortem studies have often been limited by small sample sizes, poorly matched controls, confounding effects of medications, storage conditions and preparation of brain tissue that may potentially introduce detrimental effects. In addition, most schizophrenic patients will have undergone some form of treatment at some point in their clinical history. As such, it is important to control for this as well as examine tissue samples from drug naïve patients.

Uranova and colleagues identified morphological differences in capillaries and NVU cell types in the prefrontal and visual cortex of schizophrenia patients along with vacuolar degeneration of ECs, astrocyte-foot processes and thickening of the BM (Uranova et al., 2010). In a follow-up study, reductions of capillary density in the prefrontal and visual cortex were found to associate with negative symptoms of schizophrenia (Uranova et al., 2013). Another study found significant decreases in capillary diameter in dorsal and subgenual parts of the anterior cingulate cortex in major depressive disorder and bipolar disorder patients but not in schizophrenic patients while schizophrenic patients had decreased cortical thickness (Sinka et al., 2012).

Structural abnormalities have also been detected in the brains of schizophrenic patients treated with anti-psychotic drugs including reduced capillary diameter, ECM deposition and perivascular oedema but also pinocytosis and vacuolization (Udristoiu et al., 2016). However, this study had a sample size of just three patients who were treated with anti-psychotics. Several studies have shown abnormalities in other NVU components including reductions in the number of pericapillary oligodendrocytes in the prefrontal cortex (Vostrikov et al., 2008), decreased numbers of GFAP positive astrocytes adjacent to blood vessels in the prefrontal cortex (Webster et al., 2001) and anterior cingulate cortex (Webster et al., 2005) in schizophrenia patients (Figure 1.7F).

Changes in expression of endothelial specific genes has also been investigated and have implicated the role of the BBB in the immune response in schizophrenia. Microarray analysis of ECs isolated by laser capture microdissection from post-mortem schizophrenic patients and healthy controls found downregulation of EC genes involved in ion transport, cell proliferation and adhesion, suggesting a dysfunction of the BBB (Harris et al., 2008). As the BBB enforces the "immune privileged" status of the brain, changes in BBB components such as cell adhesion molecules can increase peripheral immune cell infiltration to the brain which have previously been shown to correlate with cognitive and behavioural changes in animal models in response to systemic inflammation (D'Mello and Swain, 2014). Further evidence for the link between BBB disruption/immune response was reported by Hwang and colleagues who used RNA-seq data from the hippocampus of control and schizophrenia subjects that identified 144 genes differentially regulated in schizophrenia cases compared to unaffected controls, the majority of which are involved in the immune/inflammation response. Additionally, the majority of these differentially expressed immune system genes in this study were more likely to be expressed in ECs of the BBB, blood monocytes within blood vessels and perivascular astrocytes than in lymphocytes or microglia (Hwang et al., 2013). Furthermore, Kim and colleagues identified 23 genes up-regulated in the choroid plexus of 29 schizophrenia subjects compared to 26 unaffected controls related to biological processes involved in defence, immune and inflammatory responses and amino acid transport. The differential expression of these genes positively correlated with the amounts of inflammatory proteins in the serum and frontal cortex including c-reactive protein, cortisol, MMP-9 and tissue inhibitor of metalloproteases 1 (TIMP-1) (Kim et al., 2016). Recently, Katsel and colleagues examined 1306 genes in a microarray dataset from 15 cerebrocortical regions and the hippocampus of individuals with schizophrenia and identified 657 differentially regulated genes, 311 of which correspond to a subset uniquely enriched in ECs. Most of these EC enriched genes that were downregulated in schizophrenia are involved in angiogenesis pathways (Katsel et al., 2017). Another gene expression study examining VEGF mRNA from the dorsolateral prefrontal cortex of 16 individuals with schizophrenia and 18 psychiatrically normal controls found significant decreases in VEGF in the schizophrenia group (Fulzele and Pillai, 2009). Cerebral vascularisation is mediated by VEGF and VEGF significantly contributes to angiogenesis by stimulating neovascularisation and is intimately involved in the regulation of CBF. Additionally, VEGF has a key role in neurophysiology as suppression of neural VEGFR2

impairs hippocampal-dependent synaptic plasticity and long-term potentiation and consolidation of emotional memory (De Rossi et al., 2016). To date, studies on other BBB molecular components such as TJ proteins have not been examined in post-mortem schizophrenia brain sections.

1.2.4.2 CSF studies

The gold-standard technique for measuring BBB permeability in humans is measurement of the CSF: serum albumin ratio (QAlb) (Figure 1.7B). This test compares the concentration of albumin in the blood compared to the CSF. Albumin is typically present in the CSF at concentrations approximately 200 times lower than blood. Therefore, an increased QAlb suggests that increased quantities of albumin have been able to pass from the blood into the CSF due to an impaired barrier. This test has been used to detect BBB dysfunction in several psychiatric studies (Shalev et al., 2009). In a study of 63 psychiatric subjects and 4,100 controls, a subset of psychiatric patients (14 major depressive disorder and bipolar disorder and 14 schizophrenia) had CSF abnormalities reflecting BBB dysfunction. BBB dysfunction was represented as increased serum albumin with BBB dysfunction being the only sign of dysfunction in 24% of cases (Bechter et al., 2010). A dysfunctional blood cerebrospinal fluid barrier has also been reported in patients with several forms of dementia including AD and frontotemporal dementia with elevated QAlb (Busse et al., 2017). However, analysis of QAlb has its limitations as increased QAlb can result from other factors including low rates of CSF production, increased subarachnoid flow resistance or blocking of arachnoid villi causing reduced outflow into venous. Additional problems stem from the small sample sizes of the studies and the confounding factor of anti-psychotic medication (Bechter et al., 2010).

1.2.4.3 Blood biomarkers

The calcium-binding peptide S100β is produced mainly by astrocytes and is abundantly expressed by neurons in the brain. In healthy individuals, S100β is almost undetectable in the serum. Increased serum concentrations of S100β have therefore been used to associate CNS pathology with BBB dysfunction. There is accumulating evidence showing increased levels of S100β in the blood, CSF and brains of schizophrenic patients (Lara et al., 2001, Schroeter et al., 2003, Wiesmann et al., 1999) and depression patients (Schroeter et al., 2008) with increased levels of S100β in both acute and chronic cases. Additionally, plasma S100β levels were positively associated with the negative symptoms

of schizophrenia (Rothermundt et al., 2001, Rothermundt et al., 2004b) (Figure 1.7D). However, whether this increase in S100β is directly reflecting increases in BBB permeability or merely increased production and/or secretion by glial cells or degeneration of glial cells (Rothermundt et al., 2004a) has yet to be elucidated. Additionally, S100β has been found to be secreted by adipose tissue outside the CNS (Steiner et al., 2010a) calling into question the interpretation of the results and validity of these studies.

A limited number of studies have examined blood concentrations of BBB components. Vascular endothelial dysfunction has been suggested in several studies with increased peripheral concentrations of endothelial cell adhesion molecules such as soluble P-selectin and L-selectin in the serum and plasma of untreated acute schizophrenic patients compared to controls (Iwata et al., 2007, Masopust et al., 2011), suggesting the possibility of increased EC activation in the cerebral vasculature of individuals with schizophrenia. In addition, atypical anti-psychotics such as risperidone contributed to vascular dysfunction in diabetic rats via activation of EC adhesion molecules such as ICAM-1, VCAM-1 and soluble L-selectin (Aboul-Fotouh and Elgayar, 2013). Activation of cell adhesion molecules on the vascular endothelium may contribute to increased transendothelial migration of lymphocytes and monocytes (Figure 1.7C). Matrix metalloproteinase -9 is a 92 kDa protein that belongs to the family of zinc and calcium dependent endopeptidases. Recently, it has been shown to negatively affect CNS disorders such as epilepsy and traumatic brain injury (TBI). Few studies have investigated MMP levels in schizophrenia. Two studies reported increased concentrations of MMP-9 and TIMP in schizophrenia (Domenici et al., 2010, Yamamori et al., 2013) (Figure 1.7G), although another study found no differences between patients and controls from a total of 63 patients with chronic schizophrenia (Niitsu et al., 2014). A recent study identified elevated serum levels of VEGF in schizophrenia patients compared to controls that were associated with structural abnormalities in the prefrontal cortex (Pillai et al., 2016), however elevated serum VEGF levels are not predicted to affect BBB integrity owing to the polarised nature of the permeability response at blood-neural barriers (Hudson et al., 2014).

1.2.4.4 Neuroimaging studies

Gross anatomical changes in brain structure have also been observed with deficits in grey matter volume primarily in cortical brain regions compared to unaffected controls (Cannon et al., 2002b). Neuroimaging studies have identified consistent structural abnormalities in schizophrenic patients. Volume reductions in the medial temporal lobe (memory), left posterior superior temporal gyrus (auditory processing and language) (Shenton et al., 1992) as well as ventricular enlargement have been consistently observed (Van Horn and McManus, 1992). Neuroimaging studies have not assessed BBB changes in schizophrenia patients with the few early studies confounded by small sample size, difficult interpretation of results and imprecise techniques. Advancements in DCE-MRI for quantitative assessment of BBB permeability have since been detected that may be useful for detecting subtle BBB abnormalities, but these have yet to be applied to psychiatric patients. A recent MRI study using a 7T scanner reported alteration in the volume of small arterial and arteriolar cerebral vessels in cerebral vessels throughout the brain, suggesting that microvascular anomalies may be widespread across the brain (Hua et al., 2017). This work built on previous findings of aberrant CBF and cerebral blood volume associated with schizophrenia (Peruzzo et al., 2011). As these studies focussed on smaller vessels, it has relevance to the BBB.

Glutamate is the primary excitatory neurotransmitter in the brain and disturbances in glutamate-dependent neurotransmission have been documented in numerous psychiatric disorders including schizophrenia. This hypothesis is based on the findings that N-methyl-d-aspartate receptor (NMDAR) antagonists can induce schizophrenia-like symptoms (Moghaddam and Javitt, 2012). A meta-analysis of glutamate levels by magnetic resonance spectroscopy revealed elevations in glutamate and glutamine levels in the basal ganglia and medial temporal lobe (Merritt et al., 2016). As glutamate modulates BBB permeability (Vazana et al., 2016), regional disturbances in glutamate levels may alter regional BBB permeability. Additionally, abnormal glutamate homeostasis at the BBB may contribute to psychopathology. Glutamate is actively transported out of the brain by amino acid transporters at the BBB to maintain IF concentrations of glutamate at a fraction of the blood. Dysfunctional astroglial glutamate transporter expression has been observed in schizophrenia (McCullumsmith et al., 2016). In addition, polymorphisms of these transporters have been associated with cognitive dysfunction in schizophrenia patients (Zhang et al., 2015).

A recent study has identified regulatory mechanisms in BMVECs capable of controlling CBF by sensing neural activity to modulate CBF to dynamically regulate the changing metabolic requirements of neurons. ECs achieve this through activation of the $K_{IR}2.1$ inward rectifier K^+ channel to produce a rapidly propagating retrograde hyperpolarization that causes upstream arteriolar dilation, resulting in increased blood flow to the capillary bed. Initially this was performed *ex vivo* in brain slices via the addition of K^+ and subsequently repeated *in vivo* via addition of K^+ adjacent to a post arteriolar capillary which produced a rapid increase in red blood cell flux as measure by two-photon laser-scanning microscopy. Additionally, this effect was concentration dependent with application of 3 mM K^+ having no effect and application of concentrations >25 mM produces membrane depolarisation (Longden et al., 2017). It will be interesting to determine if dysfunction of this process is evident in schizophrenia as alterations of CBF have been observed across several brain regions in schizophrenia. Alterations in CBF have been identified in numerous brain regions in schizophrenic patients compared to controls (Andreasen et al., 2008) with reduced CBF being associated with negative symptoms of schizophrenia notably in the frontal lobe (Wang et al., 2003, Zhao et al., 2006).

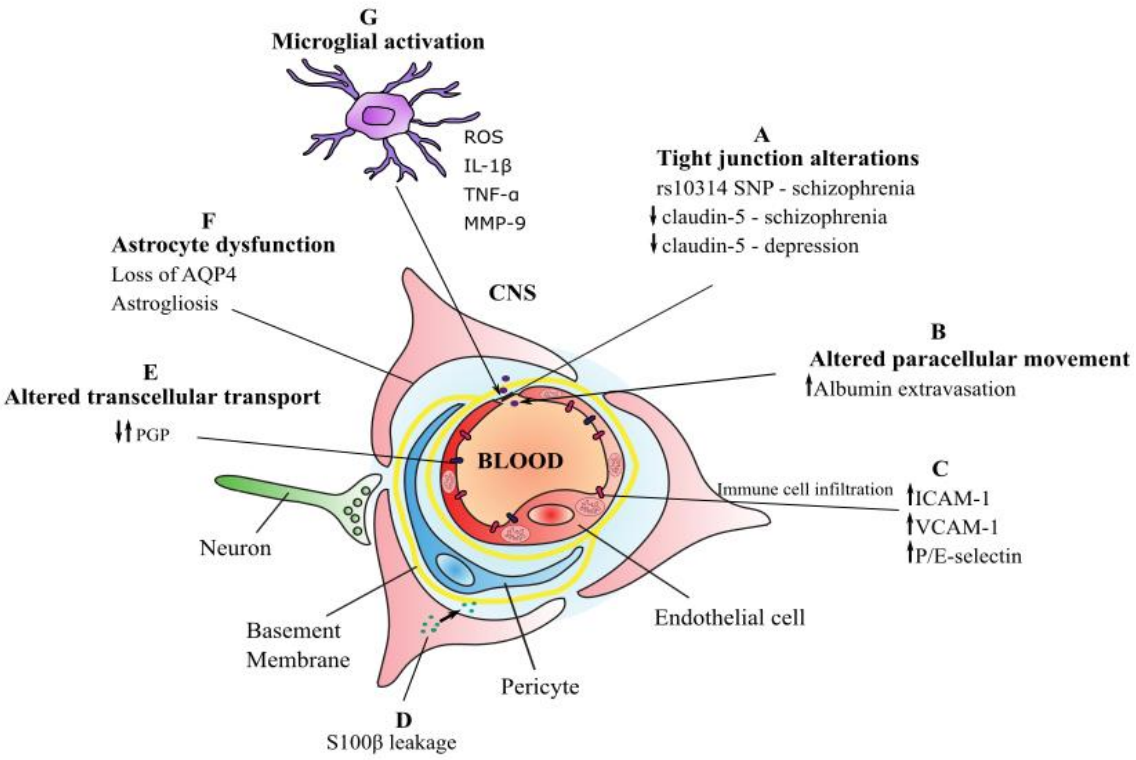

Figure 1.7: Schematic summary of experimental data of structural and functional BBB alterations in psychiatric disorders. **(A)** Alterations of tight junction proteins (such as claudin-5 gene polymorphisms) mediate increased paracellular movement of molecules. **(B)** Increased paracellular movement of macromolecules such as albumin increase CSF:serum albumin ratio. **(C)** Increased expression of cell adhesion molecules facilitates CNS entry of leukocytes and peripheral cytokines via the paracellular and transcellular pathways. **(D)** Secretion of astrocytic proteins such as S100β from damaged astrocytes, cross a leaky BBB and are detectable in the blood. **(E)** Variability in the expression and function of transcellular transporters such as PGP may affect the brain concentration of psychiatric drugs and could contribute to treatment resistance in some patients. **(F)** Dysfunction of astrocytes and other glial cells may contribute to dysfunction of the neurovascular unit. **(G)** Microglial activation results in the production of reactive oxygen species and cytokines that act on the BBB to further exacerbate BBB permeability via alterations to adherens junctions and tight junctions. Increased production of matrix metalloproteinases results in degradation of the basement membrane and junctional complexes, increasing BBB permeability.

1.2.5 Clinical outcomes

Treating schizophrenia requires a thorough understanding of each individual patient's symptoms as there are no treatments available to broadly manage all symptoms of schizophrenia and treatments vary according to the stage and severity of the illness. The advent of chlorpromazine (CPZ) over half a century ago heralded the pharmacological era in psychiatry. Anti-psychotic drugs are the only drugs available to treat the psychotic

symptoms of schizophrenia including hallucinations and delusions. Anti-psychotic drugs were discovered in the 1950's with the advent of CPZ. These "first generation" or typical anti-psychotics all function as dopamine receptor antagonists, with high affinity for dopamine d2 receptor. Studies have shown a strong correlation between the therapeutic dose of these drugs and their affinity for D2 receptors (Creese et al., 1976, Seeman, 1987), with PET studies showing that 60-80% receptor occupancy is critical for anti-psychotic efficacy. However, D2 occupancy is a risk factor for side effects with occupancy rates greater than 80% increasing the risk of extrapyramidal syndromes and hyperprolactinemia (Farde et al., 1992, Kapur et al., 2000). Conventional anti-psychotic therapies, particularly high potency drugs such as haloperidol (HAL) and fluphenazine carry high risks of extrapyramidal symptoms including akathisia (motor restlessness), dystonia and dyskinesias and parkinsonian bradykinesia (Gardner et al., 2005), however all first generation anti-psychotics can produce extrapyramidal symptoms. Indeed, this can be a disabling feature for individuals and is responsible for frequent non-compliance with medication (Gaebel, 1997). Newer, "second generation" or atypical anti-psychotic drugs were marketed as having fewer side-effects than first generation drugs, notably a reduction in extrapyramidal motor control disabilities. However, while tardive dyskinesia and extrapyramidal symptoms are rarer with atypical anti-psychotics, these drugs present a separate set of side effects. Many theories have been posited to account for the atypicality of second generation anti-psychotics such as a higher ratio of a drug's affinity for serotonin 5-HT_{2A} receptor and fast dissociation from the D2 receptor. Typical versus atypical anti-psychotics differ mainly in their side-effects and the apparent effectiveness of atypical anti-psychotics to treat negative symptoms. There is ongoing debate about the effectiveness of atypical over typical anti-psychotics, with recent evidence suggesting minimal advantage of atypical drugs (Fusar-Poli et al., 2013). While anti-psychotics generally show effectiveness at reducing positive symptoms, non-compliance due to intolerable side-effects leaves most individuals with schizophrenia substantially disabled for the rest of their lives. Therefore, it is imperative to devise new methods for treating individuals with schizophrenia to replace the need for anti-psychotic medications or to reduce the adverse side effects associated with prolonged usage.

1.3 22q11 deletion syndrome (22q11DS) and schizophrenia

22q11.2 deletion syndrome (22q11DS) is the most common chromosomal microdeletion syndrome that affects a minimum of 1 in 6000 births. Originally termed velocardiofacial

syndrome (VCFS) and DiGeorge Syndrome, it is now apparent that what were once distinct disorders are now grouped under the one nomenclature. 22q11DS involves a 0.7 – 3 Mb deletion on the short arm of chromosome 22 that leaves individuals haploinsufficient for up to 40 protein-coding genes (Figure 1.8) (McDonald-McGinn et al., 2015). The deletion arises from non-homologous meiotic recombination events resulting in a heterogeneous clinical presentation regardless of deletion size. Most cases arise from *de novo* deletions with up to 15% being inherited. The microdeletion is associated with multi-organ dysfunction including cardiac abnormalities, immune disorders, endocrine and gastrointestinal disorders, educational deficits and behavioural and psychiatric disorders. Recently, The International Consortium on Brain and Behaviour in 22q11.2 has reported the cumulative presence of schizophrenia to be 10% in adolescents (13-17 years), 24% in emerging adults (18-25 years) and over 41% in young adults (26-35 years) and mature adults (≥36 years) (Schneider et al., 2014). As such, the 22q11 locus has been an intensively studied region to find schizophrenia susceptible genes and to determine the function of genes within the region. The TJ and major BBB component, claudin-5, is located within the deleted chromosomal region. In fact, when claudin-5 was initially discovered it was termed transmembrane protein deleted in VCFS.

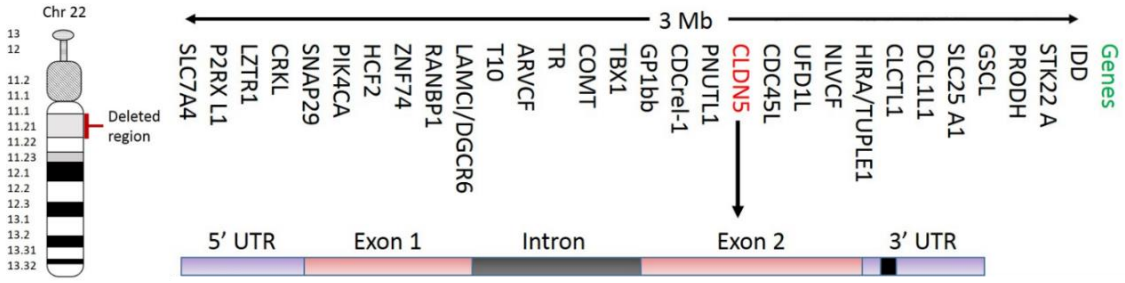

Figure 1.8: 22q11.2 deleted region. 22q11.2 DS results from microdeletions on the short arm of chromosome 22 and range in size between 0.7-3 Mb, encompassing ~40 genes. The cerebral EC-enriched TJ component claudin-5 is located within the deleted region. A 3'UTR SNP in the claudin-5 gene has previously been reported to associate with schizophrenia.

1.3.1 Clinical description of 22q11DS

Like most developmental disorders, 22q11DS has a clinical core set of features that are represented in the entire population with several other features that are more variably observed in a subset of individuals. These core clinical features include conotruncal

cardiovascular malformations of the fourth pharyngeal arch artery, craniofacial malformations including low set ears, high forehead, flattened nasal bridge and velopharyngeal insufficiency/cleft palate, hypotrophic or absent thymus and hypocalcaemia (Cheung et al., 2014). While there is consensus that these physical or behavioural features are present in all 22q11DS patients, there are varying degrees of severity ranging from mild to severe. In fact, many of these features may not require clinical attention and therapeutic intervention, with a small subset of individuals who do not come to clinical attention until they pass the deletion to an offspring with a more prominent phenotype that requires clinical attention. More variable anomalies associated with 22q11DS include regional dysmorphology of the developing forebrain including an apparent absence of the olfactory bulbs and related forebrain regions (Noel et al., 2014). These features have recently been identified in a small number of foetuses with 22q11 deletions as well as in 22q11DS patients after birth (Cheung et al., 2014, Guo et al., 2011, Herman et al., 2012, Schneider et al., 2014). 22q11DS is the second most common cause of congenital heart disease and developmental delays and the most common cause of syndromic palatal anomalies (McDonald-McGinn et al., 2015). As 22q11DS is a haploinsufficient disorder, there is a 50% chance that children of an affected individual will have the disorder.

1.3.2 Genetics of 22q11DS

The genomic location of the disorder is a highly complex region owing to large blocks of low copy repeats (LCR) (Figure 1.9). These LCRs are over 95% identical meaning the region is vulnerable to meiotic errors (Edelmann et al., 1999, Shaikh et al., 2000). Flanking the critical deleted region are the two largest repeats LCR22A and LCR22D with the deletion resulting from nonallelic homologous recombination between the two LCRs. This results in a 3 Mb deletion that is observed in approximately 85% of 22q11DS patients. Nested deletions occur in ~5-10% of all 22q11DS patient's due to the same mechanism as the major deletion. The 1.5 Mb deletion (LCR22A-LCR22B) and 2 Mb deletion (LCR22A-LCR22C) produce major phenotypic features in common with the LCR22A-LCR22D deletion. Indeed, the 1.5 Mb deletion reproduces the full spectrum of phenotypes that are observed in the 3 Mb deletion. Approximately 90 known or predicted genes are present in the 3 Mb deleted region on chromosome 22 with 46 of these known to be protein coding (41 of which are expressed in the brain), with another seven microRNAs, ten non-coding RNAs and 27 pseudogenes (Guna et al., 2015). Elucidation

of the phenotypic features of 22q11DS has been carried out through single gene analysis in genetically engineered animals. The genes located within the minimal critical deleted region are highly conserved across model organisms. The nested 1.5 Mb deletion is syntenic to chromosome 16 in mice.

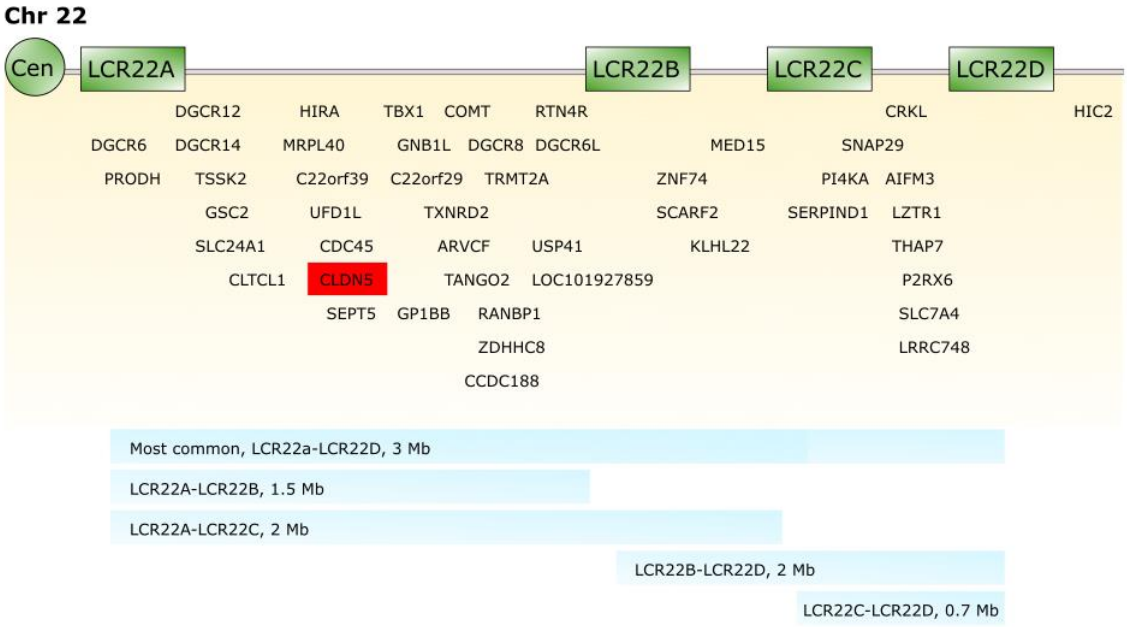

Figure 1.9: Genetics of 22q11DS. The 22q11 deletion varies between 0.7-3 Mb due to the presence of low copy repeats (LCR) leaving the region vulnerable to meiotic errors. The most common 3 Mb deletion results from nonallelic homologous recombination between LCR22A and LCR22D while the second most common 1.5 Mb deletion results from nonallelic homologous recombination between LCR22A and LCR22B. Additional deletions result from recombination between LCR22A and LCR22C resulting in a 2 Mb deletion; between LCR22B and LCR22D resulting in a 2 Mb deletion and; between LCR22C and LCR22D resulting in a 0.7 Mb deletion. Adapted from (McDonald-McGinn et al., 2015).

1.3.3 22q11DS models

Mouse models have been pivotal to understanding the expression and function of individual genes in the 22q11 deleted region and their potential contribution to 22q11DS phenotypes. The majority of genes deleted in 22q11DS are conserved together on mouse chromosome 16 so a deletion of this region is appropriate to model 22q11DS. The first approach to a 22q11DS model utilised a cre-lox approach. This resulted in the generation of two deleted lines, Df1 (Lindsay et al., 1999) and LgDel (Merscher et al., 2001) which model the 1.5 Mb deletion of 22q11.2, thus allowing for the assessment of the role of the gene dosage effects of orthologous 22q11 genes in developmental malformations in the heart, face and brain. Both Df1 and LgDel mice show aortic arch malformations in post-

natal mice like those seen in 22q11DS patients resulting from dysregulation of signalling molecules required for patterning and growth in the developing embryo including bone morphogenic protein (Bachiller et al., 2003), fibroblast growth factor (Frank et al., 2002), Shh (Maynard et al., 2013) and retinoic acid (Vermot et al., 2003). One of the most extensively characterised genes found in the major and nested deletions is T-box transcription factor (TBX1). TBX1 is a T-box transcription factor expressed in the developing pharyngeal arches (Chapman et al., 1996). Mice deficient in TBX1 had cardiac abnormalities manifested as abnormalities in the fourth pharyngeal arch arteries as well as displaying a spectrum of phenotypic effects that are common in 22q11DS (Jerome and Papaioannou, 2001, Lindsay et al., 1999). A new mouse model of 22q11DS has recently been described (Didriksen et al., 2017). The (Df(h22q11)/+) mouse displayed elevated post pubertal N-methyl-D-aspartate receptor antagonist-induce hyperlocomotion, PPI deficits and increased acoustic startle response.

1.4 RNAi-mediated barrier modulation

Numerous studies have shown that it is possible to specifically target siRNA to brain capillary ECs for targeted suppression of BBB-specific components. Delivery of siRNA to mouse brain capillary ECs *in vivo* could efficiently suppress the organic ion transporter 3 and reduce brain to blood transport of benzyl penicillin (Hino et al., 2006). More recently, RNAi-based suppression of claudin proteins has been used in numerous preclinical models of neurological disorders to improve drug penetration to the brain or to remove unwanted, neurotoxic metabolites from the brain such as amyloid-β (Aβ) (Figure 1.10). Using systemically injected siRNA targeting claudin-5, the first demonstration of RNAi-based modulation of the BBB was reported in mice by Campbell *et al.* (2008). Levels of claudin-5 mRNA were reduced between 24 and 48 hours post-siRNA injection with maximum suppression of claudin-5 occurring at 48 hours post injection compared to non-targeting siRNA injected mice. This facilitated a size-selective loosening of the BBB to molecules up to 1 kDa in size including the contrasting agent gadolinium (Gd-DTPA, 742 Da), while restricting a molecule of 4.4 kDa in size. Importantly this process was also reversible with levels of claudin-5 returning to normal at 72 hours post-siRNA injection with BBB integrity also restored (Campbell et al., 2008).

This technique was also adapted to successfully modulate the molecularly homologous inner blood-retina barrier (iBRB) in animal models of retinopathies (Campbell et al.,

2009). Using this approach, it was possible to improve visual function in mouse models of retinitis pigmentosa (RP) and a light-induced retinal degeneration model. IMPDH knockout mice are a model of autosomal recessive RP. These mice lack an enzyme involved in the *de novo* synthesis of GTP (MW: 523 Da) which is essential for visual transduction. Through targeted suppression of claudin-5 in the neural retina, systemic injection of GTP could bypass the iBRB and improve retinal function. Similarly, in BalB/c mice with light-induced retinopathy, systemic injection of the calpain inhibitor *N*-acetyl-Leu-Leu-Met-CHO (ALLM) (MW: 401 Da) could readily diffuse across the modulated iBRB and reduce photoreceptor cell death, a hallmark of light-induced retinopathy.

To adapt this process for the treatment of chronic diseases such as RP and age-related macular degeneration (AMD), Campbell and colleagues developed a doxycycline-inducible shRNA system for the transient knockdown of claudin-5 levels. The doxycycline-inducible shRNA sequence was inserted into the genome of an adeno-associated virus (AAV)-2/9 vector that can persist in retinal or brain ECs following a single localised injection. This approach achieved therapeutic benefit in a laser-induced model of choroidal neovascularisation, a hallmark of wet AMD. With this approach, it was possible to systemically deliver 17-AAG (MW: 585 Da) and Sunitinib malate (MW: 532 Da), two well characterized VEGF inhibitors, across the BRB (Campbell et al., 2011) and significantly reduce CNV volumes compared to the NT shRNA-treated contralateral eye. Importantly, this approach specifically downregulated claudin-5 at the BBB/BRB while expression patterns of other TJs remained at normal physiological levels. It is also possible to modulate TJs in specific brain regions, e.g. by direct stereotaxic injection of AAV vectors.

In the cold-induced model of TBI, application of siRNAs targeting claudin-5 can transiently open the BBB and reduce cerebral oedema and improve neurological function (Campbell et al., 2012). Claudin-3, which is also expressed in brain capillary ECs, is overexpressed in 90 % of ovarian cancers. RNAi suppression of claudin-3 reduces tumour cell proliferation and growth and tumour burden and reduces metastasis in several ovarian cancer models (Huang et al., 2009). RNAi has provided a robust method for the transient and reversible modulation of the BBB. More recently, it has been shown that sequential delivery of siRNAs targeting claudin-5 and occludin transcripts can suppress both

proteins and modulate the BBB to molecules up to 3 kDa in size. In Tg2576 mice, a murine model of familial Alzheimer's disease, suppression of claudin-5 and occludin improved cognitive function in tandem with reduced brain levels of Aβ(1-40) and increased serum levels of Aβ(1-40) indicating that it is possible to remove pathogenic agents from the brain to the blood (Keaney et al., 2015). In summary, targeted suppression of TJs at the BBB/BRB increases paracellular permeability and enhances targeted drug delivery to neuronal regions. Through use of an inducible system, it is also possible to reverse BBB permeability by withdrawal of the inducing agent. While significant attention has focussed on the therapeutic potential of modulation of the BBB in the treatment of neurological disorders, there is a scarcity of studies assessing the neurobehavioral consequences of specifically targeting BBB EC components to modulate BBB permeability.

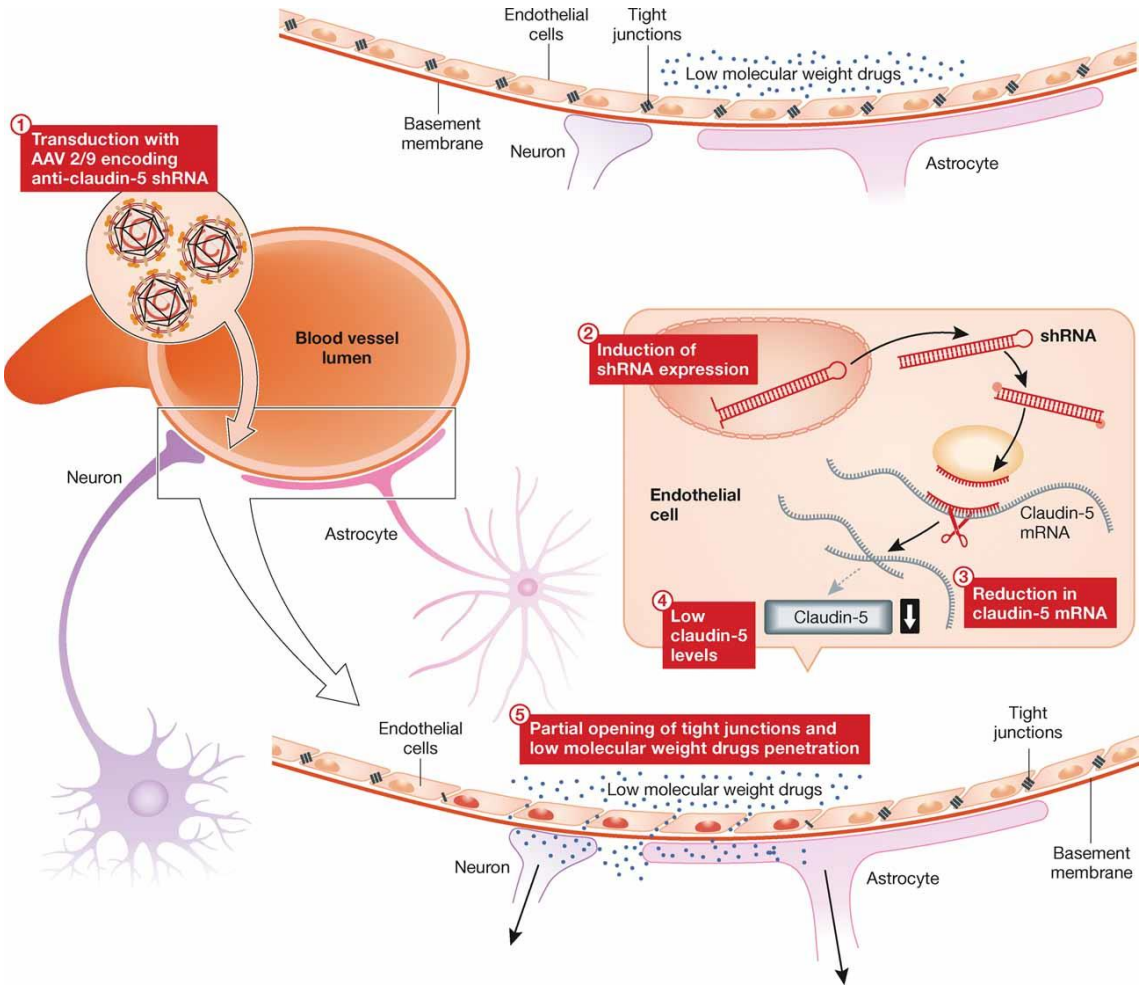

Figure 1.10: RNAi modulation of the BBB. With an intact tight junction, low molecular weight drugs are prevented from entering the CNS due to the presence of the BBB. Transduction of brain ECs with an AAV 2/9 encoding a doxycycline-inducible shRNA

targeting claudin-5 transcripts allows for reversible opening of the BBB to low molecular weight drugs. Source: (Rossi, 2011).

1.4.1 Neurobehavioral sequelae of BBB disruption

The behavioural consequences of BBB disruption in disorders such as TBI, AD and stroke have been extensively studied, however, few studies have examined the behavioural phenotype of mice following disruption/deletion of EC-specific genes. In the study by Kanoski *et al*, administration of a high energy diet to rats impaired their performance on a hippocampus dependent task on the T-maze with no impairments evident in a non-hippocampal dependent task. Additionally, this impairment was associated with decreased expression of TJ components including claudin-5 and claudin-12 in the choroid plexus and occludin, claudin-5 and claudin-12 at the BBB. BBB dysfunction was also evident with increased permeability of sodium fluorescein in the hippocampus but not in the striatum or frontal cortex following high energy diet (Kanoski et al., 2010).

As mentioned in section 1.1.3.2, PGP is an ABC transporter enriched in ECs of the BBB. Pharmacological inhibition of PGP decreases anxiety-related behaviours on the elevated plus-maze following a mild psychological stressor which is associated with brain accumulation of corticosterone (Thoeringer et al., 2007). In a study on stress response in mice, PGP knockout mice displayed a number of alterations in stress responsivity and depression-like behaviours. PGP knockout mice displayed reduced conditioned fear responses compared to WT mice. Foot shock stress decreased social interactions in knockout mice. Female PGP knockout mice also displayed several depression-like behaviours, age-related social withdrawal and hyperactivity independent of stress. Additionally, mice showed facilitated sensorimotor gating with increased in PPI and altered startle reactivity (Brzozowska et al., 2017). However, this study utilised a germline deletion of PGP and with PGP also being expressed on microglia it is difficult to decipher the contribution of EC deletion and microglial deletion of PGP to behavioural response.

Mfsd2a, a member of the major facilitator superfamily is the major transporter for docosahexaenoic acid into the brain. Mfsd2a is expressed specifically in ECs of the BBB and is critical for the formation and function of the BBB. Mice deficient for mfsd2a have a leaky BBB as well as neuronal cell loss in the hippocampus and cerebellum along with

cognitive deficits as measured by worse performance on the y-maze and novel object recognition test. Additionally, mfsd2a knockout mice displayed severe anxiety as measured by decreased arm entries on the zero-maze test, light/dark test and spent less time in the centre of the open field test (Nguyen et al., 2014).

1.5 Objectives

It is unclear whether barrier dysfunction is a cause or consequence of disease, especially in the context of schizophrenia. The overall objective of my thesis was to investigate the role of the BBB in schizophrenia. Following a review of the literature, some outstanding questions that this thesis aimed to address were:

- Is there direct evidence of BBB dysfunction in schizophrenia?
- How does BBB dysfunction influence psychiatric symptoms?
- Do anti-psychotic drugs impact BBB function?

As discussed in section 1.2.4, several studies have proposed an involvement of the microvasculature in the pathogenesis of schizophrenia (Figure 1.7) however, a functional approach to understanding the role of CNS EC-specific genes in the pathogenesis of schizophrenia has never been described. Indeed, despite the evidence pointing towards a contribution of the BBB in schizophrenia, there is a paucity of studies that have specifically examined the expression of BBB-specific components in schizophrenia as well as the relationship between *in vivo* models of dysregulated EC/BBB genes and behavioural outcomes relevant to schizophrenia. As such, the methodology employed in this thesis was multifaceted and utilised genetic association studies and post-mortem histological analysis of brain tissue from schizophrenia and control subjects. In addition, this project used preclinical animal models and behavioural assays following targeted disruption of the BBB in distinct neural regions and globally in a novel doxycycline-inducible knockdown mouse.

The first aim of this thesis was to sequence across the remining claudin-5 allele in 22q11DS patients and screen for the rs10314 SNP. Additionally, the impact of this SNP on claudin-5 function would be explored through *in vitro* experiments and *in vivo* in post-mortem human brain tissue from schizophrenia subjects and age-matched controls. As lifetime use of drugs, particularly anti-psychotics, is a potentially confounding factor, the

effect of anti-psychotic exposure to the cerebral microvasculature was explored with *in vitro* and *in vivo* experiments.

The next goal of the project was to investigate how modulation of claudin-5 in different brain regions impacted localised BBB integrity and behavioural readouts in mice. This approach involved knockdown of claudin-5 using an adeno-associated virus vector (AAV) with a doxycycline-inducible shRNA targeting claudin-5 transcripts. A key aim of this thesis was to develop an inducible claudin-5 knockdown mouse model and the generation and characterisation of this model is discussed as well as the effect on normal brain function.

The final aim of this thesis was to explore the role of circadian rhythms in regulating TJs and BBB integrity. Sleep and circadian rhythm disruptions have been reported in up to 80% of schizophrenic patients. Better understanding of TJ regulation and factors affecting BBB integrity will aid in the development of therapeutics to improve BBB function in health and disease.

Chapter 2:

Materials and Methods

2 Materials and Methods

2.1 Cell Culture Methods

All cell cultures including cell lines and primary cultures were maintained in a humidified Sterile Cycle CO_2 incubator (Hepa Class 100, ThermoScientific) at 37ºC in the presence of 5% CO_2. All cell culture procedures were carried out in a laminar flow cabinet (Holten LaminAir Model 1.2, Termo Electron Corporation). Cells were visualised using an inverted light microscope (Olympus CK30).

2.1.1 bEnd.3 cell culture

The mouse brain endothelial cells line, bEnd.3 (American Type Culture Collection, [ATCC] CRL-2299), was cultured in T75 flasks in DMEM GlutaMAX™ medium supplemented with 10% FBS and 1% P/S. To subculture the cells, the medium was aspirated, and the cells were gently washed in 1X PBS. The PBS was removed, and the cells were incubated in trypsin-EDTA in the incubator at 37ºC for 5-10 min until the cells detached from the flask. Trypsin was inactivated by the addition of growth medium and the resulting cell suspension was then centrifuged at 1,000 RPM for 5 min. The cell pellet was resuspended in fresh medium and divided into new flasks. Cells were subcultured once a week and replenished every 2-3 days with fresh medium.

2.1.2 HEK293 cell culture

The human embryonic kidney cell line, Hek293 [ATCC], was cultured in T75 flasks in DMEM GlutaMax™ supplemented with 10% FBS and 1% P/S. Cells were subcultured and fed as for the bEnd.3 cell line (see section 2.1.1).

2.1.3 Caco-2 cell culture

The human colorectal adenocarcinoma cell line, Caco-2, was cultured in T75 flasks in DMEM with 1% NEAA, 1 mM HEPES, supplemented with 10% FBS and 1% P/S. Cells were subcultured and fed as for the bEnd.3 cell line (see section 2.1.1).

2.1.4 hCMEC/D3 cell culture

The human cerebral microvascular endothelial cell line, hCMEC/D3 [Millipore], was cultured in T75 flasks coated with 50 µg/ml Fibronectin in EGM-2 MV growth medium. Prior to subculture, new T75 flasks were coated with 50 µg/ml Fibronectin for 1 h at 37ºC

and washed twice with PBS. To subculture the cells, the medium was aspirated, and the cells were gently washed in 1X PBS. The PBS was removed, and the cells were incubated in trypsin-EDTA in the incubator at 37ºC for 5-10 min until the cells detached from the flask. The resulting cell suspension was diluted with 5 ml of media and the suspension was then centrifuged at 1,000 RPM for 5 min. The cell pellet was resuspended in fresh medium and divided into new flasks. Cells were seeded at a density of $2.7*10^5$ cells/cm^2. Cells were subcultured once a week and replenished every 2-3 days with fresh medium.

2.1.5 Cell counting and trypan blue exclusion assay

Adherent cells were trypsinised as described in section 2.1.1 and centrifuged at 1,000 RPM for 5 min. Following centrifugation, the cell pellet was resuspended in 1 ml of fresh growth medium and an aliquot was diluted 1 in 10 in growth medium. This aliquot was diluted 1 in 2 with Trypan blue solution and 10 µl of the suspension was pipetted onto a cell counter slide and placed in the Luna™ Automated Cell Counter. The cell counter provides the total number of viable and dead cells and the number of viable cells/ml.

2.1.6 Cryopreservation of cells

Following trypsinisation and centrifugation, the cell pellet was resuspended in 1 ml of fresh growth medium containing 10% DMSO and placed in a Nunc™ Cryo Tube and then placed in a pre-chilled cryo-freezing container (Nalgene) and stored at -80ºC for 24 h. Cryotubes were then placed in liquid nitrogen for long term storage.

2.1.7 Construction of claudin-5 pcDNA3-EGFP

Human claudin-5 cDNAs with 3'UTRs containing G and C alleles of SNP rs10314 respectively, were synthesized by GeneArt and sub-cloned into the HindIII/ZhoI site of pcDNA3EGFP (Addgene).

2.1.8 Transformation of plasmid DNA

The following buffers were prepared prior to transformation

Lysogeny broth (LB) media: 10 g NaCl, 10 g tryptone, 5 g yeast extract, 1000 ml dH_2O

LB media containing Agar: 10 g NaCl, 10 g tryptone, 5 g yeast extract, 15 g Agar, 1000 ml dH_2O

Ampicillin: 0.1 g Ampicillin, 5 ml dH_2O

LB media and LB media containing agar were autoclaved before use and 5 ml of Ampicillin solution was added to LB media containing agar. Pour LB agar media containing antibiotic onto petri dishes and dry in laminar flow cabinet for at least 30 min. Thaw competent cells on ice and treat gently. Add 1-2 µl of plasmid DNA to be transformed to 30-100 µl of competent cells. Incubate on ice for 30 min. Heat shock at 42ºC for 45 s and incubate on ice for 2 min. Add 900-970 µl of pre-warmed LB media at 37ºC to bring volume to 1 ml, mix and incubate at 37ºC for 1 h. Plate 100 µl samples on LB agar plates containing antibiotic and incubate upside-down at 37ºC overnight. Check for colonies the following day. Plates containing transformants can be stored at 4ºC.

2.1.9 Transfection of shRNA, siRNA and plasmid DNA

Adherent cells were trypsinised as described in section 2.1.1 and centrifuged at 1,000 RPM for 5 min. Following centrifugation, the cell pellet was resuspended in 1 ml of fresh growth medium and an aliquot was removed for cell counting. $2.5*10^5$ cells were transferred to the wells of a 12 well plate and were placed in the incubator. 24 h later the cells were transfected using Lipofectamine® 2000 transfection reagent (ThermoFisher Scientific). For transfection of siRNA, 10 pmol of siRNA was diluted in 100 µl of OptiMEM reduced serum media and incubated at room temperature for 5 min. At the same time, 0.5 µl of Lipofectamine® 2000 was diluted in 100 µl of OptiMEM and incubated at room temperature for 5 min. After 5 min, the diluted siRNA and Lipofectamine® 2000 were mixed together and incubated at room temperature for 20 min to allow for complex formation. After 20 min, the complexes were dropwise pipetted onto the sub-confluent monolayer of cells.

For transfection of plasmid DNA, a ratio of 1 µg of DNA to 3 µl of Lipofectamine® 2000 was used. 500 ng/ml of plasmid DNA was diluted in 100 µl of OptiMEM reduced serum media and incubated at room temperature for 5 min. At the same time, 1.5 µl of Lipofectamine 2000 was diluted in 100 µl of OptiMEM and incubated at room temperature for 5 min. After 5 min, the diluted plasmid DNA and Lipofectamine® 2000 were mixed together and incubated at room temperature for 20 min to allow for complex formation. After 20 min, the complexes were dropwise pipetted onto the sub-confluent monolayer of cells.

2.1.10 Drug treatments

Confluent bEnd.3 and mouse BMVEC cells were treated with 0.1-100 μM CPZ, HAL, clozapine (CZP) or olanzapine (OLZ) diluted in culture medium containing 0.1 % DMSO, and 0.1-100 mM lithium chloride (LiCl) diluted in culture medium for the indicated time-points and RNA and protein was isolated as described in section 2.1.17 and 2.1.18 respectively.

2.1.11 Isolation of primary mouse brain microvascular endothelial cells (BMVEC)

The protocol for isolation of BMVEC was adapted from the method of (Abbott et al., 1992).

The following buffers were prepared prior to cell isolation:

Working buffer: Ca^{2+}/Mg^{2+} free HBSS, 10 mM HEPES, 0.5% (w/v) BSA, 1% P/S

Complete digest medium: HBSS, 1 mg/ml collagenase/dispase, 10 mM HEPES, 20 u/ml DNase I, 0.147 μg/ml TLCK, 1% P/S

Prior to starting the procedure, ensure the following are available:

A) Sterile 50 or 100 ml glass beaker
B) Sterile instruments:
   I. Brain removal — 2 pairs of large scissors and 1 pair of small; 1 pair of coarse forceps; 1 small spatula
   II. Fine dissection — 2 pairs of fine curved watchmaker's forceps; 1 spatula; 1 scalpel blade and holder
C) Whatman filter paper – sprayed with ethanol

All instruments were disinfected with 70% ethanol. C57BL/6J mice were sacrificed by CO_2 asphyxiation, the head was sprayed with ethanol and the head was removed with a large scissors. The skin was peeled back to expose the skull and two incisions were made at the base of the cerebellum on either side. An incision was made along the midline and the skull flap was peeled back from each hemisphere to expose the brain. The brain was removed using the spatula and placed in ice-cold working buffer. The process was repeated for each mouse. Using a scalpel, the cerebellum, brain stem and remaining white matter from hind- and mid-brain was removed, and the brain was gently rolled on Whatman filter paper to remove the meninges from the surface. The featureless brain was

placed in a universal container of fresh working buffer while the rest of the brains were processed. The pooled brains were homogenised using a Dounce homogeniser and centrifuged at 1,800 RPM for 5 min. Following centrifugation, the supernatant was aspirated, and the pellet was resuspended in 3 ml of complete digest medium (per 5 brains) and digested in an incubator at 37^{o}C for 1 hour with constant agitation at 200 RPM.

During the first digestion, culture plates were coated with 100 µg/ml collagen IV and 50 µg/ml fibronectin in PBS and incubated at 37^{o}C for 2 h. The suspension was centrifuged at 1,800 RPM for 5 min. The supernatant was aspirated, and the pellet was resuspended in 22% (w/v) BSA in PBS and centrifuged at 3,000 RPM for 20 min. The myelin plug, which floats to the top of the BSA solution was removed using a broken Pasteur pipette, triturated and centrifuged in a fresh BSA gradient to recover more microvessels. Tubes containing the microvessels were kept inverted on a Kimwipe sprayed with ethanol to prevent contamination by myelin. The microvessels were resuspended in 1 ml of working buffer, topped up with 4 ml of working buffer and centrifuged at 1,800 RPM for 5 min. After centrifugation the supernatant was removed, and the pellets were resuspended in the remaining 2 ml of complete digest medium and incubated at 37^{o}C for 1 h with constant agitation at 200 RPM.

The digested tissue was centrifuged at 1,800 RPM for 5 min and the supernatant was discarded. The pellet was resuspended in 5 ml of working buffer and centrifuged at 1,800 RPM for 5 min. Just before cell seeding, the coating solution was removed, and the plates were rinsed twice with PBS. The supernatant was aspirated, and the pellet was resuspended in 3 ml of filtered EGM-2 MV growth medium containing 5 µg/ml puromycin. BMVEC are resistant to puromycin due to the high levels of expression of P-glycoprotein while it is cytotoxic to contaminating cell types (Perriere et al., 2005). The vessel fragments were plated at 1 ml/4 cm^2 and left to adhere at 37^{0}C/5% CO_2. Vessel fragments should be seen when observed under a light microscope. After 24 h, cells should be observed sprouting from the vessels fragments. After 48 h the puromycin was removed and normal EGM-2 MV growth medium was added (Perriere et al., 2005). Cells typically reach confluence within 5 days of isolation (Figure 2.1).

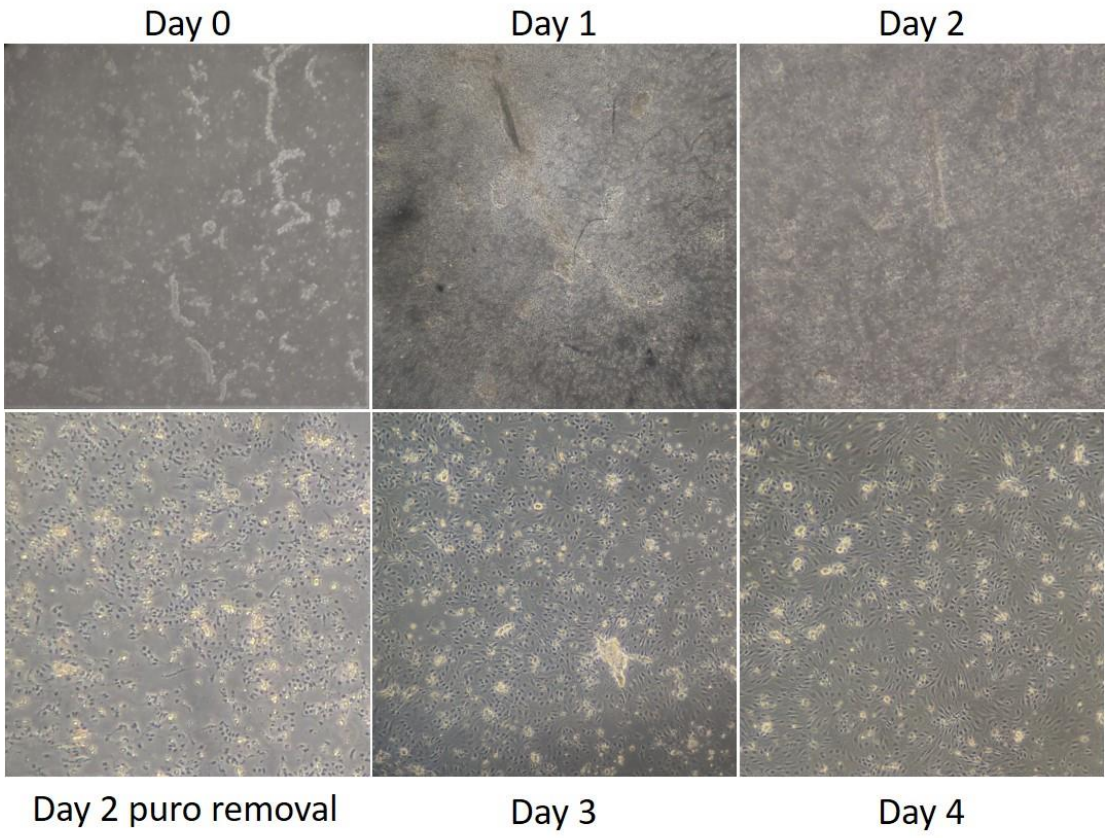

Figure 2.1: Primary mouse BMVEC isolation. Vessel fragments are clearly visible on day 0. By day 2, contaminating cells have died. Following removal of puromycin a sub-confluent monolayer of BMVEC should be observed with cells reaching confluency by day 4-5.

2.1.12 Measurement of transendothelial electrical resistance (TEER)

TEER measurements provide an indication of barrier integrity and can be used to determine the impact of growth conditions and drug treatments on barrier tightness. TEER measurements were performed on primary mouse BMVECs and bEnd.3 cells grown on 6.5 mm diameter 0.4 mm pore polyester membrane HTS transwell inserts (Corning Costar). TEER values were measured using an EVOM resistance meter fitted with "chopstick" electrodes. Prior to measurements, the apical and basolateral chambers were replaced with fresh medium and the long arm of the probe was placed in the basolateral chamber and the short arm into the apical chamber. TEER values were recorded in triplicate and the average value of a no cell compartment was subtracted from the average of the triplicate measurements. TEER values were expressed as ohm*cm^2 ($\Omega.cm^2$).

2.1.13 Transwell permeability assay

Permeability assays were performed on primary mouse BMVEC and bEnd.3 cells grown on transwell inserts (Keaney et al., 2015). After treatment of the cells with certain drugs or siRNA/shRNA/plasmids for the required time, the basolateral chamber was bathed in fresh EBM-2 medium while the apical chamber was replaced with 1 mg/ml of FITC-dextran (4-40 kDa) diluted in EBM-2 medium and the cells were incubated at 37^{o}C. Immediately following the addition of FITC-dextran a sampling aliquot was taken from the basolateral compartment and replaced with fresh medium and transferred to a 96-well plate. Further sampling aliquots were taken every 15 min for 2 h and FITC-dextran fluorescence was determined using a spectrofluorometer (Optima Scientific) at an excitation wavelength of 485 nm and an emission wavelength of 520 nm. Relative fluorescence units were converted to ng/ml of FITC-dextran using FITC-dextran standard curves. Serial dilutions and background fluorescence during the course of the experiment were corrected for. The apparent permeability coefficient (P_{app}) was calculated as follow:

$$P_{app}\ (cm/s) = dQ/dT / (A \times C_0)$$

Where dQ/dT (mg/s) is the rate of appearance of FITC-dextran in the basolateral chamber after application, A (cm^2) is the effective surface area of the insert size and C_0 (mg/ml) is the initial FITC-dextran concentration in the apical chamber. dQ/dT is the slope *m* (y = *m*x+c) calculated by plotting the cumulative amount (Q) versus time (s).

2.1.14 Polyribosome fractionation and analysis

Hek293 cells were grown to 70 % confluency and transfected as described in section 2.1.9. Polysome extracts were prepared by Dr. Susan Campbell at Sheffield Hallam University as described in (Lui et al., 2014) with the following modifications, 0.5 % (v/v) Triton X-100 and 1 mg/mL RNasin® was added to the lysis buffer. 100 µg/mL of cycloheximide (CHX) was added to cells and then incubated on ice water for 30 minutes. Cells were subsequently scraped into 10 ml of PBS containing 100 µg/mL CHX. The cells were centrifuged at 400 g for 4 min and then resuspended in lysis buffer. Following this the cells were further lysed with a 25-gauge needle and left on ice for 10 minutes. Extracts were layered onto 15 to 50 % sucrose gradients. The gradients were sedimented via centrifugation at 40,000 RPM in a Beckman ultracentrifuge for 2.5 h, and the absorbance at 254 nm was measured continuously to give the traces shown in Figure 3.5. 14 fractions were collected across the gradient into two volumes of Trizol (Life Technologies) and the RNA was extracted, precipitated, and resuspended in diethyl-

pyrocarbonate (DEPC)-treated water. cDNA was prepared and real-time reverse transcription polymerase chain reaction (RT-PCR) was carried out as described in section 2.3.1 Transcript levels in each fraction were expressed as a percentage of total RNA.

2.1.15 Serum shock of cells

Serum shocking of cells has been shown to recapitulate cycling of cells in a comparable manner to circadian rhythms (Balsalobre et al., 1998). Serum shock was performed on a confluent monolayer of cells. The media was removed, and the cells were placed in a "shock" media consisting of culture medium supplemented with 50% FBS and incubated for 2 h at 37ºC/5% CO_2. The "shock" medium was discarded, and cells were then incubated in serum-free medium for the duration of the experiment at 37ºC. RNA and protein were isolated as in sections 2.1.17 and 2.1.18 respectively at various timepoints.

2.1.16 MTS cell proliferation assay

The CellTiter 96 Aqueous One Solution Cell Proliferation Assay was used to measure cell proliferation and cell viability in *in vitro* experiments. The CellTiter 96® AQ_{ueous} One Solution Cell Proliferation Assay is composed of the novel tetrazolium compound, 3-(4,5-dimethylthiazol-2-yl)-5-(3-carboxymethoxyphenyl)-2-(4-sulfophenyl)-2H-tetrazolium, inner salt ($MTS^{(A)}$), and an electron coupling reagent, phenazine ethosulfate (PES). Metabolically active cells reduce the MTS tetrazolium compound into a coloured formazan product that is soluble in tissue culture medium. This process is thought to be accomplished by nicotinamide adenine dinucleotide phosphate (NADPH) or nicotinamide adenine dinucleotide (NADH) produced by dehydrogenase enzymes in bioactive cells.

$2*10^4$ cells were plated onto 96-well plates in 100 µl of culture medium and grown to confluence at 37ºC in 5% CO_2. Cells were then treated with various compounds (drugs, siRNA, inhibitors) and left to incubate for the required timepoints. Following treatment, medium was replaced with 100 µl of fresh medium and 20 µl/well of CellTiter AQ_{ueous} One Solution Reagent was added to each well and left to incubate for 1-4 h at 37ºC/5% CO_2. The absorbance of each well was read at 490 nm using a plate reader. The blank absorbance value of a well without cells was subtracted from all other readings and the percentage of viable cells was calculated. The amount of formazan produced by absorbance at 490 nm is directly proportional to the number of living cells in culture.

2.1.17 RNA extraction

RNA was extracted from cells grown in culture using the E.Z.N.A. Following treatment of cells in culture plates, the medium was removed, and the cells were washed once with PBS. The PBS was discarded, and the cells were lysed directly with TRK Lysis Buffer (350 µl per well) by pipetting up and down several times to disrupt and homogenise the cell monolayer. One volume of 70% ethanol was added to the cells and vortexed and up to 700 µl of the sample was transferred to a HiBind® RNA Mini Column and centrifuged at 10,000 g for 1 min. The filtrate was discarded and 500 µl of RNA Wash Buffer I was added to the column and centrifuged at 10,000 g for 30 s. The filtrate was discarded and 500 µl of RNA Wash Buffer II was added to the column and centrifuged at 10,000 g for 1 min. This washing step was repeated, followed by centrifugation at maximum speed for 2 min to dry the column. The column was transferred to a new 1.5 ml Eppendorf tube and 50 µl of NF H_2O was added directly to the column and centrifuged at maximum speed for 2 min. The eluent was added onto the column again and the centrifugation was repeated. The concentration of RNA in the sample was measured using the NanoDrop 1000 (Thermo Scientific).

2.1.18 Protein extraction

Protein was isolated from cells using 1X RIPA lysis buffer containing a protease complete mini protein inhibitor tablet (1 tablet/10 ml). Samples were pipetted up and down several times and lysed cells were collected in 1.5 ml Eppendorf tubes. The tubes were centrifuged at 12,000 RPM for 20 min and the supernatant was transferred to a new Eppendorf tube and stored at -20^{o}C. Protein quantification was performed using the Pierce® BCA Assay Kit. The BCA working reagent was prepared by mixing 50 parts of BCA Reagent A with 1 part of BCA Reagent B. 10 µl of each protein sample and standard (0, 125, 250, 500, 750, 1000, 1500, 2000 µg/ml BSA) were added in duplicate into a 96-well plate. 200 µl of Working Reagent was added to each well. The plate was covered with adhesive film, mixed and incubated at 37^{o}C for 30 min. Following incubation, the absorbance was measured at 595 nm on a Multiskan FC plate reader (Thermo Scientific). The average absorbance reading of a blank sample was subtracted from the average absorbance reading of all other samples. A standard curve was prepared in GraphPad Prism by plotting the average blank-corrected measurements for each BSA standard vs. its concentration in µg/ml and the protein concentrations of unknown samples was interpolated from the curve.

2.2 In vivo techniques

2.2.1 Animal experiments

All experiments involving the use of C57BL/6J, Tie2crexBmal$^{-/-}$, Tie2CrexCldn5 mice were assessed and approved by an internal ethics committee in Trinity College Dublin prior to all experimentation. All experiments involving the use of human samples had obtained consent from patients or next of kin. All studies carried out in the Smurfit Institute of Genetics in TCD adhere to the principles laid out by the internal ethics committee at TCD and all relevant national licences were obtained prior to commencement of all studies. All mice were bred on-site in the Specific Pathogen Free (SPF) unit at the Smurfit Institute of Genetics in TCD.

2.2.2 Injectable anaesthetics

Mice were anaesthetised with a mixture of ketamine (100 mg/ml) and domitor. Anaesthetic was administered via intraperitoneal injection (IP) at a dose of 100 µl/10 g using a 30-gauge needle. Mice were monitored until they were unconscious. To reverse anaesthetic, mice were injected with Sedastop and were maintained in an incubator until conscious and moving freely.

2.2.3 Genotyping of mice

2.2.3.1 DNA isolation from mouse ear clips

200 µl of tail lysis buffer and 15 µl of proteinase K (20 mg/ml) was added to mouse ear clips in 1.5 ml Eppendorf tubes, vortexed and incubated in a water bath at 55ºC overnight. 200 µl of 25:24:1 Phenol: Chloroform: Isoamyl alcohol was added to each tube, vortexed and centrifuged at 13,500 RPM for 5 min. The aqueous (top layer) phase was removed to a new tube and mixed with 800 µl of 96% ethanol. The tube was inverted several times to mix and centrifuged at 13,500 RPM for 10 min. The ethanol was discarded, and the DNA pellet was left open on the bench to air dry. The DNA was resuspended in 100 µl of NF H_2O and left to resuspend for a few hours at room temperature.

2.2.3.2 Polymerase chain reaction (PCR)

PCR reactions were made up as follows: 1 µl of DNA, 5 µl of Mango Taq Buffer, 0.75 µl of Mg (50 mM), 0.5 µl of dNTP mix, 0.25 µl each of forward and reverse primers (100

µM), 0.25 µl of Mango Taq Polymerase and 17 µl of NF H_2O. PCR conditions for Tie2 were as follows: 95°C for 5 min; 34 cycles of 95°C for 1 min, 54°C for 1 min, 72°C for 1 min; 72°C for 5 min; 4°C hold. The following primers were used:

Table 2.1: PCR primer sequences for cre genotyping.

Gene		**Sequence (5' – 3')**
Cre	Forward Reverse	GCGGTCTGGCAGTAAAAACTATC GTGAAACAGCATTGCTGTCACTT
Internal positive control	Forward Reverse	CTAGGCCACAGAATTGAAAGATCT GTAGGTGGAAATTCTAGCATCATCC

2.2.3.3 Agarose gel electrophoresis

PCR products were visualised on 2% agarose gels. 1 µl of ethidium bromide was added to 25 ml of melted agarose and this was poured into a gel cast with a comb and allowed to set. PCR samples were loaded onto the gel along with a 100 bp DNA ladder and the gel was run at 100 V for 20 min. The gel was viewed under UV light and images were taken with gel capture software. Expected band sizes were 100 bp for cre primers and 324 bp for IPC primers.

2.2.3.4 Genotyping of 22q11DS patients

PCR reactions were made up as follows: 100 ng of DNA from patients was amplified by PCR in a volume of 50 µl using 1 x reaction buffer, 200 µM each of dNTPs, 0.2 µM of forward and reverse primers and 1.25 units of DNA Taq polymerase. PCR conditions for the rs10314 allele were as follows: 95°C for 5 min; 34 cycles of 95°C for 1 min, 58°C for 1 min, 72°C for 1 min; 72°C for 5 min; 4°C hold. This produced an amplified product of 603bp using the following primers: forward primer 5'-CGACAAGAAGAACTACGTCT-3' and reverse primer 5'-CAGGTGGGAGAGAGTTCAAA-3'. The amplified product was digested with restriction endonuclease PvuII giving fragments of 177 + 199 + 227 and 199 + 404 for the G and C alleles respectively. DNA from the above amplification was purified using a QIAquick PCR purification kit (Qiagen) and subjected to direct sequencing using the forward primer (above).

2.2.4 AAV production and stereotaxic injections

Short hairpin RNAs (shRNAs) designed to target transcripts derived from mouse claudin-5 were incorporated into AAV-2/9 vectors. Claudin-5 shRNA was cloned into the pSingle-tTS-shRNA (Clontech) vector. The plasmid incorporating the inducible system with claudin-5 shRNA was digested with BsrBi and BsrGI and ligated into the Not1 site of the plasmid pAAV-MCS, such as to incorporate left and right AAV inverted terminal repeats (L-ITR and R-ITR). AAV-2/9 was then generated using a triple transfection system in a stably transfected Hek293 cell line for the generation of high-titre viruses (Vector BioLabs).

C57BL/6J mice were anaesthetized using a ketamine/medetomidine mixture administered via IP injection at a dose of 100 µl/10 g and monitored until unconscious. The animals fur was shaved from its head and the mice were placed in a stereotaxic frame with their jaw positioned in a mouth guard and ear bars placed into each ear socket to ensure the head remained still during surgery. Using a scalpel blade, a 2 cm incision was made anterior to posterior along the sagittal suture. The scalp was peeled to the side and clamped to allow access to the skull. Surgical spears were used to stem any bleeding. Bregma was identified and using the stereotaxic frame, the dorsal hippocampus (coordinates: A/P = -1.9 mm; M/L = ±1.55mm; D/V = 1.75mm) and medial prefrontal cortex (mPFC) (coordinates: A/P = +1.9mm; M/L = ±0.4mm; D/V = 2.5mm) were identified. Using a fine point drill tip, burr holes were made using a surgical drill above the dorsal hippocampus or the mPFC on both hemispheres. A Hamilton syringe was loaded with a doxycycline-inducible adeno-associated virus, serotype 2,9 (AAV2/9) expressing either a short hairpin RNA (shRNA) against claudin-5 or a non-targeting control (NT) and the needle was lowered slowly into the brain parenchyma. 1.0µl of the AAV solution was then injected at a rate of 0.5 µl/minute and once complete, the needle was left in place for 5 minutes before being slowly removed from the brain. The procedure was repeated in the other hemisphere. The animal was sutured, and anaesthesia was reversed with an IP injection of atipamezole and the mouse was placed in an incubator until it recovered. All mice were given 7 days of recovery before experiments began. In addition to mice receiving an injection of NT or claudin-5 AAV, a small cohort was injected with a doxycycline-inducible GFP expressing AAV2/9 to visualize the extent of AAV localization following injection.

2.2.5 Generation of knockdown mice

Mice were generated by standard blastocyst injection (Nagy et al., 2003) at Charles Rivers Laboratory in collaboration with Mirimus Inc. using their strict VAF/EliteTM health standards. A doxycycline-inducible claudin-5 shRNA (160 variant) was inserted at the Col1a1 locus on chromosome 11. Additionally, a CAG-lox-stop-lox-rtTA3-IRESmKate2 (CLR3K) allele was knocked in at the endogenous Rosa26 locus on chromosome 6. This gene utilizes the endogenous Rosa26 promoter to drive expression of the reverse tetracycline-controlled transactivator (M2rtTA) once mice are crossed to a Cre-recombinase expressing mouse (Dickins et al., 2007, Premsrirut et al., 2011, Seibler et al., 2007). Additionally, mice were generated containing a doxycycline-inducible non-targeting shRNA (REN713) inserted at the Col1a1 locus. Mice homozygous for the claudin-5 shRNA containing gene and the rtTA gene were maintained and when mice were required for experiments they were crossed to transgenic Tie-2-Cre expressing animals. Cre-negative littermate mice along with Cre-positive NT mice were used as controls.

2.2.6 Doxycycline treatment

Both the mouse AAV study and knockdown mouse involve the use of a Tet-on system. Here, the presence of doxycycline activates the expression of an shRNA to silence gene expression. The tet-on system makes use of the tetracycline transactivator (tTA) protein to activate gene expression of genes flanked by a tetracycline response element (TRE). In this system, tTA can bind TRE only in the presence of doxycycline. Doxycycline was administered to the drinking water (2 mg/ml in 2% sucrose solution). Doxycycline water was changed every three days. For short term induction of TRE controlled genes, doxycycline was administered as a single IP injection containing 2 mg of doxycycline in 400 µl.

2.2.7 Brain microvasculature fractionation

Half brains were homogenised in 5 ml of DMEM on ice using a Dounce homogeniser and the homogenate was centrifuged at 3,000 rpm for 5 min. The resulting pellet was resuspended in dissociation buffer (0.005% (w/v) dispase (Roche Diagnostics)) and incubated at 37 °C for 2 h with constant agitation at 200 RPM. Homogenates were centrifuged at 3,000 rpm for 5 min and pellets were resuspended in 12 % dextran solution (MW 70,000 from Leuconostoc spp: Sigma). Samples were vortexed and centrifuged at

3,000 rpm for 20 min. A thin red pellet should be visible at the bottom of the tube. Pellets were resuspended in PBS and centrifuged at 2,000 rpm for 5 mins. The final pellet was split in two and resuspended in RNA lysis buffer and centrifuged at 13,500 RPM for 5 min or protein lysis buffer (62.5 mM Tris, 2 % SDS, 10 mM Dithiothreitol, 10 µl protease inhibitor cocktail/100 ml (Sigma Aldrich), centrifuged at 12,000 RPM for 20 min @ 4°C and supernatant removed and stored at -20°C. The relative enrichment of endothelial markers in capillary fractions compared to neuronal, astrocyte, microglia, pericyte and myelin markers can be seen in Figure 2.2.

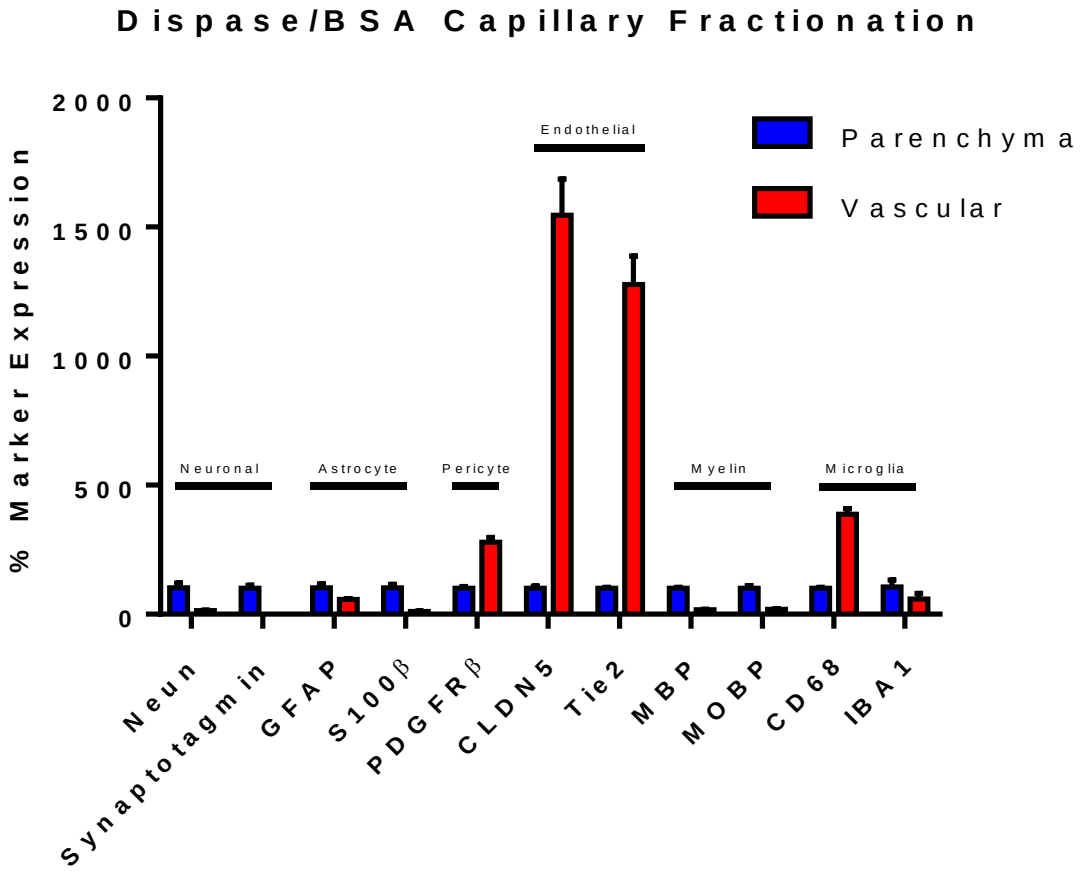

Figure 2.2: Purity of brain capillary fractionation. EC markers are enriched ~15 fold in brain capillaries isolated from the parenchyma containing myelin, neurons and astrocytes. Vascular enriched tissue had minimal expression of neuronal, astrocyte and myelin markers.

2.2.8 Perfusion of tracer molecules

The extent of BBB permeability was assessed by perfusion of tracer molecules. C57BL/6 mice or Claudin-5 KD mice were injected IV with 2 mg/ml of EZ-Link™ Sulfo-NHS-

Biotin (600 Da). Biotin was circulated for ten minutes. Following tracer molecule perfusion, brains were dissected and placed in 4 % paraformaldehyde (PFA, pH 7.4) overnight at 4^{o}C for cryosectioning.

2.2.9 Magnetic resonance imaging (MRI)

BBB integrity was assessed *in vivo* via magnetic resonance imaging (MRI), using a dedicated small rodent 7 T MRI system located at TCD (www.neuroscience.tcd.ie/technologies/mri.php). Mice were anaesthetised as described in section 2.2.2. Anaesthetised mice were physiologically monitored (ECG, respiration and temperature) and placed on an MRI-compatible support cradle, with a built-in system for maintaining the animal's body temperature at 37°C. A canulae was flushed with saline and then inserted into the tail vein. The cradle was then positioned within the MRI scanner. Accurate positioning was ensured by acquiring an initial rapid pilot image, which was then used to ensure the correct geometry was scanned in all subsequent MRI experiments. Upon insertion into the MRI scanner, high resolution anatomical images of the brain were acquired (100 µm in-plane and 500 µm through-plane spatial resolution). To visualize brain damage and lesion volumes, high resolution images were acquired using Rapid Acquisition with Relaxation Enhancement (RARE) 2-D sequence with a RARE factor of 8 and an echo time resulting in an effective time of 42.2 ms (with a flip angle of 180^{o}). With an acquisition matrix of 128 X 128 and a field of view of 1.8 X 1.8 cm^2, the pixel resolution was 0.141 mm/pixel. In the coronal plane, 15 slices, each measuring 0.25 mm in thickness were acquired. Repetition time was 7274.2 ms, and four averages were used for a total measuring time of 7 minutes 45 seconds.

Compromises of the BBB were then visualised in high resolution T1 weighted MR images (resolution, 0.156 X 0.156 X 5 mm^3; field of view: 20 X 20 X 17.9 mm^3; matrix; 128 X 128 X 30; TR/TE: 500/2.7 ms; flip angle: 30^{o}; number of averages: 3; acquisition time: 2 min, 24 sec; Repetitions: 12) following administration of 100 µl of a 1 in 3 dilution of Gd-DTPA (Gadolinium diethylene-triamine pentaacetic acid), administered via the tail vein. Gd-DTPA was administered following acquisition of the first scan (pre-Gd-DTPA). MRI analysis was performed in *ImageJ* (Fiji) where compromises of the BBB were assessed by taking the average pixel intensity of regions of interest before and after administration of Gd-DTPA.

2.2.10 Electroretinogram

ERGs were carried out by Dr. Paul Kenna. Mice were dark-adapted overnight and prepared for electroretinography under dim red light. Pupils were dilated with 2.5% phenylephrine and 1% cyclopentolate. Mice ware anaesthetised with an IP injection of ketamine (2.08 mg per 15 g body weight) and xylazine (0.21 mg per 15 g body weight). Standardised flashes of light were presented to the mice in a Ganzfeld bowl to ensure uniform retinal illumination. ERG responses were recorded simultaneously from both eyes using gold wire electrodes (Roland Consulting Gmbh) and Vidisic (Dr Mann Pharma. Germany) as a conducting agent and to maintain corneal hydration. Reference and ground electrodes were positioned subcutaneously, approximately 1 mm from the temporal canthus and anterior to the tail, respectively. Body temperature was maintained at 37°C using a heat device controlled by a rectal temperature probe. Responses were analysed using a RetiScan RetiPort electrophysiology unit (Roland Consulting Gmbh). The protocol was based on that approved by the International Clinical Standards Committee for human electroretinography. Rod-isolated responses were recorded using a dim white flash (25 dB maximal intensity, where maximal flash intensity was 3 candelas/m*/s) presented in the dark-adapted state. Maximal combined rod-cone response to the maximal intensity flash was then recorded. After a 10 min light adaptation to a background illumination of 30 candelas/m^, cone-isolated responses were recorded to the maximal intensity flash, presented initially as a single flash and subsequently as 10 Hz flickers, a-waves were measured from the baseline to the trough and b-waves from the baseline (in the case of rod-isolated responses) or from the a-wave to the trough.

2.3 Analytical Techniques

2.3.1 cDNA synthesis and real-time reverse transcription polymerase chain reaction (RT-PCR)

cDNA synthesis was carried out using the High-Capacity cDNA Reverse Transcription Kit (Applied Biosystems). The following master mix was used: 2 µl RT Buffer (10X), 0.8 µl dNTPs (100 mM), 2 µl Random Primers (10X), 1 µl MultiScribe^{TM} Reverse Transcriptase, 4.2 µl NF H_2O. 10 µl of master mix was pipetted to each well containing 100 ng of RNA. cDNA synthesis was carried out using a Miometra T3000 Thermocycler. cDNA synthesis conditions were as follows: 25^{o}C for 10 min; 37^{o}C for 120 min; 85^{o}C for 5 min; 4^{o}C hold.

RT-PCR was carried out using a SensiFAST SYBR Hi-ROX Kit (Bioline). Primers were designed using *Primer3*. The following master mix was used: 10 µl SYBR Green Mix, 1 µl Forward and Reverse Primer mix (10 µM), 4 µl NT H_2O. 15 µl of master mix was added to each well of a MicroAMP^{TM} optical 96-well RT-PCR plate. The cDNA samples were diluted 1 in 10 and 5 µl of sample was pipetted into the wells in triplicate. The plate was then covered with a MicroAmp^{TM} Optical Adhesive Film, centrifuged briefly and placed into a Step-One Plus^{TM} Real-Time PCR instrument (Applied Biosystems). RT-PCR conditions were as follows: 95ºC for 10 min; 37 cycles of 95ºC for 15 s, 60ºC for 30 s. A melt-curve stage was added of: 95ºC for 15 s, 60ºC for 1 min, 95ºC for 15 s. The comparative C_T method was used to quantify changes in mRNA levels between treatment groups. The following primers were used:

Table 2.2: RT-PCR primer sequences for tight junction mRNAs.

Gene		**Sequence (5' – 3')**
Mouse Claudin-5	Forward	TTTCTTCTATGCGCAGTTGG
	Reverse	GCAGTTTGGTGCCTACTTCA
Mouse Occludin	Forward	ACAGTCCAATGGCCTACTCC
	Reverse	ACTTCAGGCACCAGAGGTGT
Mouse ZO-1	Forward	CCACCTCTGTCCAGCTCTTC
	Reverse	CACCGGAGTGATGGTTTTCT
Mouse Tricellulin	Forward	AACCCCCTTACAGCTGTCCT
	Reverse	TAATCCCGTCAGCATCTTCC
β-actin	Forward	TCACCCACACTGTGCCCATCTACGA
	Reverse	CAGCGGAACCGCTCATTGCCAATGG

Table 2.3: RT-PCR primer sequences for brain capillary fractionation cell markers.

Gene		**Sequence (5' – 3')**
Mouse TIE2	Forward	TCAGGGCAAAAATGAAGACC
	Reverse	TCTAGGCCCTTGAGCTGGTA
Mouse PDGFRβ	Forward	AACCCCCTTACAGCTGTCCT
	Reverse	TAATCCCGTCAGCATCTTCC
Mouse GFAP	Forward	AGCCCTGCCAGCTCTCCCTTAG
	Reverse	AAGGTGTGGCTGAAATGCGCG

Mouse S100β	Forward Reverse	TCCCGGGATGTCCGAGCTGG TGTCACCCTCTCGCCCGGAG
Mouse Neun	Forward Reverse	AAACCTTCCACCGTCTCCTT GACGTGGACTTGGACTTGGT
Mouse CD68	Forward Reverse	TTCTGCTGTGGAAATGCAAG AGAGGGGCTGGTAGGTTGAT
Mouse α-smooth muscle actin	Forward Reverse	TTCAATGTCCCAGCCATGTA GAAGGAATAGCCACGCTCAG
Mouse MBP	Forward Reverse	CTTCAAAGACAGGCCCTCAG CCTGTCACCGCTAAAGAAGC
Mouse MOBP	Forward Reverse	CATTTGCTTCCCATTCACCT AGGATGCCTCCATTTCCTCT

2.3.1.1 RNA profiler array

A mouse autophagy array was used to analyse the expression profiles of a range of autophagic factors in RNA isolated from cerebral microvessels from C57BL/6J mice. cDNA synthesis was carried out using the RT^2 First Strand Kit. The genomic DNA elimination mix was prepared by mixing 100 ng of each RNA sample with 2 µl of Buffer GE and made up to 10 µl with NF H_2O. The reaction was incubated for 5 min at 42^{o}C and then placed on ice immediately for at least 1 min. For the reverse transcription step, the following reaction was prepared: 4 µl of 5X Buffer BC3, 1 µl Control P2, 2 µl RE3 Reverse Transcriptase Mix, 3 µl RNase-free water. 10 µl of the reverse transcription mix was mixed with 10 µl of the genomic DNA elimination mix and incubated for 15 min at 42^{o}C and immediately for 5 min at 95^{o}C. Each reaction was mixed with 91 µl of NF H_2O and placed on ice. RT-PCR was carried out using the RT^2 SYBR Green Mastermix. The PCR components mix was prepared in a 5 ml tube by mixing the following: 1350 µl 2x RT^2 SYBR Green Mastermix, 102 µl cDNA synthesis reaction, 1248 µl RNase-free water. 25 µl of the PCR components mix was added to each well of the RT^2 Profiler PCR Array and the plate was sealed with optical adhesive film. The plate was centrifuged for 1 min at 1000 g and placed into a StepOne Plus^{TM} Real-Time PCR instrument. RT-PCR conditions were as follows: 95^{o}C for 10 min; 40 cycles of 95^{o}C for 15 s, 60^{o}C for 1 min. A melt-curve stage was added of: 95^{o}C for 15 s, 60^{o}C for 1 min, 95^{o}C for 15 s. The

absolute quantitation method was used to quantify changes in mRNA levels between treatment groups.

2.3.2 Western blot

2.3.2.1 Bicinchoninic acid assay for protein quantification

Protein quantification was performed using the Pierce® BCA Assay Kit. The BCA working reagent was prepared by mixing 50 parts of BCA Reagent A with 1 part of BCA Reagent B. 10 µl of each protein sample and standard (0, 125, 250, 500, 750, 1000, 1500, 2000 µg/ml BSA) were added in duplicate into a 96-well plate. 200 µl of Working Reagent was added to each well. The plate was covered with adhesive film, mixed and incubated at 37^{o}C for 30 min. Following incubation, the absorbance was measured at 595 nm on a Multiskan FC plate reader (Thermo Scientific). The average absorbance reading of a blank sample was subtracted from the average absorbance reading of all other samples. A standard curve was prepared in GraphPad Prism by plotting the average blank-corrected measurements for each BSA standard vs. its concentration in µg/ml and the protein concentrations of unknown samples was interpolated from the curve.

2.3.2.2 SDS-Page gel preparation

SDS-PAGE gels were prepared according to Table 2.1 below. The resolving gel was poured into the gel plate leaving enough space for a comb plus 1 cm and allowed to set. The stacking gel was poured on top of the set resolving gel and the comb was placed into the gel and allowed to set. Once set, the rubber gasket was removed, and the gel was placed into an electrophoretic tank filled with 1X running buffer. The comb was removed, and the wells were filled with protein samples and molecular weight standards.

Table 2.4: Preparation of resolving and stacking gels.

	15% Resolving Gel	12% Resolving Gel	10% Resolving Gel	4% Stacking Gel
Deionised H_2O	4.6 ml	6.6 ml	7.93 ml	6.8 ml
1.5 M Tris-HCL (pH 8.8)	5 ml	5 ml	5 ml	-

0.5 M Tris-HCL (pH 6.8)	-	-	-	1.67 ml
30% Acrylamide	10 ml	8 ml	6.67 ml	1.33 ml
10% SDS (pH 7.2)	0.2 ml	0.2 ml	0.2 ml	0.1 ml
10% APS	0.2 ml	0.2 ml	0.2 ml	0.1 ml
TEMED	20 µl	20 µl	20 µl	10 µl

2.3.2.3 Sample preparation and electrophoresis

5 µl of 5X sample buffer was mixed with 20 µl of protein sample and the proteins were denatured at 95^{o}C for 5 min. The samples were cooled at room temperature and equal concentrations of protein were loaded into the wells along with 5 µl of protein standard. The gel rig was connected to a power pack and the gel was run at 80 V for 20 min followed by 140 V for 2 h. Once the dye front reached the bottom of the gel, electrophoresis was stopped.

2.3.2.4 Transfer of proteins

Proteins, now separated, were transferred onto a PVDF membrane. 4 sheets of filter paper were soaked in transfer buffer and placed on the transfer apparatus. The PVDF membrane was "activated" in methanol for 30 s, equilibrated in transfer buffer and placed on top of the filter paper. The gel was removed from the plate, the stacking gel was removed, and the gel was carefully placed on top of the PVDF membrane ensuring that no bubbles were introduced. 4 more sheets of filter paper were soaked in transfer buffer and layered on top of the PVDF membrane and gel. Proteins were transferred to the PVDF membrane at 12 V for 2 h.

2.3.2.5 Blocking and antibody incubations

Following transfer, the membrane was blocked with 5% Marvel in TBS Tween®-20 (0.05%) (TBS-T) for 1 h at room temperature on an orbital shaker. Blocking prevents non-specific binding of the primary antibody. The membrane was incubated in primary antibody in blocking solution at 4^{o}C on a shaker overnight. Following primary antibody incubation, the membrane was washed three times in TBS-T and then incubated with secondary antibody, anti-rabbit (IG)-horse-radish peroxidase (HRP), for 2 h at room

temperature. After incubation, the membrane was washed four times with TBS-T. The following primary antibodies were used:

Table 2.5: Primary antibodies used for western blotting.

Primary Antibody	Blocking Solution	Dilution
Rabbit anti-Claudin-5	5% Marvel	1:1000
Rabbit anti-Occludin	5% Marvel	1:500
Rabbit anti-ZO-1	5% Marvel	1:1000
Rabbit anti-Tricellulin	5% Marvel	1:1000
Rabbit anti-Axin2	5% Marvel	1:1000
Rabbit anti-Sox17	5% Marvel	1:1000
Rabbit anti-GAPDH	5% Marvel	1:5000

2.3.2.6 Enhanced chemiluminescence (ECL)

Membranes were developed in a darkroom or on a C-DiGit (LI-COR). Equal volumes of reagent A and B were mixed and poured onto the membrane. The membrane was incubated in this solution for 1 min and then sandwiched between two pieces of acetate and placed into a film cassette. In the dark room, a sheet of X-ray film was cut to the size of the membrane and placed over the membrane in the film cassette. The exposure time varied depending on the antibody. Following exposure, the X-ray film was placed in developer solution until the signal was observed. The film was then rinsed quickly in water and placed in fixer solution. The film was rinsed in water again. Alternatively, following incubation in the ECL reagent, the membrane was placed directly onto the C-DiGit and scanned for 12 min and the optimal exposure was selected. Western blots were analysed in *ImageJ* by calculating the integrated pixel density for each band and normalizing these values to the integrated pixel density of a control protein such as GAPDH or β-actin.

2.3.3 Immunohistochemistry

2.3.3.1 Fixation and cryosectioning

Following brain removal as described in section 2.1.11, brains were fixed by immersion in 4% PFA at 4^{o}C overnight. Following fixation, brains were washed three times in PBS

and then cryopreserved in a sucrose gradient (10%, 20%, 30% (w/v)) until the brains sunk. The brains were then placed into a cryomold filled with Optimal Cutting Temperature (OCT) compound and snap-frozen in liquid nitrogen-cooled isopentane and equilibrated at -20^{o}C overnight. Snap frozen brains were sectioned on a cryostat (Leica) into 12 µm thick sections and mounted onto poly-lysine slides (VWR) and stored at -20^{o}C. For immunohistochemical analysis of TJ proteins, brains were snap frozen directly in OCT compound in isopentane-cooled liquid nitrogen.

2.3.3.2 Immunohistochemistry of frozen brain sections

Mouse brain cryosections (12 µm thick) were warmed to room temperature for 30 min prior to staining. Mouse brain sections were drawn around with a PAP pen and then blocked and permeabilised with 5% NGS, 0.5% Triton X-100 in 1X PBS. For fresh frozen tissue, sections were first post-fixed with methanol for 10 min at -20^{o}C before blocking. Blocking buffer was removed and sections were incubated with primary antibodies at 4^{o}C overnight. Sections were washed 3 x 5 min in PBS and incubated with fluorescently labelled secondary antibodies for 2 h at room temperature followed by 3 x 5 min washes with PBS. All sections were counterstained with Hoechst 33258 for 30 seconds at a dilution of 1:10,000 of a stock 1 mg/ml solution and mounted with Aqua Polymount. All samples were analysed with a Zeiss LSM 710 confocal laser scanning microscope. Identical acquisition settings were used to acquire images and image processing was performed in *ImageJ*. Capillary density, length and branch points were analysed with the angiogenesis plugin in *ImageJ*. The following primary antibodies were used:

Table 2.6: Primary antibodies used for immunohistochemistry.

Primary Antibody	Blocking Solution	Dilution
Mouse anti-Claudin-5	5 % NGS	1:50
Rabbit anti-Claudin-5	5 % NGS	1:100
Rabbit anti-ZO-1	5 % NGS	1:200
Rabbit anti-Occludin	5 % NGS	1:100
Mouse anti-GFAP	5 % NGS	1:400
Rabbit anti-Fibrinogen	5 % NGS	1:100
Rabbit anti-GLUT-1	5 % NGS	1:100

Cy3-conjugated goat anti-mouse IgG and cy2-conjugated goat anti-rabbit secondary antibodies were used at a dilution of 1:200. Isolectin-IB4 Alexa Fluor 488 was used at a dilution of 1:300 to stain blood vessels in the brain. To label endogenous IgG on human samples, sections were incubated with rabbit anti-human IgG cy3 at a dilution of 1:100. To stain for Sulfo-NHS-Biotin, slides were incubated with Cy3-conjugated streptavidin at a 1:200 dilution overnight at 4^{o}C.

2.3.3.3 Immunohistochemistry of human brain sections

Free-floating 60 µm-thick sections of post-mortem human brain tissue from 24 deceased schizophrenia patients and 24 age-matched controls were obtained from the Stanley Medical Research Institute. Sections were washed in PBS and antigen retrieval was performed by boiling the sections for 2 x 5 min in sodium citrate buffer (10 mM sodium citrate, 0.05% Tween 20, pH 6.0). Sections were permeabilised with 0.5% Triton X-100 for 2 h at room temperature on an orbital shaker and then blocked with 5% NGS, 0.5% Triton X-100 in 1X PBS for 2 h at room temperature. Sections were then incubated with monoclonal mouse anti-claudin-5 (1:50; Santa Cruz) for 48 hours at 4^{o}C on an orbital shaker. Sections were washed 4 x 10 min with PBS and incubated with Cy3-conjugated goat anti-mouse IgG (1:300, Abcam) for 3 h at room temperature. Secondary antibody was removed, and sections were washed 5 x 10 min in PBS and counterstained with Hoechst 33258. Z-stacks were acquired with identical acquisition settings across samples and 3D images were rendered with Image J 3D viewer. Staining and microscopy were performed blind to diagnosis.

2.3.3.4 Immunocytochemistry

Cultured cells were plated onto 1% fibronectin-coated Nunc Lab-Tek II Chamber Slides (Thermo Scientific) in culture medium and were then treated with various materials (*e.g.* siRNA, plasmids, inhibitors) for various timepoints. Following treatment, medium in the wells was removed and the cells were washed gently twice in PBS. The PBS was discarded, and the cells were fixed with 4% paraformaldehyde (PFA) for 10 min at room temperature. Alternatively, the cells were fixed with ice-cold methanol for 10 min at room temperature. Following fixation, the cells were washed twice with PBS and blocked with 5% normal goat serum (NGS), 0.05% Triton X-100 in PBS for 1 h at room temperature. The blocking buffer was discarded, and the cells were incubated in primary antibodies overnight at 4^{o}C. The following day, the cells were washed three times with PBS and

incubated with fluorescently labelled secondary antibodies for 2 h at room temperature. The cells were then washed four times with PBS and the nuclei were stained with Hoechst 33258, Pentahydrate (bis-Benzamide) (ThermoFisher Scientific). The slide was removed from the chamber and mounted with Aqua Poly/Mount (Polysciences, Inc) before visualisation by confocal laser scanning microscopy. The following antibodies were used:

Table 2.7: Primary antibodies used for immunocytochemistry.

Primary Antibody	Blocking Solution	Dilution
Rabbit anti-Claudin-5	5 % Normal Goat Serum	1:100
Rabbit anti-ZO-1	5 % Normal Goat Serum	1:100
Rabbit anti-BMAL-1	5 % Normal Goat Serum	1:100

Cy3-conjugated goat anti-rabbit IgG secondary antibody was used at a dilution of 1:500.

2.3.3.5 Nissl staining

Prior to staining, prepare the following solution.

0.1% cresyl violet solution: 0.1 g cresyl violet acetate, 100 ml dH_2O. Add 300 µl of glacial acetic acid just before use and filter.

Sections were removed from freezer and allowed to warm to room temperature for 15 min. Sections were then rinsed twice in PBS for 5 min each followed by one min wash in dH_2O. Next, the slides were dipped in Nissl stain for 20 min at 37^oC prior to being rinsed two times in dH_2O for 5 min each. The sections were then dipped in 90%, 95% ethanol for 3 min each followed by two washes in 100% ethanol for 3 min each. Finally, the sections were dipped three times in xylene for 3 min each, cover-slipped and air dried under the fume hood.

2.3.3.6 Cerebrovascular casting of whole mouse brain

Anaesthetised mice were perfused slowly with PBS plus heparin followed by Microfil (Flow Tech, Inc) casting agent (prepared by mixing 5 ml MV diluent, 4 ml filtered MV compound and 450 µl (5%) of catalyst (MV curing agent)). Following perfusion, the brain was removed and fixed by immersion in 4% paraformaldehyde overnight at 4^oC. The brain was dehydrated in increasing concentrations of ethanol (EtOH) at room temperature as follows: 25% EtOH, 1 day; 50% EtOH, 1 day; 75% EtOH, 1 day; 95% EtOH, 2 days; and 100% EtOH, 2 days. Following dehydration, the brain was clarified by immersion in

methyl salicylate (Sigma-Aldrich) for 2 days at room temperature. The whole-brain vasculature was imaged with a bright field microscope.

2.4 Behavioural methods

2.4.1 General information and test schedule

Mice were handled for approximately 5 minutes per day for 1 week prior to behavioural testing. Except where stated, mice had free access to food and water throughout the testing schedule. Before each test, mice were taken from their holding room and allowed to habituate to the testing room for 10 minutes prior to testing. All behavioural experiments were performed during the light phase and all apparatus were cleaned with 70 % ethanol before use and between trials, except where stated. Statistical analysis was performed using Prism 7 for Windows (GraphPad Software, Inc., U.S.A.) and $P < 0.05$ was taken as being statistically significant in all cases.

The test schedule for mice that were stereotaxically injected with an AAV was as follows:

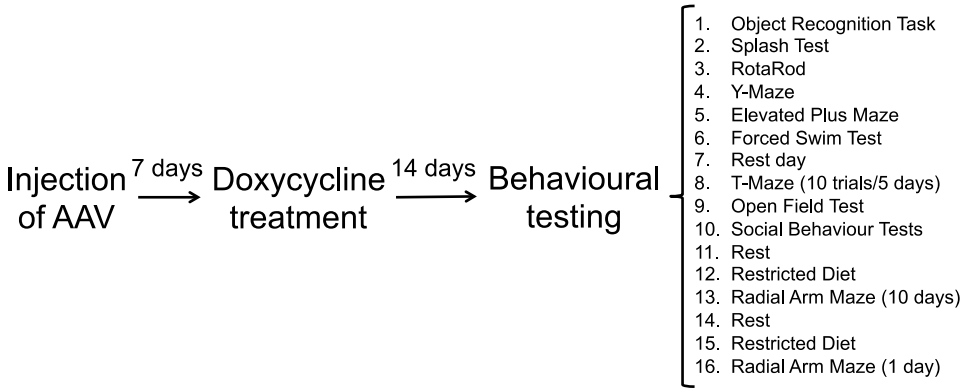

The test schedule for the doxycycline-inducible knockdown mice was as follows:

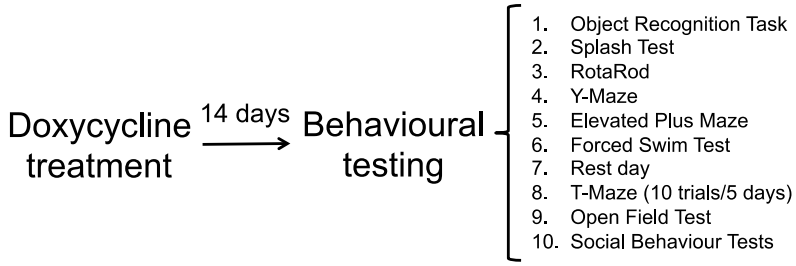

2.4.2 Object recognition task

Long-term recognition memory was assessed using the object recognition task (Leger et al., 2013). The object recognition task was performed in a plastic rectangular arena (38 x 43 x 18 cm). Three similarly sized objects were used for all mice (plastic culture tube filled with NaCl; brown glass bottle filled with water; 50 ml plastic tube filled with solution of bromophenol blue) with animals showing no preference for one object over the others. The task consisted of two 3-minute sessions:

1) Familiarisation session: Two objects are positioned at two fixed locations within the testing arena.
2) Test session: One of the objects from the Familiarisation session is placed in the same location as before (Familiar object) and the second object is replaced with a third object (Novel object).

At the beginning of each session, the test mouse was placed in the arena facing the wall and positioned equidistant from the two objects. The timer was started when the experimenter released the mouse's tail and the number of nose contacts with each object was counted (Figure 2.3). Between sessions, the arena and objects were cleaned with 70 % ethanol and the mouse was returned to its home cage for the intersession interval (ISI) of 3 hours. Each mouse's performance was assessed by calculating their discrimination index during the test session:

$$\text{Discrimination index} = \frac{\text{Nose contacts}_{\text{Novel}} - \text{Nose contacts}_{\text{Familiar}}}{\text{Nose contacts}_{\text{Novel}} + \text{Nose contacts}_{\text{Familiar}}}$$

with $\text{Nose contacts}_{\text{Novel}}$ being the number of nose contacts with the novel object and $\text{Nose contacts}_{\text{Familiar}}$ being the number of nose contacts with the familiar object from the familiarisation session. Positive values for the Discrimination index are associated with a preference for the novel object (the expected behaviour) and negative values are associated with a preference for the familiar object. Values that tend close to 0 mean that the mouse has no preference for one object over the other. Each experimental group was compared to its relevant control group via an unpaired *t*-test.

Figure 2.3: Novel object recognition task. Learning and memory was assessed on the novel object recognition task, a two-trial test of non-spatial memory.

2.4.3 Splash test

Induced grooming behaviour was assessed using the splash test (Yalcin et al., 2005). Individual mice were left in their home cage for the duration of the splash test (5 minutes); cage mates were temporarily stored in a separate cage. The mouse was sprayed on its dorsal side with a 10 % sucrose solution and a timer was started. At the end of the test, the mouse was removed to the temporary holding cage and the next mouse was placed in the home cage. Video recordings were made of the entire trial, including the spraying procedure. The videos were then analysed by an experimenter who was blind to the experimental condition looking at two measures:

1) Latency to begin grooming: The time (seconds) taken for the mouse to initiate any form of grooming behaviour.
2) Total grooming time: The total time (seconds) that the mouse engaged in any form of grooming behaviour.

Each experimental group was compared to its relevant control group via an unpaired *t*-test.

2.4.4 Rotarod

Motor co-ordination was assessed using the RotaRod (Deacon, 2013). Mice were run on the RotaRod (Ugo Basile, Italy) along with all their cage mates to reduce anxiety in performing the task. The RotaRod was started at a constant speed of 4 rotations per minute (rpm) and each mouse from the cage was placed on a lane in the RotaRod. Once all the

mice were in position, the RotaRod was set to accelerate from 4 to 60 rpm over 3 minutes. Two measures were taken:

1) The time (seconds) at which the mouse fell from its lane.
2) The acceleration (rpm) at the time at which the mouse fell from its lane.

Each experimental group was compared to its relevant control group via an unpaired *t*-test. The RotaRod was cleaned with 70 % ethanol between each trial and reset to 4 rpm for the next cage.

2.4.5 Y-maze

Working spatial memory was assessed using the spontaneous alternation on a Y-Maze (Maurice et al., 1994). Individual mice were placed in the centre zone of a Perspex Y-Maze (three 30 x 5 cm joined by a 20 cm diameter central area; bounded by wall 15 cm high) and allowed to freely explore the apparatus for 8 minutes (Figure 2.4A). Arm entries were counted by the experimenter when the mouse placed all four paws into an arm, delineated by the slot for guillotine doors associated with the apparatus (the doors themselves were not used in this task). Each arm entry was recorded in the order in which they occurred. Spontaneous alternation was assessed after the experiment was over; a successful alternation being defined as the mouse entering all three arms of the Y-Maze over any 4-arm entry span (e.g. if the mouse entered the arms in the order 1, 2, 1, 3, 1, 3 then it would count as two alternations out of a possible three). Errors were counted if the mouse exited an arm and then returned to that arm before visiting either of the other two arms. Each experimental group was compared to its relevant control group via an unpaired *t*-test.

2.4.6 Elevated plus maze

Anxiety-like behaviour was assessed using the elevated plus maze (Komada et al., 2008). Individual mice were placed in the centre zone of a Perspex elevated plus maze (four 30 x 5 cm arms; two open arms and two closed arms with wall height = 20 cm; apparatus raised on Perspex legs to a height of 40 cm) and allowed to freely explore the apparatus for 10 minutes (Figure 2.4B). Arm entries were logged by a computerised tracking system (ANY-Maze, Version 4.99m, Stoelting Co., U.S.A.) on a Hewlett-Packard ProBook running Windows 8.1 with the total closed arm entries and open arm entries being taken for analysis. Levels of anxiety-like behaviour were analysed by comparing the number of

entries into the open arms between the groups. Each experimental group was compared to its relevant control group via an unpaired *t*-test.

2.4.7 T-maze

Working spatial memory was assessed using the alternating T-Maze paradigm (Deacon and Rawlins, 2006). Mice were individually placed into the start arm of a Perspex T-Maze (three arms 30 x 10 cm; wall height 20 cm) with a guillotine door preventing them from accessing the maze (Figure 2.4C). Each mouse underwent 10 sessions with each session comprising of two trials. One session was performed in the morning and another in the evening over 5 days. During the first trial in each session, a Perspex divider was present to encourage the selection of one arm over the other. The trial began when the guillotine door in the start arm was removed and a stopwatch was started at the same time. The stopwatch was stopped when the mouse entered one of the choice arms. An arm entry was defined as the point when entire mouse, including its tail, was in the arm and at this point a guillotine door was placed at the entrance of the arm to prevent the mouse from going back into the start arm. The time taken to enter an arm and the name of the arm selected (A or B) was noted by the experimenter and the guillotine door to the start arm was replaced. The mouse was then returned to the start arm for the second trial.

Before beginning the second trial, the divider between the two choice arms and the guillotine arm from the choice arm from the first trial was removed. The apparatus was not cleaned between trials, as mice should use olfactory cues to make a choice on this task (see Deacon & Rawlins, 2006). The second trial again began when the guillotine door for the start arm was removed and ended when the mouse fully entered one of the two arms, again using a stopwatch to time performance in the task. The mouse was contained in the choice arm with a guillotine door before being returned to its home cage. The time taken to enter the arm and the name of the arm selected was again noted. Each mouse was scored for each session using a binary system: 1 for alternating between the arms; and 0 for visiting the same arm twice in a session. The time taken to enter an arm on the second trial of each session was also analysed as a response time. Each experimental group was compared to its relevant control group via unpaired *t*-tests.

2.4.8 Radial arm maze

Working and long-term spatial memory was assessed using the 8-armed radial arm maze (Crusio et al., 1993). Mice were familiarised with the food reward (chocolate flavoured cereal, Aldi, Ireland) for two days before the test. Mice were also placed on a restricted diet for three days prior to the start of the test until the end of the final day of testing to encourage the mice to search for the food rewards. The radial arm maze consisted of two phases:

1) Standard radial arm maze protocol of one trial per day over 10 days.
2) A single retention trial 10 days after the final trial of the standard protocol.

One day before testing, mice were habituated to the Perspex radial arm maze (eight 30 x 5 cm joined by a 20 cm diameter central area; bounded by wall 15 cm high); mice were placed on the maze with their cage mates and allowed to freely explore the apparatus in groups for 5 minutes. This was to minimise any anxiety effects during learning in the radial arm maze. On test days, the radial arm maze was baited with four food rewards. These were each placed into four of the eight arms, leaving four empty arms. The food rewards were put into recessed food wells so that mice could not see whether a food reward was present or not until they had traversed down the arm to directly check the well. Baited arms were pseudorandomly assigned for each mouse before the experiment started. The radial arm maze was cleaned with 70 % ethanol between all trials and after placement of the food rewards to minimise olfactory cues.

For each trial, mice were individually placed in the central start zone of the radial arm maze and allowed to explore until they had consumed all four of the food rewards or until the trial had run for 15 minutes (Figure 2.4D). At the end of the trial, mice were returned to their home cage. All trials were recorded using a computerised tracking system (ANY-Maze, Version 4.99m, Stoelting Co., U.S.A.) on a Hewlett-Packard ProBook running Windows 8.1 with the number of arm entries, average speed and trial duration being measured. Working memory errors were counted when a mouse entered an arm that it had already visited during that trial and reference memory errors (reflecting long-term storage of food reward locations) were counted when a mouse entered an arm that does not contain a food reward. Each experimental group was compared to its relevant control group via unpaired *t*-tests for measures made over the total experiment and via repeated

measures analyses of variance (ANOVAs) for data that had been analysed on a trial-by-trial basis. The first two trials were considered as training trials and were not included in the statistical analysis of the task (Crusio et al., 1993).

For the retention trial, mice were run in the same manner to see whether treatment affected retention of the food reward locations over several days of rest. Again, working and reference memory errors were analysed along with average speed and trial duration. Each experimental group was compared to its relevant control group via an unpaired *t*-test.

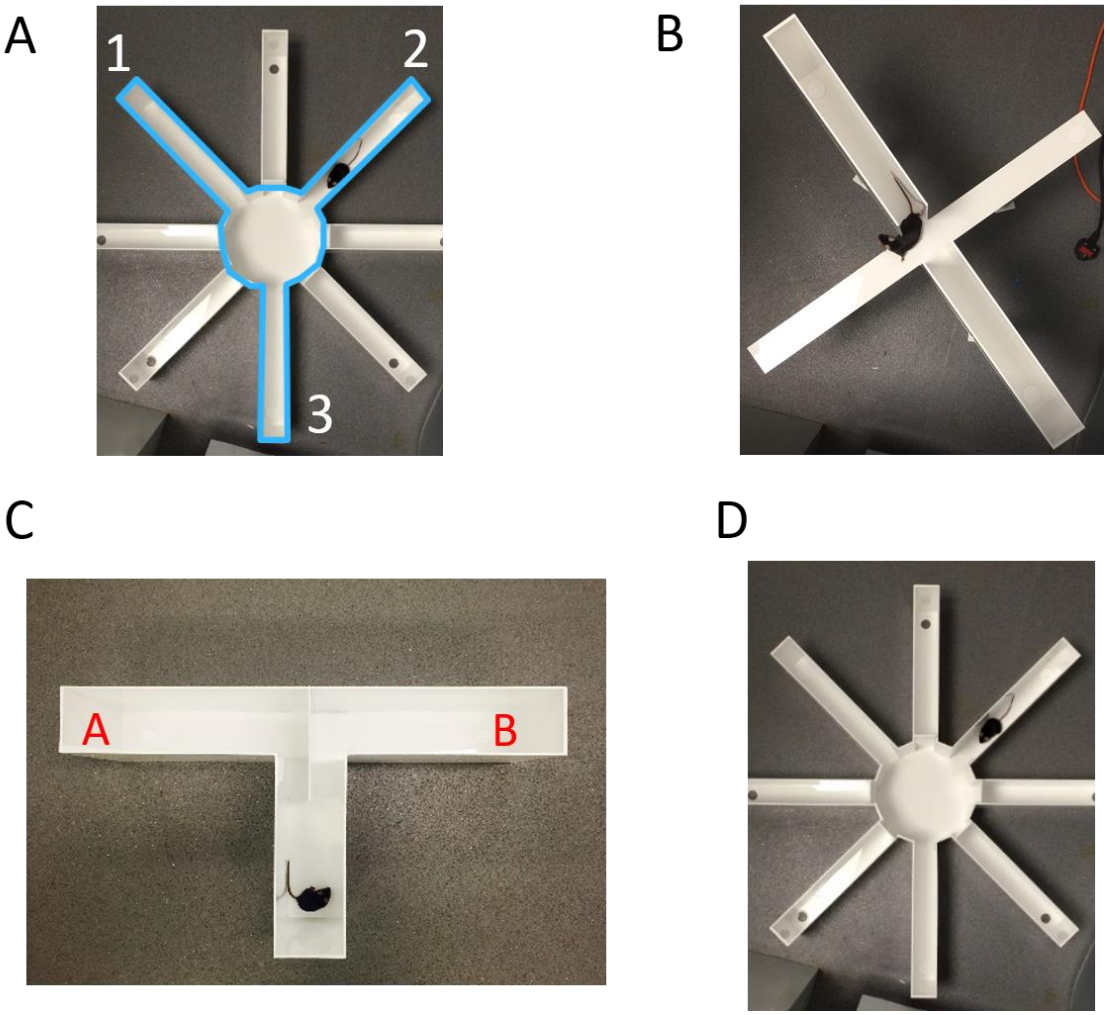

Figure 2.4: Learning and memory mazes. **(A)** Working memory was assessed on the hippocampal dependent Y-maze. **(B)** Anxiety-related behaviour was assessed on the elevated plus maze, an elevated 4-armed maze containing two open and two closed arms. **(C)** Working spatial memory was assessed on the hippocampal dependent T-maze. **(D)** Working and long-term memory was assessed on the hippocampal dependent radial arm maze.

2.4.9 Forced swim test

Depression-like behaviour was assessed using the forced swim test (Can et al., 2012). A large transparent plastic beaker (diameter 17 cm; height 21 cm) was filled with lukewarm water (20-21 °C). Mice were slowly placed individually into the water and a timer was started the moment the experimenter released the mouse's tail. Mice were allowed to swim for 6 minutes and were then removed from the apparatus and dried off with paper towel. Mice were then allowed to dry off under a heating lamp before returned to the cage rack. Video recordings were made covering the placement of the mouse into the apparatus up until the end of the swimming period. The videos were then analysed by an experimenter who was blind to the experimental condition, recording the total time (in seconds) spent engaged in escape behaviour during the final 4 minutes of the swimming period (Can et al., 2012). This value was subtracted from the total time (240 seconds) to give the time spent immobile. Each experimental group was compared to its relevant control group via an unpaired *t*-test.

2.4.10 Open field test

General locomotor activity and anxiety-like behaviour was assessed using the open field test (Bailey and Crawley, 2009). Mice were individually placed into a Perspex open field arena (30 x 30 x 21 cm) and allowed to freely explore for 30 minutes. The mice were tracked using a computerised tracking system (ANY-Maze, Version 4.99m, Stoelting Co., U.S.A.) on a Hewlett-Packard ProBook running Windows 8.1, which automatically recorded distance, average speed, time spent in the three zones (outer perimeter; middle perimeter; centre zone) and time spent freezing. The experimenter overseeing the test used hot keys to record the time spent rearing and grooming during the 30 minutes test. Each experimental group was compared to its relevant control group via unpaired *t*-tests for measures made over the total time and via repeated measures analyses of variance (ANOVAs) for data from the three zones and for data that had been time-binned into 5 minute intervals.

2.4.11 Social behaviour tests

Social behaviour was assessed using the social preference and social novelty tasks (Kaidanovich-Beilin et al., 2011). The apparatus used was a plastic arena (38 x 43 x 18 cm) divided into three areas by Perspex dividers. The central start zone was empty but the two zones on either side contained circular dome-shaped transparent plastic housing

containers (diameter 15 cm; height 9 cm) that had several air holes drilled around their circumference. There were three trials in every session and each mouse was given one session each. In the habituation trial, mice were placed individually into the central start zone and allowed to freely explore the empty apparatus for 5 minutes. For the social preference trial, the mouse being tested was placed in the start zone and allowed to explore the apparatus (containing one empty housing container and one with an unfamiliar mouse in it) for 10 minutes (Figure 2.5). Another unfamiliar mouse was then placed the previously empty housing container. For the social novelty trial, the mouse being tested was placed in the start zone and allowed to explore the apparatus (now containing two housing containers; one containing a familiar mouse from the social preference trial and the other containing a novel mouse) for 10 minutes (Figure 2.5). At the end of the session, all mice were returned to their respective home cages. The apparatus was cleaned with 70 % ethanol before all trials. In the social preference and social novelty trials, the mice were tracked using a computerised tracking system (ANY-Maze, Version 4.99m, Stoelting Co., U.S.A.) on a Hewlett-Packard ProBook running Windows 8.1. The time (in seconds) spent in the area around each housing container was measured and a social interaction index was calculated for each trial. For the social preference trial, the social interaction index was calculated as:

$$\text{Social interaction index}_{\text{Preference}} = \frac{\text{Time}_{\text{Mouse}} - \text{Time}_{\text{Empty}}}{\text{Time}_{\text{Mouse}} + \text{Time}_{\text{Empty}}}$$

with $\text{Time}_{\text{Mouse}}$ being the time spent in the zone surrounding the unfamiliar mouse and $\text{Time}_{\text{Empty}}$ being the time spent in the zone surrounding the empty housing container. For the social novelty trial, the social interaction index was calculated as:

$$\text{Social interaction index}_{\text{Novelty}} = \frac{\text{Time}_{\text{Novel}} - \text{Time}_{\text{Familiar}}}{\text{Time}_{\text{Novel}} + \text{Time}_{\text{Familiar}}}$$

with $\text{Time}_{\text{Novel}}$ being the time spent in the zone surrounding the novel mouse and $\text{Time}_{\text{Familiar}}$ being the time spent in the zone surrounding the familiar mouse from the previous social preference trial.

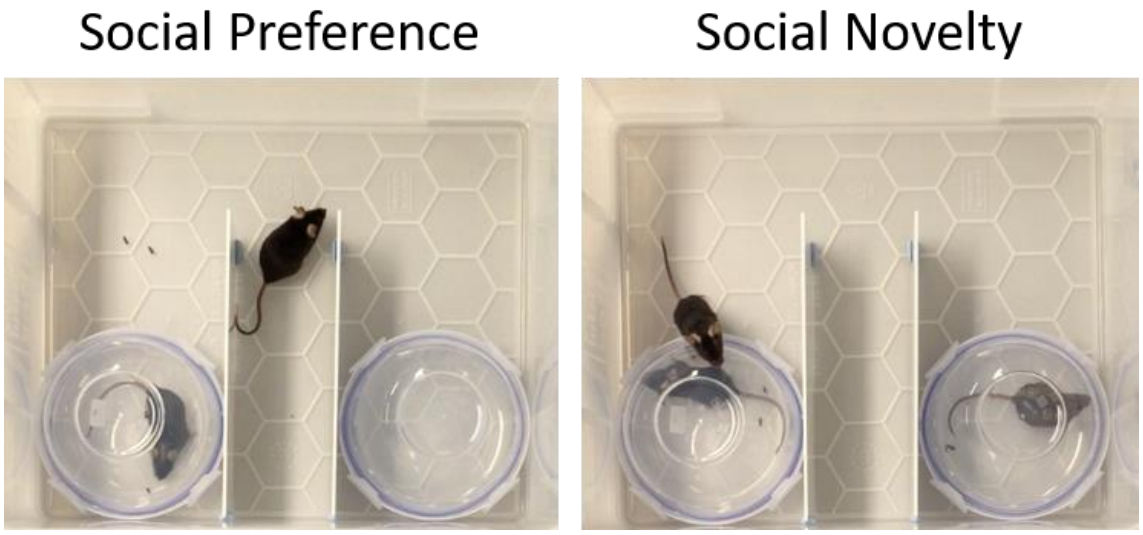

Figure 2.5: Social tests. Sociability was assessed on the social preference task where mice are free to explore an arena containing an empty cage or a cage with an unfamiliar mouse. Sociability was then assessed on the social novelty task where mice are free to explore an arena containing a cage with a familiar mouse and a cage containing an unfamiliar mouse.

2.4.12 Pre-pulse inhibition (PPI) of the acoustic startle response

Sensorimotor gating was assessed by prepulse inhibition (PPI) of the acoustic startle response. The PPI apparatus consisted of a soundproof PPI chamber with a weighing scale positioned in the centre of the chamber beside a loudspeaker. Mice were maintained in a holding chamber placed on the scale. Each mouse was given two days to habituate to the holding chamber and PPI chamber with a constant background white noise (65 dB). Before the beginning of the experiment, all instruments were calibrated and startle stimulus (71, 77, 83, 100, 110, 120 dB) were set. The animal holding chamber was cleaned with 70% ethanol between trials and allowed to airdry. PPI was divided into 3 stages:

1) 2 min habituation with constant background noise of 65 dB.
2) Presentation of random combinations of prepulse (71, 77, 83 dB) and pulse (100, 110, 120 dB) intensities to habituate animals to startle stimulus.
3) 10 blocks of random combinations of prepulse alone, pulse alone, prepulse plus pulse and no stimulus trials.

Startle stimulus were presented as 20 ms bursts of white noise with an interstimulus (time between presentation of prepulse and pulse stimuli) interval of 100 ms. The PPI program

was written in MATLAB and the sound files were generated in Microsoft Visual Studios. Raw data was exported from MATLAB to Excel. Excel files for each block were then loaded into MATLAB and the data were averaged across the 10 blocks for each prepulse, pulse, prepulse plus pulse and no stimulus trial and PPI was calculated as:

$$\%PPI = 100\ x\ \frac{pulse - (prepulse + pulse)}{pulse\ alone}$$

2.4.13 Statistical Analyses

Statistical analysis was performed using Student's t-test, with significance represented by a P value of ≤ 0.05. For multiple comparisons, ANOVA was used with a Tukey-Kramer post-test and significance represented by a P value of ≤ 0.05. For survival analysis, a Log-rank (Mantel-Cox) test was performed to compare the survival distribution between two groups.

Chapter 3:

Association of a single nucleotide polymorphism (SNP) with schizophrenia in 22q11DS patients and characterisation of brain endothelial tight junctions in human schizophrenia cases

3.1 Introduction

Emerging evidence points to BBB hyperpermeability and microvascular dysfunction as being involved in several neuropsychiatric disorders including schizophrenia (Najjar et al., 2017, Pollak et al., 2017, Katsel et al., 2017). While studies of BBB dysfunction in schizophrenia have been limited, there is evidence for TJ abnormalities in other neuropsychiatric disorders. In autism spectrum disorder, (ASD), post-mortem studies have identified increases in levels of claudin-3/5/12 mRNA and tricellulin mRNA in the cortex with increased levels of claudin-5/12 in the cerebellum. Additionally, levels of claudin-5 protein were increased in the cortex and cerebellum of ASD patients while claudin-12 was decreased in the cortex of ASD patients (Fiorentino et al., 2016). Additional insights into the role of the BBB in neuropsychiatric disorders has been garnered from animal models. In a stress-induced model of depression, stress was associated with reduced expression of claudin-5 and occludin and neurovascular dysfunction (Santha et al., 2015). Similarly, stress induced increases in the permeability of the BBB to intravenously injected tracers (Esposito et al., 2001) and to Evans blue (Sharma and Dey, 1981). However, the link between stress and BBB dysfunction is controversial (Roszkowski and Bohacek, 2016). Recently, the role of claudin-5 in depression was evaluated in the chronic social defeat stress model, a mouse model of depression, where loss of claudin-5 in the nucleus accumbens was associated with increased depression-like behaviours and infiltration of the peripheral cytokine interleukin-6. This behavioural phenotype could be rescued following chronic anti-depressant treatment (Menard et al., 2017). However, functional studies of BBB specific components and their involvement in schizophrenia and other neuropsychiatric disorders have been limited.

3.1.1 The rs10314 variant

The rs10314 SNP is a G to C base change in the 3’ untranslated region (UTR) of the claudin-5 gene. Previous association studies have identified a nominal but significant association between the rs10314 SNP with schizophrenia (Sun et al., 2004, Ye et al., 2005, Wu et al., 2010, Omidinia et al., 2014). In a study of 176 Chinese trios consisting of mothers, fathers and affected patients with schizophrenia, three SNPs were analysed with rs10314 being the only SNP associated with schizophrenia (Sun et al., 2004). In a replication study with a larger sample size, Ye and colleagues identified a stronger

association (P = 0.007) of the rs10314 SNP with schizophrenia (Ye et al., 2005). The rs10314 SNP has also been shown to strongly associate with schizophrenia in combination with other variants. A study of the combined effects of the rs10314 SNP with SNPs of the DQB1 gene revealed a significant association between rs10314 and rs3189152 with schizophrenia (Wei and Hemmings, 2005a). In an association study of 131 British trios consisting of mothers, fathers and affected offspring, the rs10314 SNP strongly associated with schizophrenia in combination with the BanI SNP in the PLA2G4A gene which is involved in the phospholipid metabolism pathway (Wei and Hemmings, 2005b). These findings suggest that abnormalities of TJs may be involved in schizophrenia as a result of changes in permeability in the brain and gut. As 22q11DS patients contain only one copy of the claudin-5 gene, the main goal of this chapter was to identify if the rs10314 allele was associated with schizophrenia in a cohort of individuals with 22q11DS with or without a diagnosis of schizophrenia. Working with collaborators in the Department of Psychiatry, RCSI (*Dublin, Ireland*), Department of Paediatrics, Duke University (*North Carolina, United States*) and the Department of Psychological Medicine and Neurology, Cardiff University (*Cardiff, United Kingdom*). DNA samples were obtained from 22q11DS patients for sequencing across their remaining claudin-5 allele. Additionally, how the rs10314 allele impacts claudin-5 protein expression and function was explored by transfecting wild-type and rs10314-containing plasmid constructs into Hek293 and caco-2 cells. Working in collaboration with the Stanley Medical Research Institute, post-mortem formalin-fixed free-floating brain tissue was obtained from 48 schizophrenia disease donors and age-matched controls for analysis of BBB TJ proteins in these conditions. While I conducted these experiments blind to neuropathological diagnosis, I received the diagnostic information from the Stanley Medical Research Institute afterwards. Additionally, the chapter explores the effect of anti-psychotic drugs on TJ protein expression and barrier integrity in *in vitro* models of the BBB as well as *in vivo* in wild-type C57BL/6 mice.

3.1.2 Objectives

- To examine the association of the rs10314 allele with schizophrenia in 22q11DS patients
- To determine the effect of the rs10314 allele on claudin-5 function *in vitro*
- To examine schizophrenia donor brain tissue for BBB dysfunction

- To investigate the biological activity of anti-psychotic drugs in primary mouse BMVECs
- To examine the effects of anti-psychotic drugs on BMVEC in C57BL/6 mice

3.2 Results

3.2.1 The rs10314 variant is associated with schizophrenia in 22q11DS patients

Given the previous findings of an association of the claudin-5 rs10314 allele in the general schizophrenia population, the first aim of this chapter was to examine the association of the rs10314 SNP with schizophrenia in individuals with 22q11DS. 22q11DS patients are haploinsufficient for claudin-5 so they contain either the G or C allele. DNA samples were obtained with consent prior to sequencing studies from a cohort of 65 22q11DS patients consisting of 52 individuals with no diagnosis of psychosis and 13 individuals with a diagnosis of schizophrenia. Following sequencing across the remaining claudin-5 allele, there was a significant association (*P = 0.038, Chi-square test) between the claudin-5 C variant (rs10314) and those 22q11DS patients who had developed schizophrenia (Figure 3.1). Five out of 13 22q11DS patients with schizophrenia contained the C allele and 8 out of 52 22q11DS patients without schizophrenia contained the C allele (Figure 3.1A).

A

Patients	Normal (G-allele)	rs10314 (C-allele)
Schizophrenia	8	5
No schizophrenia	44	8

B

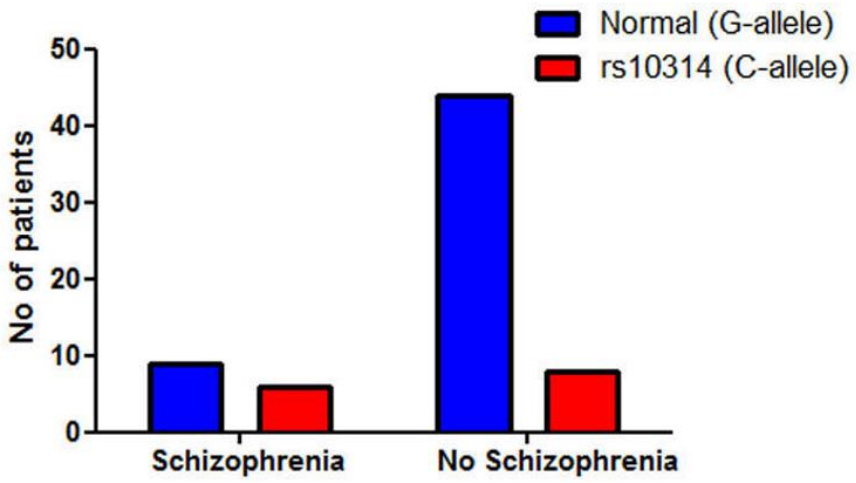

Figure 3.1: The rs10314 SNP is significantly associated with schizophrenia in 22q11DS patients. **(A)**, **(B)** A 3'UTR SNP, rs10314, on the remining claudin-5 allele in a cohort of 65 22q11DS patients is significantly associated with schizophrenia. *P = 0.0388, Chi-square test.

3.2.2 Effect of the rs10314 variant on claudin-5 expression *in vitro*

Having identified an association between the rs10314 SNP and schizophrenia, *in vitro* experiments were designed to investigate the functional effect of this SNP on claudin-5 protein and transcript levels. To address this, two human claudin-5 cDNAs with 3'UTRs containing the G and C alleles of the rs10314 SNP respectively, were sub-cloned into the HindIII/XhoI site of the pcDNA3EGFP vector. The expression plasmids were then transfected into Hek293 cells and claudin-5 levels were determined by western blot and RT-PCR analysis. Following transfection of the plasmid constructs into Hek293 cells, western blot analysis revealed the rs10314 variant (C allele) lead to lower levels of claudin-5 protein in cells (Figure 3.2 A, C) with no change in claudin-5 mRNA expression (Figure 3.2E) compared to normal (G allele). This experiment was repeated in a cell line with established TJ proteins. The Caco-2 cell line is a human colorectal adenocarcinoma cell line that expresses several TJ components including claudin-2, claudin-3, claudin-4, occludin and ZO-1. Following transfection of the plasmid constructs, western blot analysis revealed the rs10314 variant (C allele) lead to lower levels of claudin-5 protein in cells (Figure 3.2 B, D) with no change in claudin-5 mRNA expression (Figure 3.2 F) compared to normal (G allele) similar to the results obtained in the Hek293 experiment.

The distribution of claudin-5 protein was observed in Hek293 cells by immunocytochemical analysis. Following transfection of the normal and variant alleles, claudin-5 expression was detected primarily at the cell periphery in normal-transfected cells with intense staining evident at cell-cell contacts. However, in the variant transfected cells, claudin-5 localisation at cell-cell contacts was disrupted with increased perinuclear staining of claudin-5 as well as overall reduced staining intensity compared to normal (Figure 3.3).

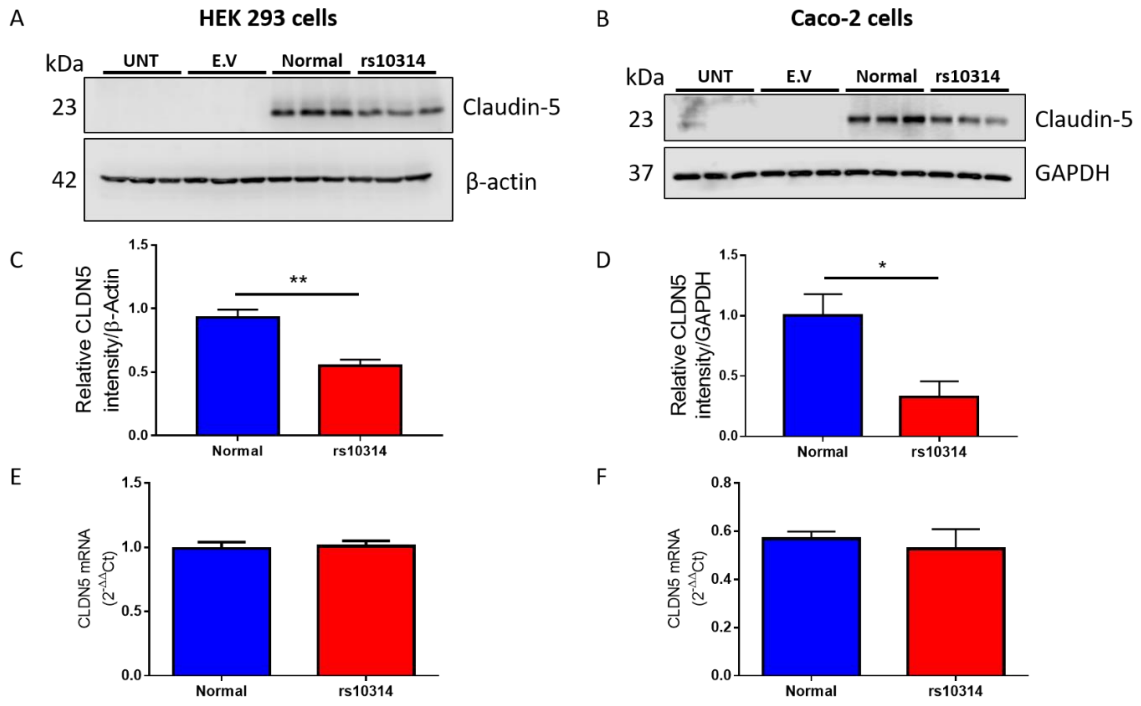

Figure 3.2: The rs10314 SNP leads to reduced claudin-5 protein levels *in vitro*. Western blot analysis of claudin-5 protein in **(A)** Hek293 cells and **(B)** Caco-2 cells 24 h post-transfection of normal or rs10314 plasmid constructs. Densitometry analysis of the western blots in **(A)** and **(B)** of claudin-5 protein levels 24 h post-transfection of normal or rs10314 plasmid constructs in **(C)** Hek293 cells and **(D)** Caco-2 cells. Image quantification was performed in *ImageJ*. β-actin and GAPDH were used to normalise the blots. RT-PCR analysis of claudin-5 in **(E)** Hek293 cells and **(F)** Caco-2 cells 24 h post-transfection of normal or rs10314 plasmid constructs. *P<0.05, **P<0.01 by Student's t-test compared to normal. All data are means ± SEM with n = 3 independent experiments.

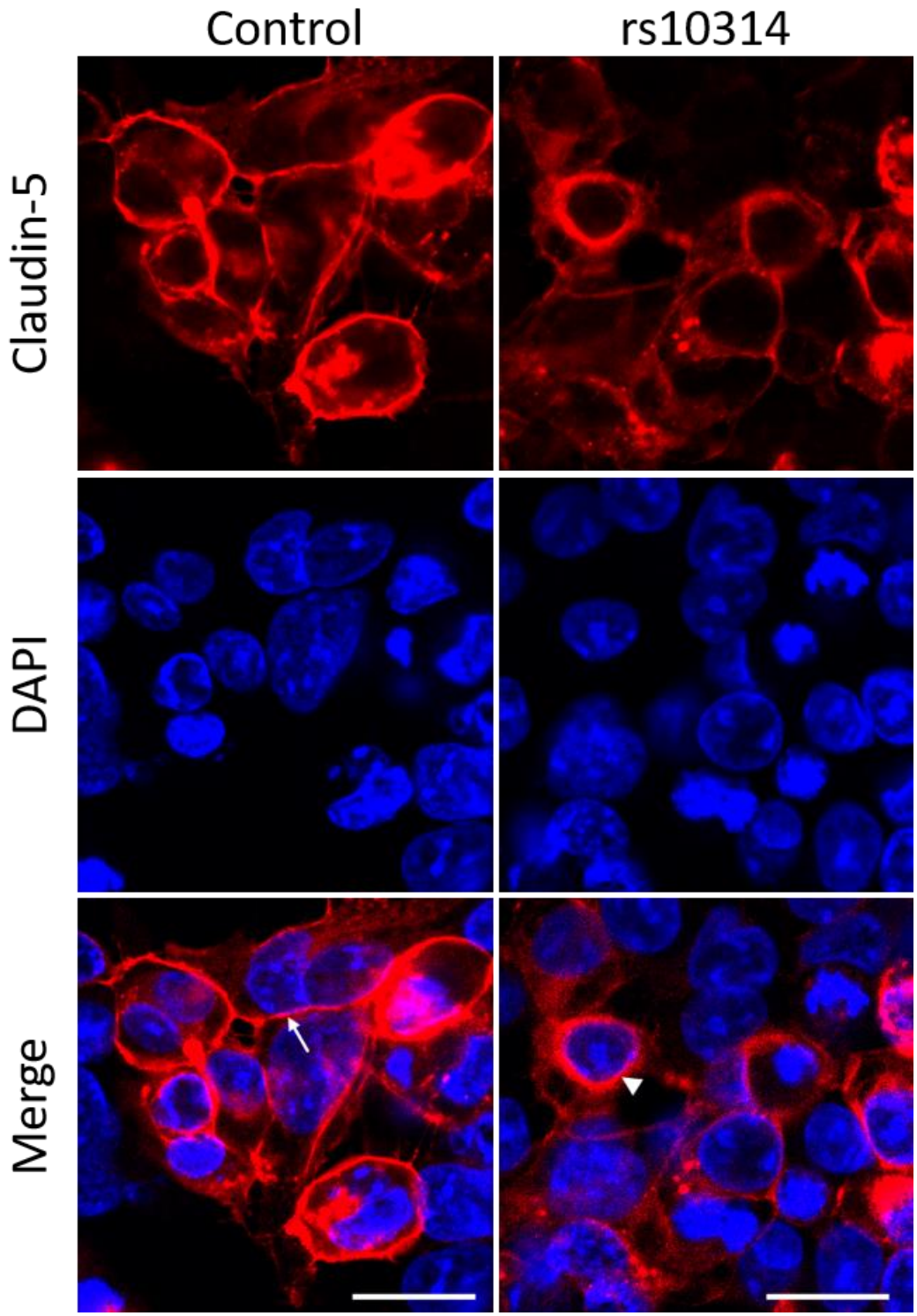

Figure 3.3: Immunocytochemical analysis of normal and rs10314 alleles in Hek293 cells. Immunocytochemical analysis of claudin-5 72 h post-transfection of normal or rs10314 plasmid constructs in Hek293 cells. Arrow points to membrane localisation of claudin-5 protein at cell-cell contacts. Arrowhead points to intracellular accumulation of claudin-5 protein. Scale bar – 20 µm.

3.2.3 Regulation of claudin-5 expression in the 3'UTR

The 3'UTRs of mRNA transcripts contain important sequences governing the fate of mRNA transcripts and subsequent protein synthesis. Together with many RNA-interacting partners, UTRs regulate stability of mRNA transcripts, export of mRNA to the cytoplasm, subcellular localisation and translational efficiency which all influence the amount of synthesised protein (Moore, 2005). RT-PCR analysis of Hek293 cells transfected with normal or risk alleles revealed no change in the expression of claudin-5 transcript between normal and rs10314 variants between 24 and 96 h post transfection (Figure 3.4A). Thus, it was hypothesised that the 3'UTR SNP could confer novel binding sites for trans-acting regulatory elements that could be influencing subsequent protein synthesis. Indeed, sequence analysis of the claudin-5 3'UTR revealed putative microRNA binding sites that may be affected by the rs10314 variant. Luciferase assays in Hek293 cells transfected with the normal and rs10314 variant revealed significant reductions in the promoter activity of cells containing the rs10314 variant. This reduction in promoter activity was rescued following transfection of two different miRNAs with binding capabilities in the claudin-5 3'UTR. where luciferase activity was restored to normal levels (Figure 3.4B, C).

Ribosomes dictate mRNA translation and protein synthesis, with polyribosomes (complex of mRNA and two or more ribosomes) contributing to translation of mRNA transcripts by synthesising the same protein at separate locations on the same mRNA. Polyribosome profiling separates translated mRNAs across a sucrose gradient according to the number of bound ribosomes with subsequent extraction of RNA providing a measure of the expression of mRNA in each ribosomal subunit. Hek293 cells were transfected with normal and risk rs10314 expression plasmids and 24 h post-transfection, polyribosome fractions were isolated, and RNA was extracted from each fraction. Subsequent analysis of polyribosome fractions isolated from Hek293 cells transfected with normal and rs10314 variant constructs revealed no differences in the A_{254} trace which shows the corresponding peaks of the 40S, 60S, 80S ribosomal subunits with each subsequent peak representing the polysome subunits. RT-PCR analysis of claudin-5 mRNA levels from individual ribosomal fractions revealed differences in the abundance of claudin-5 mRNA of each construct in the polyribosome fractions (Figure 3.5) inferring alterations in the translational efficiency of the claudin-5 protein occurs in the presence of the rs10314 variant.

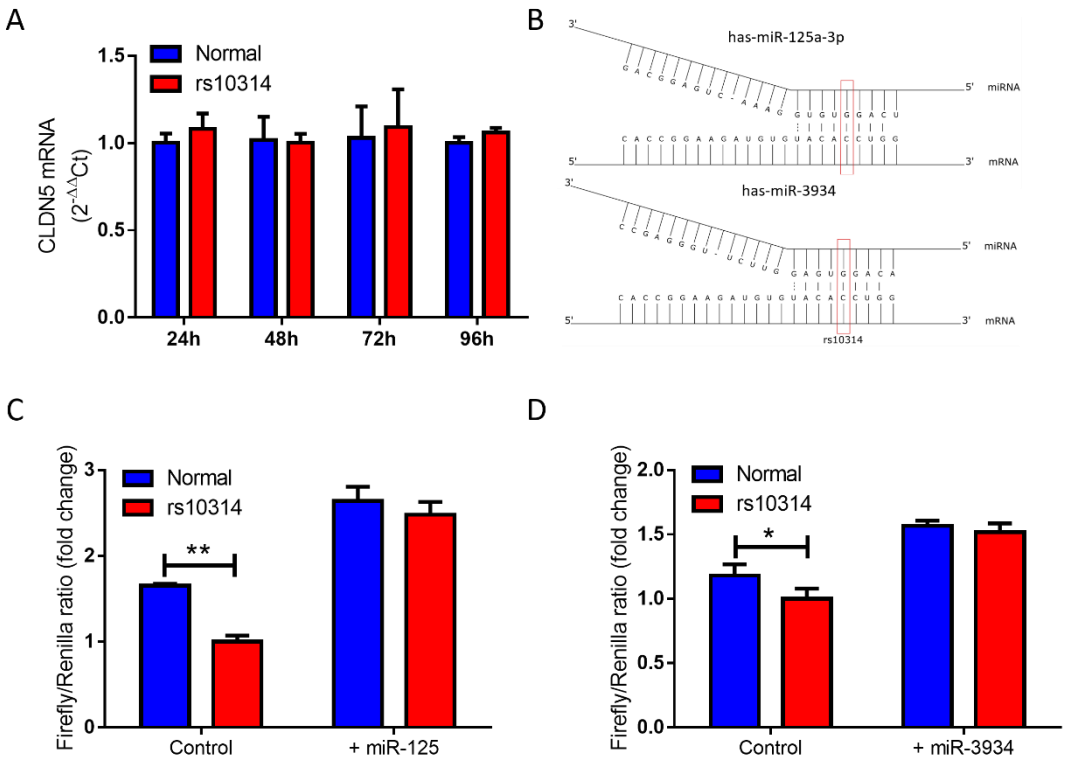

Figure 3.4: MicroRNA binding sites in the claudin-5 3'UTR. RT-PCR analysis of claudin-5 in **(A)** Hek293 cells 24-96 h post transfection of normal or rs10314 pcDNA3EGFP plasmid constructs. Luciferase analysis of Firefly/Renilla ratio (fold change) in Hek293 cells following co-transfection of normal or rs10314 plasmid and control or **(B)** hsa-mir-125a-3p or **(C)** hsa-mir-3934 microRNA. *P<0.05, **P<0.01 by two-way ANOVA with Bonferroni post-test. All data are means ± SEM with n = 3 independent experiments. Luciferase expression data was generated in conjunction with the lab of Jianghui Hou in Washington University.

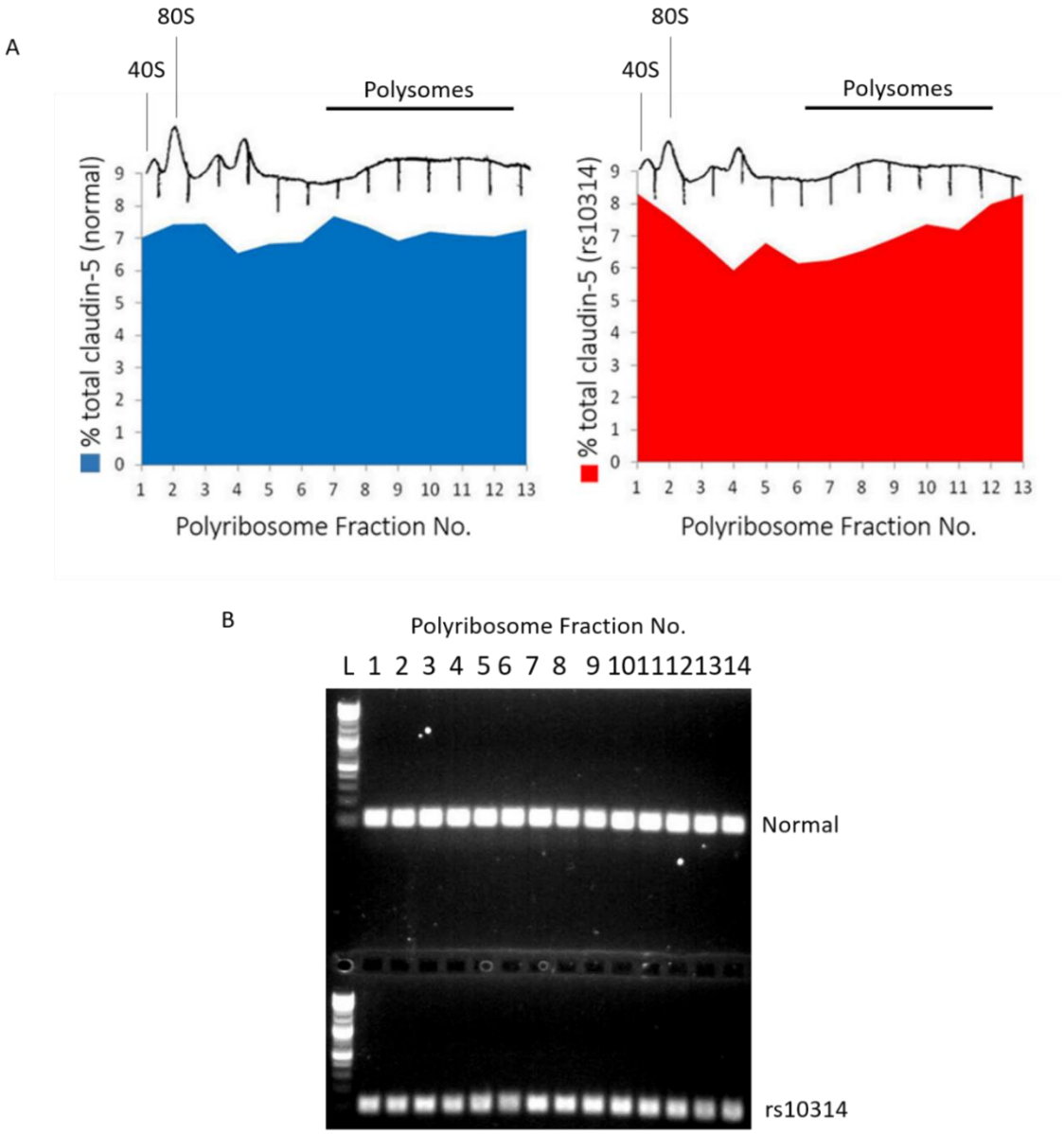

Figure 3.5: Polyribosome fractionation and RT-PCR analysis of claudin-5 mRNA. **(A)** RT-PCR analysis of claudin-5 mRNA in polyribosome fractions expressed as a percentage of total claudin-5 mRNA across all fractions. **(B)** Agarose gel of claudin-5 PCR products of mRNA isolated from polyribosome fractions from the normal (upper gel) and rs10314 (lower gel) alleles showing distinct differences in the levels of claudin-5 in the polyribosome fractions. Polyribosome fractionation was performed in conjunction with the lab of Susan Campbell at Sheffield Hallam University.

3.2.4 Reduced claudin-5 expression in post-mortem schizophrenia brain tissue

In collaboration with the Stanley Medical Research Institute (*Kensington, United States*), formalin fixed free-floating brain sections from a neurological disease cohort (48 patients in total) was obtained with the aim of characterising TJ protein integrity in the cerebral vasculature. Details on age, cause of death and post-mortem index (PMI) are detailed in Table 3.1. No individuals with 22q11DS were present in the examined cohort and the rs10314 genotype status was determined by DNA sequencing (Table 3.2). Blind to the neuropathological diagnosis, 60 µm thick free-floating brain sections from the inferior parietal lobule (IPL) were prepared for TJ protein immunohistochemistry.

Brain sections from each patient in the neurological disease cohort were analysed using the Nissl stain and separately, sections were labelled for GLUT-1 and the TJ protein claudin-5. Additionally, sections were dual-labelled with fibrinogen and IgG to assess barrier leakage in the patient cohort. Quantification of TJ staining pattern and intensity was accomplished with the Angiogenesis Analyzer for *ImageJ* which calculates the total stained length, number of branch points and breakages in the staining pattern. This was followed by confirmation of the neuropathological diagnoses from the Stanley Medical Research Institute. Initial analysis revealed a greater density of claudin-5 immunoreactivity in the grey matter compared to the white matter (data not shown), likely reflecting differences in capillary density in each region (Ballabh et al., 2004). Owing to these regional differences in capillary density, subsequent immunohistochemical analysis focussed on the grey matter only. Quantification of capillary density by immunohistochemical analysis of GLUT-1 revealed no significant differences between groups (Figure 3.6). Preliminary characterisation revealed discontinuous claudin-5 immunoreactivity in over 60% of schizophrenia patients when assessed in a blinded manner (Figure 3.7). 3D reconstructed images from Z-stacks of claudin-5 staining revealed intact claudin-5 vessel immunoreactivity in patient samples from control cases. In contrast, discontinuous claudin-5 vessel immunoreactivity was evident in schizophrenia patient brain tissue (Figure 3.8). Subsequent analysis revealed that discontinuous claudin-5 immunoreactivity correlated with the presence of the rs10314 variant (Figure 3.8). Finally, immunohistochemical analysis revealed that fibrinogen (340 kDa) and IgG (150 kDa) were retained within the cerebral vasculature of control and schizophrenia cases (Figure 3.9).

Table 3.1: Descriptive variables of brain tissue used in this study.

Characteristics of the sample group used in this study		
Characteristics	Normal	Schizophrenia
Patient number	24	24
Sex	M	M
Age (years)	44.3 ± 9.3	39.8 ± 10.8
Brain pH	6.68 ± 0.21	6.53 ± 0.23
PMI	29.42 ± 10.8	29.08 ± 11.6
Causes of death		
Cardiac	18	8
Cirrhosis	0	1
Myocarditis	1	0
Pneumonia	0	3
Suicide	0	6
Acute Pancreatitis	0	1
Pulmonary embolism	1	0
Alcohol poisoning	1	0
OD	0	2
MVA	2	0
Bronchopneumonia	0	1
Asthma	1	1
Unknown	0	1

Table 3.2: Genotype status for rs10314 SNP.

Rs10314	G/G	G/C	C/C
Control	19	5	0
Schizophrenia	18	6	0

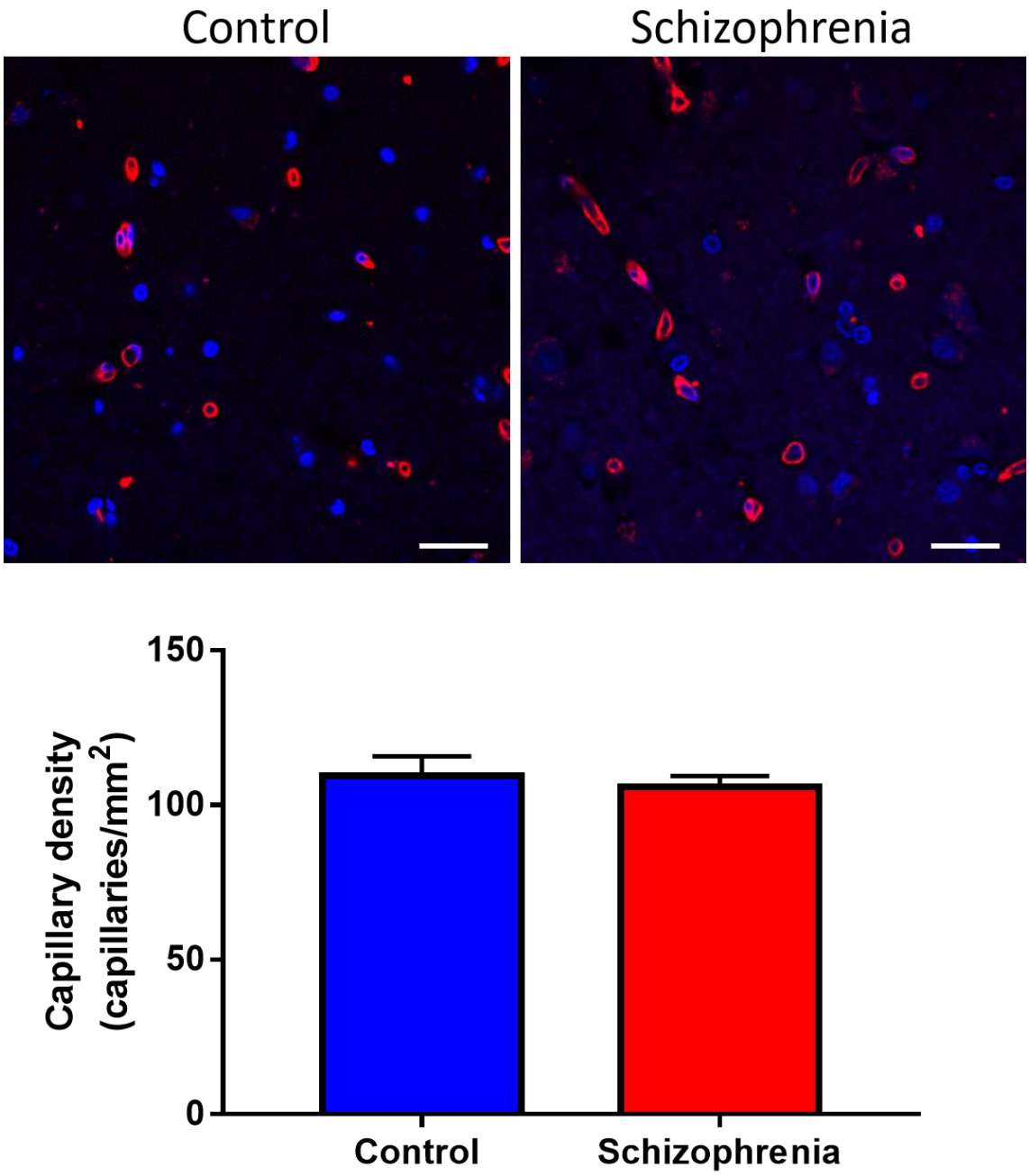

Figure 3.6: Immunohistochemicacl analysis of GLUT-1 in the IPL. Top image – Immunohistochemical analysis of GLUT-1 in control and schizophrenia IPL. Bottom image – quantification of capillary density. Scale bar – 50 µm. All data are means ± SEM.

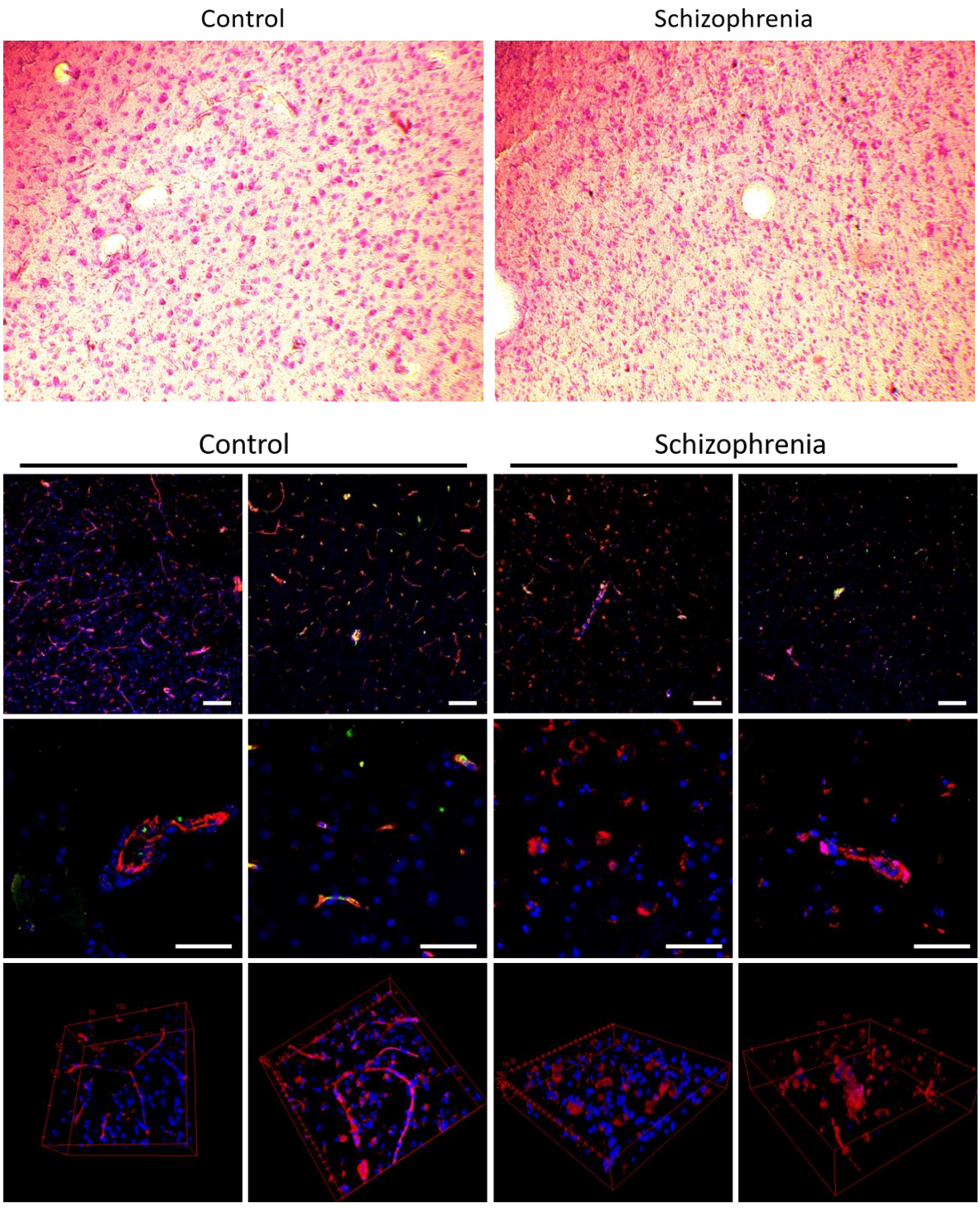

Figure 3.7: Immunohistochemical analysis of claudin-5 in the IPL. Top image – Free-floating IPL brain sections stained with cresyl violet acetate to identify Nissl bodies in neurons. Bottom images - Free-floating IPL brain sections stained with claudin-5. 3D reconstructed images of Z-stacks are shown on the bottom panel. Scale bar (top panel) – 50 µm, (middle panel) – 20 µm.

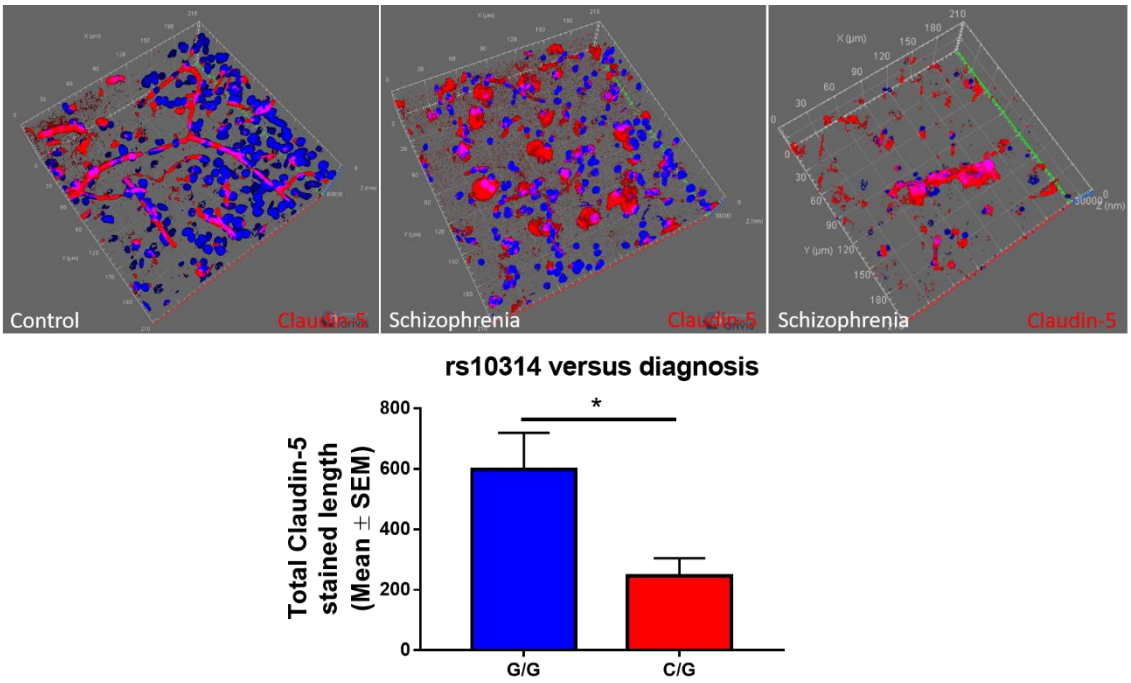

Figure 3.8: Claudin-5 dysfunction in schizophrenia brain tissue. Top - 3D reconstructions of Z-stack images showing claudin-5 distribution in control and schizophrenia donor sections. Bottom - Claudin-5 levels are significantly decreased in schizophrenic individuals harbouring one copy of the C allele. Image analysis was performed with the Angiogenesis Analyzer plugin in *ImageJ.* *P<0.05 by Student's t-test. All data are means ± SEM with n = 6 for G/G and n = 5 for C/G genotypes.

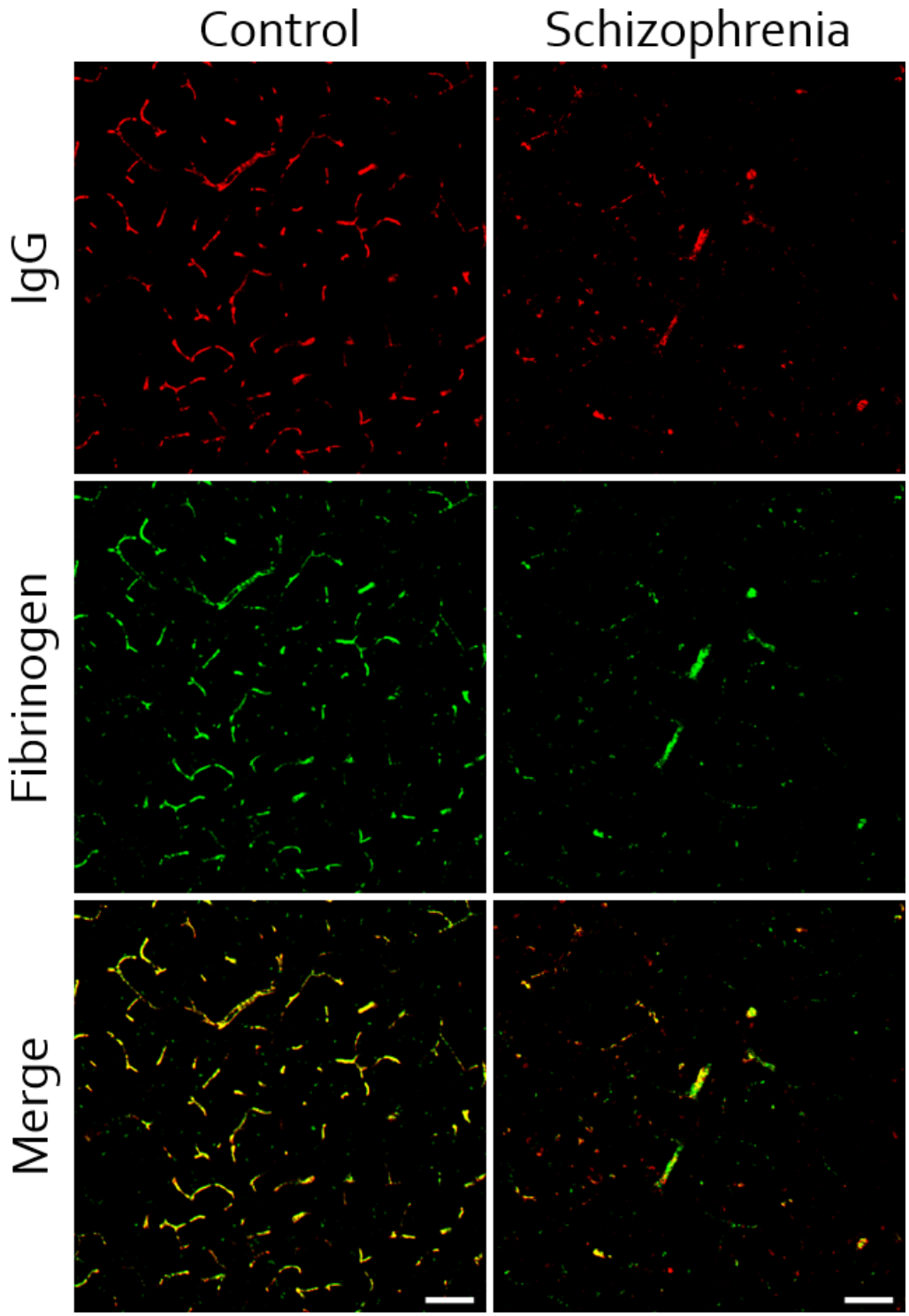

Figure 3.9: Immunohistochemical assessment of BBB leakage in the IPL of control and schizophrenia cases. Immunohistochemical analysis of IgG (150 kDa) and fibrinogen (300 kDa) in the IPL of schizophrenia and age-matched control brains. Scale bar – 50 µm.

3.2.5 Anti-psychotic drugs regulate TJ protein levels and barrier permeability *in vitro*

Characterisation of claudin-5 at the BBB in schizophrenia patients indicated that reductions in levels of claudin-5 were pervasive in the IPL of these patients. Previous studies have identified potential physiological roles for anti-psychotics in regulating microvascular endothelial cell integrity and viability (Elmorsy et al., 2014, Elmorsy and Smith, 2015). As the patient cohort assessed in this study had history of anti-psychotic use, the following experiments investigated the effect of anti-psychotic drugs on BBB components *in vitro* and *in vivo*. Primary mouse BMVEC were isolated from C57BL/6 mice and treated with increasing concentrations of the anti-psychotic drugs CPZ and HAL for 24 h. Cells were also treated with LiCl, a clinically used treatment for schizoaffective disorder. Western blot analysis of protein lysates revealed dose-dependent increases in the protein levels of claudin-5 in LiCl, HAL and CPZ treated cells (Figure 3.11).

Results from the western blot analyses indicated that anti-psychotic drugs increased claudin-5 protein levels. To further investigate the relationship between anti-psychotic drugs and BBB integrity, flux analysis was performed. Primary mouse BMVECs were grown on transwell inserts and TEERs were recorded daily to determine cell confluency as TEER values increase until confluency is reached. Once confluency was reached, LiCl, HAL or CPZ was added to the apical chamber and cell permeability was measured 24 h later. A FITC-dextran paracellular tracer flux assay was conducted to analyse cell permeability. 70 kDa FITC-dextran was applied to the apical chamber of the transwell insert and the amount of FITC-dextran that moved into the basolateral chamber was measured over a 2 h period by taking samples from the basolateral compartment every 15 minutes and measured by fluorescence spectrophotometry. The concentration of FITC-dextran and the apparent permeability (P_{app}) was significantly decreased in cells treated with LiCl and CPZ but not HAL compared to untreated cells indicating that anti-psychotic drugs decreased the permeability in these cells and that FITC-dextran was more restricted from moving across the monolayer of primary mouse BMVEC from the apical to basolateral chambers (Figure 3.12). Immunocytochemical analysis of TJ proteins revealed no major morphological differences or levels of claudin-5 and ZO-1 in primary mouse BMVEC treated with each anti-psychotic (Figure 3.13).

In the subsequent set of experiments, the effect of anti-psychotic drugs on cell viability was determined. Primary mouse BMVECs were examined after administration of LiCl, HAL, CPZ, OLZ and CZP at physiological and non-physiological concentrations. Cell viability was measured using the MTS assay in response to increasing doses of LiCl, HAL, CPZ, OLZ and CZP for 24 h, 48 h and 72 h. Anti-psychotics were cytotoxic to primary mouse BMVEC as assessed by the inability of BMVECs to reduce tetrazolium to formazan at concentrations above 10 µM in LiCl, CPZ, HAL and CZP treated cells, concentrations of drugs typically observed in overdose patients (Figure 3.14).

The WNT signalling pathway is a known regulator of claudin-5 and previous studies have shown that LiCl can activate WNT signalling by inhibiting GSK3β activity. Therefore, it was next examined if anti-psychotic drugs could activate this pathway by examining downstream targets of the WNT signalling pathway including axin-2 and sox-17. Treatment of primary mouse BMVEC with anti-psychotics produced a non-significant trend for increased expression of axin-2 and sox-17 (Figure 3.15).

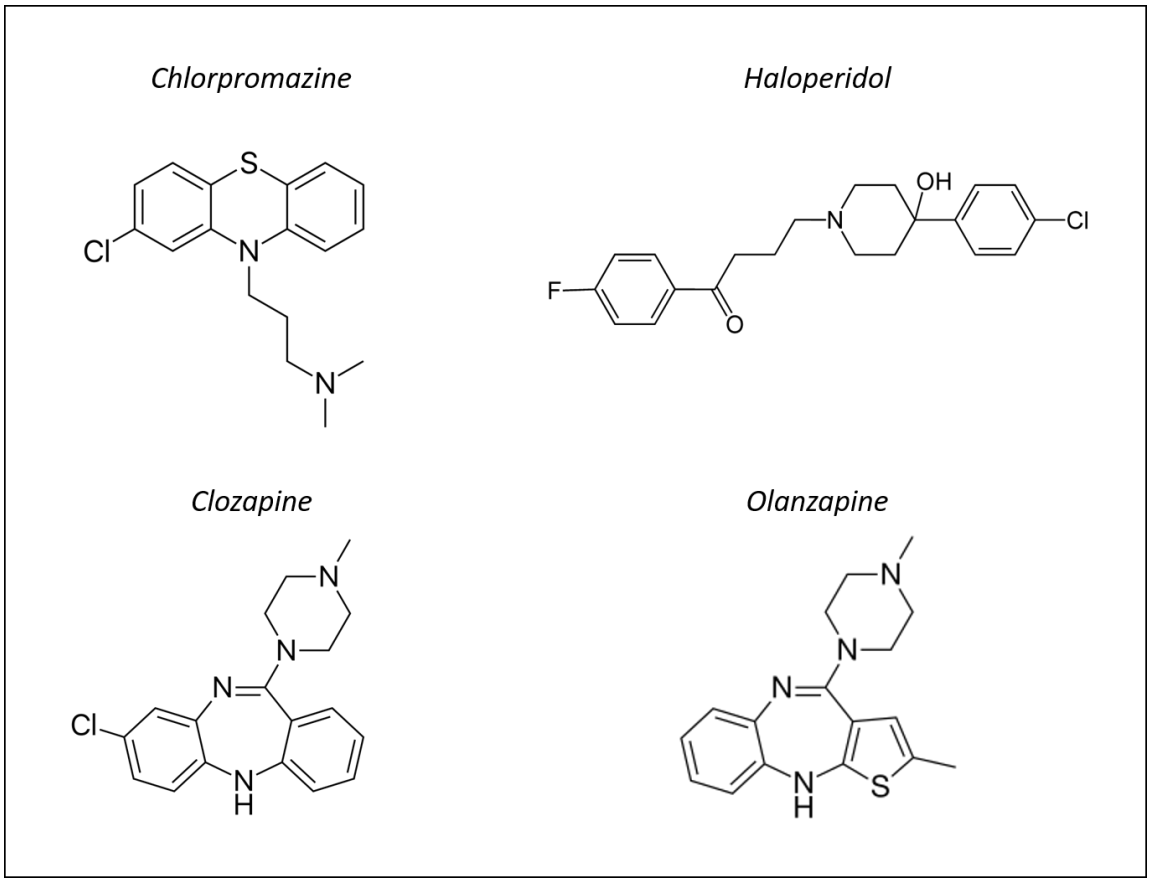

Figure 3.10: Chemical structures of the various anti-psychotics used.

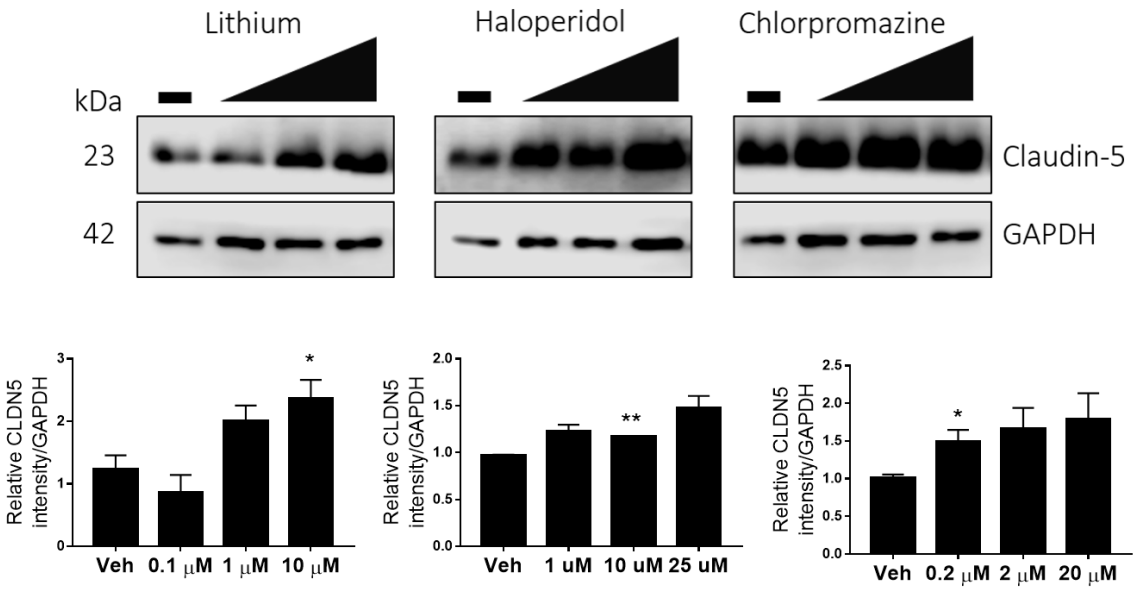

Figure 3.11: Effect of anti-psychotic drugs on claudin-5 protein levels in primary mouse BMVECs. Western blot analysis and densitometric analysis of claudin-5 in primary mouse BMVECs treated with increasing concentrations of Lithium chloride (LiCl) (0.1, 1, 10 mM), haloperidol (HAL) (0.2, 2, 20 µM) and chlorpromazine (CPZ) (0.2, 2, 20 µM) for 24 h. GAPDH was used to normalise the blots. *ImageJ* was used for densitometry analysis. *P<0.05, **P<0.01 by ANOVA with Bonferroni post-test. All data are means ± SEM with n = 3 independent experiments.

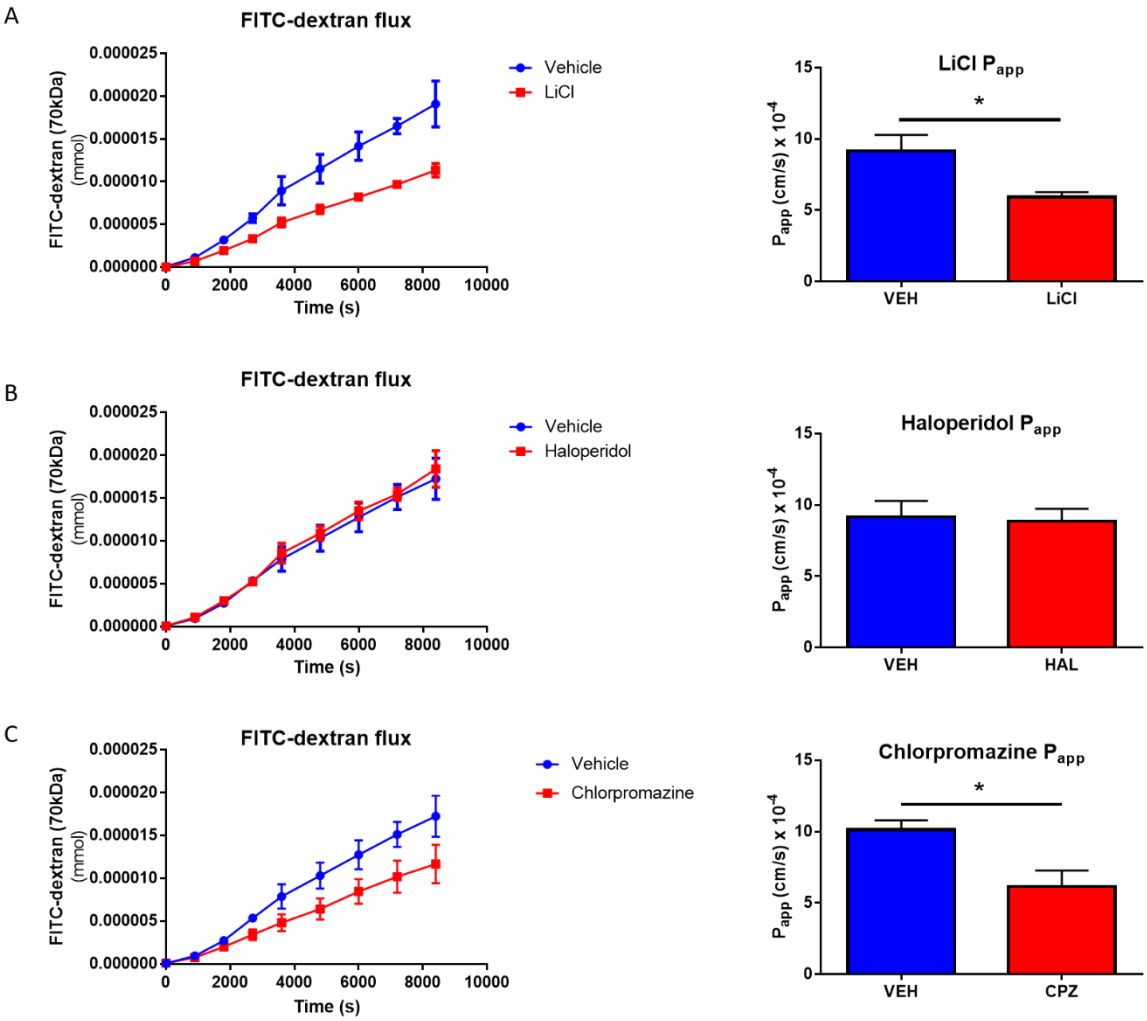

Figure 3.12: Assessment of paracellular permeability in primary mouse BMVECs following anti-psychotic treatment. Primary mouse BMVECs were grown on collagen IV/fibronectin coated transwell inserts and treated with **(A)** LiCl, **(B)** HAL and **(C)** CPZ for 24 h before application of 70 kDa FITC-dextran (1 mg/ml) to the apical compartment. Flux of FITC-dextran across primary mouse BMVEC was monitored over a 2 h time course by fluorescence spectrophotometry. The P_{app} was calculated for all treatments. *P<0.05 by Student's t-test. All data are means ± SEM with n = 3 independent experiments.

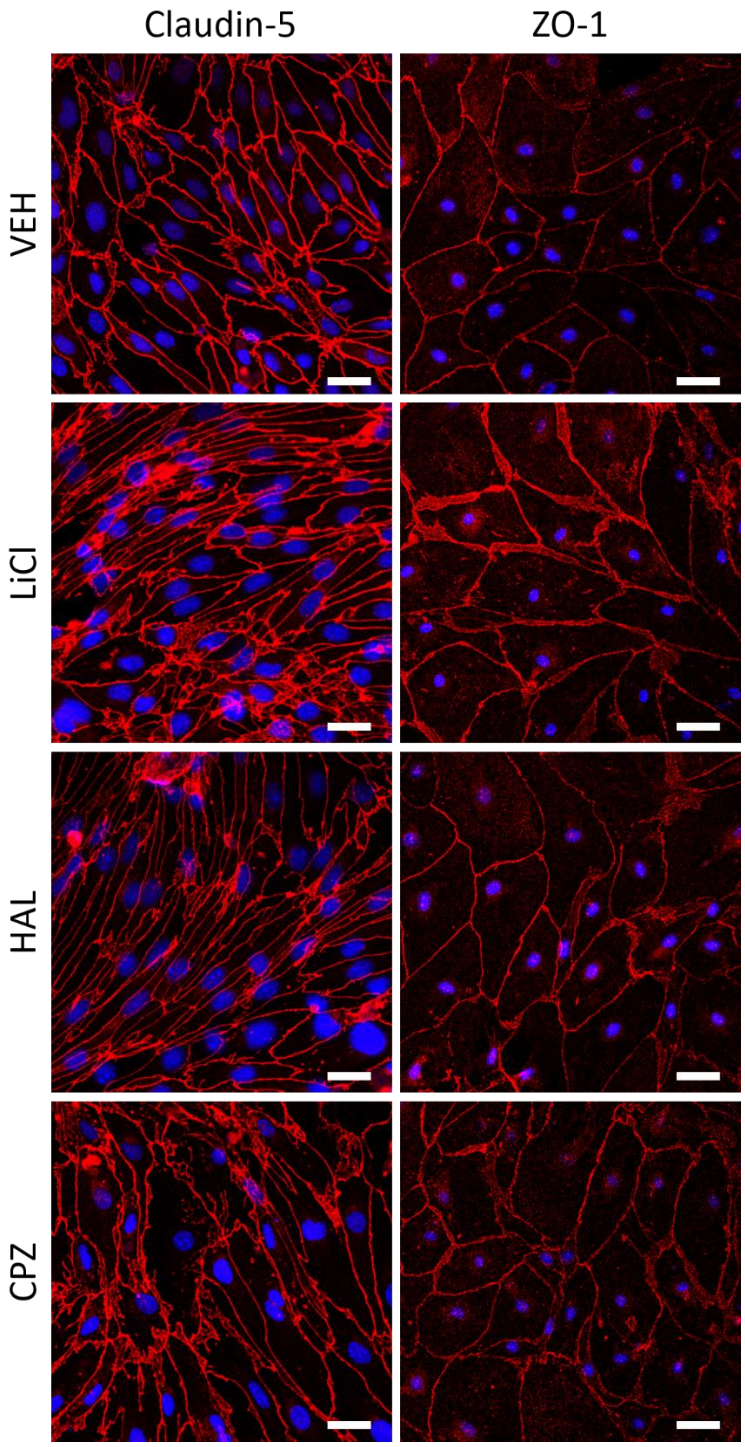

Figure 3.13: Immunocytochemical analysis of TJ proteins following anti-psychotic treatment. Immunocytochemical analysis of claudin-5 and ZO-1 in primary mouse BMVEC 24 h following treatment with LiCl, HAL and CPZ. Scale bar - 50µm.

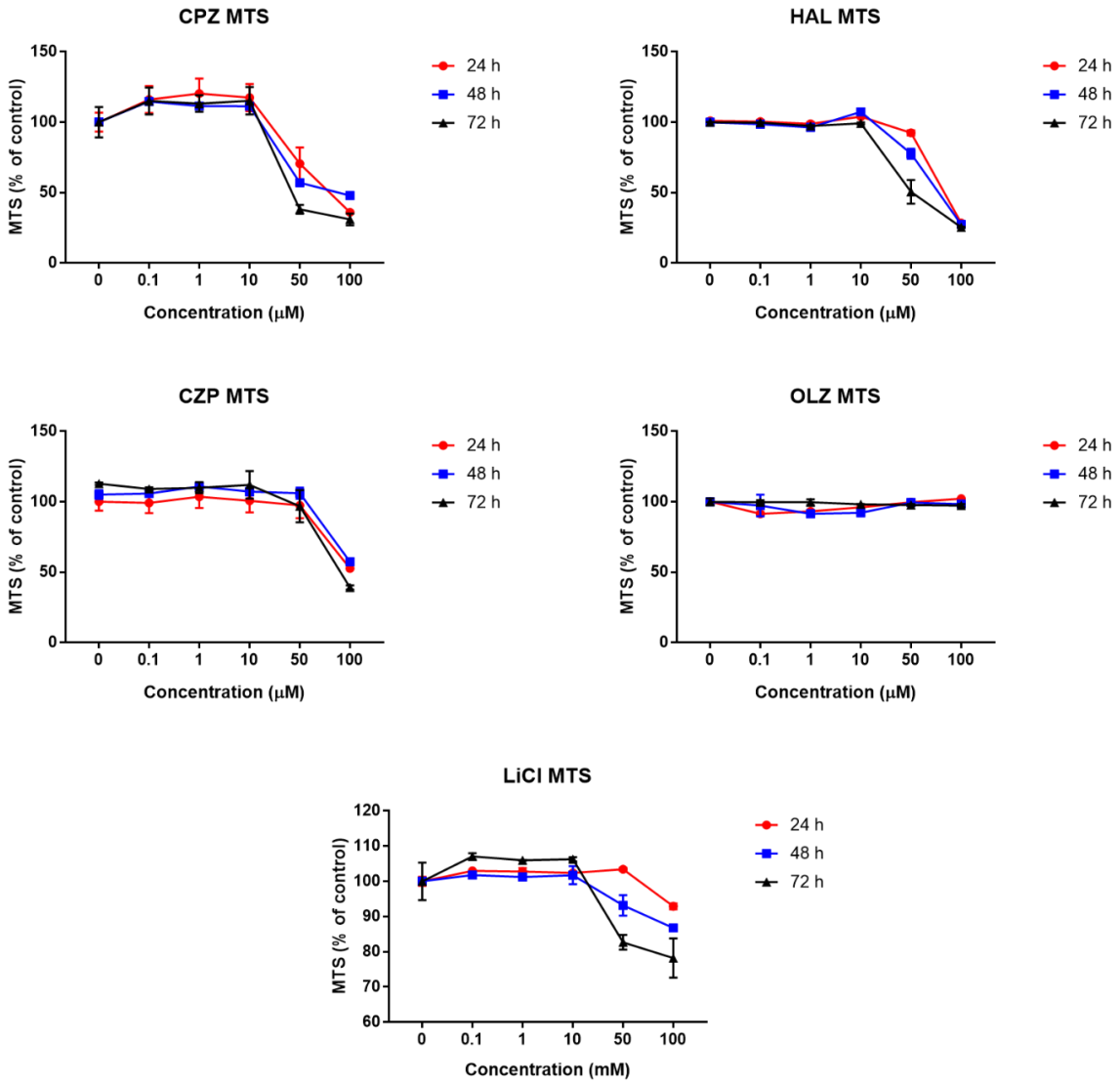

Figure 3.14: Effect of anti-psychotic drugs on primary mouse BMVEC cell viability. MTS assay following treatment with the indicated anti-psychotic drugs on primary mouse BMVEC cells for 24, 48 and 72 h. CPZ = chlorpromazine, HAL = haloperidol, CZP = clozapine, OLZ = olanzapine, LiCl = lithium chloride.

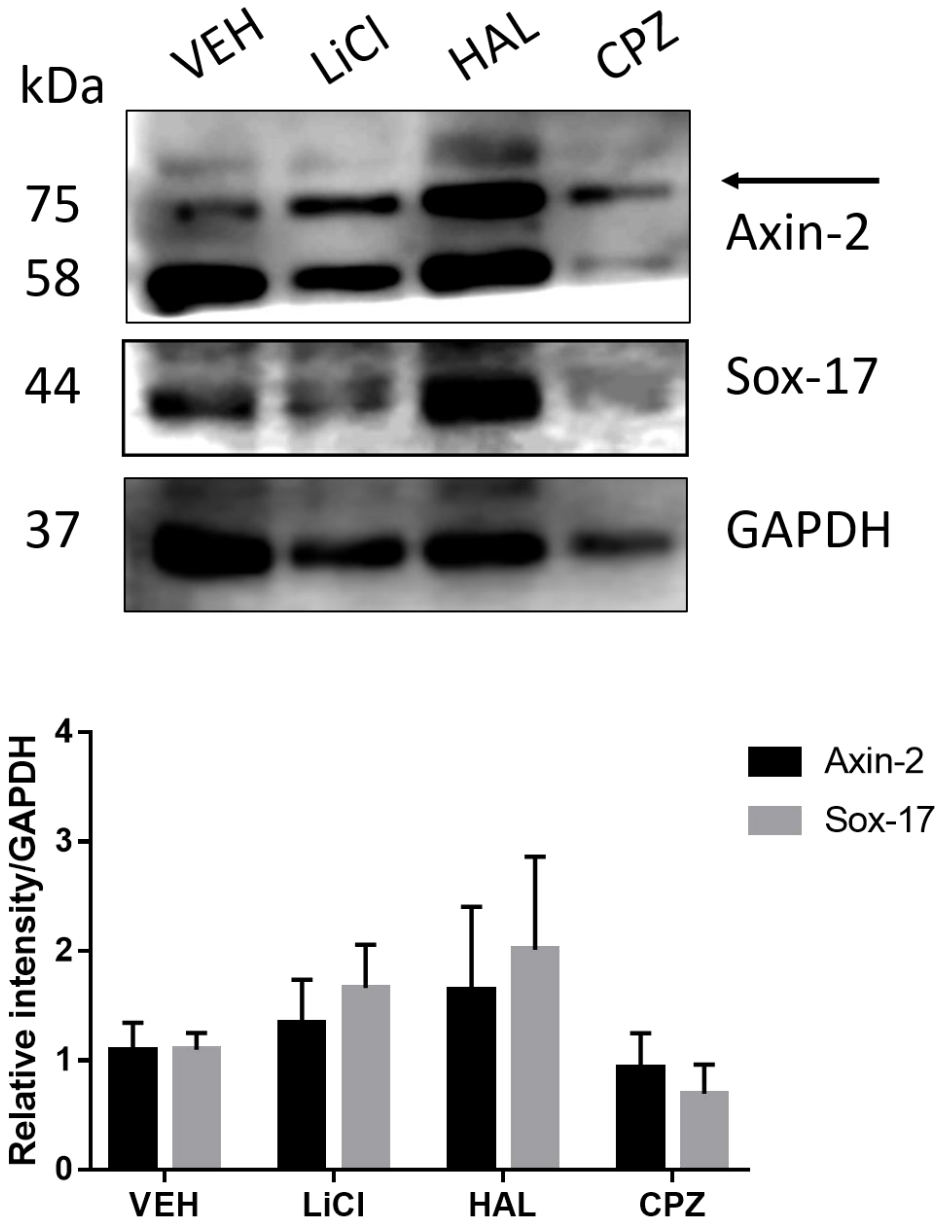

Figure 3.15: Effect of anti-psychotics on WNT signalling components in primary mouse BMVECs. Western blot analysis of Axin-2 and Sox-17 protein in primary mouse BMVECs treated with LiCl, HAL and CPZ for 24 h. GAPDH was used to normalise the blot. *ImageJ* was used for densitometry analysis. All data are means ± SEM with n = 3 independent experiments.

3.2.6 Effect of anti-psychotic drugs on BMVEC *in vivo*

The data presented here indicates that anti-psychotic drugs can potently regulate TJ protein levels in cultured ECs *in vitro* and regulate the paracellular permeability of cultured primary mouse BMVEC, however the physiological role of anti-psychotic drugs on ECs *in vivo* has never been established. To explore this, C57BL/6 mice were injected with a single I.V dose of vehicle control (PBS, 2.5 % polyethylene glycol 400), 100 mg/kg LiCl, 1 mg/kg CPZ and 1 mg/kg HAL via the tail-vein. 24 h later, mice were sacrificed, and the brains were removed for subsequent isolation of capillaries for western blot and RT-PCR analysis. Western blot analysis revealed significantly increased levels of claudin-5 protein in LiCl, HAL and CPZ injected mice compared to vehicle control injected mice. RT-PCR analysis revealed significantly increased levels of claudin-5 transcript in CPZ treated mice (Figure 3.16) with no change in transcript levels of occludin, ZO-1 or tricellulin. Additionally, LiCl and HAL treatment significantly increased occludin protein levels in primary mouse BMVEC 24 h following treatment (Figure 3.17 A, B) while CPZ increased ZO-1 protein levels and HAL and CPZ significantly increased tricellulin protein levels in cerebral microvessels isolated from C57BL/6 mice (Figure 3.17 D, F).

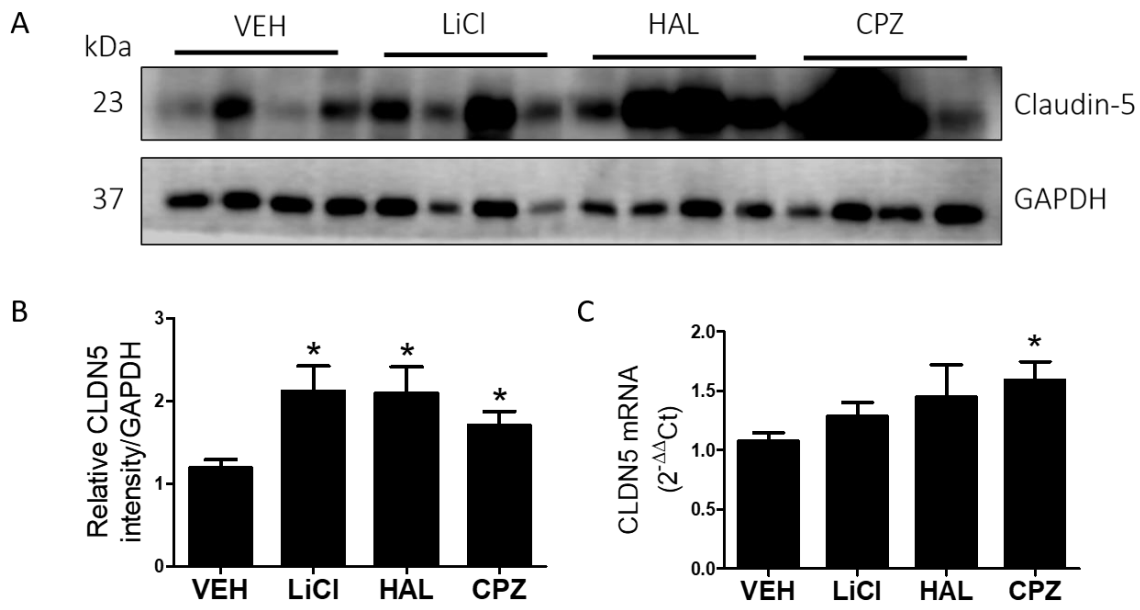

Figure 3.16: Systemic injection of anti-psychotics increase claudin-5 protein and mRNA levels in C57BL/6 mice. **(A)** Western blot analysis of claudin-5 in cerebral microvessels isolated from C57BL/6 mice 24 h following I.V injection of LiCl (100 mg/kg), HAL (1 mg/kg) and CPZ (1 mg/kg). **(B)** *ImageJ* was used for densitometry analysis. **(C)** RT-PCR analysis of claudin-5 in cerebral microvessels isolated from C57BL/6 mice 24 h following treatment with LiCl (100 mg/kg), HAL (1 mg/kg) and CPZ (1 mg/kg) by I.V injection. *P<0.05 by ANOVA with Bonferroni post-test. All data are means ± SEM with n = 4 per group.

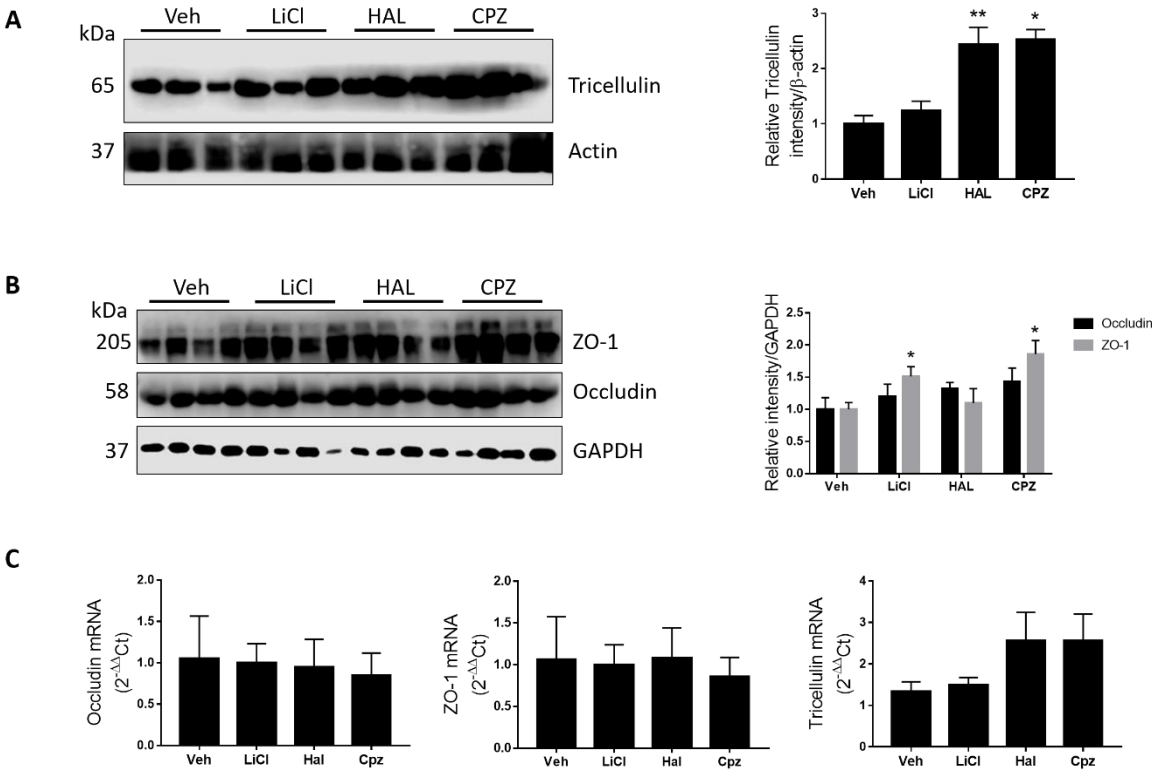

Figure 3.17: Anti-psychotic drugs regulate TJ protein levels *in vivo*. Western blot analysis of **(A)** tricellulin and **(B)** occludin and ZO-1 protein levels in isolated cerebral microvessels from C57BL/6 mice 24 h following I.V injection of LiCl (100 mg/kg), HAL (1 mg/kg) and CPZ (1 mg/kg). GAPDH and β-actin was used to normalise the blots. *ImageJ* was used for densitometry analysis. **(C)** RT-PCR analysis of occludin, ZO-1 and tricellulin in isolated cerebral microvessels from C57BL/6 mice 24 h following I.V injection of LiCl (100 mg/kg), HAL (1 mg/kg) and CPZ (1 mg/kg). *P<0.05, **P<0.01 by ANOVA with Tukey post-test All data are means ± SEM with n = 3-4 per group.

3.3 Discussion

In this study, DNA samples were collected from individuals with 22q11DS and their remaining claudin-5 allele was sequenced for the rs10314 SNP. By sequencing across the remaining claudin-5 allele in a cohort of 65 individuals with 22q11DS, it was confirmed that the rs10314 C allele significantly associated with schizophrenia in 22q11DS patients. This agreed with the previous findings in the general schizophrenia population. Within the 22q11 deleted region there are 6 susceptibility genes that have been reported as candidate genes for association with schizophrenia. Of these genes (COMT, PRODH, ZDHHC8, CLDN5, DGCR14, DGCR2), COMT has been the most intensively studied (Arinami, 2006) however several independent association studies have now highlighted the association between a SNP in the claudin-5 3'UTR with schizophrenia.

While the overall numbers of participants in this association study were small, the numbers reflect similar numbers used in several other studies of 22q11DS (Carmel et al., 2014, de Koning et al., 2015, Radoeva et al., 2014) and is in fact one of the largest cohorts of 22q11DS patient samples in the world. 22q11DS patients have only one functioning copy of the claudin-5 allele and the presence of 3'UTR mutations could have major impacts on the paracellular flux of molecules between the blood and brain in these individual. As such, the next aim of this chapter was to determine the effect of the rs10314 variant on the expression, regulation and localisation of the protein product of claudin-5. 3'UTR mutations are known to interfere with the processing, localisation and translation and degradation of mRNA transcripts. Transfection studies in Hek293 cells revealed that the rs10314 variant allele **(C)** produced up to 50% less claudin-5 protein compared to the normal allele **(G)**. Hek293 cells do not contain TJ components so this first experiment was designed to determine the effect of the SNP on claudin-5 expression in the absence of endogenous TJ components. Additional studies in Caco-2 cells revealed that this deficit in claudin-5 protein expression was not cell-type specific with similar changes detected comparable to Hek293 transfected cells. This shows that the presence of endogenous TJ components does not abrogate the reductions in claudin-5 protein expression observed with the C allele. If individuals with 22q11DS were to also harbour the rs10314 risk allele they may theoretically produce up to 75% less claudin-5 protein compared to individuals with two copies of the claudin-5 allele. It will be important in future to perform expression analysis on brain tissue from 22q11DS patients to determine the level of expression of claudin-5 in individuals with and without the rs10314 risk allele. However, at present

there are no brain banks containing 22q11DS donor brains. One post-mortem study has been performed from four individuals with 22q11DS. Kiehl and colleagues revealed post-mortem neuropathological features in four individuals with a confirmed diagnosis of 22q11DS and schizophrenia. Three out of four cases displayed severe astrocytic gliosis as well as abundant collection of macrophages in the cerebral white matter. Cerebrovascular hypertensive-type changes were also evident with vascular thickening and perivascular pallor (Kiehl et al., 2009). These findings suggest a potential microvascular pathology in the brains of 22q11DS patients with a confirmed diagnosis of schizophrenia. Further evidence for microvascular anomalies in 22q11DS patients has been identified by ocular examination of 90 patients. 34% of individuals with 22q11DS were found to have a tortuous retinal vasculature along with several other ocular defects (Forbes et al., 2007). Cerebral and retinal vessels share similar embryological origins and are as such, structurally and functionally homologous (Patton et al., 2005). Imaging retinal vessels may provide a non-invasive method to identify vascular abnormalities in individuals with 22q11DS and indeed, in the wider schizophrenia population. In fact, in a recent study, Meier *et al* used *in vivo* retinal imaging in 27 individuals with schizophrenia and identified wider retinal venules in schizophrenics compared to controls. Additionally, wider retinal venules were associated with childhood psychosis symptoms and with a dimensional measure of adult psychosis symptoms (Meier et al., 2013). Wider retinal venules are suspected to result from cumulative structural damage to the microvasculature and indicate problems with oxygen supply to the brain (de Jong et al., 2008).

Having established an effect of the rs10314 on levels of claudin-5 protein, the subsequent experiments were designed to determine the mechanism behind this. Overall, while claudin-5 mRNA levels were unchanged, luciferase assays revealed significant differences between the normal and rs10314 allele indicating differences in transcriptional regulation of the mRNA transcript. Given the number of regulatory sequences present in the 3'UTR of genes, microRNA binding sites were identified, and two microRNAs were found to bind and upregulate claudin-5 mRNA to levels that were similar between the normal and rs10314 allele. It is likely that the 3'UTR SNP is interfering with the function of some trans-interacting factor. The 3'UTRs contain binding sites for ribosome binding proteins and as such, future studies are required to determine the exact nature of these claudin-5 deficits especially given the differences

observed in the abundance of claudin-5 mRNA in polyribosomal subunits in the rs10314 risk allele compared to normal.

Post-mortem histological studies have been paramount to identifying dysfunctional proteins and aberrant cellular networks in the schizophrenic brain. One of the least studied regions that is known to be involved in schizophrenia is the inferior parietal lobe (IPL). The IPL forms part of the posterior parietal cortex, a region involved in integrating sensory information from various modalities and is important in language processing. The IPL along with the superior parietal lobe are key regions for the recognition of self and for integrating incoming sensory information (Singh-Curry and Husain, 2009). One of the earliest and most common symptoms in schizophrenia is a disruption of sensory integration. Despite this, the IPL has been one of the least studied regions. Several studies have identified structural differences in the IPL with 6 out of 10 studies reporting significant decreases in volume, 3 reporting increases and another identifying positive correlations between decreased volume and the severity of symptoms (Torrey, 2007). Reduced CBF has also been reported in the IPL (Liddle et al., 1992), hinting at microvasculature disruption in the region. Here, it was assessed if there was evidence for BBB dysfunction in the brains of 24 schizophrenia cases and 24 age-matched controls. This was the first such study examining TJ components in schizophrenia brains. Initially the abundance of capillaries in control and schizophrenic brains was examined by immunohistochemical analysis of GLUT-1. The density of capillaries was calculated, and no significant differences were detected between control and schizophrenia groups. Next, TJ patterns of immunoreactivity and intensity was examined. Immunohistochemical analysis revealed discontinuous, mis-localised claudin-5 staining in the brains of the schizophrenia donors. Interestingly, by genotyping each patient for the presence of the rs10314 allele, it was found that the rs10314 allele was associated with reduced claudin-5 expression in individuals with schizophrenia, suggesting that the rs10314 allele affects the expression levels of claudin-5 *in vivo*, reaffirming the results from the *in vitro* investigations. Claudin-5 is known to be crucial for impeding the paracellular diffusion of material from blood to brain, therefore an assessment was made of the permeability of the microvasculature to endogenous serum proteins. Fibrinogen is a 340 kDa glycoprotein that is involved in the maintenance of processes involved in blood clotting. Leakage of serum proteins into the brain parenchyma is a known consequence of CNS insults. Previous studies have shown that fibrinogen leakage into the brain parenchyma can

induce microglial activation and exacerbate BBB dysfunction (Ryu and McLarnon, 2009). It was found that the IPL of schizophrenia brains remained intact to the larger molecular weight proteins (>150 kDa) IgG and fibrinogen. In the absence of low molecular weight markers to detect BBB dysfunction in post-mortem studies, estimates of the size-selectivity of the BBB in post-mortem schizophrenia brain tissue was difficult to deduce. In this regard, high-resolution MRI scans will be pivotal to determining slight changes in vessel permeability in individuals with schizophrenia, or indeed by *in vivo* retinal imaging as mentioned above. More recently, a study was carried out assessing the intensity and localisation of claudin-5 in post-mortem schizophrenia donor brain tissue. Here, Nishiura *et al.* found significant decreases in claudin-5 protein in the prefrontal cortex but not the visual cortex of schizophrenia patients compared to controls. The authors also observed increases in claudin-5 mRNA levels in the prefrontal cortex. Additionally, the barrier remained intact to fibrinogen and IgG (Nishiura et al., 2017).

The primary treatment option for schizophrenia is anti-psychotic therapy, however, these drugs are used to treat psychosis symptoms of the disorder including delusions, hallucinations and paranoia with limited treatment options available for the negative symptoms of schizophrenia. Many studies have highlighted the adverse effects of anti-psychotic drugs in psychiatric patients, yet few studies have examined the impact of these drugs on the cerebral vasculature. Indeed, brain ECs are one of the first cell types that these drugs will encounter prior to entering the CNS and previously, it has been shown in *in vitro* models of the BBB that anti-psychotic drugs have adverse effects on microvascular ECs at high therapeutic concentrations (Elmorsy et al., 2014, Elmorsy and Smith, 2015). In the study by Elmorsy and colleagues, human brain microvascular endothelial cells were exposed to high therapeutic doses of the typical anti-psychotics CPZ and HAL and the atypical anti-psychotics CZP and risperidone and cell viability, programmed cell death and barrier permeability were assessed. At high therapeutic doses, all drugs significantly reduced cell viability as a result of caspase activation and apoptosis. At EC_{50} concentrations, anti-psychotics enhanced the permeability of Evans blue across a monolayer of ECs. Intriguingly, at lower concentrations the drugs were found to reduce the permeation of tracer molecules across a monolayer of BMVEC and to increase the transendothelial electrical resistance (TEER), indicating an enhancement of barrier properties (Elmorsy et al., 2014). In this chapter, it was found that several typical and atypical anti-psychotic drugs could increase the expression levels of claudin-5 protein in

an *in vitro* model of the BBB using primary mouse BMVEC. This increase in the expression of TJ proteins may explain the findings from previous studies where at certain concentrations, anti-psychotic drugs could enhance barrier properties in an *in vitro* BBB model. Additionally, administration of anti-psychotic drugs to the apical chamber of a monolayer of primary mouse BMVEC could reduce the permeation of a 70 kDa tracer molecule, indicating that they could enhance barrier tightness. To investigate the potential mechanism behind the regulation of TJ protein levels, components of the WNT signalling pathway including Axin-2 and SOX-17 were analysed by western blot. LiCl is a potent inhibitor of GSK3β that prevents degradation of β-catenin in the proteasome (van Noort et al., 2002). Western blot analysis of WNT signalling components revealed no differences between anti-psychotic treated cells and controls, however further effectors of the WNT pathway should be interrogated.

As CNS ECs have a crucial role in the uptake of anti-psychotic drugs to the brain parenchyma, assessing the safety and toxicity of anti-psychotic drugs in BMVEC is of importance. Short term addition of physiological and non-physiological doses of anti-psychotic drugs onto primary mouse BMVEC significantly reduced BMVEC cell viability and disrupted morphology. Therapeutic plasma concentrations for CPZ, HAL, CZP, OLZ have been reported at 50 to 300 ng/ml (0.15 to 1 μM), 5 to 12 ng/ml (0.01 to 0.03 μM), 300 to 700 ng/ml (1 to 2 μM) and 20 to 40 ng/ml (0.06 to 0.13 μM) respectively (Rivera-Calimlim et al., 1976, Van Putten et al., 1992, Chang et al., 1997, Rao et al., 2001). Anti-psychotic concentrations above therapeutic doses were cytotoxic to BMVEC for CPZ and CZP while concentrations over 30 times greater than therapeutic doses were required to induce cytotoxic effects for HAL. BMVEC were resistant to OLZ at concentrations up to 100 μM. To assess the effect of anti-psychotic drugs on the BBB *in vivo,* C57BL/6 mice were injected with therapeutic concentrations of LiCl, HAL and CPZ and capillary fractions were isolated from the brains of these mice 24 h following I.V injection. Western blot data of capillary lysates isolated from the brains of the injected mice showed an increase in TJ protein levels after anti-psychotic administration. In addition to the negative side-effects associated with anti-psychotic drugs, up to 23% of schizophrenia patients show no response to therapy (Lally et al., 2016). ECs of the CNS restrict the entry of amphiphilic compounds such as anti-psychotics to the brain. Anti-psychotics acting on neurotransmission need access to the brain and differences in PGP functionality leading to variable brain concentrations of these drugs may be responsible

for this variability in therapeutic response. One study found that behavioural changes in Mdr1a/b knockout mice following treatment with the atypical anti-psychotic risperidone was dependent on the expression of PGP (Pacchioni et al., 2010). Several anti-psychotics are potent PGP substrates including: amisulpride, aripiprazole, olanzapine, risperidone and paliperidone. One anti-psychotic therapy that is not a PGP substrate is clozapine which is of interest given its efficacy in treatment-resistant schizophrenia. In addition, PGP polymorphisms have been associated with clinical drug response, particularly with regards to clozapine, olanzapine and risperidone (Wolking et al., 2015). The impact of anti-psychotics on the BBB, particularly on the activity of PGP, may influence clinical drug response in individuals with schizophrenia. In addition, findings in this thesis showing that anti-psychotic drugs can upregulate TJ proteins and strengthen the barrier may influence the bioavailability of these drugs in the CNS. Further studies are required to determine the chronic effect of anti-psychotic drugs on the BBB and on the brain uptake of these drugs.

Taken together, these results show that claudin-5 deficits are evident in individuals with schizophrenia, with a 3'UTR SNP associating with schizophrenia in individuals with 22q11DS, one of the largest known genetic risk factors for schizophrenia. The result of this SNP is a dysfunctional claudin-5 protein that is also evident in post-mortem tissue from individuals with schizophrenia. Additionally, anti-psychotic drugs are biologically active in brain ECs and can upregulate the expression of key TJ proteins that are fundamental to the barrier properties of the BBB. In chapter 4, the role of claudin-5 in regulating the BBB will be explored and mouse models of localised BBB disruption will be used to determine the effect of regional specific suppression of claudin-5 towards the development of schizophrenia-like behaviour will be explored.

3.5 Conclusions

- The rs10314 SNP is associated with schizophrenia in 22q11DS patients.
- The rs10314 SNP interferes with claudin-5 protein synthesis.
- Claudin-5 is downregulated in the brains of schizophrenia patients.
- The rs10314 allele is associated with reduced claudin-5 expression in post-mortem schizophrenic brain tissue.
- Anti-psychotic drugs dose-dependently increase BBB proteins *in vitro* and *in vivo.*

- Anti-psychotic drugs at higher than therapeutic concentrations induce EC cytotoxicity and barrier breakdown.

Chapter 4:

Assessment of behavioural phenotype in wild-type mice *in vivo* following RNAi-mediated down-regulation of claudin-5 in specific neural regions and in a doxycycline-inducible knockdown mouse

4.1 Introduction

A small number of neurons (<8) are supplied by a single capillary with some suggestions that every neuron in the brain has its own capillary (Zlokovic, 2008). As such, it can be hypothesised that BBB dysfunction can increase the permeability of the BBB to potentially damaging endogenous blood components that may impact the surrounding NVU and subsequently animal neurophysiology and behaviour. It is known that CNS disorders can induce localised BBB breakdown. In TBI, localised BBB dysfunction is associated with post-traumatic epilepsy. Likewise, in Alzheimer's disease, vascular deposition of Aβ is associated with loss of TJ proteins and increased BBB permeability (Biron et al., 2011, Hartz et al., 2012, Marco and Skaper, 2006). While *in vitro* models of the BBB based on the culture of primary or immortalized brain ECs have been used to study various aspects of BBB biology, it is difficult to model all aspects of a functional NVU *in vitro*. This includes interactions between several cell types and basement membranes and the cerebral circulation. As a result, *in vitro* models of the BBB have been able to recapitulate some but not all of the features of the BBB such as high TEER, low rate of flux, strong AJ and TJ protein expression and polarised expression of receptors. Therefore, *in vivo* measurements of BBB permeability remain the most reliable method to assess BBB permeability in pathological conditions.

As shown in chapter 3, a SNP in the 3'UTR of the claudin-5 gene was associated with schizophrenia in 22q11DS patients. The SNP was associated with reduced levels of claudin-5 protein *in vitro.* Additionally, levels of claudin-5 protein was found to be reduced in post-mortem schizophrenia brains as well as having discontinuous staining patterns. However, it is difficult to determine the contribution of reduced levels of claudin-5 to the development of schizophrenia including the development of various abnormal behaviours without relevant preclinical animal models. Thus, the first aim of this chapter was to assess the effect of downregulated expression of claudin-5 in distinct neural regions in the brains of C57BL/6 mice to determine the impact of downregulated claudin-5 levels on schizophrenia-related behaviour. The second aim of this chapter was to generate a mouse model that would facilitate inducible suppression of claudin-5 across the entire brain in mice. To this end, shRNAs designed to target claudin-5 transcripts were examined *in vitro* in mouse brain ECs and subsequently used for the generation of a doxycycline-inducible claudin-5 knockdown mouse. Subsequently, mice were characterised for claudin-5 suppression and size-selectivity of the BBB to tracer

molecules *in vivo*. Additionally, mice underwent phenotypic characterization for behaviours analogous to psychiatric disorders.

4.1.1 Objectives

- To site-specifically suppress claudin-5 with AAV vectors
- To examine the behavioural phenotypes in claudin-5 suppressed mice
- To generate and characterise a doxycycline-inducible claudin-5 knockdown mouse
- To explore the behavioural phenotype in claudin-5 knockdown mice

4.2 Results

4.2.1 Site-specific modulation of the BBB in C57BL/6 mice

To determine the effect of reduced levels of claudin-5 protein on BBB integrity *in vivo*, C57BL/6 mice were stereotaxically injected with an adeno-associated virus vector containing a doxycycline-inducible shRNA targeting claudin-5 transcripts or a NT scrambled control shRNA (Figure 4.2A), bilaterally into the dorsal hippocampus and medial prefrontal cortex (mPFC). The AAV contains a doxycycline-inducible shRNA targeting claudin-5 transcripts, the expression of which is activated in the presence of doxycycline. Doxycycline (2 mg/ml) was supplemented to the drinking water with 2 % sucrose. Injection of an AAV vector containing a doxycycline-inducible GFP showed the distribution of the virus in the dorsal hippocampus (Figure 4.2B) and mPFC (Figure 4.2C) following three weeks of doxycycline treatment. Immunohistochemical analysis of claudin-5 and isolectin-IB4 revealed significantly fewer claudin-5 positive blood vessels in the dorsal hippocampus and mPFC following three weeks of doxycycline treatment compared to NT injected control mice (Figure 4.3).

Following three weeks of doxycycline treatment, mice were injected I.V with a 2 mg/ml solution of Sulfo-NHS-biotin (600 Da) which was circulated for ten minutes before mice were sacrificed for brain removal. Immunohistochemical analysis of Sulfo-NHS-Biotin detected with a streptavidin cy3 conjugate revealed significant leakage of biotin in the dorsal hippocampus and mPFC compared to NT control mice where biotin was retained within the microvasculature. (Figure 4.4). As loss of TJs may be compensated for by up-

regulation of associated TJ components, immunohistochemical analysis of occludin and ZO-1 was performed. Suppression of claudin-5 did not affect the expression or localisation of occludin or the scaffolding protein ZO-1 in the mPFC (Figure 4.5 A) or dorsal hippocampus (Figure 4.5B). To determine the efficiency of AAV uptake, the number of GFP infected vessels was analysed to calculate the proportion of vessels containing the doxycycline-inducible AAV. Immunohistochemical analysis of GFP and isolectin-IB4 (Figure 4.6A) revealed approximately 45 % of vessels were infected with the AAV as determined by colocalization of GFP with isolectin-IB4. Additionally, suppression of claudin-5 in the dorsal hippocampus or mPFC did not induce vascular remodelling events as measured by isolectin-IB4 staining intensity and localisation (Figure 4.6C). Low magnification images revealed numerous leaky vessels in the region of interest (Figure 4.6D).

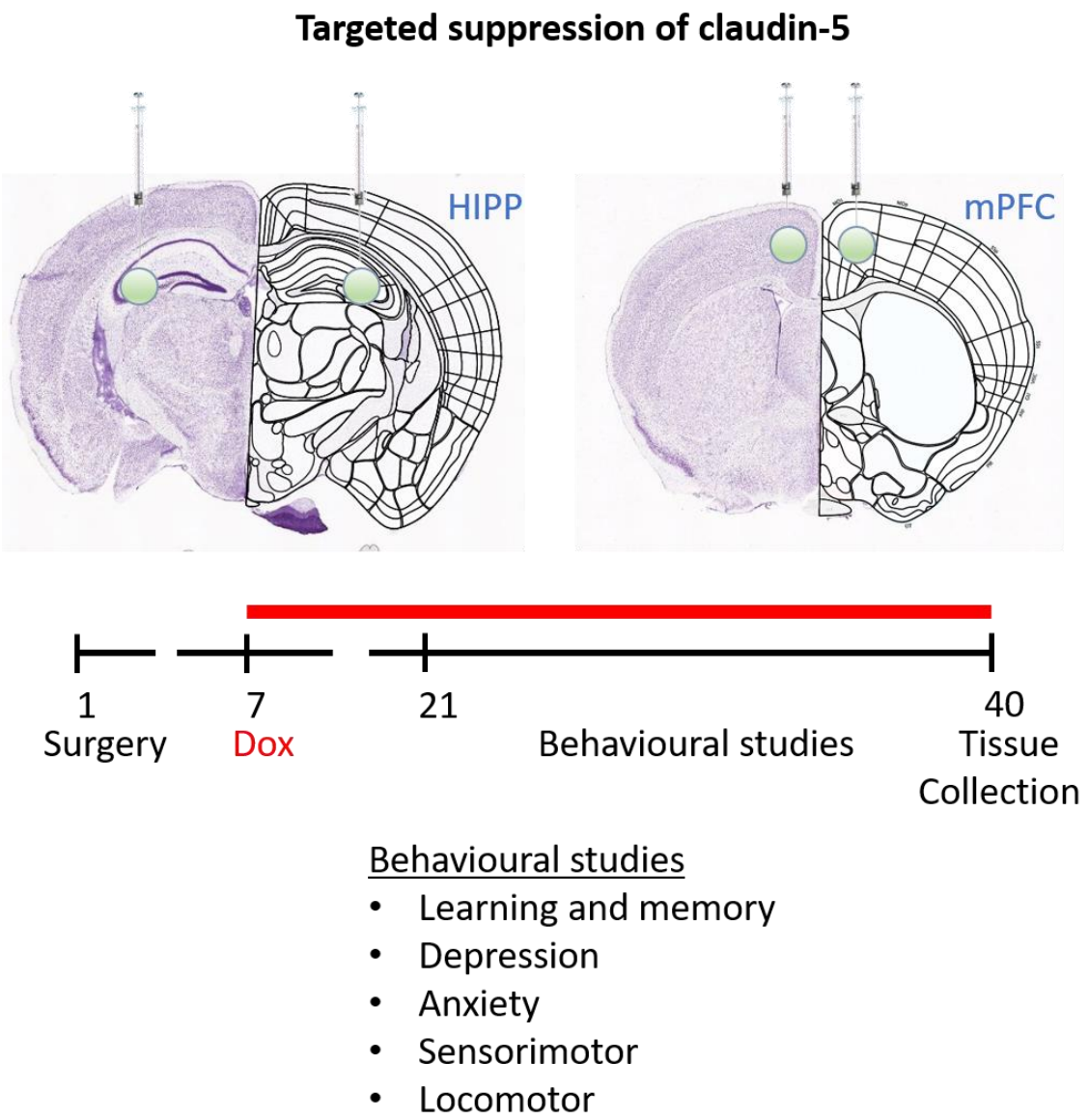

Figure 4.1: Experimental design for AAV2/9 studies. Stereotaxic injection coordinates were determined using the reference mouse brain atlas. C57BL/6 mice were bilaterally injected with adeno-associated virus vectors containing a doxycycline-inducible shRNA targeting claudin-5 transcript or a scrambled control shRNA into the dorsal hippocampus or mPFC. Mice were left to recover from surgery for 1 week before doxycycline (2 mg/ml, 2 % sucrose) was introduced to the drinking water. Behavioural studies began on day 21 and tissue was collected on day 40.

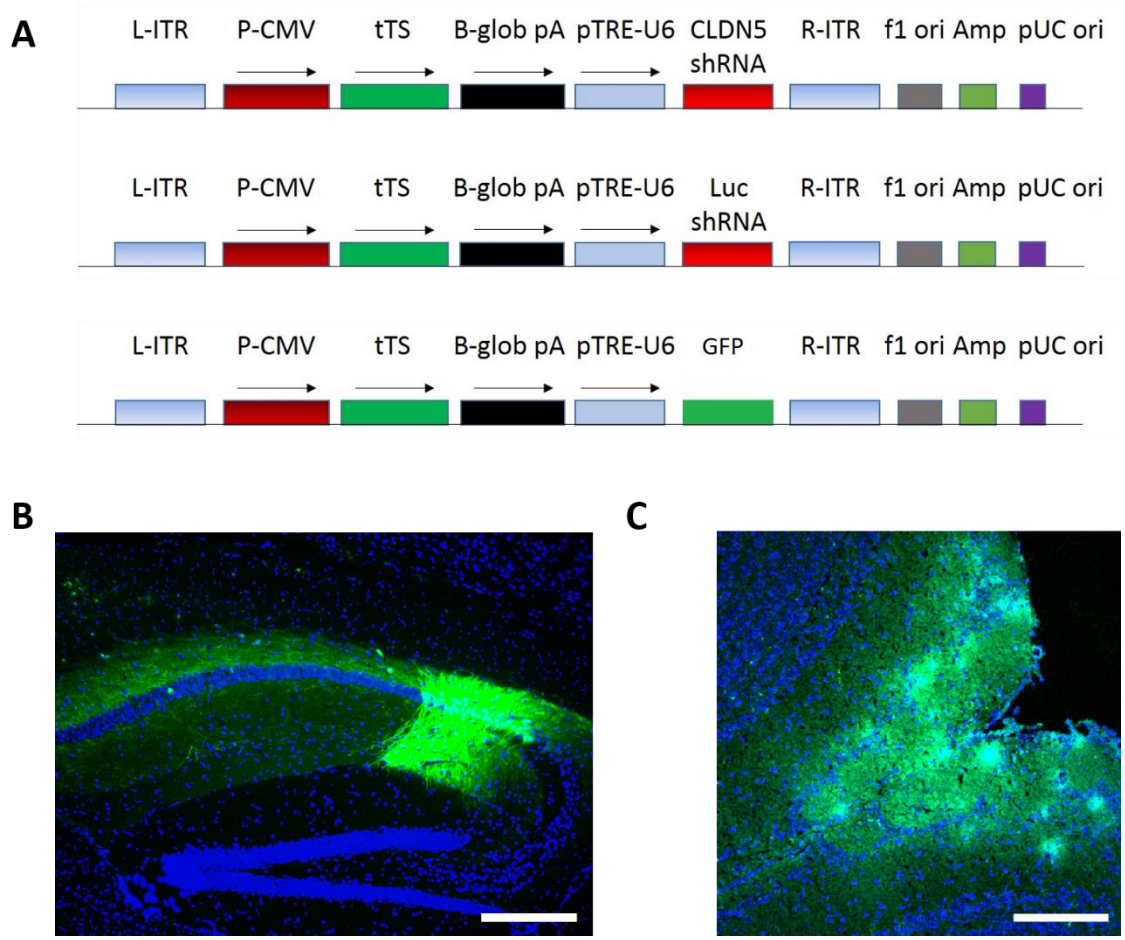

Figure 4.2: Distribution of AAV vectors injected in the dorsal hippocampus and mPFC. **(A)** AAV2/9 vector design of a doxycycline inducible claudin-5 or luciferase (non-targeting) shRNA and a doxycycline inducible GFP. Distribution of an adeno-associated virus containing a doxycycline-inducible green fluorescent protein in the **(B)** dorsal hippocampus and **(C)** mPFC. Scale bar – 200 µm.

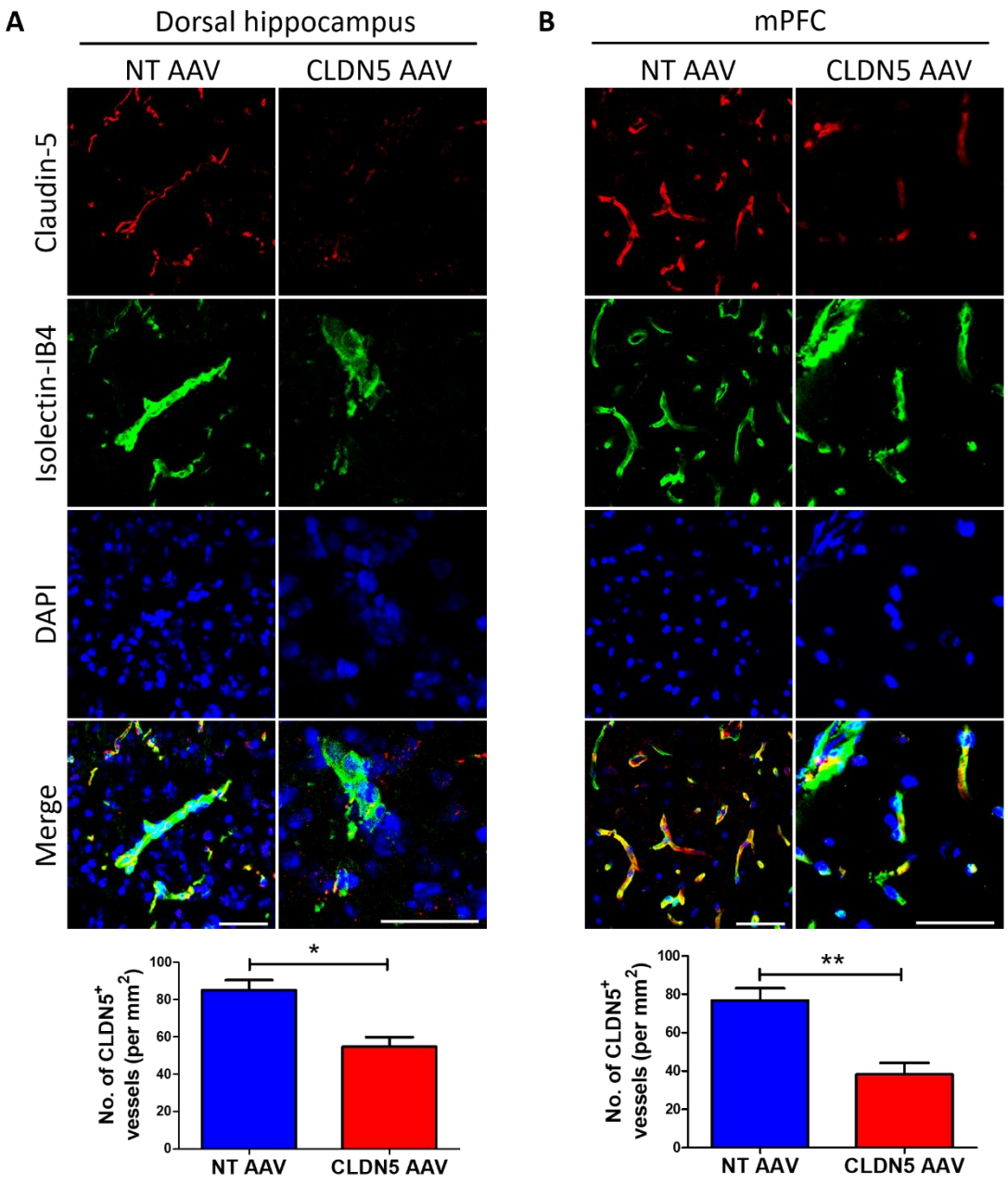

Figure 4.3: Claudin-5 suppression in the dorsal hippocampus and mPFC. Immunohistochemical analysis of claudin-5 (red) and isolectin-IB4 (green) staining in the **(A)** dorsal hippocampus and **(B)** mPFC of C57BL/6 mice injected with a NT AAV or CLDN5 AAV and treated with doxycycline for three weeks. Scale bar – 50 µm. *P<0.05, **P<0.01 Student's t-test. All data are means ± SEM with n = 7 per group.

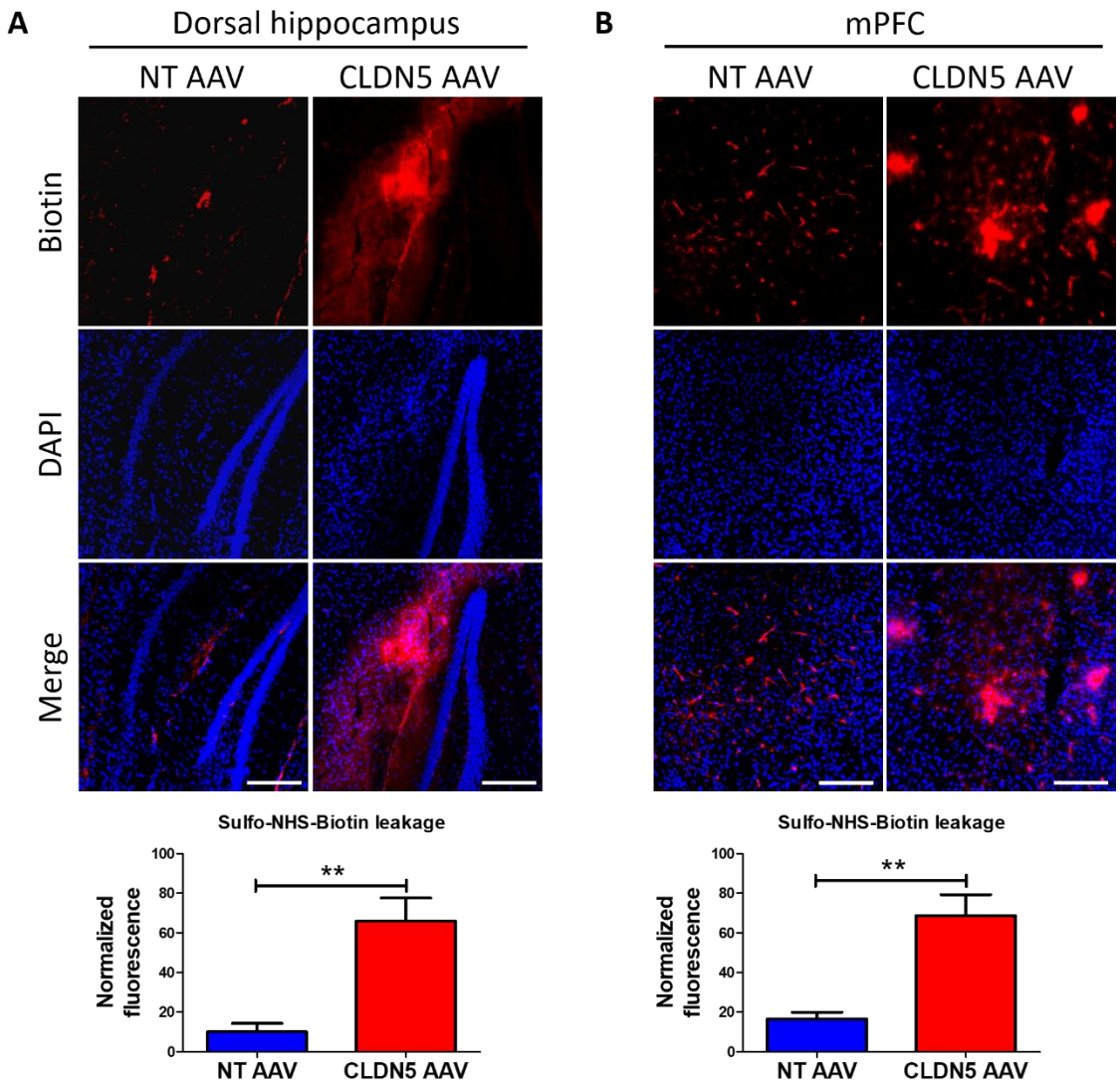

Figure 4.4: BBB permeability following suppression of claudin-5 in the dorsal hippocampus and mPFC. Immunohistochemical analysis of Sulfo-NHS Biotin (red) staining in the **(A)** dorsal hippocampus and **(B)** mPFC of C57BL/6 mice injected with a NT AAV or CLDN5 AAV and treated with doxycycline for three weeks. Scale bar – 200 µm. **P<0.01 Student's t-test. All data are means ± SEM with n = 7 per group.

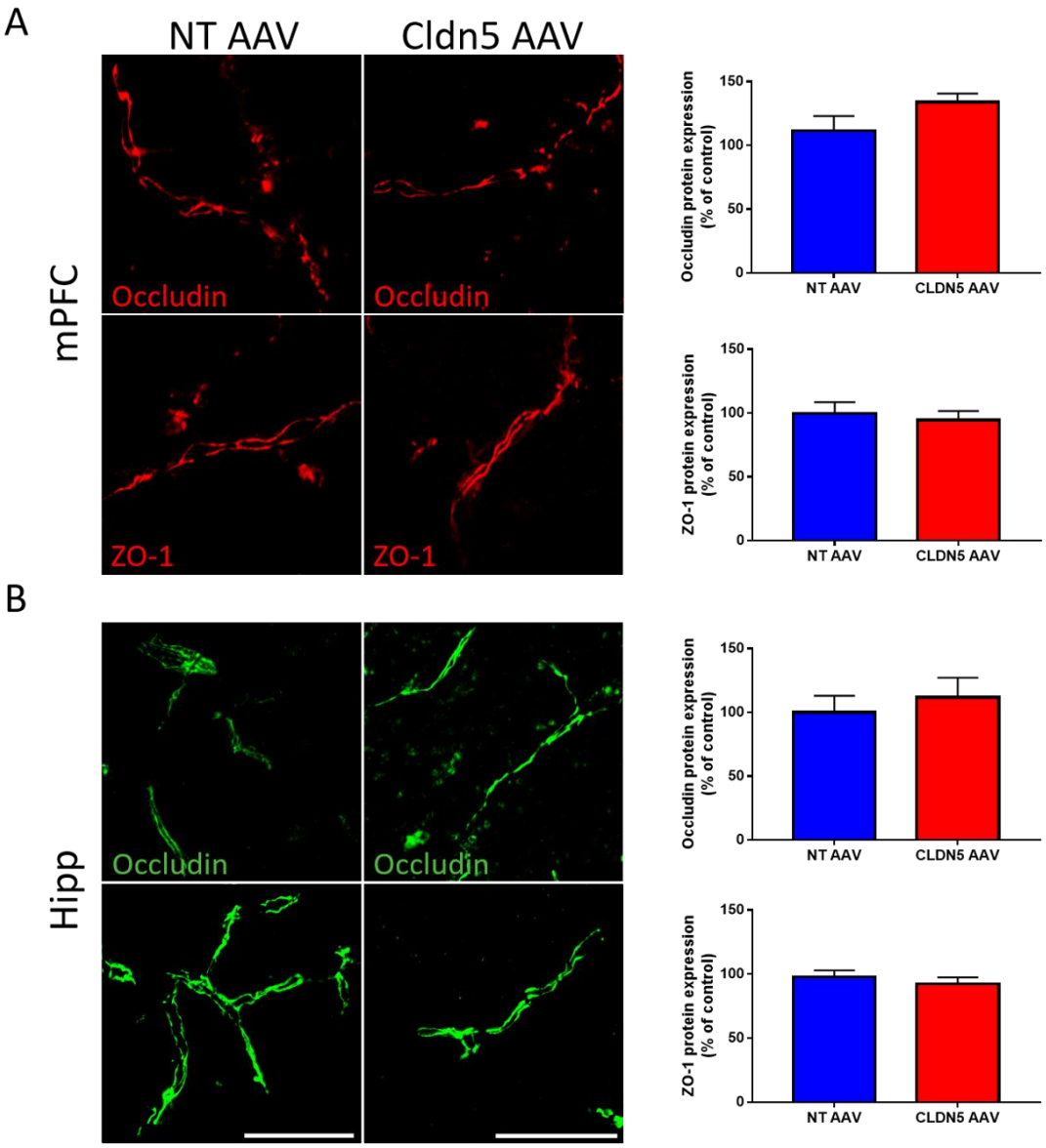

Figure 4.5: Immunohistochemical analysis of occludin and ZO-1 following suppression of claudin-5 in the dorsal hippocampus and mPFC. Immunohistochemical analysis of occludin and ZO-1 staining in the **(A)** mPFC and **(B)** dorsal hippocampus of C57BL/6 mice injected with a NT AAV or CLDN5 AAV and treated with doxycycline for three weeks. Scale bar – 50 µm. ANOVA with Tukey post-test compared to NT AAV control. All data are means ± SEM with n = 4 per group.

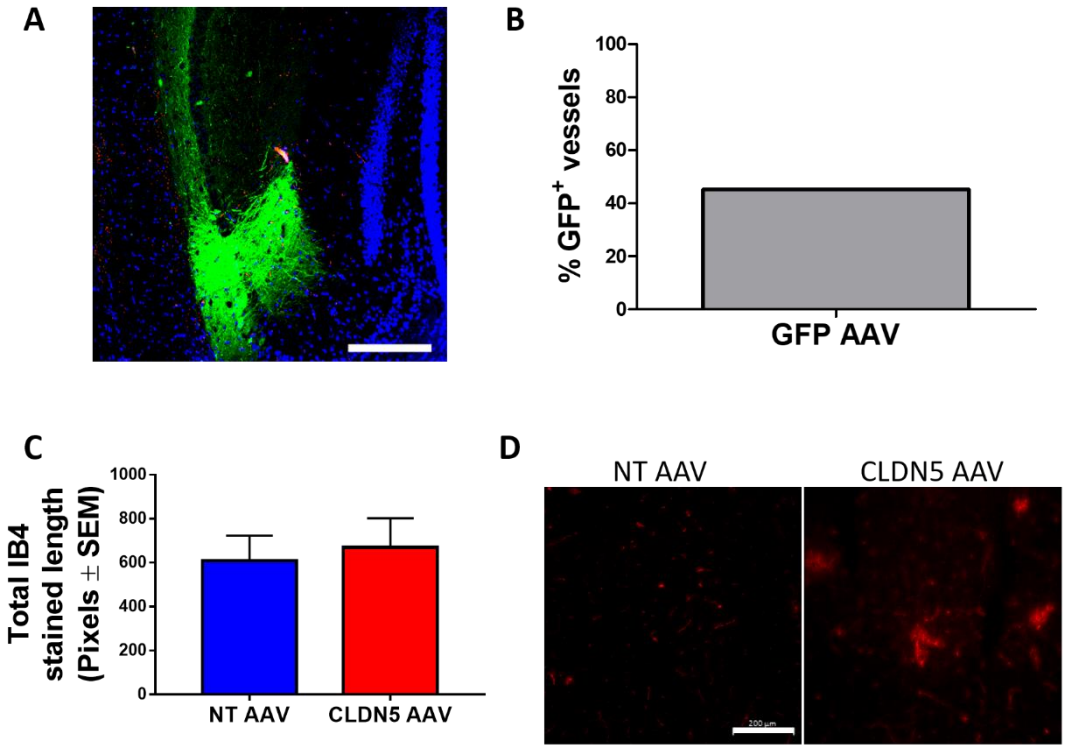

Figure 4.6: Examination of AAV infection rate and vascular patterning. **(A)** Immunohistochemical analysis of GFP and isolectin-IB4 staining in C57BL/6 mice injected with a doxycycline-inducible AAV containing GFP and treated with doxycycline for two weeks, scale bar – 200 µm. **(B)** Percentage of GFP positive blood vessels in the brain of mice injected with a GFP AAV. **(C)** Total isolectin-IB4 vessel length and signal intensity in C57BL/6 mice injected with a NT AAV or CLDN5 AAV and treated with doxycycline for three weeks. **(D)** Immunohistochemical analysis of Sulfo-NHS biotin leakage in C57BL/6 mice injected with a NT AAV or CLDN5 AAV and treated with doxycycline for three weeks. Scale bar – 200 µm. All data are means ± SEM with n = 4 mice per group.

4.2.2 Behavioural impairments following suppression of claudin-5 in the dorsal hippocampus

Neurological deficits are evident in several CNS disorders with apparent BBB disruption, however a direct assessment of the neurobehavioral sequelae following deletion or knockdown of EC specific components has never been investigated. Following two weeks of doxycycline treatment, C57BL/6 mice were subjected to a range of behavioural tests designed to evaluate their learning and memory, depression, anxiety, social interaction and locomotor skills. Details of the experiments are outlined in the methods section 2.4. Learning and memory impairments were assessed with both spatial and non-spatial tests which included the radial arm maze, novel object recognition test, spontaneous alternation y-maze and spontaneous alternation T-maze. Affective impairments were assessed with several anxiety and depressive-related tests including the elevated plus maze, forced swim test, splash test (forced grooming), social behaviour tests and open field test. Additionally, locomotor activity was assessed on the rotarod, radial arm maze, beam walk and open field test by calculating average speeds, distance travelled and rearing actions.

Site-specific suppression of claudin-5 in the dorsal hippocampus by an AAV containing a doxycycline-inducible shRNA targeting claudin-5 transcripts had no effect on learning or memory behaviours (Figure 4.7), however mice showed a significantly reduced latency to complete trials on the spontaneous alternation T-maze (Figure 4.7B). Mice also developed a non-significant trend for an increased side-bias in the spontaneous alternation Y-maze (Figure 4.7A). No impairments in long term memory were detected as measured on the radial arm maze (Figure 4.7D, E). Suppression of claudin-5 had significant effects on affective behaviours with impairments in social interaction as assessed by the social preference and social novelty test (Figure 4.8B) with mice spending significantly less time exploring a cage containing a novel mouse. In addition, mice displayed a significantly increased latency to groom as measured in the splash test and open field test (Figure 4.8A, C). Mice performed normally on the rotarod (Figure 4.9A) and beam walk (Figure 4.9C) and travelled similar distances on the open field test (Figure 4.9D). Both groups of mice also travelled at similar speeds on the radial arm maze (Figure 4.9B) and open field test and had similar rearing behaviour (Figure 4.9D). These mobility tests indicated normal locomotor function between NT and CLDN5 AAV injected groups.

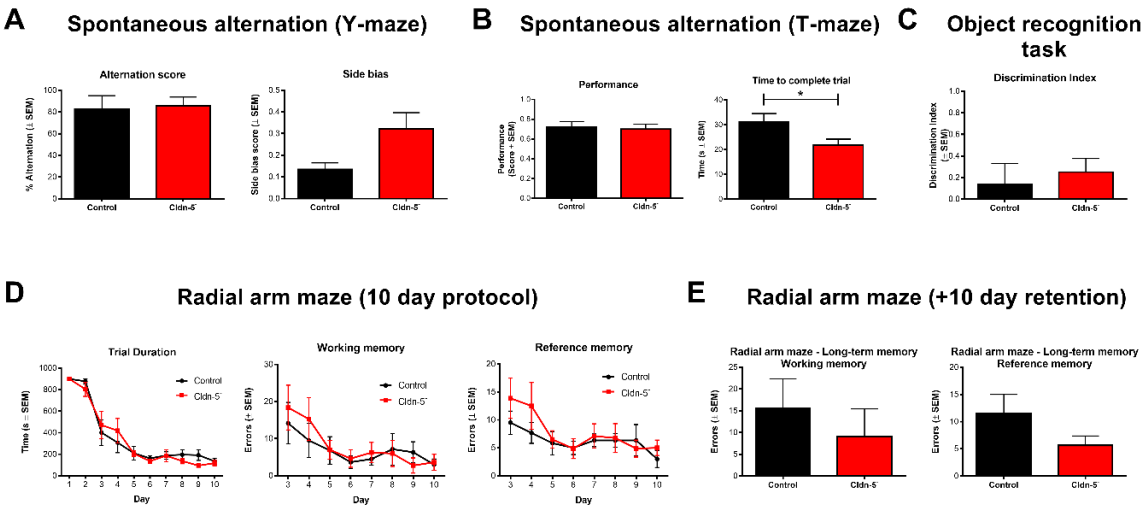

Figure 4.7: Suppression of claudin-5 in the dorsal hippocampus has no effect on learning or memory. Behavioural analysis of learning and memory on the **(A)** y-maze, **(B)** T-maze, **(C)** Radial arm maze and **(D)** object recognition task in C57BL/6 mice injected with a NT AAV or CLDN5 AAV in the dorsal hippocampus and treated with doxycycline for three weeks. *P < 0.05 by Student's t-test compared to NT AAV control. All data are means ± SEM with n = 6 for NT and n = 8 for CLDN5 groups.

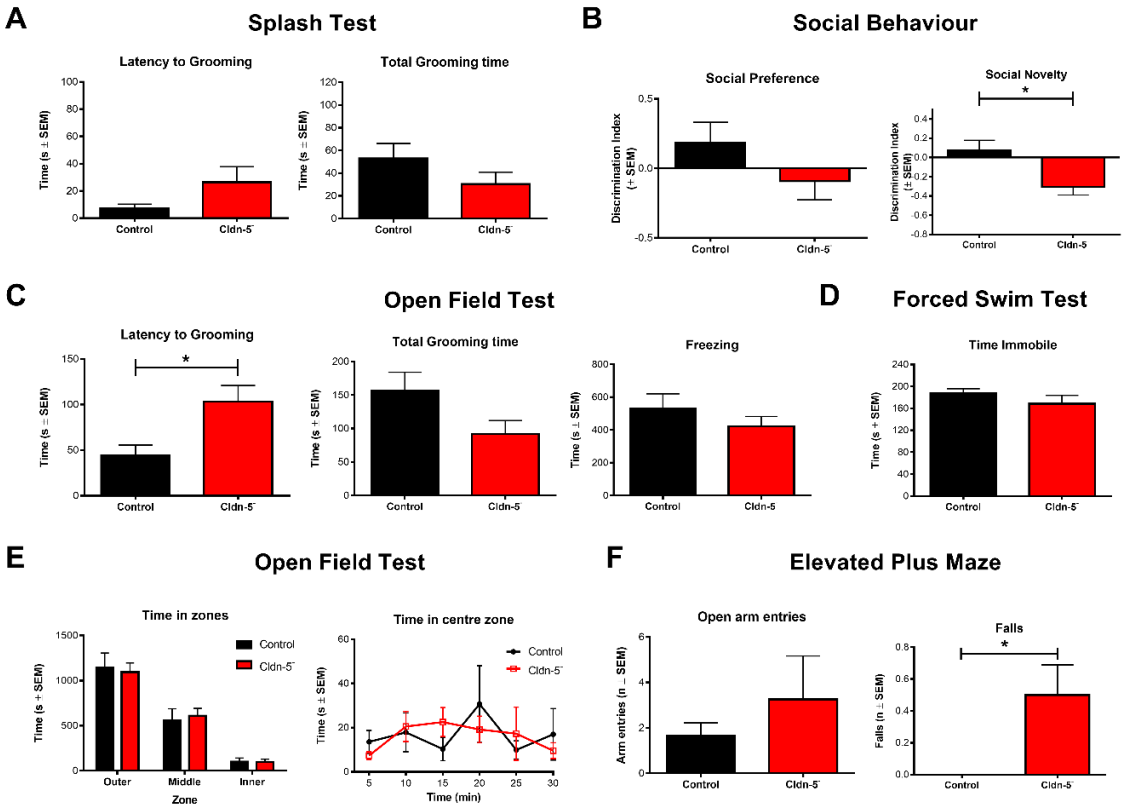

Figure 4.8: Suppression of claudin-5 in the dorsal hippocampus increases depressive-like behaviours. Behavioural analysis of affective behaviour on the **(A)** splash test, **(B)** social novelty task, **(C)** open field test, **(D)** forced swim test and **(E)** elevated plus maze in C57BL/6 mice injected with a NT AAV or CLDN5 AAV in the dorsal hippocampus and treated with doxycycline for three weeks. *P<0.05 by Student's t-test compared to NT AAV control. All data are means ± SEM with n = 6 for NT and n = 8 for CLDN5 groups.

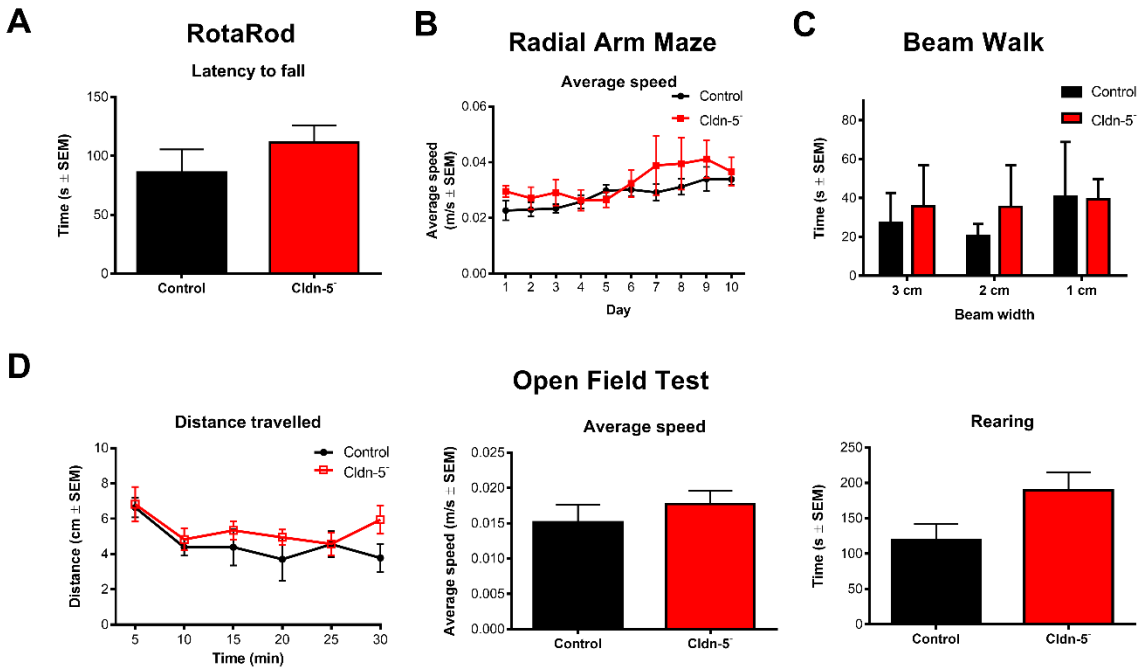

Figure 4.9: Suppression of claudin-5 in the dorsal hippocampus has no effect on locomotor activity. Behavioural analysis of locomotor activity on the **(A)** rotarod, **(B)** radial arm maze, **(C)** beam walk and **(D)** open field test in C57BL/6 mice injected with a NT AAV or CLDN5 AAV in the dorsal hippocampus and treated with doxycycline for three weeks. ANOVA with Tukey post-test compared to NT AAV control. All data are means ± SEM with n = 6 for NT and n = 8 for CLDN5 groups.

4.2.3 Behavioural impairments following suppression of claudin-5 in the mPFC

In contrast to mice injected with AAVs in the dorsal hippocampus, mice injected with AAVs in the mPFC showed significant deficits on several learning and memory tasks with significant impairments on the T-maze (Figure 4.10B) and object recognition task (Figure 4.10C). There were also alterations in affective behaviour with mice spending significantly less time immobile in the forced swim task (Figure 4.11D). To control for potential neurological deficits resulting from surgical procedures, mice were assessed on several locomotor tasks to assess mobility, speed and rearing behaviour. No differences were detected between groups injected with NT or Claudin-5 AAV vectors (Figure 4.12). Mice performed equally well on the rotarod (Figure 4.12A) and beam walk (Figure 4.12C) and travelled similar distances on the open field test (Figure 4.12D). Both groups of mice also travelled at similar speeds on the radial arm maze (Figure 4.12B) and open field test and had similar rearing behaviour (Figure 4.12D). The data presented here provides evidence that BBB integrity is critical for maintaining homeostasis within the NVU and for normal animal behaviour with localised BBB disruption inducing impairments in learning and memory tasks as well as inducing affective disorder phenotypes and social withdrawal.

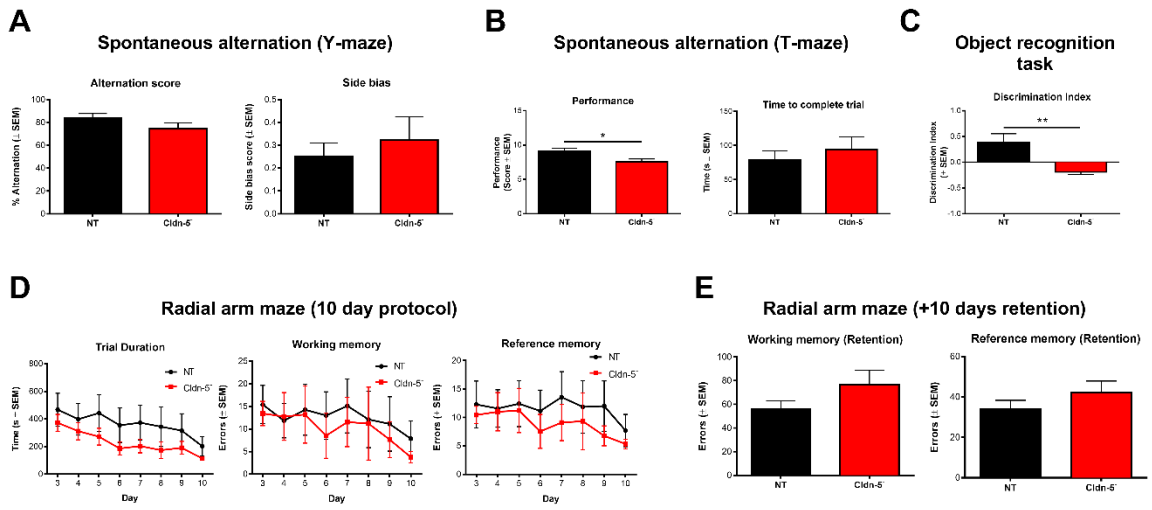

Figure 4.10: Suppression of claudin-5 in the mPFC impairs learning and memory. Behavioural analysis of learning and memory on the **(A)** Y-maze, **(B)** T-maze, **(C)** Radial arm maze and **(D)** object recognition task in C57BL/6 mice injected with a NT AAV or CLDN5 AAV in the mPFC and treated with doxycycline for three weeks. *P<0.05, **P<0.01 by Student's t-test compared to NT AAV control. All data are means ± SEM with n = 7 for NT and n = 9 for CLDN5 groups.

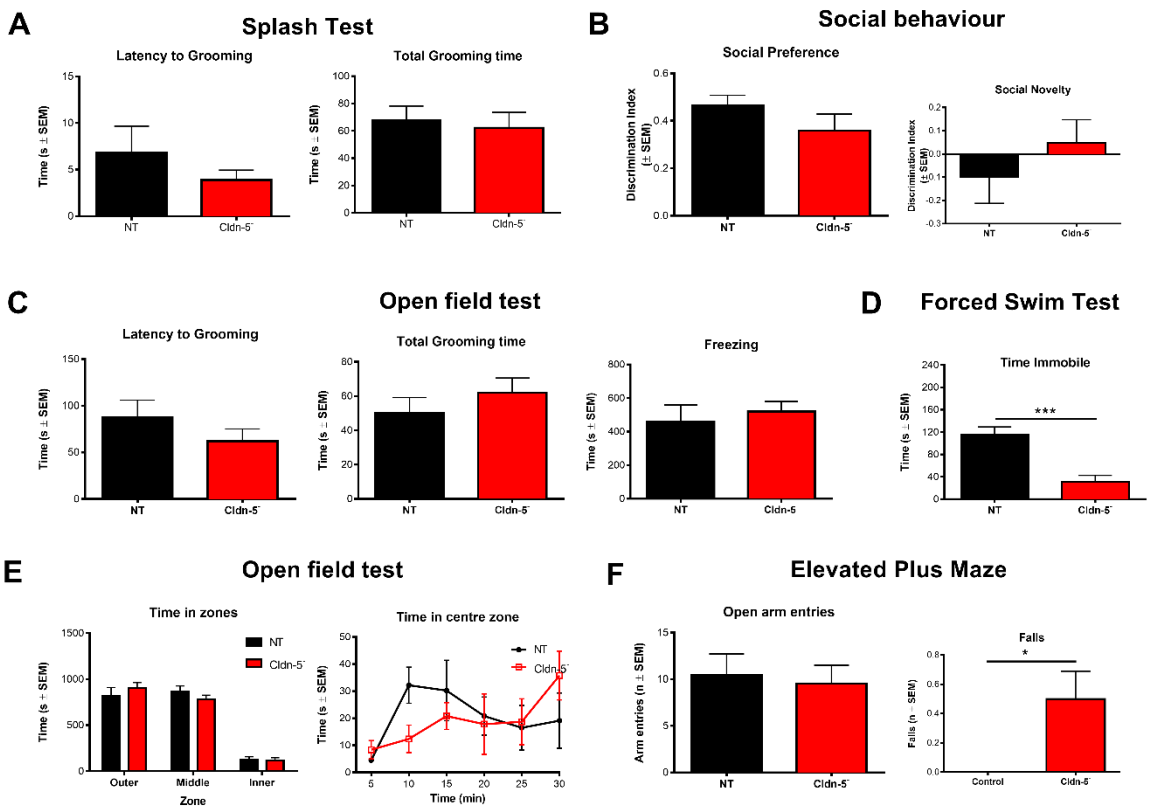

Figure 4.11: Suppression of claudin-5 in the mPFC increases mobility in the forced swim task. Behavioural analysis of affective behaviour on the **(A)** splash test, **(B)** social novelty task, **(C)** open field test, **(D)** forced swim test and **(E)** elevated plus maze in C57BL/6 mice injected with a NT AAV or CLDN5 AAV in the mPFC and treated with doxycycline for three weeks. ***P<0.01 by Student's t-test compared to NT AAV control. All data are means ± SEM with n = 7 for NT and n = 9 for CLDN5 groups.

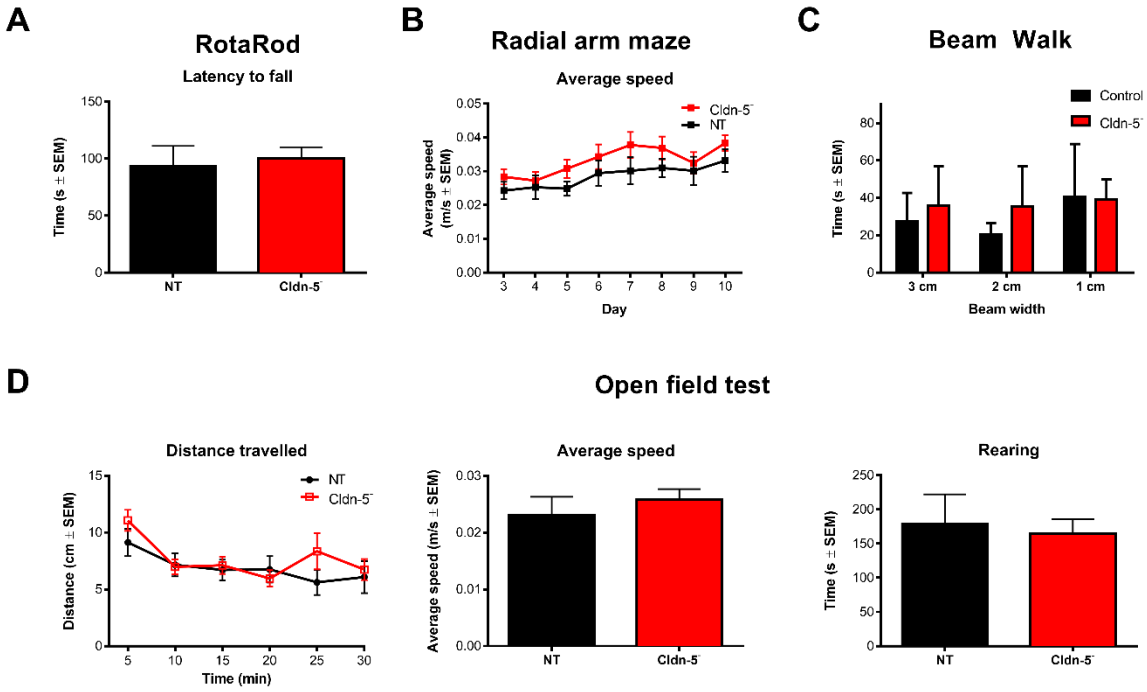

Figure 4.12: Suppression of claudin-5 in the mPFC has no effect on locomotor activity. Behavioural analysis of locomotor activity on the **(A)** rotarod, **(B)** radial arm maze, **(C)** beam walk and **(D)** open field test in C57BL/6 mice injected with a NT AAV or CLDN5 AAV in the mPFC and treated with doxycycline for three weeks. ANOVA with Tukey post-test compared to NT AAV control. All data are means ± SEM with n = 7 for NT and n = 9 for CLDN5 groups.

4.2.4 Generation and characterisation of an inducible claudin-5 knockdown mouse

The previous results section demonstrated profound alterations in animal behaviour following site-specific suppression of claudin-5 in the dorsal hippocampus and mPFC. Therefore, a key aspect of this chapter was to generate a BBB mouse model that would allow for inducible and reversible RNAi-based suppression of claudin-5 at the BBB.

Initially, the brain endothelial cell line, bEnd.3, was transfected with shRNAs targeting different regions of the claudin-5 mRNA transcript (Figure 4.13). Several shRNAs suppressed claudin-5 mRNA and protein (Figure 4.14A). Immunocytochemical analysis of claudin-5 24 h following transfection of claudin-5 160 shRNA showed reduced staining intensity compared to UNT and NT shRNA transfected controls (Figure 4.14B). Using the selected shRNA sequences, mice were then generated by Mirimus Inc such that a gene containing a doxycycline-inducible claudin-5 shRNA was inserted at the Col1a1 locus on chromosome 11. Additionally, a CAG-lox-stop-lox-rtTA3-IRES-mKate2 (CLR3K) allele was knocked in at the endogenous *Rosa26* locus on chromosome 6. This gene utilizes the endogenous *Rosa26* promoter to drive expression of the reverse tetracycline-controlled transactivator (M2rtTA). Immediately upstream of the CLR3K allele is a stop codon flanked by loxP sites so that mice that are crossed to a Cre-recombinase expressing mouse express the rtTA. Crossing of the bi-allelic mice outlined above to Tie-2-Cre mice generates mice with activated rtTA specifically in endothelial cells. Supplementation of doxycycline to the diet then allows for doxycycline to interact with rtTA to subsequently bind to tetracycline response elements (TRE) upstream of the inserted claudin-5 shRNA to allow for transcription of the GFP-tagged claudin-5 shRNA (Figure 4.14A). Claudin-5 knockdown mice administered doxycycline in their diet developed normally with no macroscopic differences (Figure 4.15B). Claudin-5 x Tie2 cre positive mice were genotyped by PCR with PCR products separated by agarose gel electrophoresis. Cre positive mice had a band of 100 bp representing cre (Figure 4.15C). Immunohistochemical analysis of brain cryosections from claudin-5 knockdown mice using mKate (red) and GFP (green) reporter genes confirmed expression of rtTA and claudin-5 shRNA respectively in the vasculature. NT cre positive and claudin-5 cre positive mice received a 1 mg dose of doxycycline I.P and 72 h later capillaries were isolated from the brain and protein and RNA were extracted. Western blot analysis of isolated cerebral microvessels revealed significantly reduced claudin-5 protein compared to NT control mice. RT-PCR analysis revealed significantly reduced claudin-5 mRNA

compared to NT controls (Figure 4.16). Additionally, suppression of claudin-5 did not impact on expression levels of other TJ protein (Figure 4.17A) or transcripts (Figure 4.17B) including ZO-1, occludin and tricellulin. There were no abnormalities in the cerebral vasculature of claudin-5 knockdown mice as assessed by whole brain imaging of a vascular cast on a light microscope (Figure 4.18A). Additionally, no defects were detected as measured by the total stained length of isolectin-IB4 in control and claudin-5 knockdown mice (Figure 4.18B).

4.2.5 Size selective loosening of the BBB in claudin-5 knockdown mice

To assess the barrier phenotype of mice following suppression of claudin-5 in the inducible knockdown model, dynamic contrast-enhanced MRI (DCE-MRI) was performed to monitor the real-time perfusion of a gadolinium tracer molecule into brain parenchyma in claudin-5 knockdown mice treated with doxycycline for two weeks. Gadolinium extravasation into extravascular spaces was quantified over the course of a 20 minute DCE-MRI scan and analysed with *ImageJ* software by plotting the mean signal intensity of gadolinium normalised to the signal intensity prior to injection of gadolinium. Suppression of claudin-5 resulted in increased extravasation of gadolinium over the course of the scan compared to controls (Figure 4.19).

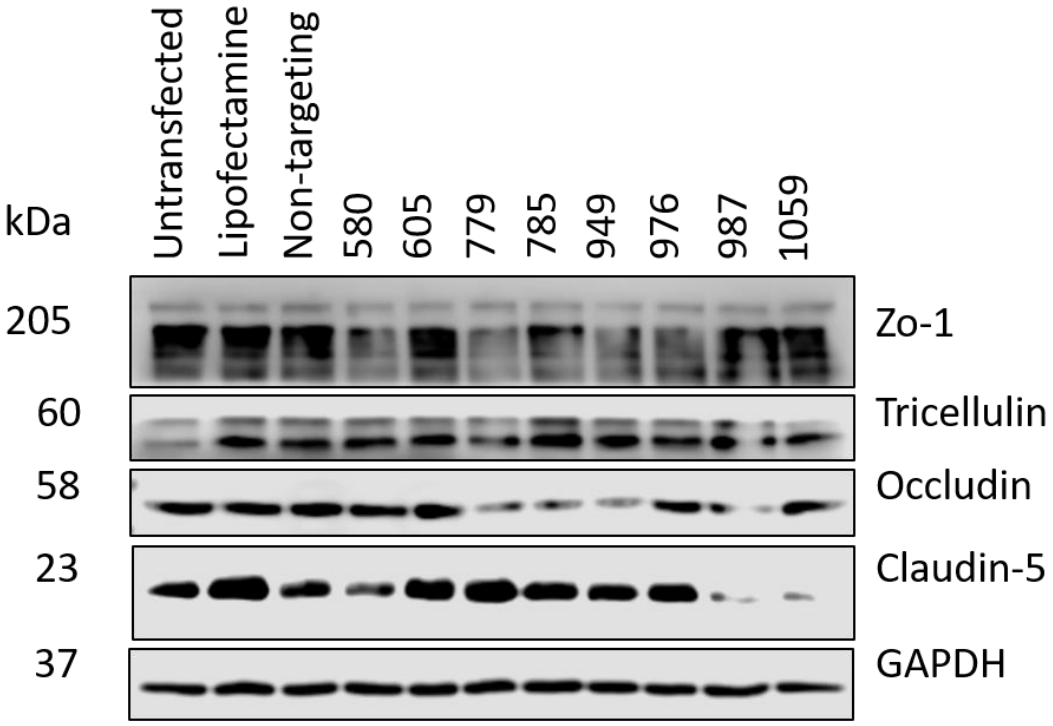

Figure 4.13: Screening of claudin-5 shRNAs *in vitro*. Western blot analysis of ZO-1, tricellulin, occludin and claudin-5 in bEnd.3 cells 24 h post-transfection of the indicated claudin-5 shRNAs or NT shRNA.

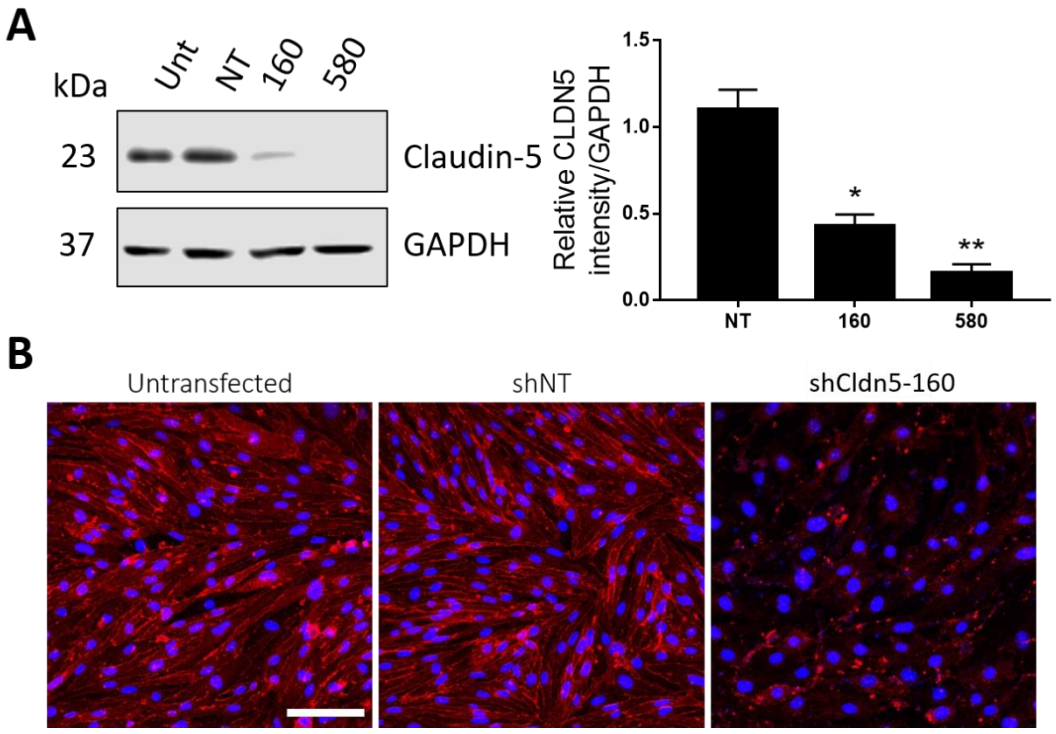

Figure 4.14: Transfection of shRNAs targeting claudin-5 transcript in bEnd.3 cells. **(A)** Western blot analysis of claudin-5 and densitometric analysis 24 h post-transfection of claudin-5 shRNA or NT shRNA in bEnd.3 cells. **(B)** Immunocytochemical analysis of claudin-5 24 h post-transfection of claudin-5 shRNA in bEnd.3 cells. *P<0.05, **P<0.01 by ANOVA with Tukey post-test compared to NT control. Scale bar – 100 µm. All data are means ± SEM with n = 3 and are representative of three independent experiments.

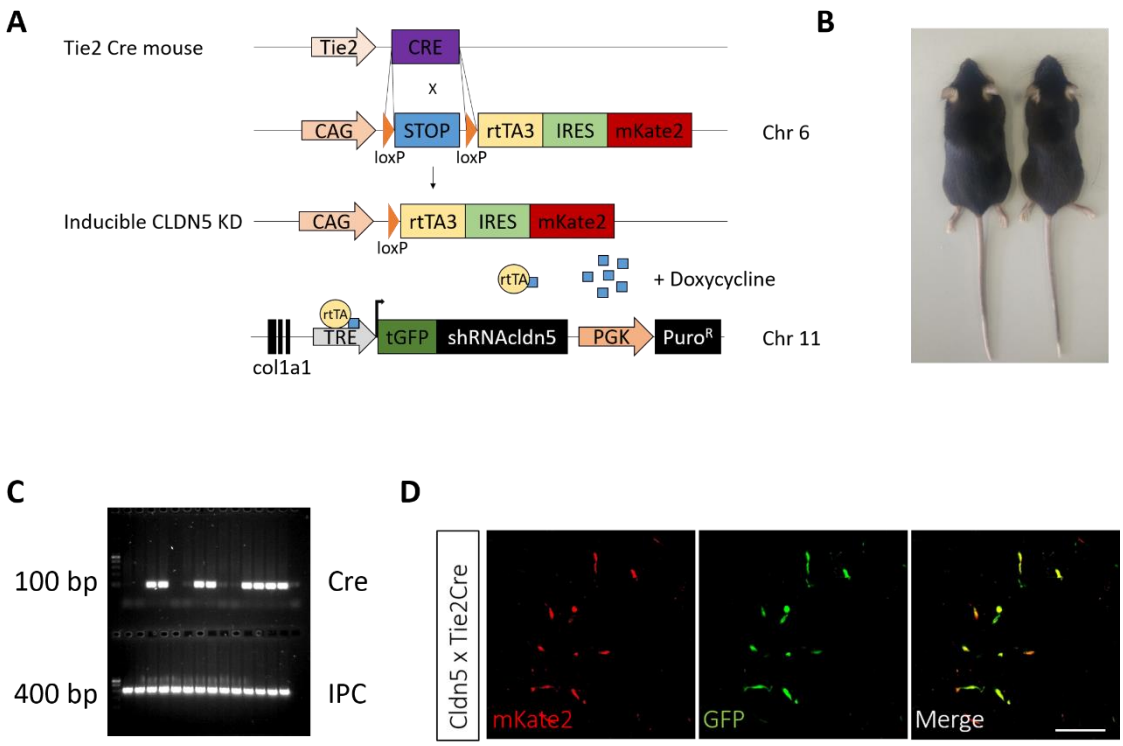

Figure 4.15: Doxycycline-inducible claudin-5 knockdown mouse. **(A)** Schematic diagram showing the inducible claudin-5 knockdown system with the associated genetic elements knocked in on chromosome 6 and 11. **(B)** No macroscopic differences are apparent between cre – and cre + claudin-5 knockdown mice. **(C)** DNA samples from cre – and cre + claudin-5 knockdown mice were amplified with cre primers (top gel) and internal positive control primers (bottom gel). A product of 100 base pairs is observed representative of the cre product and a band of 400 base pairs is observed representative of the IPC product. **(D)** mKate2 (red) and GFP (green) staining in the brain of cre + claudin-5 knockdown mice treated with doxycycline for 72 h showing specific distribution of rtTA3 and claudin-5 shRNA in blood vessels. Scale bar – 50 µm.

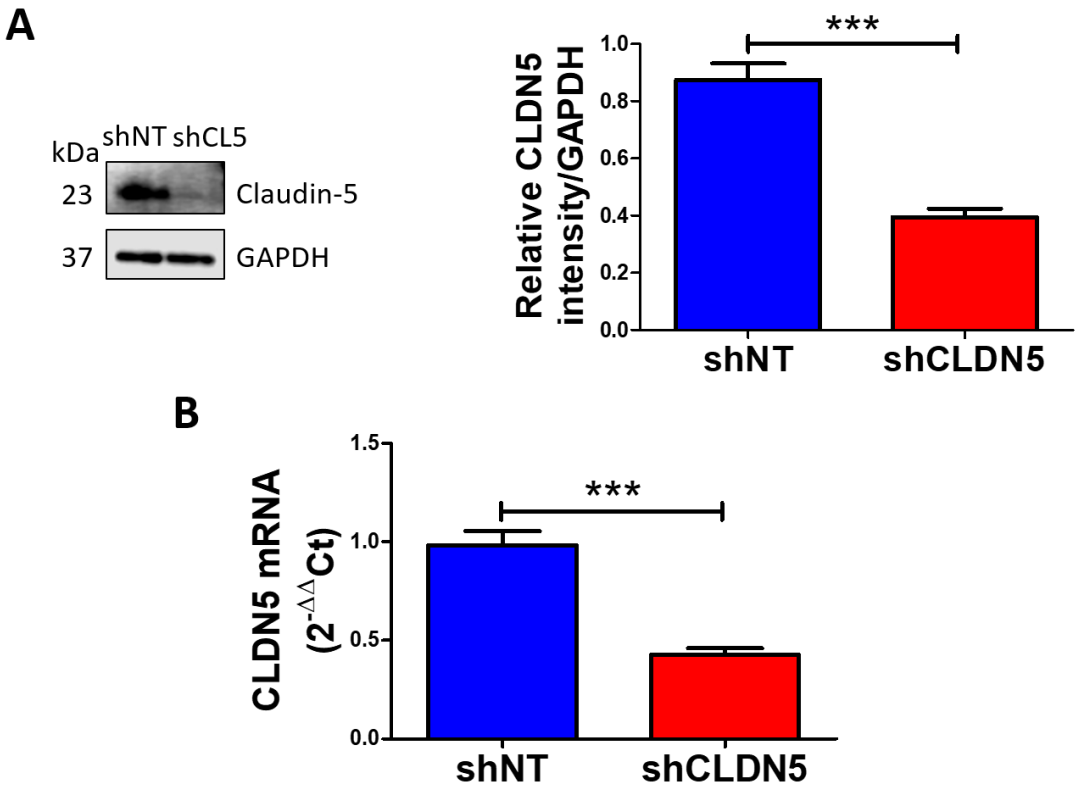

Figure 4.16: Characterisation of claudin-5 suppression in claudin-5 knockdown mice. **(A)** Western blot analysis of claudin-5 in cerebral microvessels isolated from Tie2 cre positive claudin-5 knockdown mice treated with 2 mg IP of doxycycline for 72 h. GAPDH was used to normalise the blots. ImageJ was used for densitometry analysis. **(B)** RT-PCR analysis of claudin-5 in cerebral microvessels isolated from Tie2 cre positive claudin-5 knockdown mice treated with 2 mg IP of doxycycline for 72 h. ***P<0.001 by Student's t-test compared to NT controls. All data are means ± SEM with n = 4 mice per group.

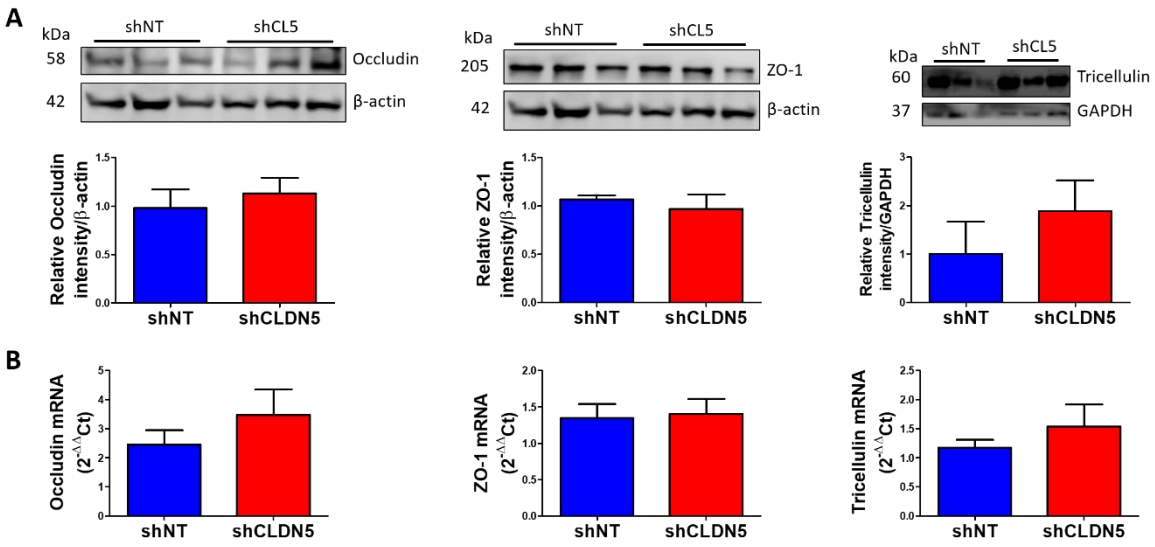

Figure 4.17: Suppression of claudin-5 does not impact other TJ components. **(A)** Western blot analysis of occludin, ZO-1 and tricellulin in cerebral microvessels isolated from Tie2 cre positive claudin-5 knockdown mice treated with 2 mg IP of doxycycline for 72 h. β-actin or GAPDH was used to normalise the blots. ImageJ was used for densitometry analysis. **(B)** RT-PCR analysis of occludin, ZO-1 and tricellulin in Tie2 cre positive claudin-5 knockdown mice treated with 2 mg IP of doxycycline for 72 h. Data was analysed by Students t-test. All data are means ± SEM with n = 3 mice per group.

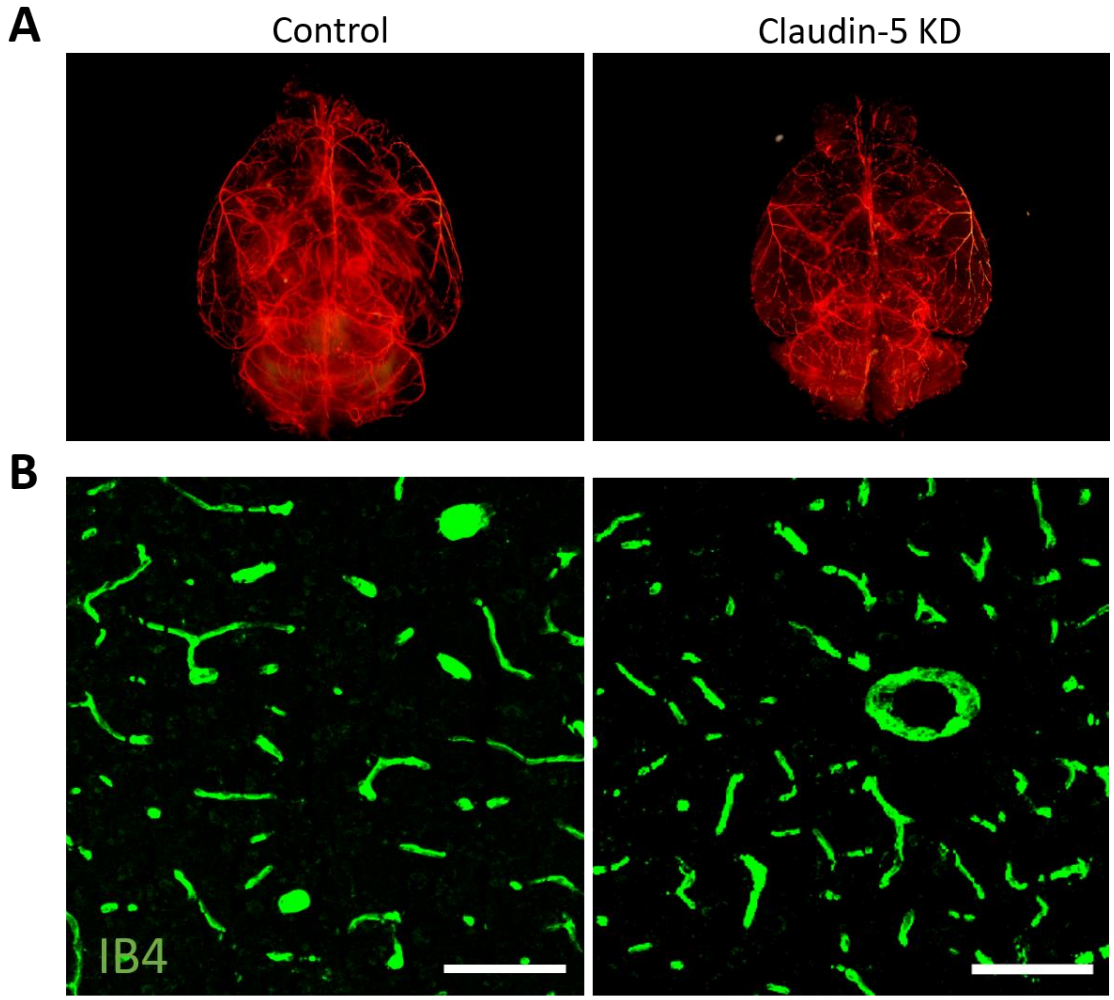

Figure 4.18: Normal vascular patterning in claudin-5 knockdown mice. **(A)** Microvascular cast of control and claudin-5 knockdown mice treated with doxycycline for 3 weeks. **(B)** Immunohistochemical analysis of isolectin-IB4 in control and claudin-5 knockdown mice. Scale bar – 100 µm.

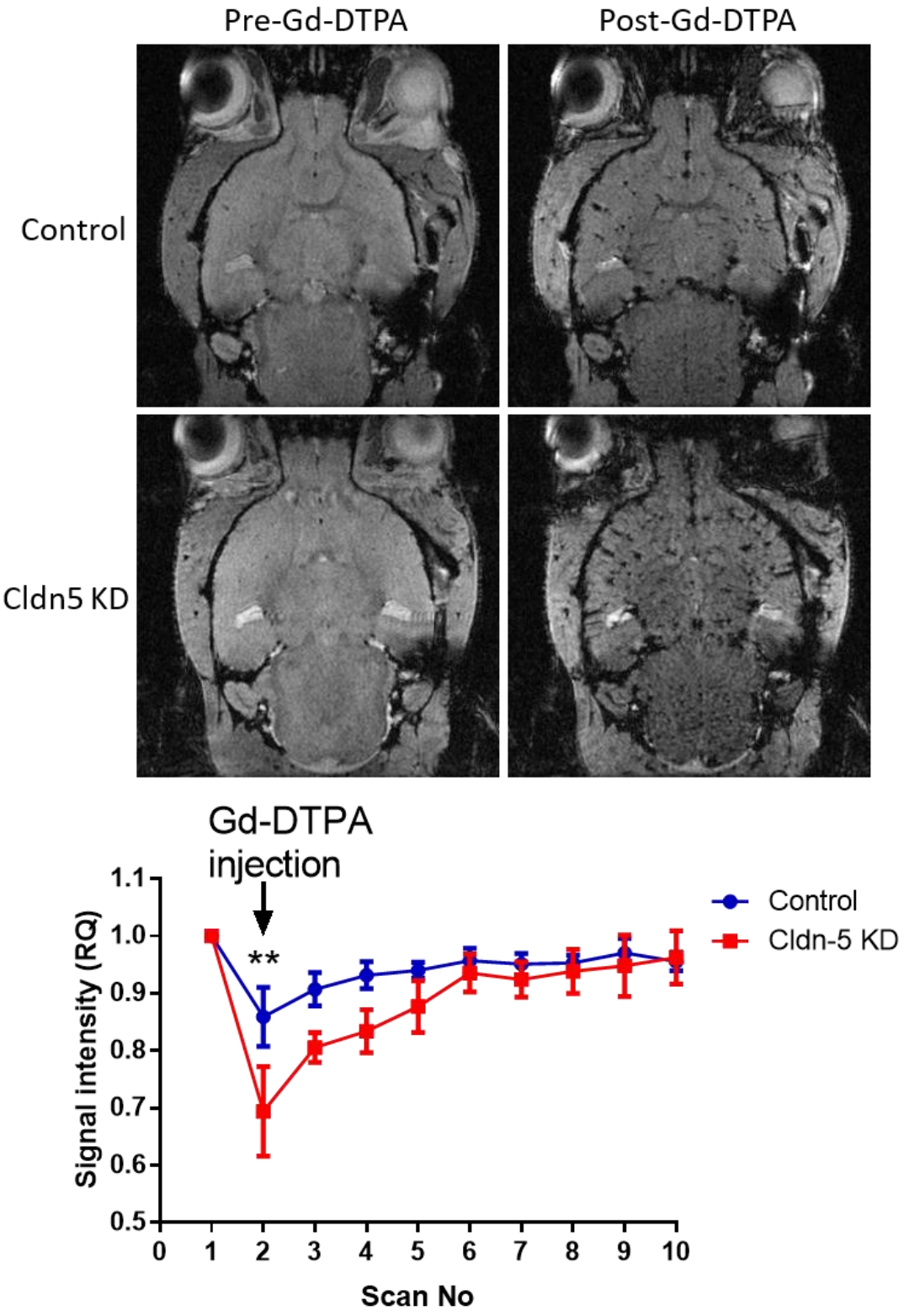

Figure 4.19: Dynamic contrast-enhanced MRI analysis in claudin-5 knockdown mice. Top panel - Representative images pre- and post-injection of 2 mg/ml Gd-DTPA in control and claudin-5 knockdown mice treated with doxycycline for two weeks. Lower panel - Analysis of signal intensity changes across the 10 scans. **P<0.01 by two-way ANOVA with Bonferroni post-test. All data are means ± SEM with n = 4 mice per group.

4.2.6 Behavioural impairments in the claudin-5 knockdown mouse

As claudin-5 knockout mice die soon after birth, we utilised our inducible claudin-5 knockdown model to examine behavioural phenotypes post-suppression of claudin-5 across the entire brain. Following three weeks of doxycycline administration to the drinking water, mice were subjected to a range of behavioural tasks designed to evaluate learning and memory, anxiety, depression, social interaction, locomotor activity and sensorimotor behaviour similar to C57BL/6 mice which received bilateral injections of AAVs. Claudin-5 knockdown mice showed significant impairments on multiple learning and memory tasks, with significant impairments in the T-maze (Figure 20B) and object recognition task (Figure 20C). These mice also showed a significant side bias on the Y-maze (Figure 20A). Cre positive mice also displayed increased anxiety as assessed by a significant reduction in the number of open arm entries in the elevated plus maze (Figure 21E). There were also non-significant trends for decreased social interaction and increased locomotion in the open field test (Figure 4.22). Control and claudin-5 knockdown mice performed similarly on locomotor-related tasks with no differences detected in distance travelled, average speed or rearing behaviour on the open field test (Figure 4.22A) in addition to performing similarly on the rotarod (Figure 4.22B).

4.2.7 Sensorimotor gating deficits in claudin-5 knockdown mice

Acoustic pre-pulse inhibition (PPI) is a sensorimotor gating phenomenon that is preserved across species and has previously been shown to strongly associate with schizophrenia. Indeed, numerous proposed mouse models of schizophrenia use acoustic PPI as a correlate of a schizophrenia-like phenotype. PPI refers to the ability of a non-startling "prepulse" stimulus to inhibit the response to a subsequent "pulse" startling stimulus. Here, NT and claudin-5 knockdown mice were assessed for PPI at 71, 77, 83 dB prepulse sound levels with 100, 110 and 120 dB pulse sound levels. Claudin-5 knockdown mice display a significantly reduced acoustic PPI response with a 77 dB prepulse at a 110 dB pulse (Figure 4.23A) and a 77 and 83 dB prepulse at a 120 dB pulse (Figure 23B). NT and claudin-5 knockdown mice showed similar startle responses at 100, 110 and 120 dB indicating that these deficits in PPI are not just a result of an impaired startle response or due to impaired hearing (Figure 4.23D). These mice also displayed normal a-wave and b-wave responses as measured by ERG analysis (Figure 4.24). Taken together, the molecular and behavioural data presented here suggest a profound link between the gene dosage effect of claudin-5 and the development of behavioural impairments governing

learning and memory and increased anxiety observed in several neuropsychiatric disorders as well as reductions in PPI typically observed in individuals with schizophrenia.

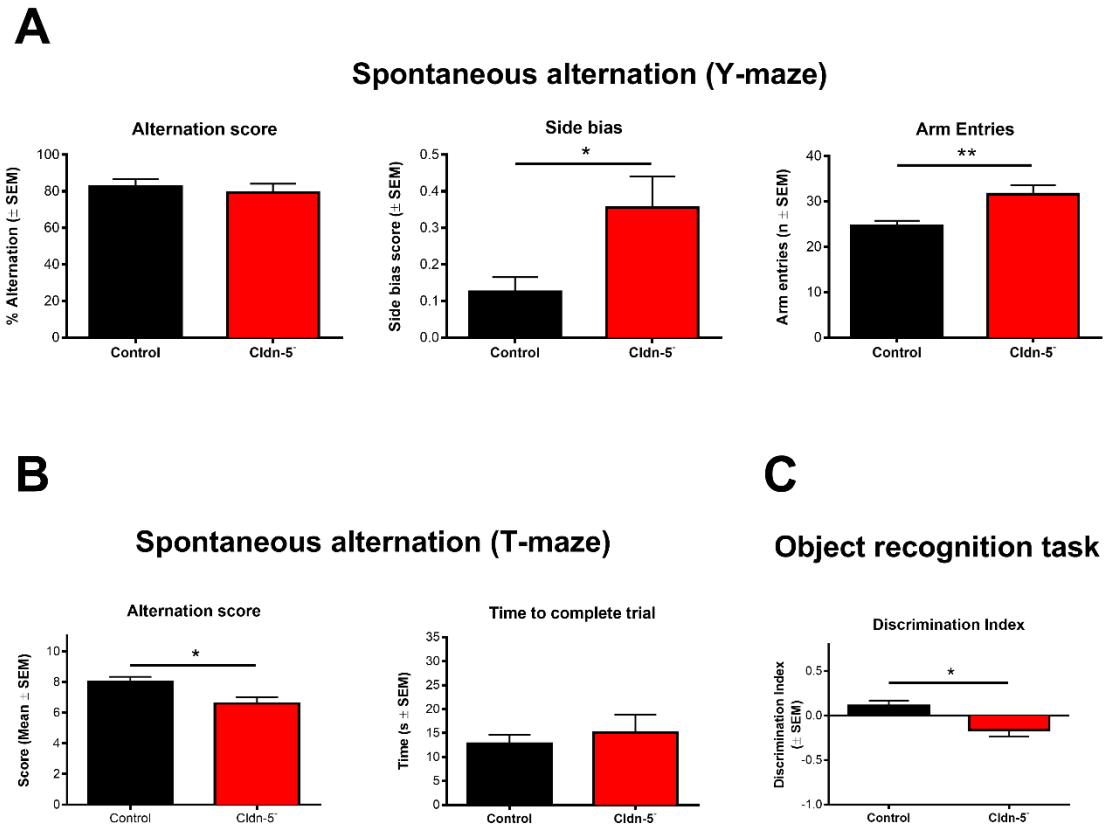

Figure 4.20: Learning and memory impairments in claudin-5 knockdown mice. Behavioural analysis of learning and memory on the y-maze **(A)**, T-maze **(B)** and object recognition task **(C)** in cre positive and cre negative claudin-5 KD mice treated with doxycycline for three weeks. *P<0.05 by Student's t-test compared to cre negative littermate controls. All data are means ± SEM with n = 13 for NT and n = 6-8 for CLDN5 groups.

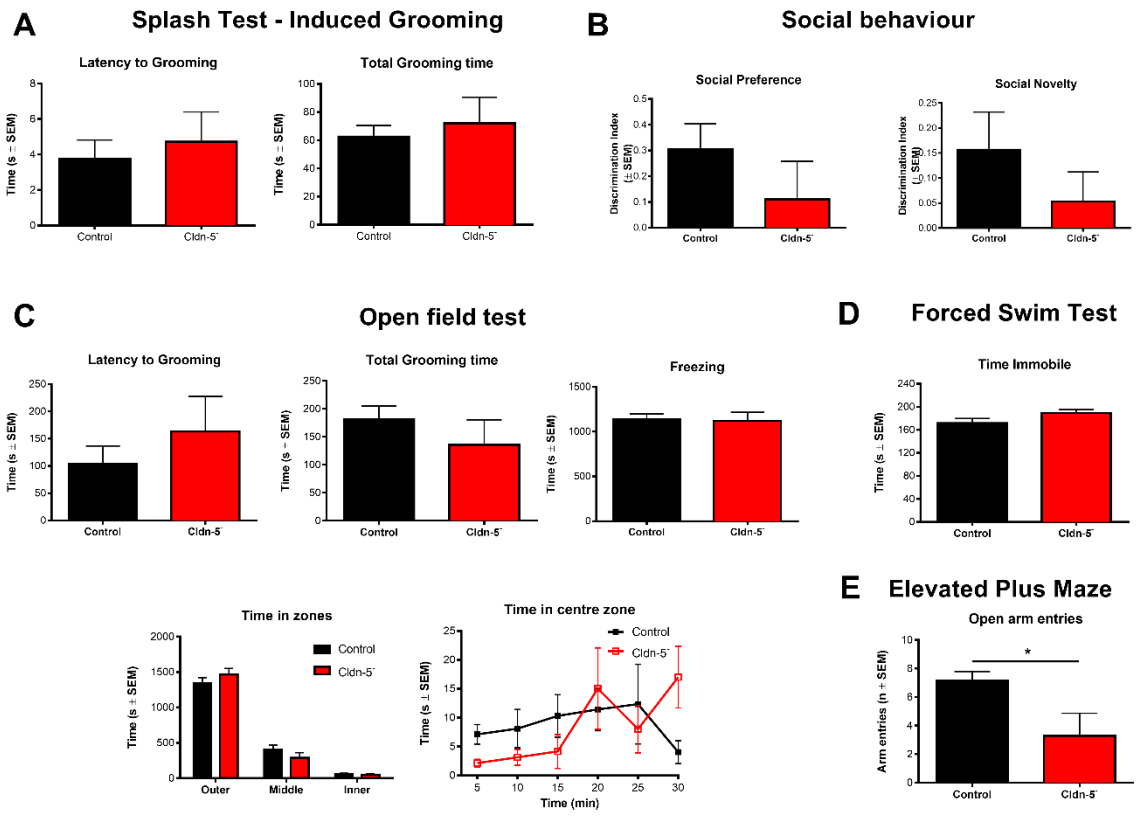

Figure 4.21: Increased anxiety in claudin-5 knockdown mice. Behavioural analysis of affective behaviour on the **(A)** splash test, **(B)** social novelty task, **(C)** open field test, **(D)** forced swim test and **(E)** elevated plus maze in cre + and cre - claudin-5 KD mice treated with doxycycline for three weeks. *P<0.01 by Student's t-test compared to cre negative littermate controls. All data are means ± SEM with n = 13 for cre - and n = 6-8 for cre + groups.

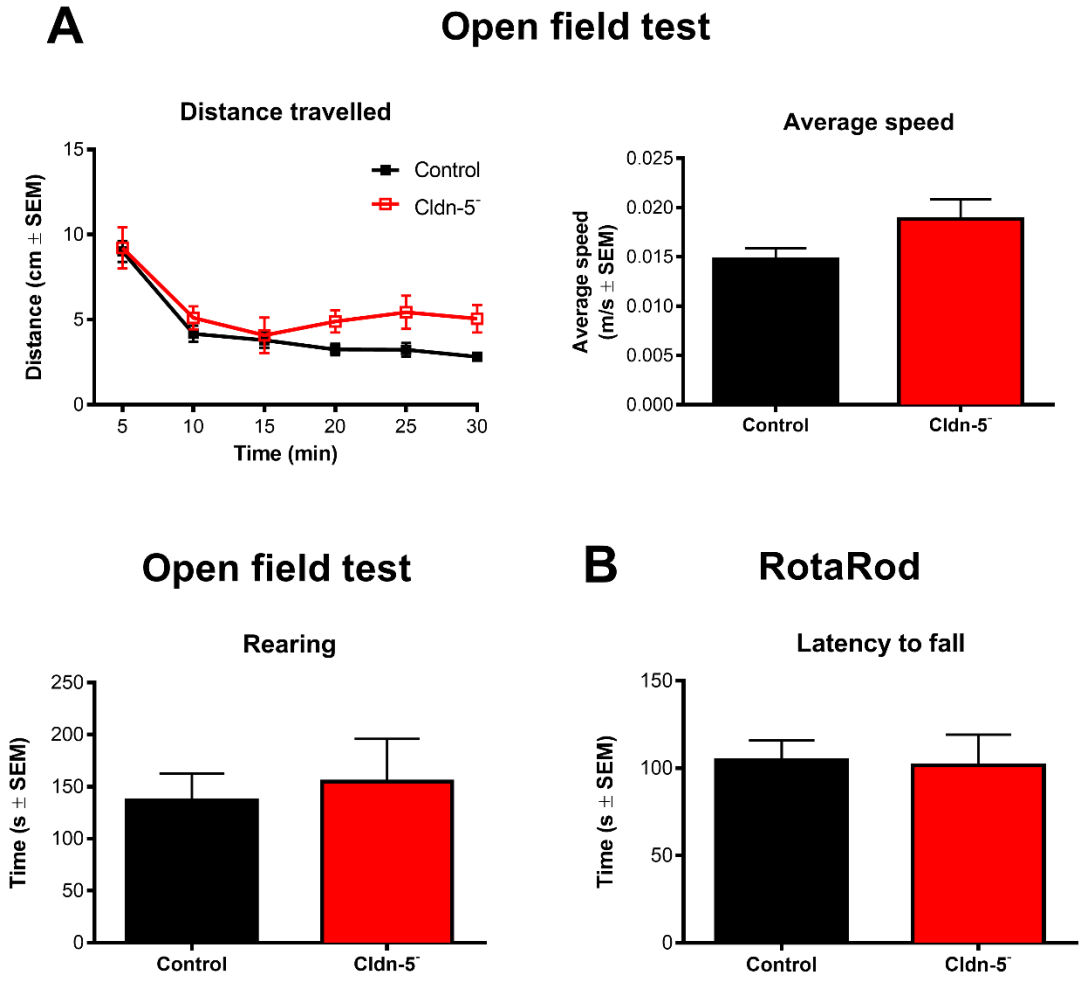

Figure 4.22: Examination of locomotor skills in claudin-5 knockdown mice. Behavioural analysis of locomotor activity on the **(A)** open field test and **(B)** rotarod in cre + and cre – claudin-5 knockdown mice treated with doxycycline for three weeks. ANOVA with Tukey post-test compared to cre – littermate controls. All data are means ± SEM with n = 13 for NT and n = 7-9 for cre + groups.

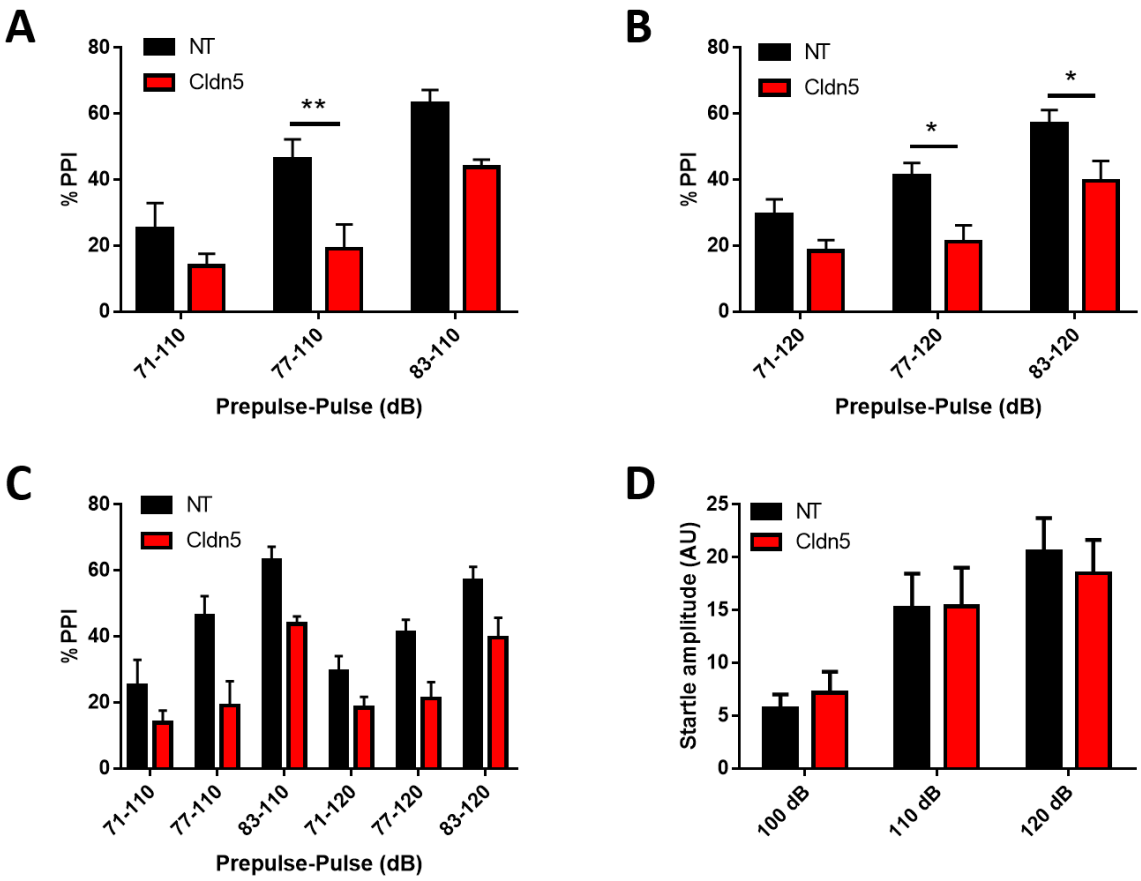

Figure 4.23: Sensorimotor gating deficits in claudin-5 knockdown mice. Analysis of prepulse inhibition of the acoustic startle response in NT and cre positive claudin-5 KD mice at 71, 77 and 83 dB pre-pulse sound levels with **(A, C)** 110 and **(B, C)** 120 dB pulse sound levels. **(D)** Analysis of startle amplitude at 100, 110 and 120 dB pulse sound levels. *P<0.05, **P<0.01 by two-way ANOVA with Bonferroni post-test. All data are means ± SEM with n = 10 for NT and n = 7 for CLDN5 groups.

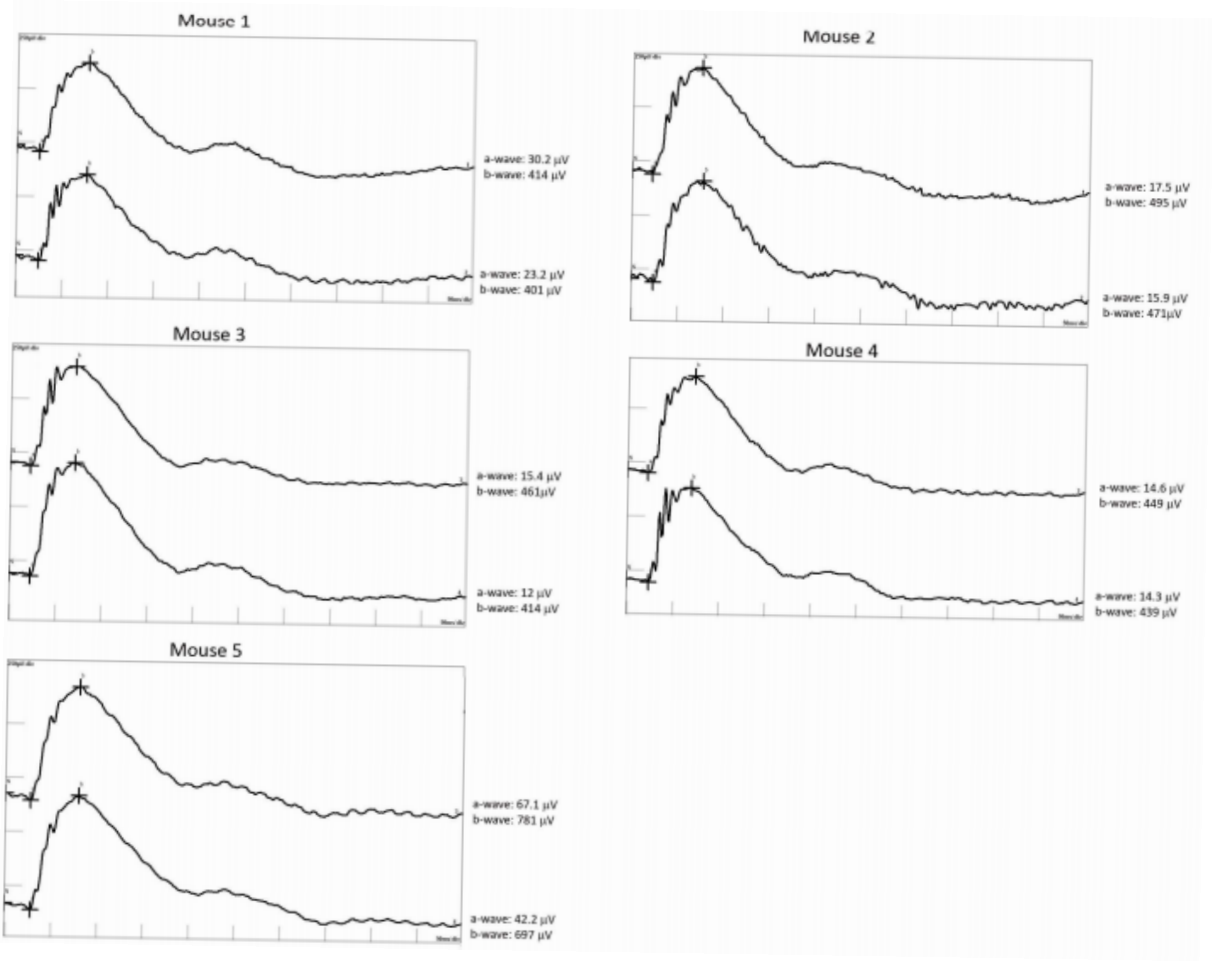

Figure 4.24: ERG readouts in claudin-5 knockdown mice. Sample ERGs from cre positive claudin-5 knockdown mice treated with doxycycline for 4 weeks that were dark adapted overnight.

4.2.8 Seizure activity and early mortality in claudin-5 knockdown mice

By the end of the behavioural testing of claudin-5 mice, a dramatic change in behaviour occurred. Persistent suppression of claudin-5 in this mouse model lead to mortality of all mice within approximately 5 weeks of constant doxycycline supplementation when compared to cre negative littermate control mice, NT control mice and claudin-5 knockdown mice not treated with doxycycline (Figure 4.25). All mice examined presented with similar phenotypes before death. Approximately 48 h prior to death the mice suffered from seizures and displayed hyperactivity followed by subsequent immobility. Mice ceased feeding and drinking and died approximately 48 h after the onset of seizures Mice were sacrificed at the onset of seizure activity and the brains were removed for analysis. Immunohistochemical analysis of the brains of mice following seizure activity revealed significant leakage of the large molecular weight glycoprotein fibrinogen in multiple brain regions including the frontal cortex and hippocampus (Figure 4.26). Seizures are typically characterised by NVU cell activation including astrocytic gliosis and microglial activation. Immunohistochemical analysis of the astrocyte marker GFAP revealed significantly increased staining primarily in the CA1, CA3 and dentate gyrus regions of the hippocampus of claudin-5 knockdown mice that displayed seizure activity compared to control mice (Figure 4.27). Following four weeks of doxycycline treatment, claudin-5 transcript remained suppressed with no change in the expression of ZO-1 transcript between claudin-5 knockdown mice and littermate controls (Figure 4.28A, C). RT-PCR analysis of whole brain RNA fractions revealed significantly increased transcript levels of GFAP with no change in transcript levels of the neuronal marker neun between claudin-5 knockdown mice and littermate controls (Figure 4.28B, D).

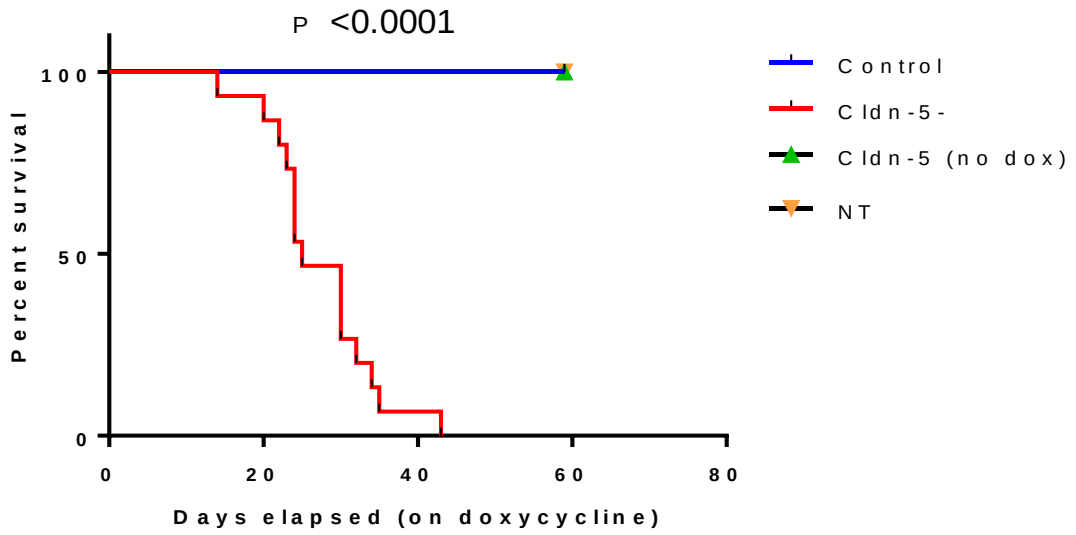

Figure 4.25: Early mortality in claudin-5 knockdown mice. Survival analysis of NT mice, cre negative claudin-5 knockdown mice, cre positive claudin-5 knockdown mice minus doxycycline and cre positive claudin-5 knockdown mice plus doxycycline. Cre positive mice supplemented with doxycycline in their diet all die by 42 days with a median survival time of 25 days compared with NT mice, cre negative mice, and cre positive mice not supplemented with doxycycline. ***P<0.001 by Log-rank (Mantel-Cox) test.

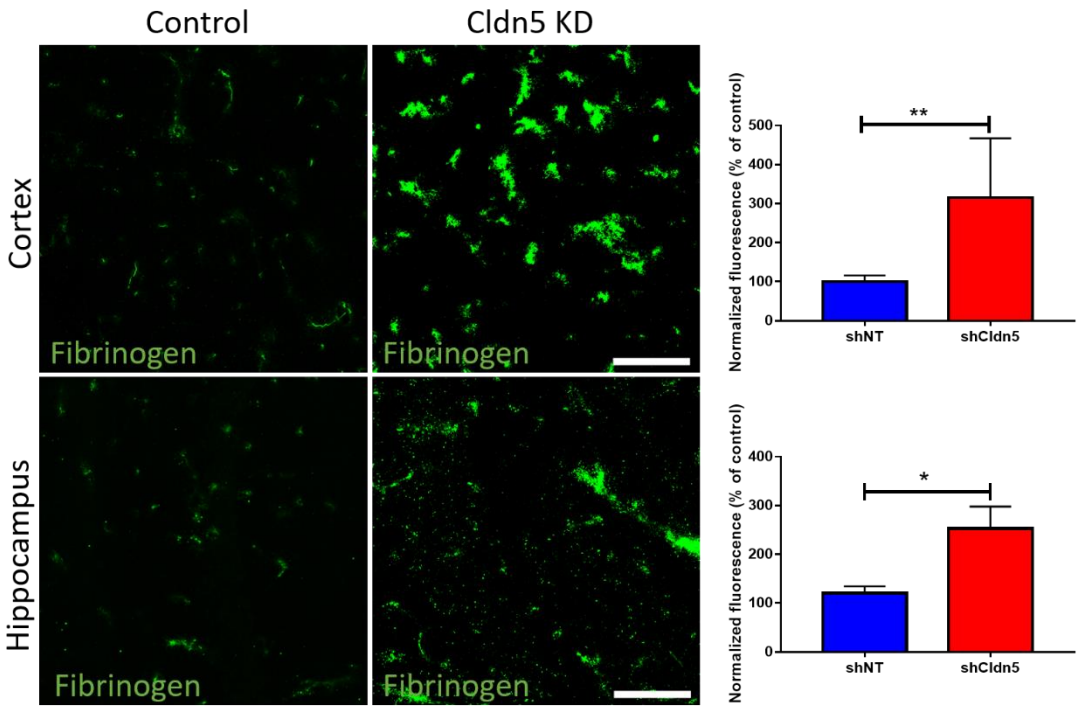

Figure 4.26: Fibrinogen extravasation in the brains of claudin-5 knockdown mice. Immunohistochemical analysis of fibrinogen in the brains of claudin-5 knockdown mice 4 weeks following treatment with doxycycline in the cortex and hippocampus. Scale bar – 100 µm. *P<0.05, **P<0.01 by Student's t-test. All data are means ± SEM with n = 5 mice per group.

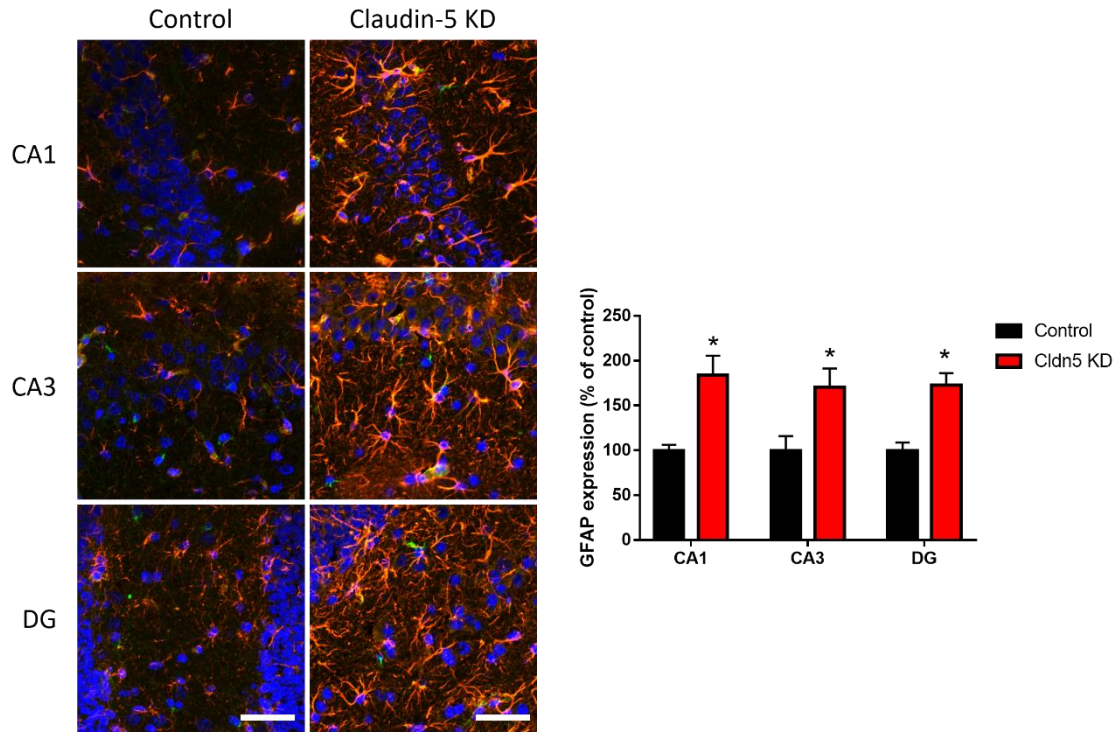

Figure 4.27: Reactive gliosis following seizure activity in the hippocampus of claudin-5 knockdown mice. Immunohistochemical analysis of GFAP in the brains of claudin-5 knockdown mice 4 weeks following treatment with 2 mg/ml doxycycline in the CA1, CA3 and dentate gyrus (DG) regions of the hippocampus. Quantification of GFAP levels was done in *ImageJ*. Scale bar – 50 µm. *P<0.05 by two-way ANOVA with Bonferroni post-test. All data are means ± SEM with n = 4 mice per group.

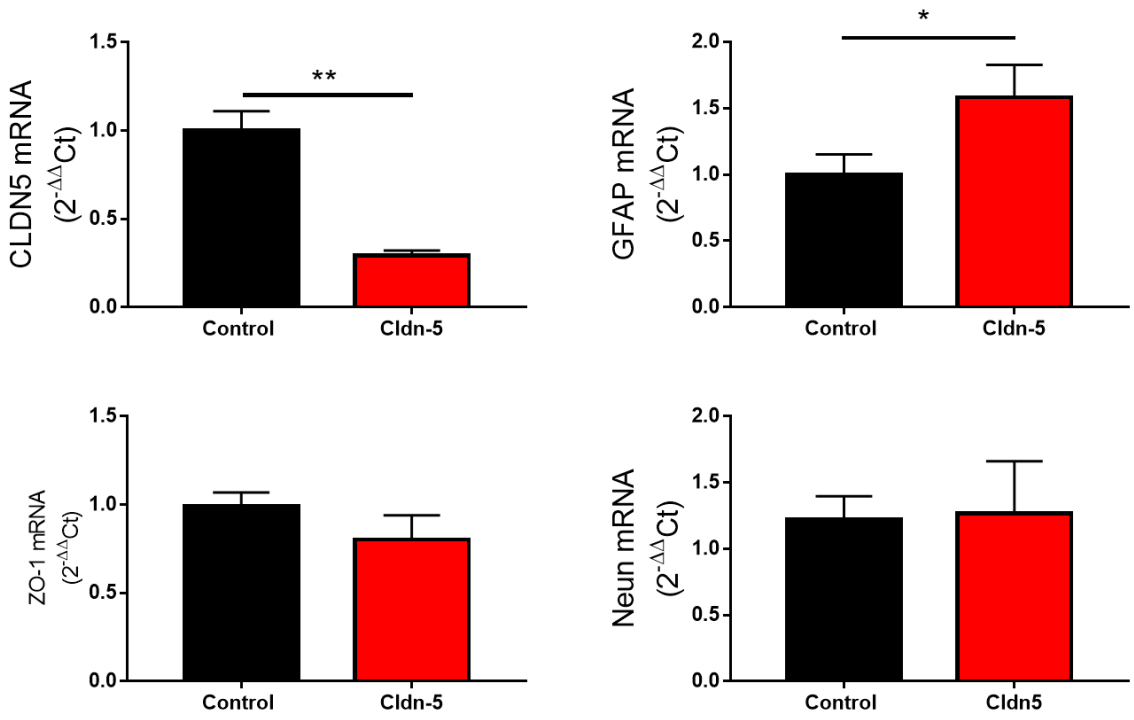

Figure 4.28: Transcript levels of TJ, astrocyte and neuron markers in claudin-5 knockdown mice. RT-PCR analysis of claudin-5, GFAP, ZO-1 and Neun in the brains of claudin-5 knockdown mice 4 weeks following treatment with doxycycline. *P<0.05, **P<0.01 by Student's t-test. All data are means ± SEM with n = 6 per group.

4.3 Discussion

Based on the findings in chapter 3 of an association between a claudin-5 SNP and schizophrenia and the down-regulation of claudin-5 in the brains of schizophrenia patients, a key aspect of this chapter was to understand the neurobehavioral sequelae of TJ disruption. Is it possible to induce schizophrenia-like behaviours in mice by specifically suppressing claudin-5? By utilising an AAV2/9-based approach, it was shown that stereotaxic injections of AAVs containing a doxycycline-inducible shRNA targeting claudin-5 transcript could specifically suppress claudin-5 in the dorsal hippocampus and mPFC which resulted in localised BBB permeability. Following three weeks of doxycycline supplementation, mice were subjected to an array of behavioural tests designed to identify impairments in several domains including learning and memory, depression, anxiety and locomotor. Suppression of claudin-5 in the dorsal hippocampus impaired affective behaviours in C57BL/6 mice with mice spending less time exploring a container containing a novel mouse in the social preference task and spending significantly less time exploring a novel mouse in the social novelty task. *Mus musculus* is a social species with high levels of reciprocal social interactions. Recent evidence has shown that the CA2 region of the hippocampus is essential for recognising a novel mouse as CA2 pyramidal neuron deficient mice spent less time exploring a novel mouse compared to controls in the social novelty test (Hitti and Siegelbaum, 2014). As can be seen in Figure 4.1, the primary site of accumulation of the stereotaxically injected AAV is the CA2 region of the hippocampus, suggesting that this region will invoke the greatest efficacy of suppression of claudin-5 and subsequently increase BBB permeability. Localised disruption of the BBB and increased permeability in the CA2 region produced significant deficits in the social novelty test. Several neuropsychiatric disorders including ASD, bipolar disorder and schizophrenia are characterised by reduced social behaviour and social isolation. Additionally, claudin-5 suppressed mice spent less time grooming in the spontaneous grooming test assessed on the open field test and in the forced grooming splash test. The mice also took longer to initiate grooming behaviours in both tests. Disruption of the neural microenvironment in this study by increasing localised BBB permeability may be affecting neural activity and synaptic signalling.

In contrast to the behavioural phenotype observed following suppression of claudin-5 in the dorsal hippocampus, suppression of claudin-5 in the mPFC significantly impaired the performance of mice on several learning and memory tasks. Mice performed worse on

the spontaneous alternation T-maze compared to controls as well as performing worse in the object recognition task, a non-spatial memory task. The object recognition task is a non-spatial memory task that is dependent on the perirhinal cortex, a region that has reciprocal connections with the mPFC. It has been shown that novel object recognition is dependent on the perirhinal cortex as lesions to it significantly impair performance. Lesions to the perirhinal cortex and mPFC significantly impairs performance in the object in place and temporal order memory tasks (Barker et al., 2007). Despite the proximity of the hippocampus to the perirhinal cortex, the hippocampus is not involved in object recognition memory as rodents with lesions to the hippocampus perform similarly to controls (Winters et al., 2004). Results outlined here suggest that BBB modulation in the mPFC and not the hippocampus may be affecting the neural circuitry between the mPFC and perirhinal cortex and subsequently impairing object recognition.

Interestingly, suppression of claudin-5 in the mPFC significantly reduced the time spent immobile in the forced swim test. The forced swim test is a well characterised measure of depressive-like behaviour and this result suggests that mice are resilient to the stressor. Hyperactive mice may spend less time immobile however suppression of claudin-5 in the mPFC had no impact on locomotor function. Alternatively, reduced immobility could point to increased anxiety in mice. However, mice showed no impairments in the elevated plus maze and performed similarly to control mice in the open field test. Development of resilience to a stressor is a highly complex process involving genetics, environment and neural circuitry. Several studies have identified several limbic regions in the forebrain that regulate emotional states. Research suggests that the mPFC, amygdala and hippocampus form a dynamic neural circuit that is key to acute stressor responses (Feder et al., 2009). Additionally, several hormones, neurotransmitters and neuropeptides are involved in the acute response to stress, for example cortisol, and changes in localised BBB permeability may interfere with this process (Feder et al., 2009). To control for potential loss of motor coordination following stereotaxic surgery that could confound the results of the various behavioural tests, several locomotor tests were performed. All groups of mice remained on the rotarod for similar lengths of time, travelled similar distances in the open field test and travelled at similar speeds in the open field test and radial arm maze.

It is evident that regional suppression of claudin-5 produces a dissociative phenotype in mice with several correlates of schizophrenia including reduced social interaction and cognitive decline. The next aim of this chapter was to determine the effect of claudin-5 suppression across all brain regions. To achieve this, a mouse model was developed that would facilitate inducible RNAi-based suppression of claudin-5 levels in the brain. Initially, shRNAs were screened in the brain endothelial cell line, bEnd.3, and an shRNA that could suppress claudin-5 mRNA was selected to be incorporated into embryonic stem cells for subsequent blastocyst injection for the development of a knockdown mouse. Doxycycline is a tetracycline antibiotic routinely used in tet-inducible gene expression systems. This knockdown system utilises the tet-on regulation of gene expression, where the presence of doxycycline activates expression. This system makes use of the rtTA protein which can bind to specific TetO operator sequences only in the presence of doxycycline (Das et al., 2016). By administering doxycycline to the water of cre positive claudin-5 knockdown mice, expression of claudin-5 shRNA could be observed localised with rtTA in microvessels. Western blot data and RT-PCR data showed reduced levels of claudin-5 with no effect on the levels of other TJ components including occludin, tricellulin and the scaffolding protein ZO-1. Suppression of claudin-5 in knockdown mice produced BBB disruption that was assessed by DCE-MRI with comparable results observed in previous studies that have used claudin-5 siRNA to suppress claudin-5 (Campbell et al., 2012, Keaney et al., 2015). Knockdown of claudin-5 induced BBB permeability but the normal patterning of vascular networks was maintained.

Claudin-5 knockdown mice were treated with doxycycline for two weeks prior to assessing the behavioural phenotype. These mice had several learning and memory impairments with mice performing worse on the T-maze, a hippocampal dependent task of spatial memory. Additionally, mice showed impairments on the object recognition task, a test designed to evaluate recognition memory and the natural propensity of mice to explore a novelty. In rodents, the parahippocampal regions of the temporal lobe are important for visual object recognition with damage to the region impairing performance (Hammond et al., 2004). Claudin-5 knockdown mice showed no differences on the Y-maze compared to controls however this potentially be explained by the development of a significant side-bias, that is, the mice preferentially turned in one direction. Hippocampectamised animals typically develop a strong side preference (Deacon and Rawlins, 2006), e.g., always turning right in the Y-maze. Because of a side-preference,

mice in the Y-maze have the potential to outperform controls and it is difficult to identify memory errors. Claudin-5 knockdown mice also displayed heightened anxiety as measured on the elevated plus maze. Claudin-5 knockdown mice preferred the sheltered, enclosed arms, rarely venturing out onto the open arms. No differences were detected on various locomotor-based tasks between claudin-5 knockdown mice and controls, with similar performances observed on the rotarod, open field test and radial arm maze. ERG analysis of claudin-5 KD mice treated with doxycycline for four weeks revealed normal a-wave and b-wave responses indicating normal visual function.

The final behavioural domain assessed in the inducible knockdown mice was sensorimotor gating. Specifically, PPI of the acoustic startle response was assessed in claudin-5 knockdown mice. PPI is a measure of sensorimotor gating that is conserved across species. It is a neurological phenomenon whereby a non-startling stimulus can inhibit or condition an animal's response to a subsequent startling stimulus. PPI can be assessed by different parameters including tactile, acoustic and light stimulus. While deficits in PPI are found in several psychiatric conditions including obsessive compulsive disorder, Huntington's disease, panic disorder and adults with autism (Powell et al., 2009), PPI deficits in schizophrenia patients are the most widely replicated and consistently observed behavioural abnormalities in schizophrenia patients (Kumari et al., 2008, Ludewig et al., 2003, Mackeprang et al., 2002). In this thesis, PPI of the acoustic startle response was examined at three prepulse sound levels (71 dB, 77 dB and 83 dB) in combination with 3 pulse sound levels (100 dB, 110 dB and 120 dB). Claudin-5 knockdown mice had significant deficits in PPI at 77 dB prepulse with 110 dB pulse and at 77 dB and 83 dB prepulse with 120 dB pulse. Examination of the acoustic startle response of these mice revealed no significant differences between claudin-5 knockdown and control mice.

The initial claudin-5 knockout mouse described by Nitta et al dies within hours of birth from unknown causes (Nitta et al., 2003). In this chapter, chronic suppression of claudin-5 in adult mice caused early mortality with a median survival time of 30 days. Additionally, the mice showed severe changes in behaviour that preceded death that included hyperactivity and seizures that was followed by a cessation of movement and subsequent death within 48 h of seizure onset. Accompanying seizure activity was a more profound loss of BBB integrity with extravasation of fibrinogen, a 340 kDa glycoprotein

involved in the clotting of blood. Indeed, a possible explanation for the behavioural impairments that are evident following site-specific and global suppression of claudin-5 in the mouse brain is neuronal excitability resulting from imbalances in ionic concentrations of potassium and glutamate due to impaired BBB integrity. Glutamate is the major excitatory neurotransmitter in the brain and neuronal excitotoxicity from impaired glutamate regulation may cause status epilepticus and seizure activity in the claudin-5 knockdown mice. Additionally, leakage of high molecular weight molecules normally present in the circulation into the brain parenchyma of claudin-5 knockdown mice may exacerbate seizure activity and behavioural outcome. Fibrinogen is known to extravasate into the brain following TBI and can inhibit neurite outgrowth (Schachtrup et al., 2007). Additionally, fibrinogen deposits are found in human AD patients and mouse models of AD and reductions of fibrinogen can decrease neuronal degeneration (Cortes-Canteli et al., 2015). Leakage of blood components into the CNS is a common pathological finding in TBI (Chodobski et al., 2011) and epilepsy (Roch et al., 2002). Albumin extravasation into the CNS is found in humans after status epilepticus and in rat models where surrounding cell types could engulf albumin including neurons, microglia and astrocytes. Additionally, artificial opening of the BBB exacerbated seizure activity in rats (van Vliet et al., 2007). It is known that BBB disruption is associated with seizures, with seizures and epilepsy commonly observed in combination with stroke and TBI, conditions known to disrupt the BBB. BBB disruption has been associated with seizures in both congenital disorders such as GLUT-1 deficiency and in acquired disorders such as those resulting from TBI (De Giorgis and Veggiotti, 2013, Friedman, 2011). However, there is much debate over whether BBB breakdown occurs before, during or after seizure or whether a compromised BBB is a component of the aetiology of epilepsy or a consequence of seizure. Animal studies have provided some insight. Seiffert and colleagues induced focal disruption of the BBB via application of bile salts to the rat cortex. This resulted in the long-lasting extravasation of serum albumin to brain parenchyma. Electrophysiological recordings of brain slices identified epileptiform discharges that developed within one week of treatment and could be recorded for up to 49 days. Additionally, albumin extravasation was associated with astrocyte activation without an immunological response (Seiffert et al., 2004). In the claudin-5 knockdown mouse, chronic treatment with doxycycline induced seizure-like activity and large molecule leakage from blood to brain. RT-PCR analysis revealed elevated GFAP transcripts along with prominent astrocytic gliosis notably in the CA1, CA3 and dentate

gyrus of the hippocampus. However, without electroencephalograms to monitor electrical activity in the brains of these mice, it is difficult to ascertain the nature of this seizure-like activity or the point of origin in the brain.

Future studies will be required to investigate the effect of anti-epileptic drugs on the seizure-activity in claudin-5 knockdown mice. Several studies have examined the therapeutic effect of anti-epileptic medications in animal seizure models and their impact on restoring BBB integrity. For example, previous studies have shown that levetiracetam can attenuate BBB dysfunction and reduce permeability resulting from pilocarpine-induced status epilepticus in mice. In the study by Itoh et al, levetiracetam efficiently reduced astrogliosis, microglia activation, angiogenesis and neuronal cell loss (Itoh et al., 2016). In the hyperthermia-induced seizure model in rats, treatment with levetiracetam can reduce leakage of sodium fluorescein and restore levels of occludin protein (Ahishali et al., 2010). Pretreatment of rats with levetiracetam for one week prior to pentylenetetrazol kindling reduced sodium fluorescein extravasation and pinocytotic vesicle formation (Gurses et al., 2009).

In summary, suppression of claudin-5 in distinct brain regions and across the brain in an inducible knockdown model impairs the behaviour of mice with some phenotypic correlates of schizophrenia, notably a reduction of PPI and reduced grooming and social interaction as well as signs of subtle cognitive decline (Figure 4.29 and Table 4.1). Additionally, persistent suppression of claudin-5 induces dramatic behavioural changes, with tail-flickering, seizure activity and cessation of movement and subsequent death. Analysis of the brains of mice revealed leakage of high molecular weight serum proteins as well as activation of astrocytes. This chapter has shown that disruption of homeostasis within the CNS via increased permeability of the BBB can impair normal neurological function in mice to induce behavioural abnormalities typically observed in individuals with schizophrenia and other neuropsychiatric disorders.

4.3.1 Comparisons with other animal models of schizophrenia

The development of reliable, predictive clinical models for complex disorders such as schizophrenia is vital to understanding the neurobiological basis of the disorder and for the development of novel drugs with better therapeutic efficacy. Animal models of schizophrenia fall under 4 categories: developmental models, drug-induced models,

lesion models and genetic models. The major limitation of animal models of schizophrenia is identifying a model that uniquely recapitulates the positive, negative and cognitive dysfunction symptoms of schizophrenia. Typically, models show behavioural phenotypes that resemble positive symptoms with few showing negative symptoms such as impaired social interaction and learning and memory deficits. There are several core domains of cognition that have been identified as deficient in schizophrenia: working memory, attention, verbal learning and memory and social cognition (Young et al., 2009) and assessment of animal models should focus on a behavioural battery of tests that comprises these domains.

Raising rats in social isolation is a well described developmental model to understand the developmentally linked emergence of neural and behavioural abnormalities in schizophrenia patients. For example, isolation rearing of rats leads to deficits in PPI (Powell and Geyer, 2002, Geyer et al., 2001). The neonatal ventral hippocampal lesion model is a particularly translational animal model of schizophrenia. This model involves the infusion of an excitotoxin into the ventral hippocampus during the first postnatal week. This model has several behavioural abnormalities including hyperlocomotion, PPI deficits, impaired working memory and addictive behaviour. Additionally, most of these abnormalities don't manifest until post adolescence (Brady, 2016).

As described in section 1.3.3 the core group of deleted genes at the 22q11DS locus are conserved on chromosome 16 in mice. Several 22q11DS models have been developed with the most recent model displaying behavioural characteristics of schizophrenia including PPI deficits, altered acoustic startle response and hyperlocomotion (Didriksen et al., 2017). Disrupted in schizophrenia (DISC1) is a strong candidate schizophrenia susceptibility gene for schizophrenia, bipolar disorder and depression. Mice carrying a DISC1 orthologue have deficits in short-term plasticity and cognitive deficits in working memory tasks (Kvajo et al., 2008). Furthermore, transgenic mice expressing a dominant-negative DISC1 displayed deficits in cognitive control of adaptive behaviour as well as reduced social interaction in the social novelty test (Johnson et al., 2013). COMT is a schizophrenia susceptibility gene located in the 22q11DS locus. It encodes catechol-O-methyltransferase, an enzyme involved in the catabolism of dopamine. COMT knockout mice had dysregulated dopamine levels particularly in the frontal cortex of male mice. Behaviourally, female mice displayed impaired emotional reactivity in the dark/light

exploratory model of anxiety while male mice exhibited increased aggressive behaviour (Gogos et al., 1998) with no changes in PPI in either sex.

The glutamate hypothesis of schizophrenia, similarly to the dopamine hypothesis, was based on a chance clinical observation that NMDA receptor antagonists such as phencyclidine (PCP) and ketamine produced symptoms and cognitive deficits in volunteers like those observed in schizophrenia, resulting from neurotransmission blockade at NMDA-type glutamate receptors. PCP is a non-competitive NMDA receptor antagonist that when administered to rodents, reproduces a schizophrenia-like psychosis including positive symptoms, negative symptoms and cognitive dysfunction. PCP treated animals exhibit hyperlocomotion, social behaviour deficits in the social interaction test and increased immobility in the forced swim test. Additionally, PCP treated animal have PPI deficits and cognitive deficits in several learning and memory tests (Enomoto et al., 2007).

Like the above-mentioned models, the inducible claudin-5 knockdown mouse model displays a reduction in PPI, along with impaired working memory. In addition, targeted suppression of claudin-5 is specific neural regions induces learning and memory impairments. Moving ahead, it will be worthwhile to determine if these abnormalities manifest in pre-adolescent mice.

4.4 Conclusions

- Site specific BBB modulation alters behaviour in mice
- Suppression of claudin-5 across the whole brain induces a wide range of behavioural impairments in mice
- Claudin-5 knockdown mice have PPI deficits
- Large molecule leakage is evident following chronic suppression of claudin-5 in the induce knockdown mouse
- Persistent suppression of claudin-5 causes spontaneous seizure activity and early mortality in claudin-5 knockdown mice

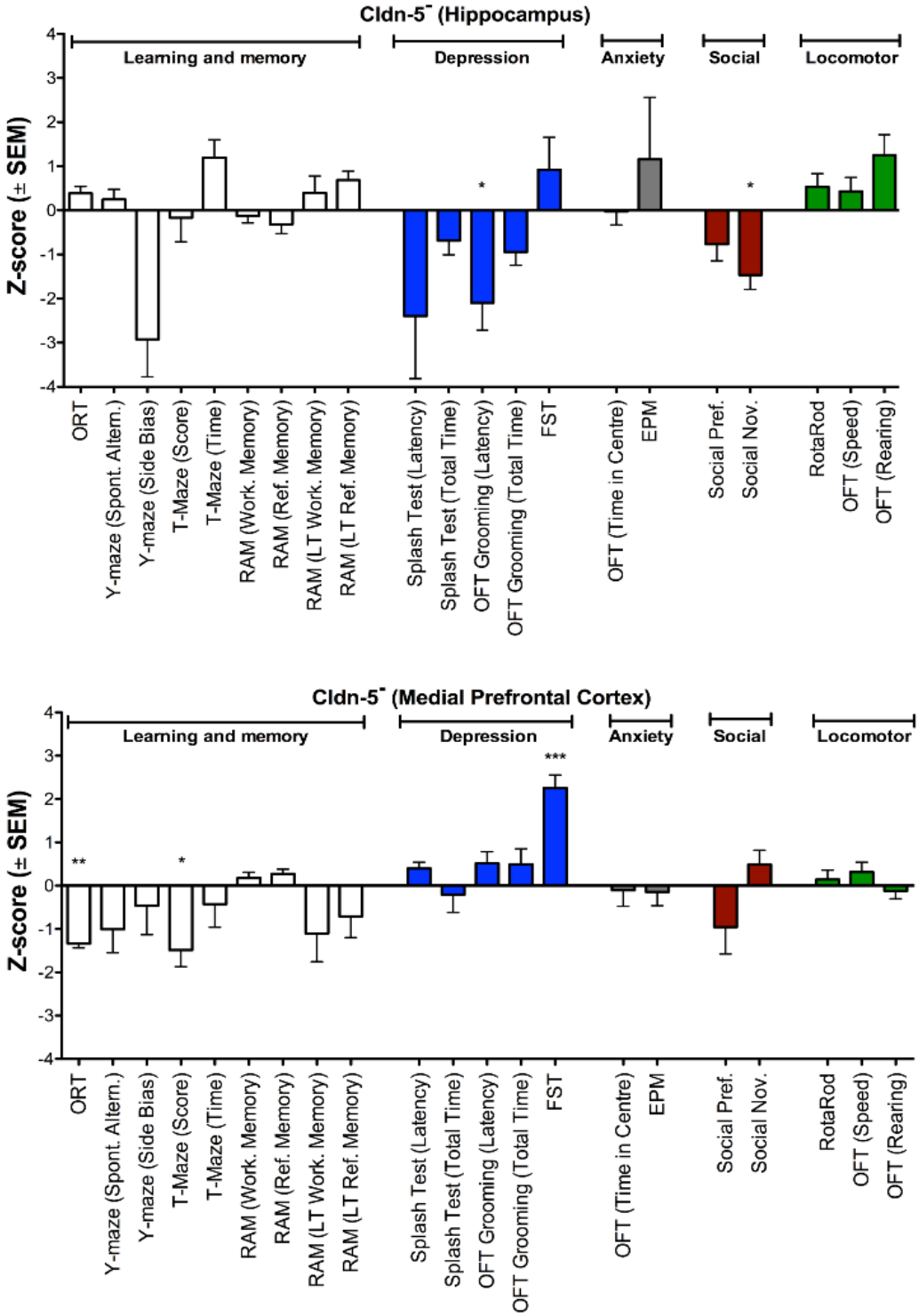

Figure 4.29: Summary of the complete behavioural readout following suppression of claudin-5 in the dorsal hippocampus and mPFC in C57BL/6 mice treated with doxycycline for three weeks. All data are Z-scores ± SEM. Summary slides were created by Dr. John Kealy.

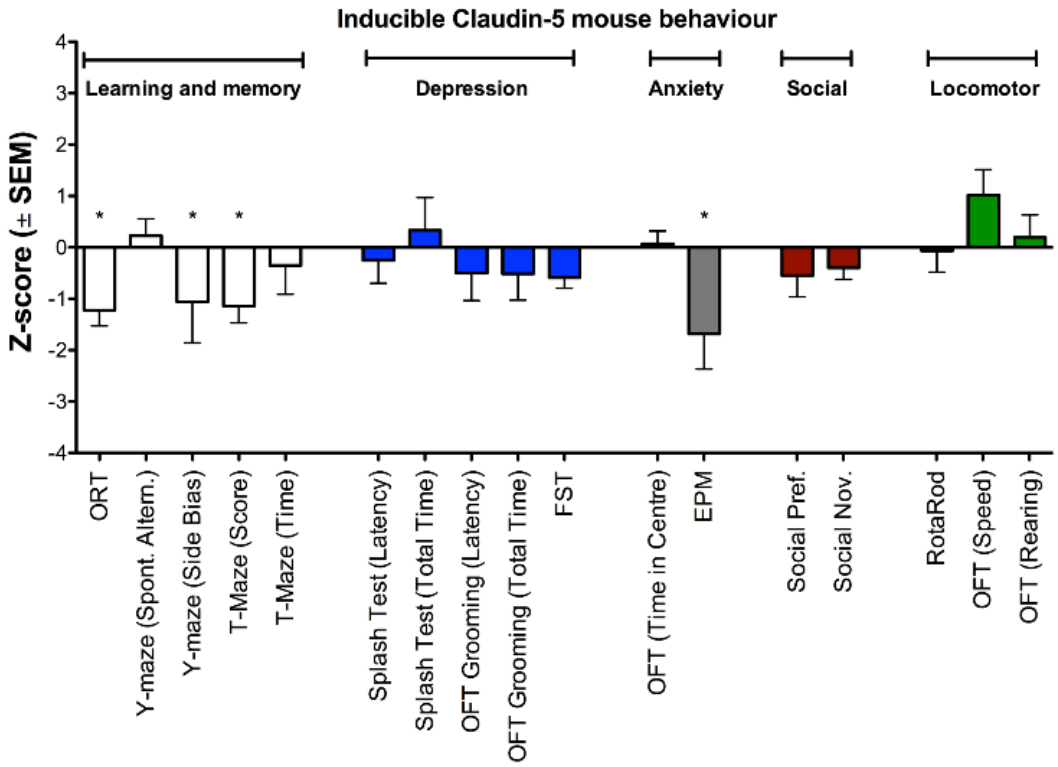

Figure 4.29 continued: Summary of the complete behavioural readout following suppression of claudin-5 in doxycycline-inducible claudin-5 knockdown mice treated with doxycycline for three weeks. All data are Z-scores ± SEM. Summary slides were created by Dr. John Kealy.

	DH	mPFC	KD
ORT	-	↓↓	↓
Y-Maze (Spont. Altern.)	-	-	-
Y-Maze (Side Bias)	-	-	↓
T-Maze (Score)	-	↓	↓
T-Maze (Time)	-	-	-
RAM (Work. Memory)	-	-	-
RAM (Ref. Memory)	-	-	-
RAM (LT Work. Memory)	-	-	-
RAM (LT Ref. Memory)	-	-	-
Splash Test (Latency)	-	-	-
Splash Test (Total Time)	-	-	-
OFT Grooming (Latency)	↓	-	-
OFT Grooming (Total)	-	-	-
Forced Swim Test	-	↓↓↓	-
OFT (Time in Centre)	-	-	-
EPM	-	-	↓
Social Pref.	-	-	-
Social Nov.	↓	-	-
Rotarod	-	-	-
OFT (Speed)	-	-	-
OFT (Rearing)	-	-	-
PPI	-	-	↓↓
ASR	-	-	-

Table 4.1: Behavioural phenotype following suppression of claudin-5 in the dorsal hippocampus (DH), mPFC and claudin-5 knockdown mouse. ORT – object recognition task, OFT – open field test, EPM – elevated plus maze, RAM – radial arm maze, LT – long term, PPI – prepulse inhibition, ASR – acoustic startle response.

Chapter 5:

Assessment of circadian rhythms in brain endothelial cells in wild-type mice *in vivo* and *in vitro* following serum shock treatment

5.1 Introduction

Many aspects of mammalian behaviour and physiology show circadian rhythmicity, including sleep, body temperature, hormone levels, blood pressure and immune function. These diverse rhythms are controlled by a single portion of the anteroventral hypothalamus called the suprachiasmatic nucleus (SCN), a paired neuronal structure with each nucleus consisting of approximately 10,000 neurons in mice (Abrahamson and Moore, 2001). The SCN functions to synchronise all circadian clocks in the body to one another and to the 24 h day. Lesions to the SCN eliminate 24 hour circadian rhythms (Stephan and Zucker, 1972) while transplantation of a donor SCN can restore behavioural rhythms (Drucker-Colin et al., 1984). The SCN receives photic information from photosensitive ganglion cells in the retina via the retinohypothalmic tract (Eckel-Mahan and Sassone-Corsi, 2013) (Figure 5.1). Interactions between retinal ganglion cells and SCN neurons leads to glutamate release, membrane depolarisation and subsequent calcium influx. This then leads to the activation of multiple kinases such as MAPK and AMPK and phosphorylation of CREB. Phosphorylated CREB can then induce CREB targets by binding to calcium/cAMP response elements of genes, such as PER1/PER2 (Meijer and Schwartz, 2003). Induction of PER1 occurs within 15 min of a light pulse and could mediate clock resetting owing to its involvement in the core clock feedback loop (Welsh et al., 2010). The central mechanism driving circadian rhythms is the circadian clock. The clock is a biochemical mechanism that generates molecular rhythms with 24 h periodicity when entrained by external environmental cues, primarily daylight and darkness. The major components of the circadian clock are; a self-sustained oscillator with a period of 24 hours that keeps time; input pathways (environment) to allow entrainment of the clock and; output pathways that regulate overt biochemical, physiological or behavioural rhythms in an organism (Buhr and Takahashi, 2013). The clock is reset through external time cues that are sensed by the organism, the primary one of which is light. Such is the importance of a normal circadian rhythm that disruptions have been linked to various neurological disorders, most notably depression and sleep disorders; but it has also been linked with cancer and cardiovascular function. In fact, many molecular gears constituting the circadian clock have been found to functionally interplay with regulators of the cell cycle and malfunctions in these can lead to aberrant cell proliferation (Savvidis and Koutsilieris, 2012).

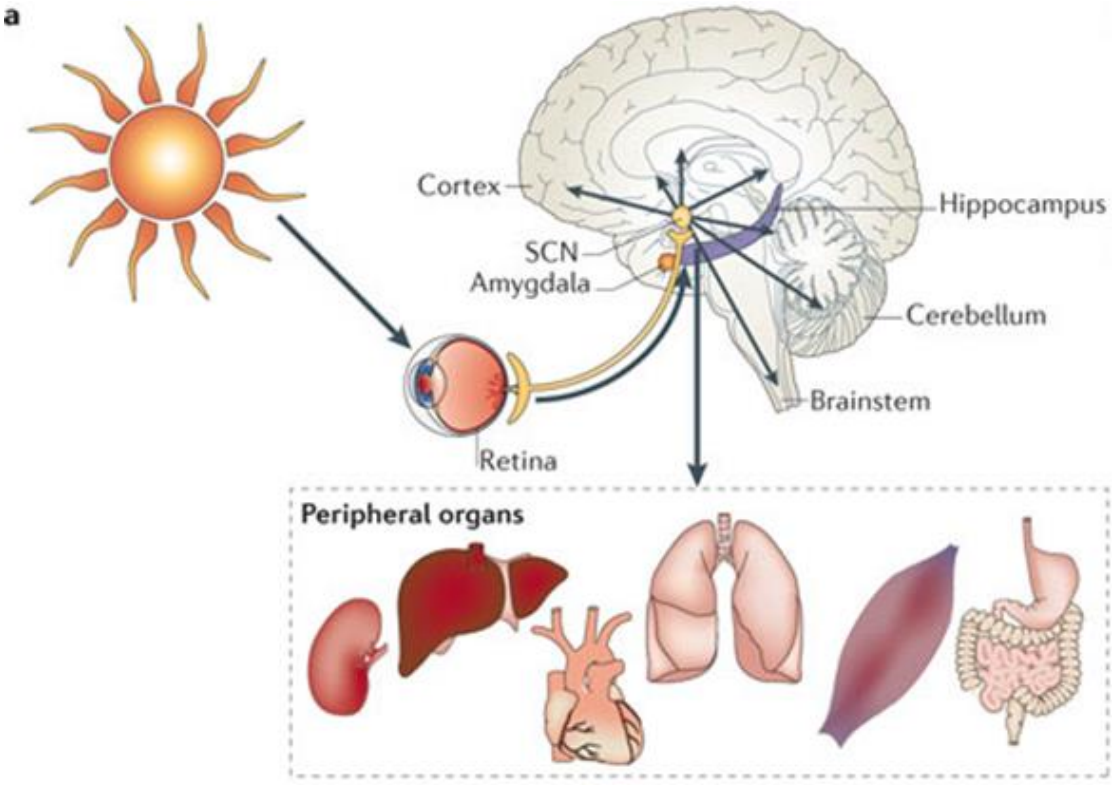

Figure 5.1: Circadian rhythms**.** The SCN of the hypothalamus receives information from light sensitive ganglion cells in the retina which allows for entrainment of daily rhythms to the 24-hour cycle in nature. Source: (Kondratova and Kondratov, 2012)

5.1.1 Feedback loops drive circadian rhythms

Circadian rhythms are approximately 24 h oscillations in behaviour and physiology controlled by the SCN of the hypothalamus. Circadian rhythms are formed at the cellular level by transcription factors that form a transcriptional activator/repressor feedback loop that governs gene expression of circadian controlled genes. In mammals, the circadian oscillation system is controlled by a "master" clock in the SCN of the anterior hypothalamus which regulates downstream oscillators in peripheral tissues (Ralph et al., 1990). A recent RNA-seq study identified that 43% of protein-coding genes oscillate in at least one organ in mice (Zhang et al., 2014). Core clock components refer to genes, the protein product of which are necessary for the generation and regulation of circadian rhythms. Several clock genes have been identified including circadian locomotor output cycles protein kaput (CLOCK) and brain and muscle aryl hydrocarbon receptor nuclear translocator-like protein-1 (BMAL-1) which are members of the basic helix-loop-helix family of transcription factors. The positive loop is comprised of BMAL-1 and CLOCK. In the cytoplasm, CLOCK and BMAL-1 dimerise and, upon translocation to the nucleus,

bind to specific E-box cis regulatory enhancer sequences in the promoter region of clock-controlled genes. CLOCK/BMAL-1 promote expression of genes involved in the negative loop including period (PER) and cryptochrome (CRY). The repressor feedback loop is formed when PER and CRY dimerise, translocate to the nucleus and repress their own transcription by inhibiting CLOCK: BMAL-1 dimers from interacting with E-box sequences (Gekakis et al., 1998, Griffin et al., 1999, Kume et al., 1999). Another regulatory loop is created when CLOCK: BMAL-1 dimers activate transcription of members of the REV-ERB (α and β) and ROR (α, β and γ), two retinoic acid-related orphan nuclear receptors. The promoter region of BMAL-1 contains retinoic acid-related orphan nuclear receptor response elements (ROREs), which members of ROR and REV-ERB can bind to regulate expression of BMAL-1. It has been shown that ROR members can activate transcription of BMAL-1 while REV-ERBs repress transcription (Guillaumond et al., 2005). Overall, the molecular pattern of circadian rhythms can be considered as a genetic network of interconnected negative feedback loops governing the transcription of core clock genes (Ueda et al., 2005).

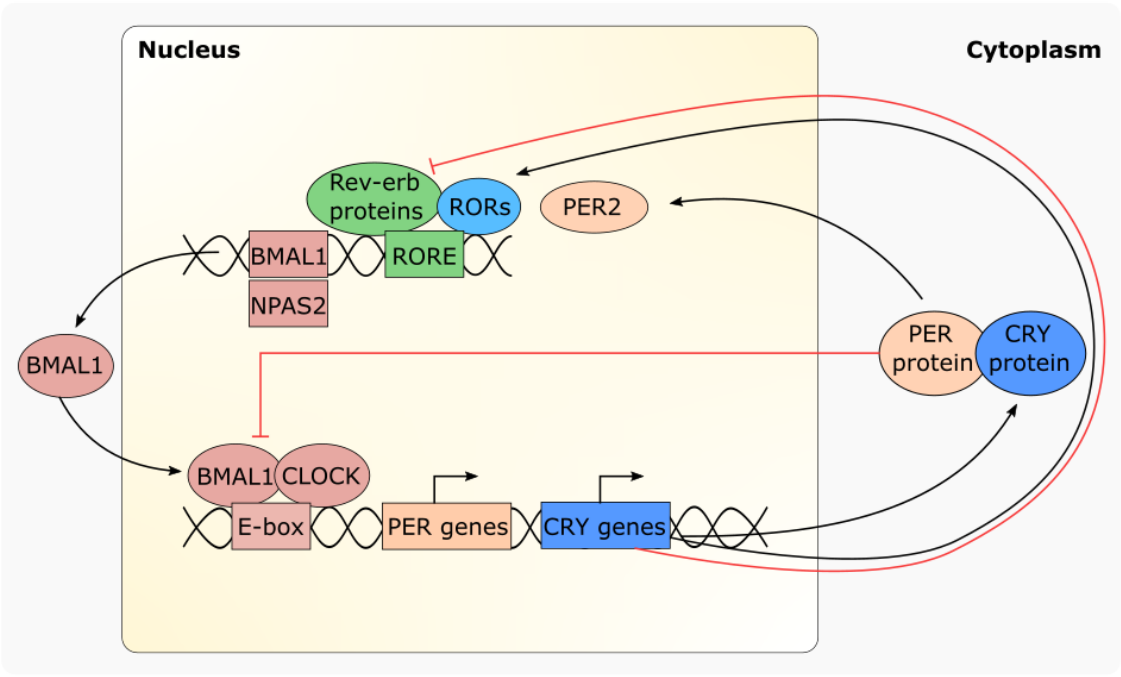

Figure 5.2: Molecular organisation of circadian rhythms. The generation of circadian rhythms is regulated by a transcriptional, translational regulatory feedback loop. In the nucleus, BMAL-1 and CLOCK dimers can bind to E-box sequences in the promoter region of clock-controlled genes such as PER and CRY. In the cytoplasm, dimers of the recently synthesised PER and CRY proteins translocate to the nucleus where they inhibit BMAL-1:CLOCK binding to E-box sequences to ultimately repress their own transcription. Additional regulatory loops are formed when BMAL-1:CLOCK activate transcription of ROR and REV-ERB which can activate and inhibit transcription of BMAL-1 respectively.

Disorders associated with disruption of circadian rhythms have also been associated with loss of BBB integrity. Sleep disruption is known to be common in a wide range of neurological disorders including schizophrenia with abnormalities in the phases of sleep being correlated with the severity of symptoms in schizophrenia for example. Additionally, anti-psychotic treatment is known to cause further perturbation of sleep (Miller, 2004). Up to 80% of individuals with schizophrenia report sleep disruption as a common co-morbidity of the condition (Wilson and Argyropoulos, 2012). Sleep is a universal and essential state among animals that is characterized by decreased sensory responsiveness and reduced muscle tone. The biological functions and necessity of sleep are still largely unclear though sleep likely assists in tissue repair, consolidation of memories and immune system function. Sleep deprivation can lead to significant and permanent impairments in neurocognitive function and increases the risk of developing conditions such as Alzheimer's disease (Musiek et al., 2015). Two recent studies have found that sleep deprivation, in the form of chronic sleep restriction (CSR) or selective rapid-eye-movement (REM) sleep deprivation, can increase BBB permeability. Firstly, REM sleep restriction increased BBB permeability to Evans blue. Subsequently it was determined that CSR was associated with reduced GLUT-1 and TJ mRNA and protein expression at the BBB, decreased brain glucose uptake and increased paracellular permeability to sodium fluorescein and biotin tracer molecules. In both studies, sleep recovery restored BBB structure and function including a return to baseline TJ protein levels (Gomez-Gonzalez et al., 2013, He et al., 2014). Related work has also elucidated the role of sleep in regulating the exchange of material such as Aβ between the CSF and interstitial fluid (ISF) along paravenous drainage pathways (the so-called ‘glymphatic’ system) (Xie et al., 2013). These combined findings suggest that sleep regulation of cerebrovascular clearance pathways is vital to maintaining brain homeostasis. The aim of this chapter was to explore the role of the circadian clock in regulating TJ components and BBB integrity.

5.1.2 Objectives

- To screen brain capillary ECs for clock components
- To determine the effect of time of day on BBB integrity
- To establish circadian rhythms *in vitro* and examine the disruption of circadian components on BBB integrity

5.2 Results

5.2.1 Clock transcription factors are expressed in mouse BMVEC

To investigate the effect of circadian rhythms on BBB components, C57BL/6 mice were housed on a 12 h light-dark cycle with lights on at 8 am and lights off at 8 pm. Five mice were sacrificed at 8 am (ZT0), 2 pm (ZT6), 8 pm (ZT12) and 2 am (ZT18) and cerebral microvessels were isolated for RT-PCR and western blot analysis. RT-PCR analysis revealed that capillaries expressed the core clock transcription factors BMAL-1, REV-ERBα and PER2 and that these transcription factors cycled throughout the day (Figure 5.3). To determine if the expression of clock transcription factors was circadian, mice were subsequently housed in complete darkness and microvessels were isolated as before. C57BL/6 mice that were housed in complete darkness for 24 h showed the same expression patterns of these transcription factors indicating that they continue to cycle in the absence of light stimulus in CNS ECs.

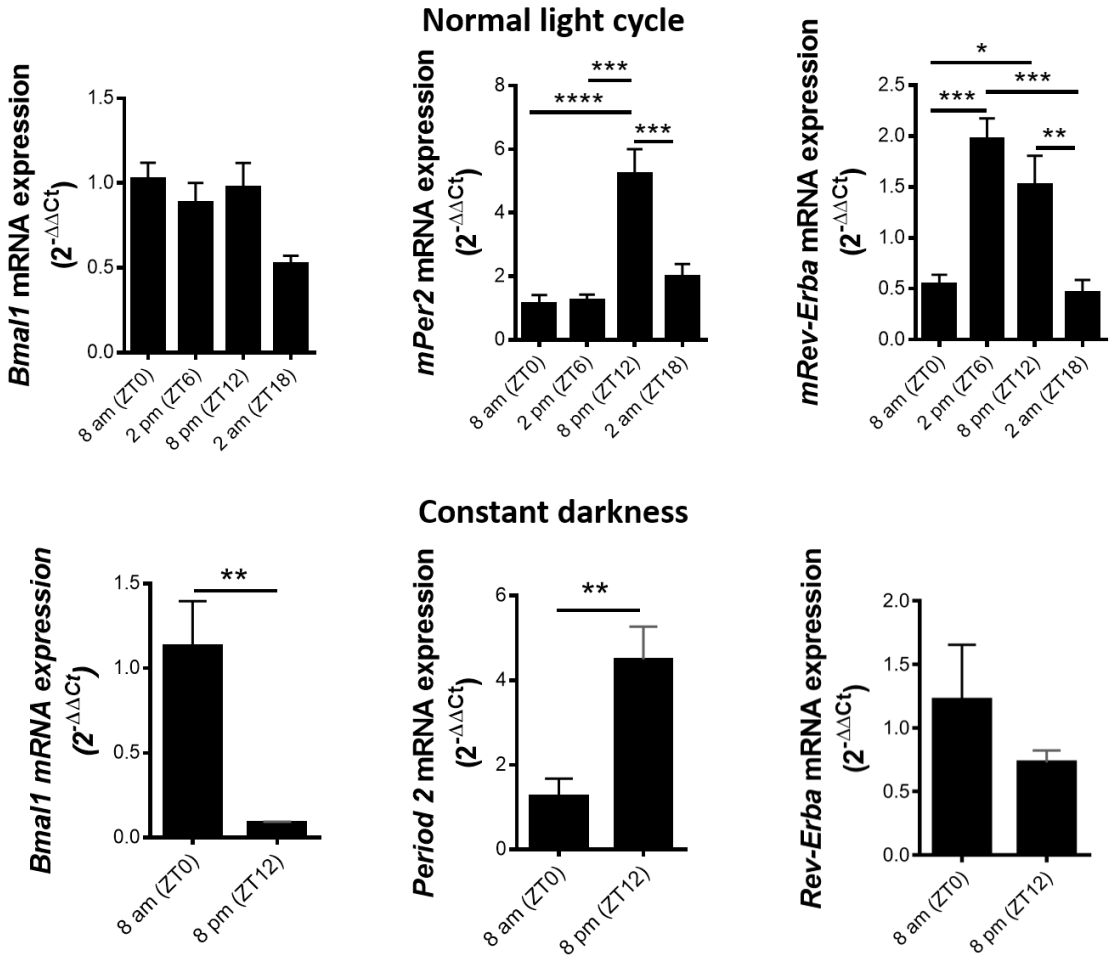

Figure 5.3: Circadian clock components cycle throughout the day in C57BL/6 mice. RT-PCR analysis of BMAL-1, Per2, and REV-ERBα in cerebral microvessels isolated from C57BL/6 mice kept on a normal light-dark cycle (top panel) and in constant darkness (bottom panel) at 8 am (ZT0), 2 pm (ZT6), 8 pm (ZT12) and 2 am (ZT18). *P<0.05, **P<0.01, ***P<0.001 by Student's t-test or ANOVA with Bonferroni post-test. All data are means ± SEM with n =5 per group.

5.2.2 TJ components cycle throughout the day in C57BL/6 mice

RT-PCR analysis revealed that clock transcription factors cycled in brain ECs *in vivo* so it was next determined if TJ components also displayed a circadian rhythmicity. RT-PCR analysis of TJ transcripts revealed that claudin-5 cycled throughout the day with minimal mRNA expression detected at ZT12 for claudin-5. Additionally, ZO-1 levels were significantly increased at ZT12 with no differences detected in the levels of occludin at any timepoint. RT-PCR analysis of claudin-5 from mice housed in complete darkness showed the same pattern of expression from ZT0 to ZT12 with significantly reduced claudin-5 mRNA levels at ZT12. Levels of ZO-1 were unchanged and occludin was significantly decreased at ZT12. To determine if this cycling of claudin-5 was specific to brain ECs or was evident in other tissues, RNA was isolated from retinas and hearts of C57BL/6 mice at ZT0 and ZT12. RT-PCR analysis for claudin-5 revealed similar expression patterns as observed in brain ECs with significantly reduced claudin-5 transcript levels at ZT12 (Figure 5.5A, B). The circadian database is an online repository of gene expression studies identifying genes that have a circadian pattern of expression. Microarray data taken from the Circadian database showed that claudin-5 cycles in numerous organs including the heart, adrenal gland, skeletal muscle and hypothalamus (Figure 5.5C-F).

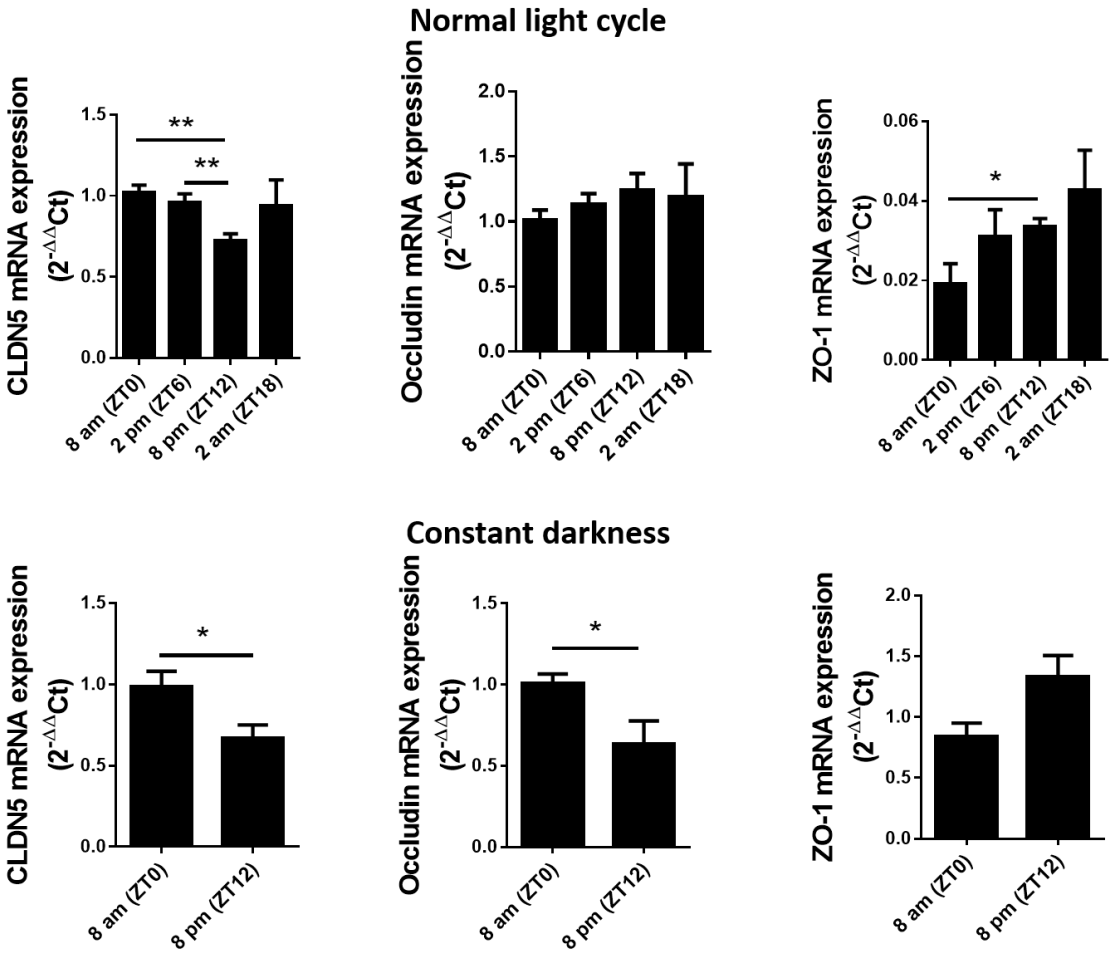

Figure 5.4: TJ components cycle throughout the day in C57BL/6 mice. RT-PCR analysis of claudin-5, occludin and ZO-1 in cerebral microvessels isolated from C57BL/6 mice kept on a normal light-dark cycle (top panel) and in constant darkness (bottom panel) at ZT0, ZT6, ZT12 and ZT18. *P<0.05, **P<0.01 by Student's t-test or ANOVA with Bonferroni post-test. All data are means ± SEM with n = 5 per group.

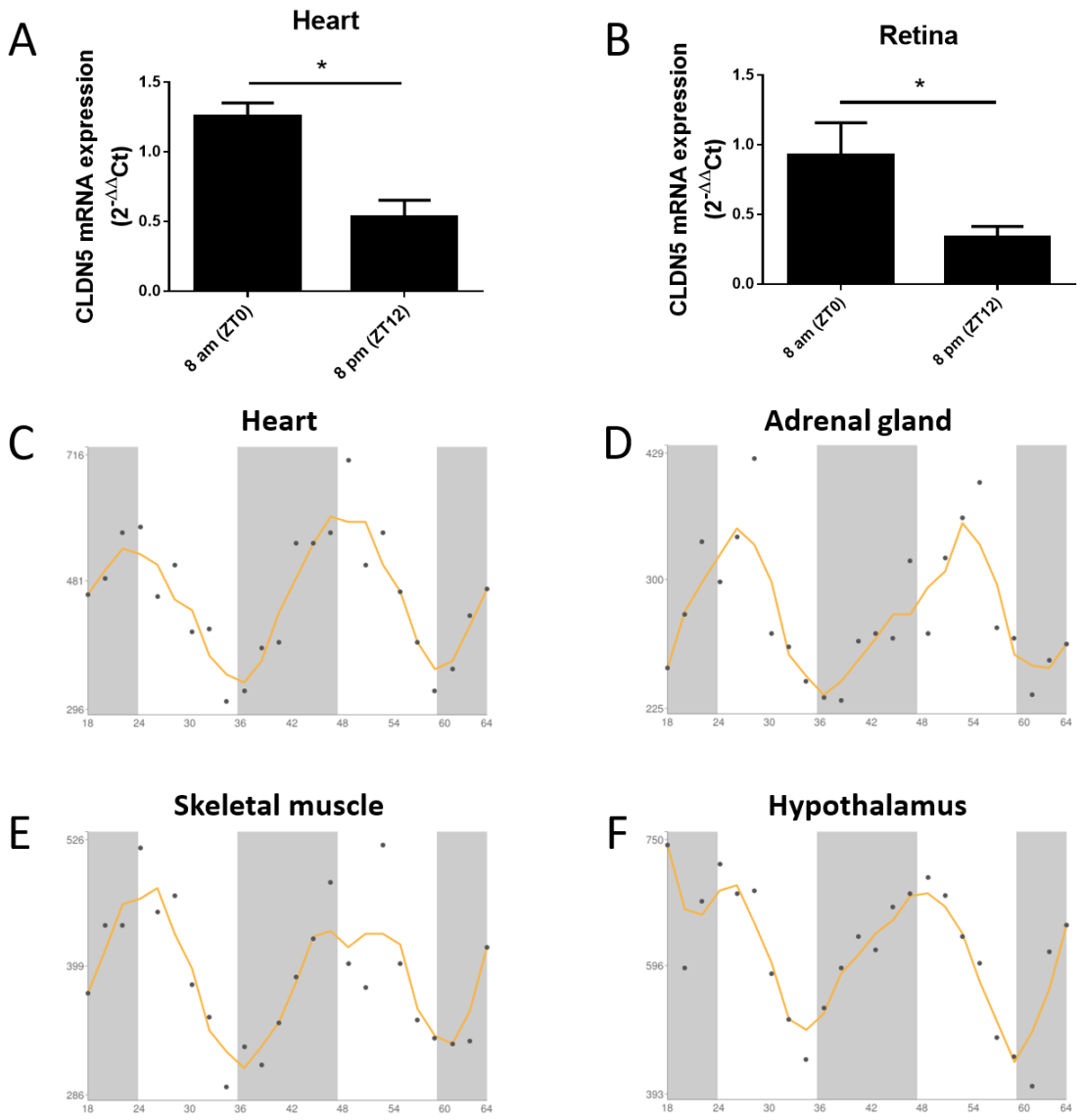

Figure 5.5: Claudin-5 cycles in peripheral organs. RT-PCR analysis of claudin-5 in the **(A)** heart and **(B)** retina of C57BL/6 mice at ZT0 and ZT12. Expression profiles taken from the circadian database showing claudin-5 expression across numerous timepoints in the **(C)** heart, **(D)** adrenal gland, **(E)** skeletal muscle and **(F)** hypothalamus. *P<0.05 by Student's t-test. All data are means ± SEM with n = 3-5 per group.

5.2.3 Diurnal variation of BBB integrity in C57BL/6 mice

Next, it was determined if changes in levels of claudin-5 mRNA manifested as differences in protein levels. Western blot analysis of capillary enriched protein fractions isolated from the brains of C57BL/6 mice at ZT0 and ZT12 revealed significantly reduced levels of claudin-5 protein at ZT0 compared to ZT12 (Figure 5.6). This reduction was confirmed by immunocytochemical analysis of claudin-5 in isolated cerebral microvessels with significantly reduced claudin-5 staining intensity evident in the morning (Figure 5.7). Given the differential expression patterns of claudin-5 throughout the day in mice, BBB integrity was determined by DCE-MRI analysis. C57BL/6 mice were anaesthetised and placed in an MRI scanner at 7 am. The tail-vein was cannulated and 200 µl of Gd-DTPA was injected slowly. This was repeated at 7 pm with the same mice to allow for paired analysis. Analysis of Gd-DTPA extravasation in the brains of the same C57BL/6 mice at 7 am and 7 pm revealed increased permeation of the Gd-DTPA contrast agent at 7 am compared to 7 pm (Figure 5.8). Following the MRI scanning, mice were injected I.V with a 2 mg/ml solution of Sulfo-NHS-biotin which was circulated for 10 min before mice were sacrificed and the brain was removed. Immunohistochemical analysis of Sulfo-NHS-biotin revealed significantly increased extravasation of the biotin tracer at ZT0 compared to ZT12 (Figure 5.9).

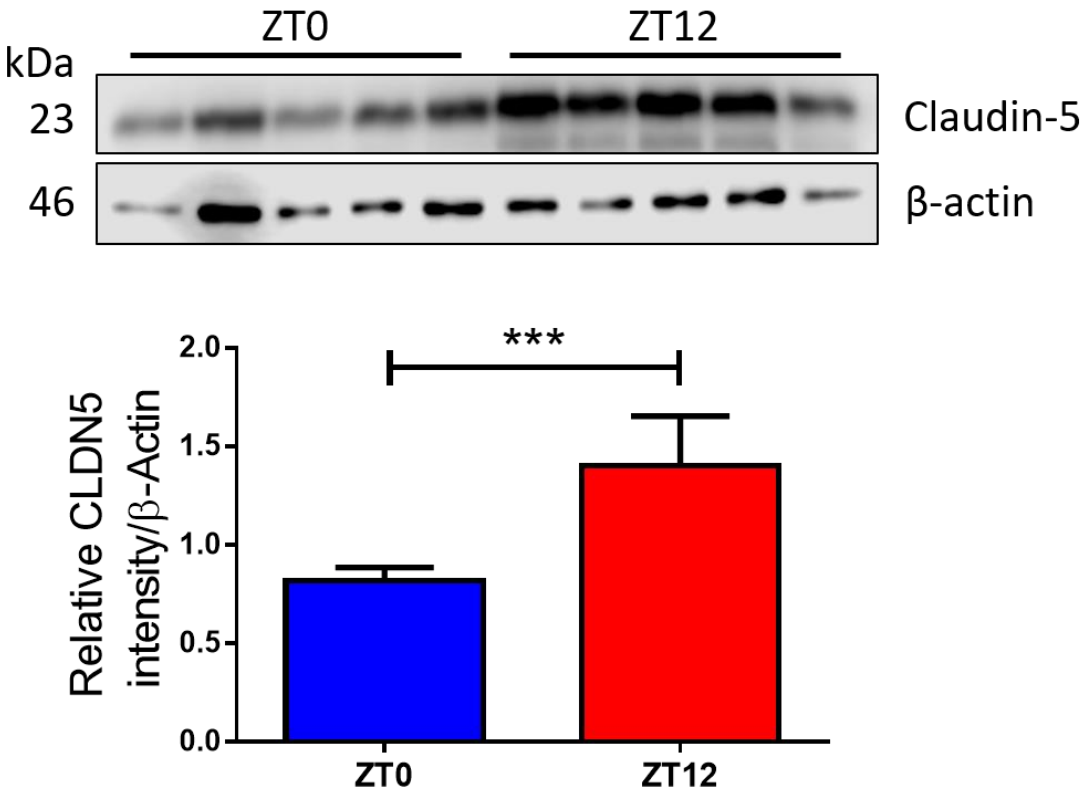

Figure 5.6 Claudin-5 protein levels are reduced in the morning. Western blot analysis of claudin-5 in cerebral microvessels isolated from C57BL/6 mice at ZT0 and ZT12. ***P<0.001 by Student's t-test. All data are means ± SEM with n = 5 per group.

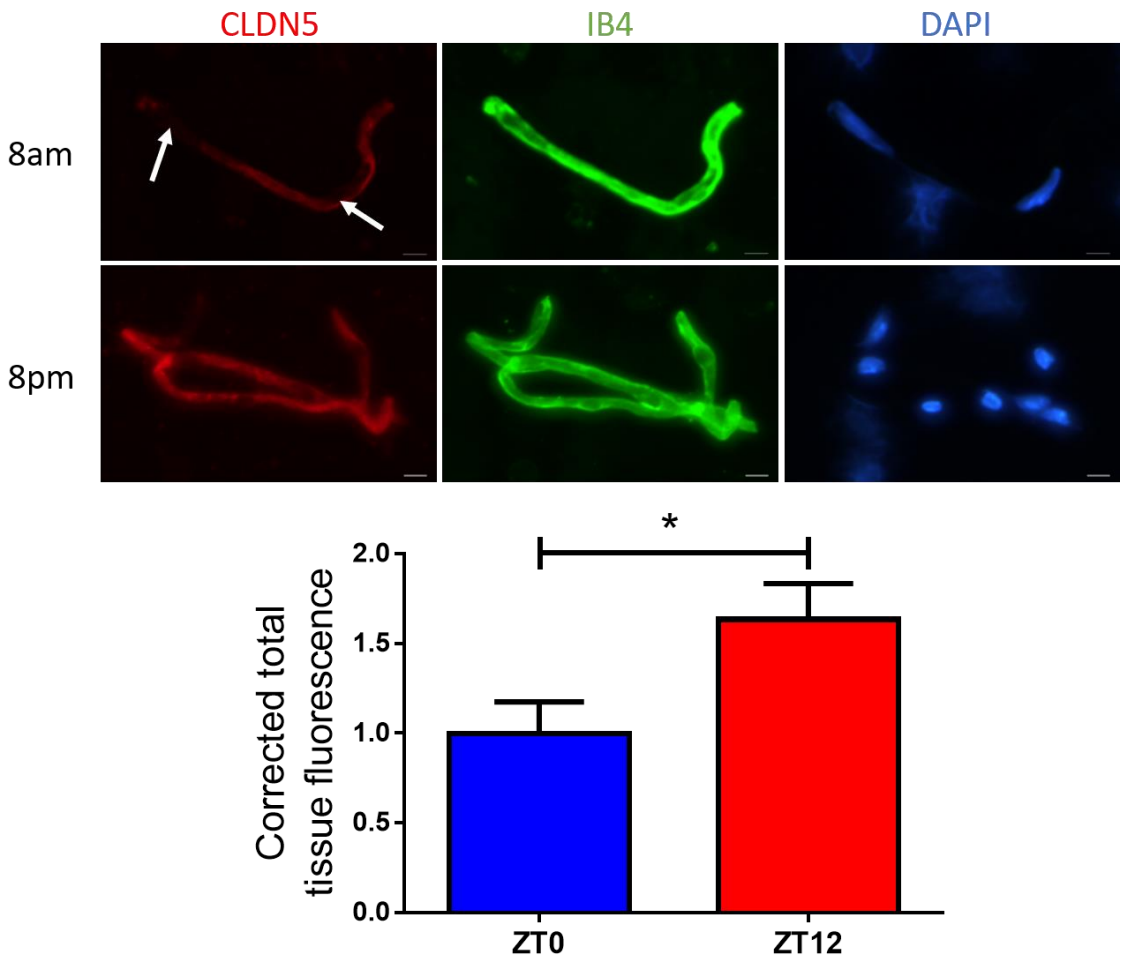

Figure 5.7 Immunohistochemical analysis of claudin-5 at 8 am and 8 pm. Immunohistochemical analysis of claudin-5 and isolectin-IB4 in isolated microvessels from C57BL/6 mice at ZT0 and ZT12. *P<0.05 by Student's t-test. All data are means ± SEM with n = 3 per group.

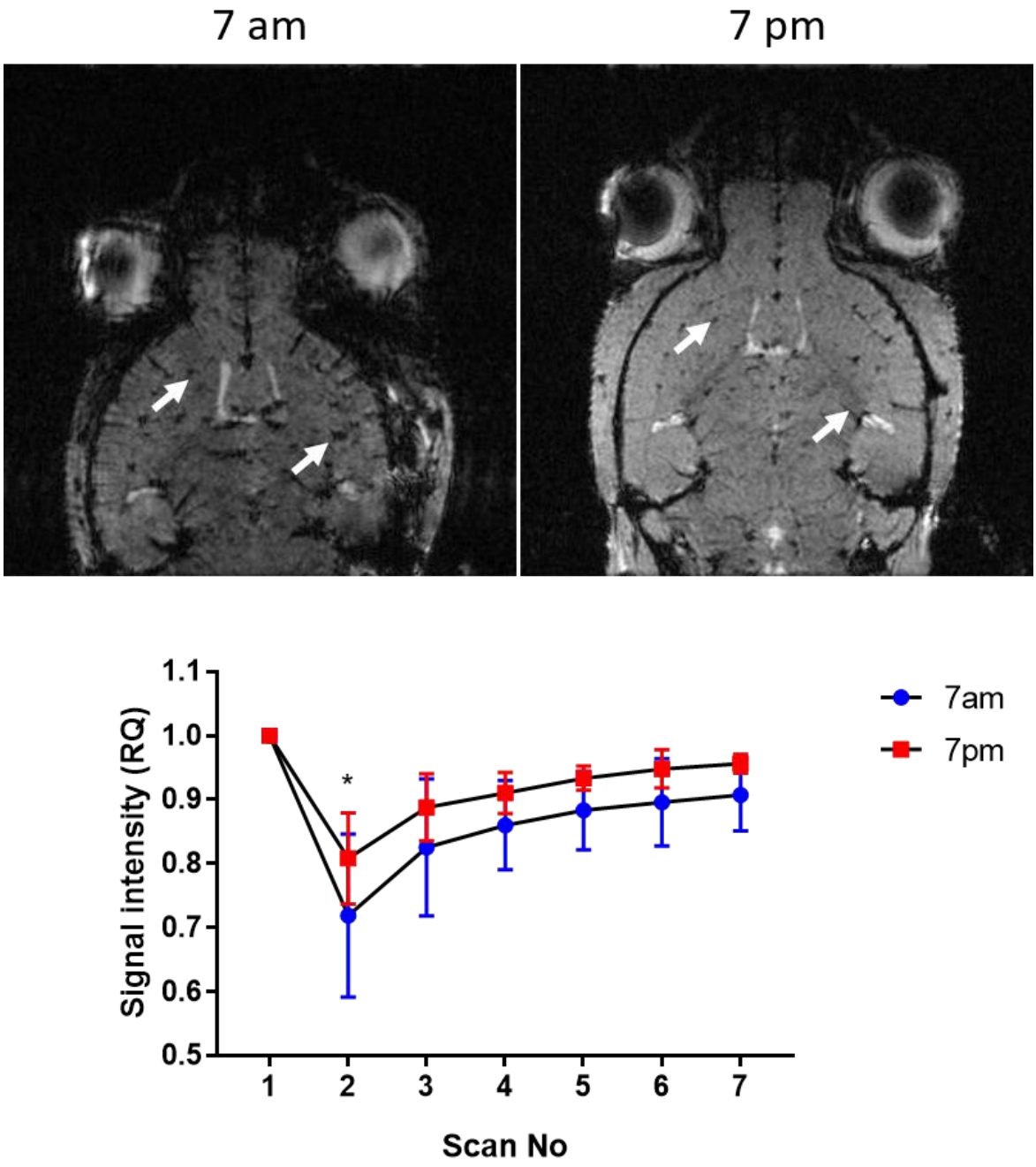

Figure 5.8: DCE-MRI analysis of C57BL/6 mice at 7 am and 7 pm. Top panel: DCE-MRI images from the same C57BL/6 mice taken at 7 am and 7 pm show increased contrast of Gd-DTPA in the morning indicative of a more permeable BBB. Lower panel: quantification of Gd-DTPA signal intensity across 7 scans. *P < 0.05 by two-way ANOVA with Tukey post-test. All data are means ± SEM with n = 4 per timepoint.

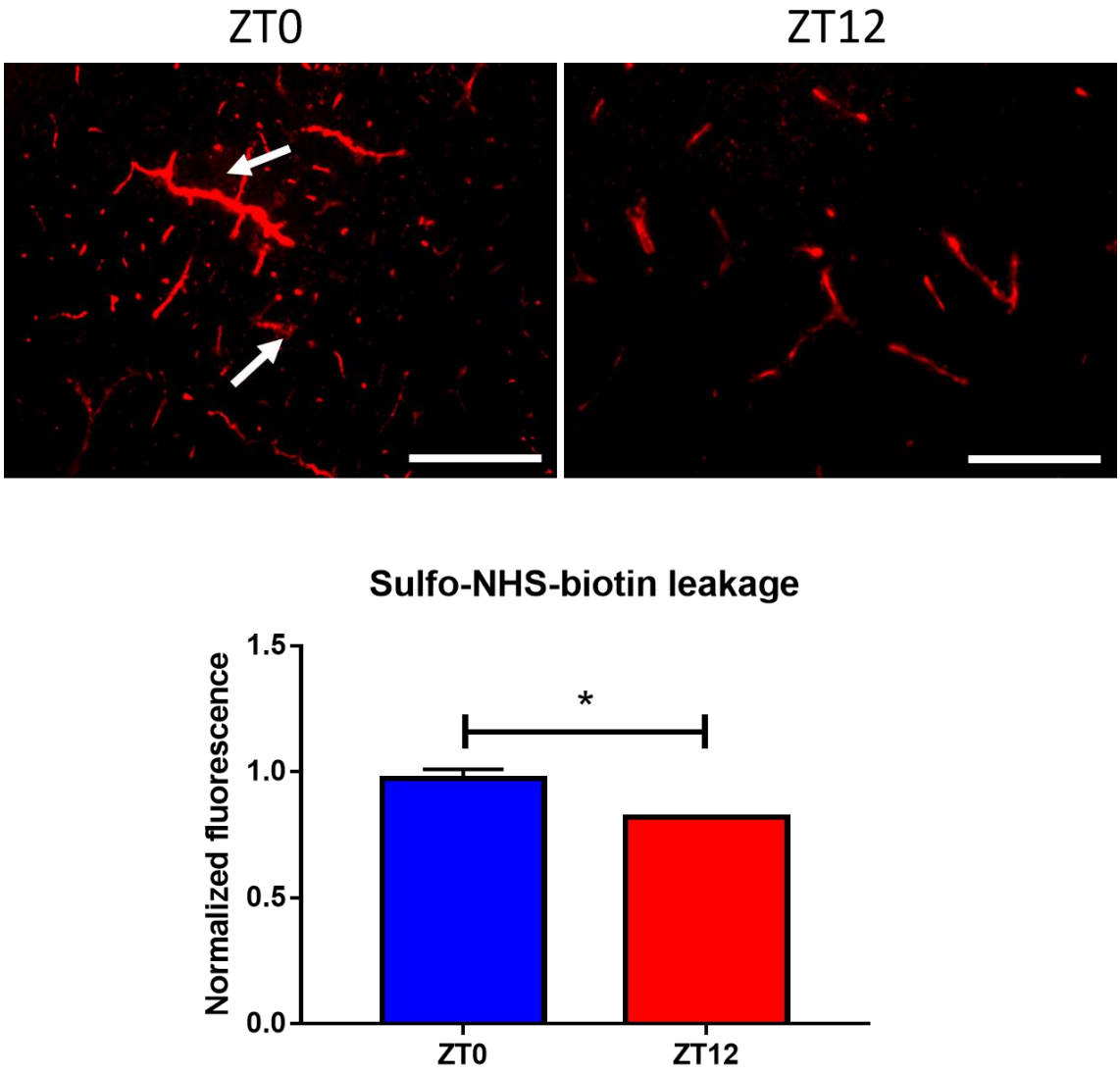

Figure 5.9: Sulfo-NHS-biotin extravasation at 8 am. Top panel: Immunohistochemical analysis of Sulfo-NHS-biotin in C57BL/6 mice at ZT0 and ZT12. Bottom panel: Quantification of Sulfo-NHS-biotin extravasation in C57BL/6 mice at ZT0 and ZT12. *P<0.05 by Student's t-test. Scale bar – 50 µm. All data are means ± SEM with n = 4 per timepoint.

5.2.4 Serum shock re-establishes circadian rhythms *in vitro*

RT-PCR analysis of clock transcription factors in primary mouse BMVEC and isolated cerebral capillaries revealed expression of the clock transcription factors BMAL-1, REV-ERBα and PER2. To explore the role of these transcription factors in regulation TJ protein and mRNA levels, an *in vitro* circadian rhythm model was established with mouse brain ECs and human brain ECs. Previously it has been shown that it is possible to reconstitute circadian rhythms *in vitro* to produce a sustained cycling of clock transcription factors and proteins controlled by the clock for up to 72 h. Sequence analysis of the claudin-5 promoter revealed E-box sequences (Figure 5.10) conserved in the claudin-5 promoter region in humans and mice. Canonical E-box sequences are known binding sites of BMAL-1 with subsequent binding of BMAL-1-CLOCK dimers activating gene expression. Confluent bEnd.3 cells "shocked" with 50% FCS for 2 h showed characteristic circadian cycling of claudin-5 protein (Figure 5.11). To assess the influence of clock transcription factors on claudin-5 cycling, bEnd.3 cells were transfected with siRNA targeting mouse BMAL-1 mRNA for 48 h before cells were serum shocked for 2 h to assess the effect of suppression of the key circadian-associated inducer of gene expression. RNAi based suppression of BMAL-1 attenuated the serum shock induced cycling of claudin-5 in mouse bEnd.3 cells (Figure 5.12). Similar experiments were then performed in the human cerebral microvascular endothelial cell line, hCMEC/d3, transfected with human BMAL-1 siRNA for 48 h before cells were serum shocked for 2 h and subsequently cultured in serum-free media. Suppression of BMAL-1 in hCMEC/d3 cells significantly reduced the serum-shock induced cycling of claudin-5 mRNA (Figure 5.13).

To further assess the influence of *in vitro* circadian rhythms on BBB integrity, permeability studies were performed. To determine the barrier function following BMAL-1 suppression, mouse bEnd.3 cells were cultured on transwell inserts. TEER measurements were recorded daily until they plateaued indicating cells had reached confluency. bEnd.3 cells were transfected with NT or BMAL-1 siRNA for 72 h and TEER measurements were recorded. Suppression of BMAL-1 significantly reduced TEER measurements indicating reduced barrier integrity (Figure 5.14A). A FITC-dextran paracellular tracer flux assay was conducted to analyse cell permeability. 40 kDa FITC-dextran was applied to the apical chamber of the transwell insert and the amount of FITC-dextran that moved into the basolateral chamber was measured over a 2 h period by taking

samples every 15 minutes and measured by fluorescence spectrophotometry. The concentration of FITC-dextran and the P_{app} was significantly increased in cells transfected with BMAL-1 siRNA compared to cells transfected with a NT siRNA indicating that suppression of BMAL-1 increased the permeability in these cells and that FITC-dextran moved more freely across the monolayer of bEnd.3 cells from the apical to basolateral chambers (Figure 5.14B). Additionally, immunocytochemical analysis of claudin-5 in brain ECs following transfection of BMAL-1 siRNA revealed discontinuous and reduced claudin-5 staining intensity compared to NT transfected cells (Figure 5.14C).

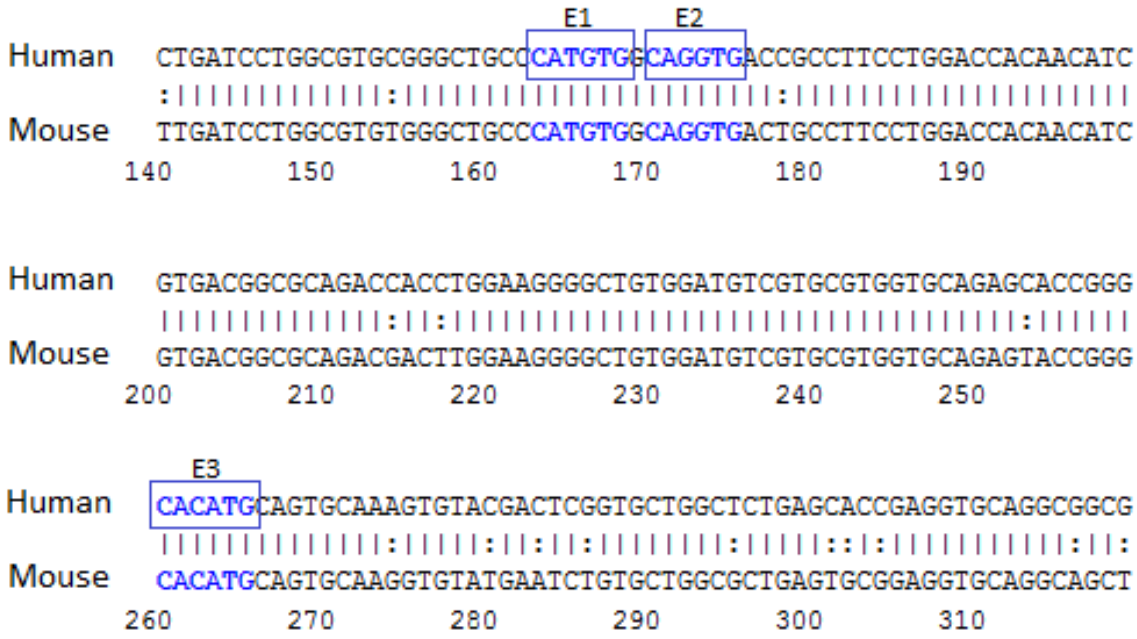

Figure 5.10: E-box binding sites in the claudin-5 promoter. Canonical E-box binding sites are conserved between mouse and human claudin-5 promoter regions. E-box sites can be canonical (CACGTG), non-canonical (CANNTG) or E-like (CGAGCG).

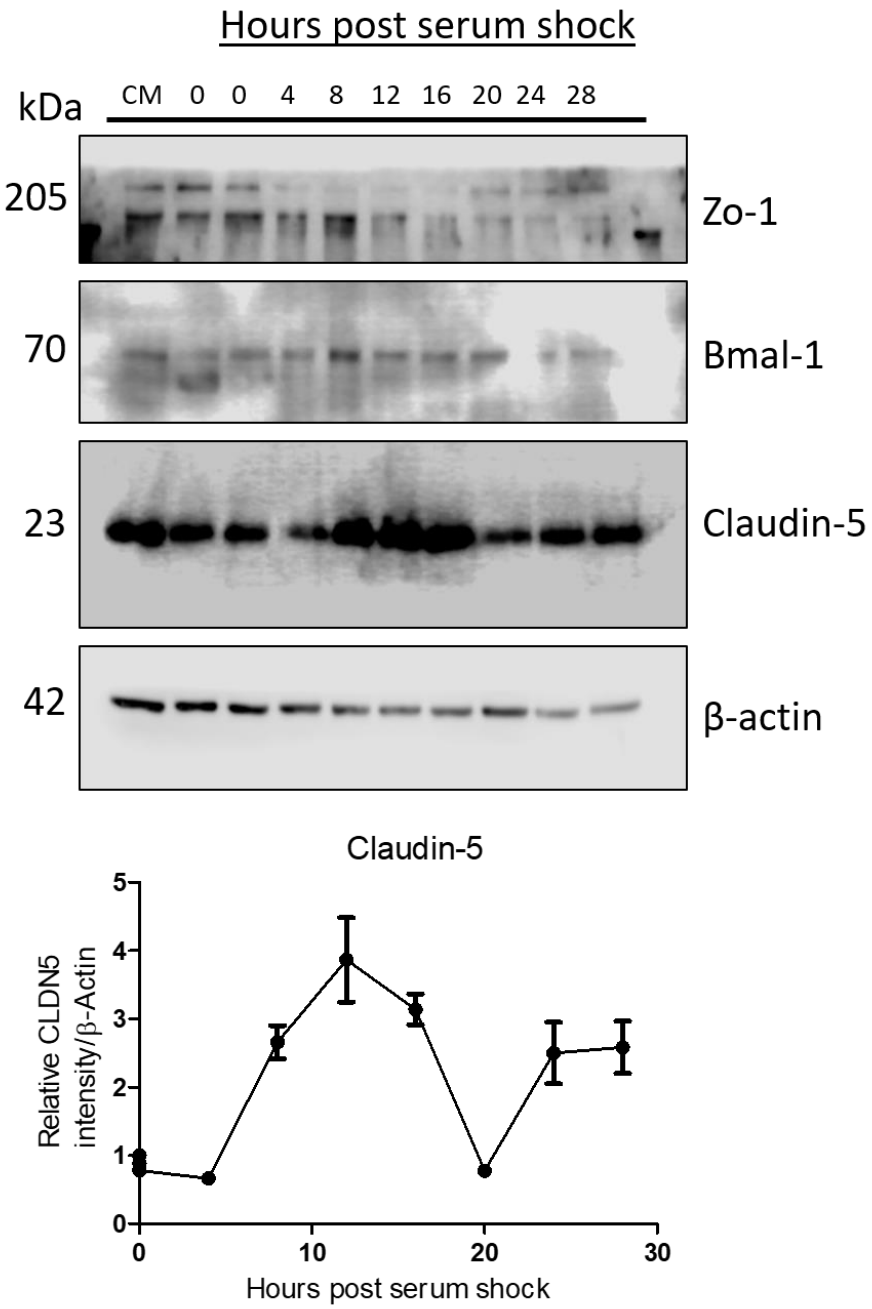

Figure 5.11: Serum shock induces cycling of TJ components. Top - Western blot analysis of ZO-1, BMAL-1 and claudin-5 in bEnd.3 cells treated with 50% FBS for 2 hours and incubated in serum-free media for the indicated times. Bottom – Densitometry analysis of claudin-5 protein. All data are means ± SEM with n = 3 independent experiments.

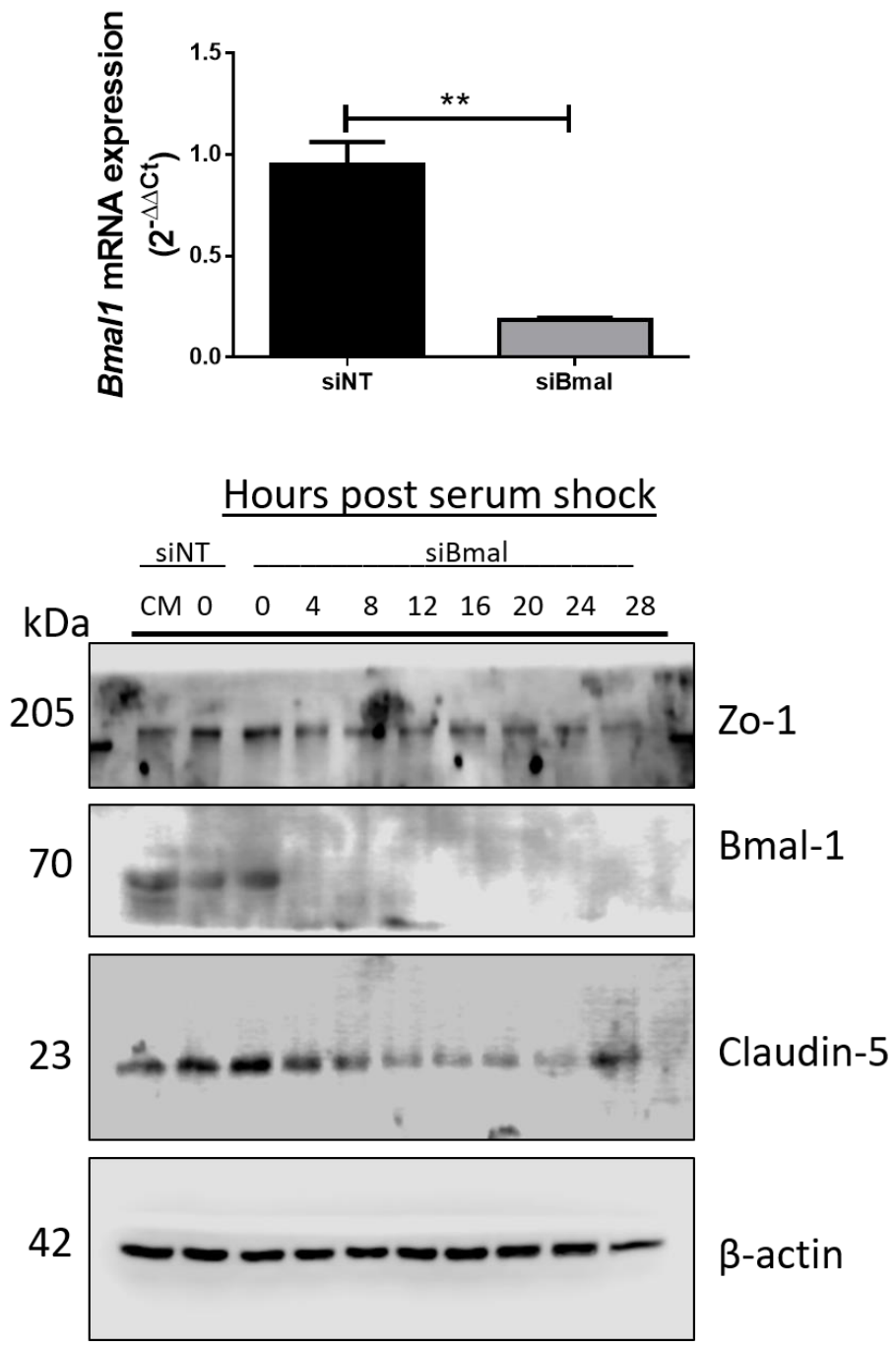

Figure 5.12: Suppression of BMAL-1 attenuates serum shock induced cycling of claudin-5. Top - RT-PCR analysis of BMAL-1 transcript 24 h following transfection of NT and BMAL-1 siRNA in bEnd.3 cells. Bottom - Western blot analysis of ZO-1, BMAL-1 and claudin-5 in bEnd.3 cells transfected with BMAL-1 siRNA and treated with 50% FBS for 2 h. **P < 0.01 by Student's t-test. All data are means ± SEM with n = 3 independent experiments.

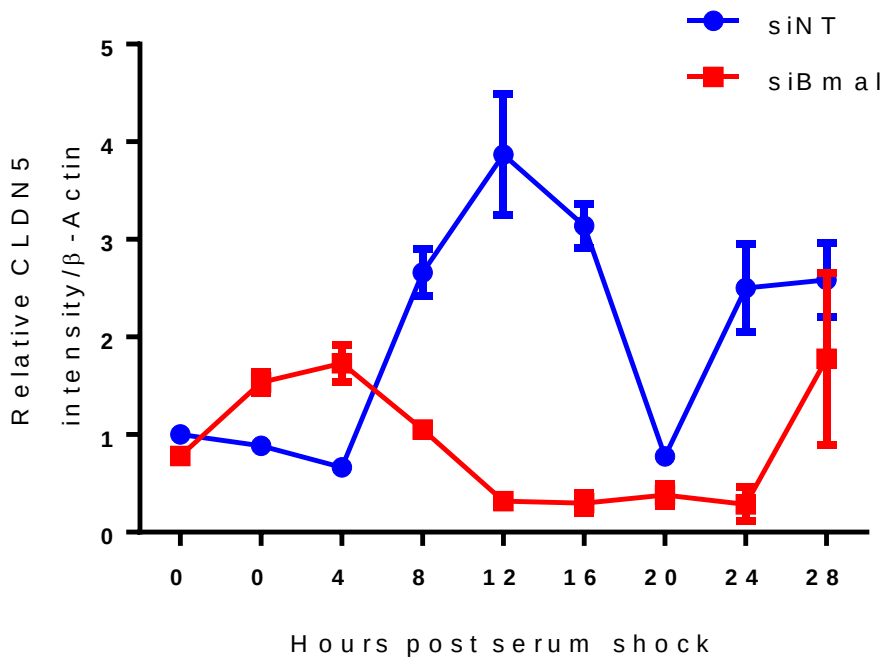

Figure 5.12 continued: Suppression of BMAL-1 attenuates serum shock induced cycling of claudin-5. Densitometry analysis of the western blot above. All data are means ± SEM with n = 3 independent experiments.

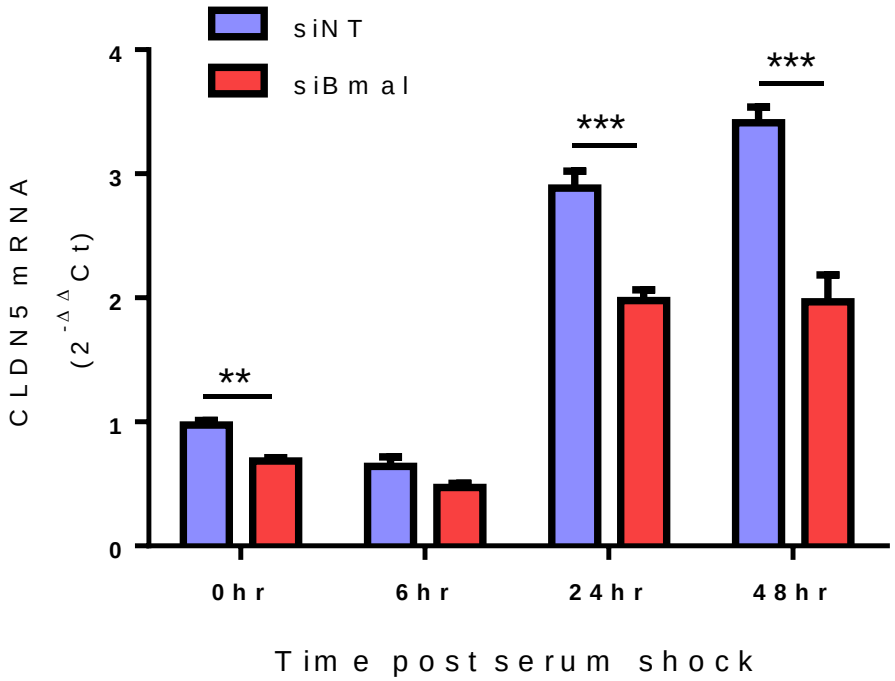

Figure 5.13: BMAL-1 is required for serum-shock induced claudin-5 cycling in human brain ECs. RT-PCR analysis of claudin-5 in hCMEC/d3 cells transfected with NT or BMAL-1 siRNA and treated with 50% FBS for 2 h. **P < 0.01, ***P < 0.001 by two-way ANOVA. All data are means ± SEM with n = 3 independent experiments.

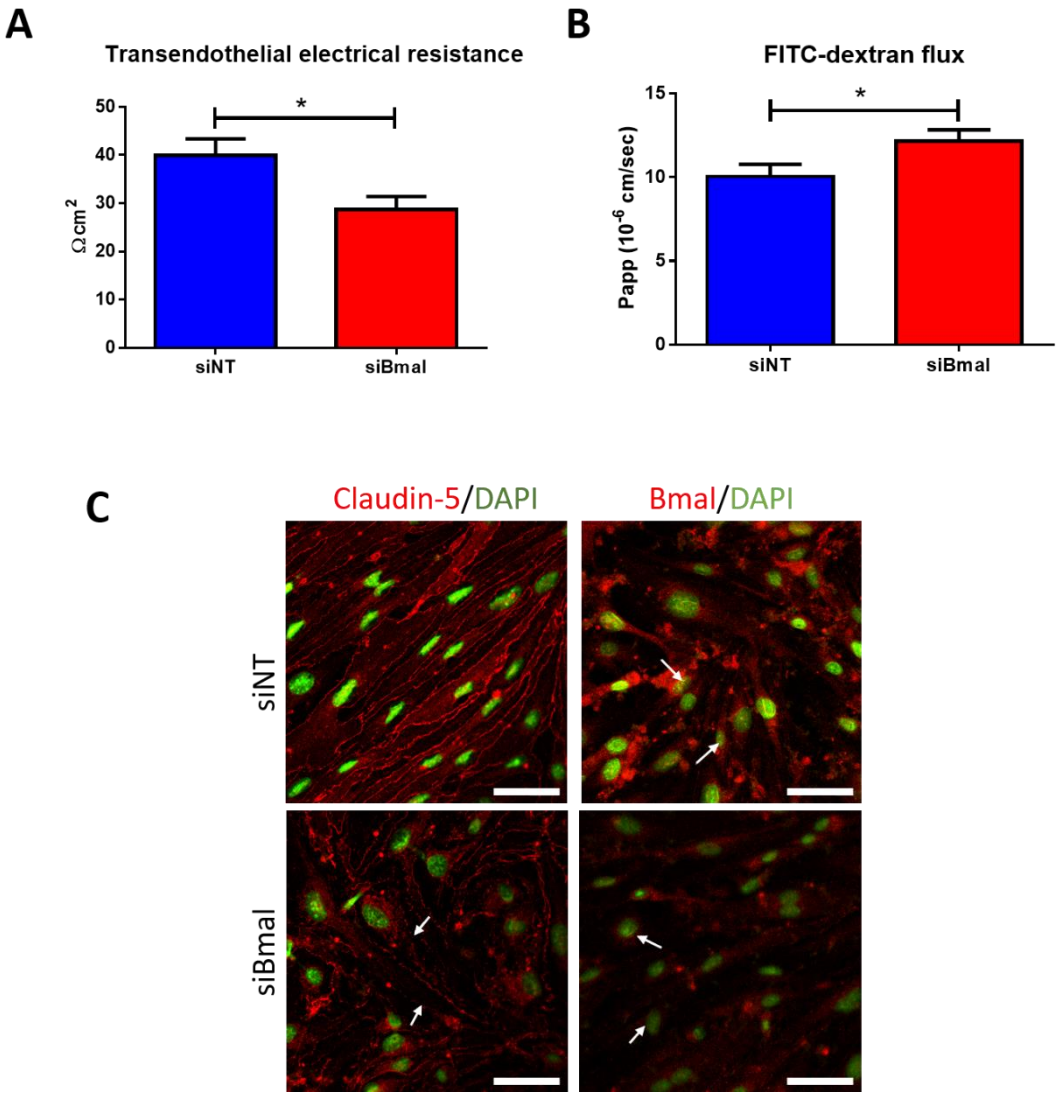

Figure 5.14: BMAL-1 is required for barrier integrity in bEnd.3 cells. **(A)** TEER measurements 24 h following transfection of BMAL-1 siRNA in bEnd.3 cells. **(B)** bEnd.3 cells were grown on collagen IV/fibronectin coated transwell inserts and transfected with BMAL-1 siRNA for 24 h before application of 70 kDa FITC-dextran (1 mg/ml) to the apical compartment. Movement of FITC-dextran across bEnd.3 cells was monitored over a 2 h time course by fluorescence spectrophotometry. The P_{app} was calculated for all treatments. **(C)** Immunocytochemical analysis of claudin-5 and BMAL-1 24 h post-transfection of NT or BMAL-1 siRNA in bEnd.3 cells. Scale bar – 50 µm. *P<0.05 by Student's t-test. All data are means ± SEM with n = 3 independent experiments.

5.3 Discussion

Circadian rhythms dictate some of the most basic and vital biological process, from the sleep-wake cycle to blood pressure, neurotransmitter release and cellular metabolism. In the CNS, neurons and synaptic signalling require a dynamic microenvironment to meet the ionic and fluid needs to function efficiently. While circadian rhythm disturbances are well-established in neurological disorders such as schizophrenia (Wilson and Argyropoulos, 2012), how these disruptions effect homeostatic imbalances remains poorly understood. At the level of the microvasculature, the BBB is highly dynamic in physiology and pathology to regulate the neural microenvironment. It has been shown that disruptions of homeostasis mediated by BBB dysfunction are intrinsically linked to neuropathologies including AD and stroke (Ryu and McLarnon, 2009, Sandoval and Witt, 2008). While much insight has been garnered about the regulation of BBB components from neurological disorders, little is known about the dynamism of the BBB in maintaining daily homeostasis. The development of therapies to treat CNS disorders including schizophrenia is dependent on the identification of new pathways that are involved in the disabling features of these conditions. It has been reported that CSR downregulates TJ components such as claudin-5 and occludin and increases the paracellular permeability of the BBB to potentially damaging serum proteins (He et al., 2014). Sleep disruption, a disruption of circadian rhythms, is one of the most widely documented disabling features in schizophrenic patients (Wilson and Argyropoulos, 2012). In this regard, the daily dynamics of the BBB were investigated to determine if the BBB is regulated by the circadian clock and if this in turn impacts BBB integrity.

For this chapter, the expression of BBB TJ components was compared at various timepoints throughout the day *in vivo* in wild-type mice. Intriguingly, it was found that the core clock transcription factors BMAL-1, REV-ERBα and PER2 were expressed in the cerebral ECs of C57BL/6 mice. Additionally, these clock transcription factors cycled throughout the day at the BBB in C57BL/6 mice and their cycling persisted in the absence of light stimulus. While circadian rhythms are endogenous, they are entrained to the local environment by external factors called zeitgebers, the primary one of which is light. RT-PCR analysis of TJ components revealed that claudin-5 cycled throughout the day with minimum levels detected at 8 pm. Additionally, claudin-5 cycling persisted in constant darkness. Interestingly, claudin-5 mRNA also cycled in several other organs examined including the retina and heart. Moreover, expression patterns of claudin-5 in numerous

other organs such as the heart, adrenal gland, skeletal muscle and hypothalamus taken from the online Circadian database revealed that claudin-5 cycled in an identical manner, reinforcing the findings of this study. While up to 43 % of known protein-coding genes cycle in at least one organ (Zhang et al., 2014), it is unusual to observe a gene cycling in numerous organs. This may reflect the crucial role of claudin-5 in regulating permeability at biological barriers. In contrast to the mRNA data, western blot analyses revealed an inverse relationship between claudin-5 mRNA and protein levels with minimum levels of protein detected at 8 am. In turn, this reduction in levels of claudin-5 protein at the BBB manifested as increased paracellular permeability to Sulfo-NHS-Biotin in brain cryosections from C57BL/6 mice and could be observed in living mice by DCE-MRI, revealed as increased Gd-DTPA extravasation in the morning compared to the same mice imaged in the evening. Further confirmation of reduced claudin-5 protein was observed through immunocytochemical analysis of claudin-5 in isolated cerebral microvessels. Further mechanistic insights on the role of circadian rhythms and cycling of BBB components was explored in *in vitro* BBB models. Various endothelial cell lines were screened for the presence of transcription factors that control the molecular formation of circadian rhythms. Human and mouse cell lines were found to express the core clock transcription factors. To determine the physiological effect of the clock on BBB integrity *in vitro*, a circadian rhythm *in vitro* model was applied. Treatment of cultured cells with high concentrations of serum induces the circadian expression of various genes including PER2 and REV-ERBα, the transcription of which also oscillates in living animals (Balsalobre et al., 1998). Treatment of the immortalized mouse brain endothelial cell line bEnd.3 and human endothelial cell line hCMEC/d3 with high concentrations of serum induced the circadian expression of claudin-5. The circadian expression of claudin-5 was governed at least in part by the expression of the core clock transcriptional transactivator BMAL-1 as siRNA mediated downregulation of BMAL-1 in cultured human and mouse brain ECs attenuated the circadian expression of claudin-5. Suppression of BMAL-1 had no effect on the levels of ZO-1. Furthermore, suppression of BMAL-1 was sufficient to increase the paracellular leakage of brain ECs to a fluorescent tracer and reduce TEER, reflecting increased barrier permeability and decreased barrier tightness. As E-box sequences, which are binding sites for clock transcription factors such as BMAL-1, are present in the human and mouse claudin-5 promoter region, it is likely that the circadian expression of claudin-5 is dictated by BMAL-1 binding to these E-box sequences and activating expression of claudin-5. Future work should confirm this through chromatin

immunoprecipitation experiments to determine the binding capability of BMAL-1 and other clock transcription factors to E-box sequences in the claudin-5 promoter region.

The purpose of circadian regulation of BBB components remains underexplored however recent studies have shed some light. A recent study has reported that conditional knockout of BMAL-1 in astrocytes resulted in astroglial activation, age-dependent loss of pericyte coverage of blood vessels and increased BBB permeability owing to down-regulation of PDGFRβ (Nakazato et al., 2017). With regard to neurological function, circadian rhythms dictate the transport of leptin across the BBB with greatest influx at 8 pm (Pan and Kastin, 2001). Leptin is a neuroendocrine hormone vital for regulating feeding behaviour and these results show that circadian rhythms are linked to regulating the transport of material from blood to brain. In an *in vivo* study of positron emission tomography imaging of PGP functionality, PGP displayed a daily rhythm with decreased function in the early active phase as measured by increased uptake of a radiolabelled PGP substrate (Savolainen et al., 2016). Diurnal regulation of PGP may allow for greater CNS penetration of known PGP substrates such as anti-psychotics or anti-epileptics based on a strategically timed dosing regimen. The circadian regulation of cytokines at the BBB has also been observed. In mice, IL-1α shows peak amplitude in the spinal cord at 8 am with the nadir at midnight (Banks et al., 1998). Also, TNFα showed a circadian rhythm in transport from blood to spinal cord of mice with peaks before lights on and nadir at noon (Pan et al., 2002).

Enhanced paracellular permeability of Sulfo-NHS-Biotin and gadolinium Gd-DTPA in the morning reflecting functional changes in the expression of claudin-5 protein and mRNA suggests that dynamic regulation of TJ proteins at the BBB by circadian rhythms could offer a novel approach in the treatment of neurological disorders by improving the penetration of CNS therapeutics based on a timed-dosing. Indeed, in epileptic patients that were unresponsive to therapy, administration of carbamazepine and phenytoin at night improved seizure control. In the study by Yegnanarayan et al., a group of epileptic patients unresponsive to standard treatment were subjected to treatment with all or most of their anti-seizure medication at 8 pm and showed better therapeutic response and reduced toxicity (Yegnanarayan et al., 2006). Chronotherapy is a form of therapy where medications are administered at specific times to improve the overall control of a disease and minimise side-effects. In one study, 56 out of the top 100 best-selling drugs in the United States were found to target the product of a circadian gene (Zhang et al., 2014).

Coupled with the short half-lives of some of these drugs, the time of administration could have an impact on their action.

Another potential function of circadian rhythms at the BBB is the clearance of material from brain to blood. Normal function of the CNS depends on a constant supply of essential molecules such as glucose and amino acids from the cerebral circulation, exchange of electrolytes between brain extracellular fluids and blood and efficient clearance of metabolic waste products. One of the key functions of CSF is the removal of waste products of metabolism, excess neurotransmitters and cellular debris. Novel investigations have identified a new waste clearance system in the brain termed the "glymphatic system" that actively interchanges CSF and IF along paravenous drainage pathways mediated by the astrocytic water channel AQP4. Intriguingly, this process is heightened during sleep and may be circadian dependent (Xie et al., 2013). This has implications for the study of neurodegenerative diseases and it has been shown that Aβ is cleared by the glymphatic system along the paravenous efflux pathway. Additionally, AQP4 knockout mice have a 55 % reduction in Aβ clearance (Iliff et al., 2012). However, the extent of the contribution of the glymphatic system towards CSF convective flow remains controversial with recent studies failing to support these findings (Hladky and Barrand, 2014, Smith et al., 2017, Holter et al., 2017). Results here suggest that circadian regulation of TJ components enhances the paracellular leakage of small molecules. The BBB is the major site for exchange of Aβ, with estimated clearance of 80-85 % of Aβ species (some of which are involved in Alzheimer's Disease) through transvascular transport (Sweeney et al., 2018). Recently in the host lab, it was shown for the first time that the paracellular pathway of the BBB is also involved in the exchange of soluble, low molecular weight species of Aβ. Additionally, co-suppression of claudin-5 and occludin in brain ECs could enhance the paracellular clearance of Aβ1-40 from brain to blood and improve cognitive function in the Tg2576 mouse model of Alzheimer's disease (Keaney et al., 2015). The circadian regulation of BBB integrity may therefore point to a process of removal of low molecular weight, potentially neurotoxic products such as Aβ and glutamate from the brain to maintain cerebral homeostasis. This is supported by findings of sleep disruption in Alzheimer's Disease patients and in animal models where sleep disruption is associated with enhanced Aβ aggregation in the brain (Roh et al., 2012).

5.4 Conclusions

- Clock transcription factors are expressed in BBB ECs
- Claudin-5 oscillates in BBB ECs in C57BL/6 mice
- BBB integrity is diurnally regulated
- Circadian rhythms can be re-established in cultured mouse BMVEC
- RNAi-based suppression of BMAL-1 attenuates claudin-5 cycling

Chapter 6:

Concluding Remarks and Future Studies

6 Concluding Remarks and Future Studies

With the lifespan of individuals in the developed world set to increase past 80 years, mental disorders are set to dramatically rise and affect 1 in 4 people globally. Over 21 million people worldwide live with schizophrenia. This severe mental disorder affects not only patients but has an enormous impact on families. The cost of treating and managing schizophrenia and supporting people with the illness and their families in the US alone are estimated at over $100 billion (Chong et al., 2016). Even though some symptoms of schizophrenia can be managed with treatment, over 50% of people with schizophrenia don't receive appropriate care (2016). As such, investigations to detect new ways to identify at risk individuals or to enable the generation of novel therapeutics to treat these disorders are essential. Current treatment options for schizophrenia almost exclusively rely on anti-psychotic therapies such as CZP, CPZ and OLZ. However, intolerable side-effects resulting from anti-psychotic use have significant impacts on the quality of life of individuals with schizophrenia. Moreover, studies have shown that up to 20% of first-episode patients do not respond to conventional anti-psychotic treatment after 1 year of medication (Lieberman, 1993). Accumulating evidence is highlighting the involvement of the cerebral vasculature in the pathogenesis of schizophrenia. The work described in this thesis outlines the involvement of the BBB in the context of schizophrenia and results suggest that BBB dysfunction is a hallmark of schizophrenia with *in vivo* data showing a profound link between the gene dosage effects of claudin-5 and the development of neuropsychiatric symptoms. Preliminary *in vitro* data is also shown of the involvement of a claudin-5 SNP in conferring the risk for schizophrenia. Additionally, a novel claudin-5 knockdown mouse model is described and suppression of claudin-5 in the brain was found to produce translatable schizophrenia phenotypes including impaired PPI and cognitive dysfunction. Finally, regulation of TJ proteins by circadian processes was examined and the circadian clock transcription factor BMAL-1 was found to act as a genetic modifier of claudin-5 expression.

In chapter 3, the rs10314 SNP, a claudin-5 3'UTR mutation was found to associate with schizophrenia in 22q11DS patients. The focus of these studies centred on elucidating the role of the rs10314 variant on claudin-5 expression. It was observed that the rs10314 risk allele was associated with an approximate 50% reduction in claudin-5 protein levels compared to the normal allele. Previous reports have hypothesised on the involvement of the BBB in schizophrenia, however no study to date has assessed the involvement of the

TJ in the schizophrenic brain. Given the finding that the claudin-5 levels were reduced in post-mortem schizophrenia cases, it is imperative to identify the extent of claudin-5 disruption in individuals with 22q11DS as they may theoretically produce up to 75% less claudin-5 factoring in the deleted gene with the rs10314 variant on the remaining claudin-5 allele compared to an individual with two copies of the normal claudin-5 allele. It is worth noting that previous studies examining the retinal microvasculature *in vivo* in schizophrenia patients revealed several ocular abnormalities including wider retinal venules (Meier et al., 2013). As 22q11DS patients are known to have several ocular abnormalities including tortuous retinal veins, an interesting future study may involve fluorescein angiography in individuals with 22q11DS. Not only would this provide information on the extent of ocular malformations, it would also provide a direct assessment of the integrity of the BRB. As the BBB and BRB are functionally and structurally homologous, by analysis of the genotypes of these individuals it would be possible to associate the genotype status of the rs10314 allele in these individuals with the extent of BRB leakage. Additionally, by taking blood samples, it would be possible to examine indirect measurements of BBB integrity by screening plasma and serum isolated from the blood for markers of BBB dysfunction including S100β, MMP-9 and albumin. Recent studies have also highlighted that it is possible to detect circulating levels of TJ proteins following BBB disruption, so this approach may be useful for determining the integrity of TJ components (Jiao et al., 2015, Zhu et al., 2017).

In chapter 4, the involvement of BBB dysregulation was explored in several animal models of BBB breakdown. Utilising AAV2/9 based vectors to site-specifically suppress claudin-5 in the dorsal hippocampus and mPFC, increased BBB permeability was observed that was associated with behavioural impairments in learning and memory and social interaction behaviours. To further evaluate the role of BBB dysfunction to phenotypic correlates of schizophrenia, a novel doxycycline-inducible claudin-5 knockdown mouse was developed. This model, based on the expression of shRNA targeting claudin-5 transcripts, allows for reversible suppression of claudin-5 at the BBB to modulate BBB permeability. In addition to showing reduced protein and transcript levels of claudin-5, these mice also developed several learning and memory impairments, increased anxiety and sensorimotor gating deficits. The importance of claudin-5 levels in the maintenance of BBB integrity was also revealed in the premature mortality of this knockdown model that was preceded by seizure-like activity and hyperactivity which led

to immobility and subsequent death. Immunohistochemical analyses of the brains of claudin-5 knockdown mice revealed a late-effect of seizure activity which resulted in the extravasation of large serum proteins as well as activation of astrocytes.

Cognitive behavioural impairments characterised in schizophrenia patients fall under seven domains: attention/vigilance, working memory, reasoning and problem solving, visual learning and memory, verbal learning and memory, and social cognition. Identifying a model that encompasses these domains is paramount to improving our understanding of the neurobiochemical basis for cognitive impairments in schizophrenia. However, mouse models of schizophrenia rarely factor in environmental causes. Indeed, schizophrenia is a neurodevelopmental, genetic and environmental disorder. As such, future studies with schizophrenia mouse models including the mouse models described in this thesis could include environmental stressors which may unmask latent psychopathology. Indeed, a future study could assess the role of environment and genetic abnormalities in the development of psychiatric disorders by combining social isolation with targeted suppression of claudin-5 at the BBB to discern the environmental contribution to BBB dysfunction and behavioural abnormalities evident in schizophrenia.

Finally, in chapter 5, circadian rhythms were found to be essential regulators of claudin-5 levels and BBB integrity. Initially, various brain microvascular endothelial cell lines were screened for the presence of BMAL-1 and REV-ERBα, the key positive and negative regulators of the transcriptional feedback loop that drives the circadian oscillation of target genes. BMAL-1 and REV-ERBα were found to be expressed in primary mouse BMVEC and isolated capillary fractions from C57BL/6 mice. As the clock transcription factors cycle in every organ (Zhang et al., 2014), an experiment was designed whereby capillary fractions were isolated from C57BL/6 mice at various timepoints during the day to determine if a) do clock transcription factors cycle in CNS ECs? and b) do clock transcription factors regulate BBB components? Indeed, it was found that several clock factors, BMAL-1, REV-ERBα PER2 cycle in CNS ECs. Interestingly, claudin-5 was found to cycle at the BBB with an approximate 25% reduction in transcript levels at 8 pm (ZT12). It was found that light did not influence the expression of claudin-5 as mice housed in total darkness displayed the same expression of claudin-5 as mice housed on a normal light-dark cycle. Additionally, clock transcription factors also remained unaffected by constant dark conditions. To determine

the effect of this variation in expression of claudin-5 on the BBB, several methods were employed to determine the extent of BBB modulation. DCE-MRI of C57BL/6 mice at 7 am and 7 pm found increased permeability of the BBB to Gd-DTPA in the morning with an associated reduction in the expression of claudin-5 protein in isolated capillary fractions. Additionally, by systemically injecting Sulfo-NHS-Biotin in these mice at each timepoint, the increased extravasation of the tracer was confirmed in the morning by immunohistochemical analysis of biotin in brain cryosections. To further elucidate the role of the circadian clock on BBB integrity, *in vitro* BBB models were used to re-establish circadian rhythms *in vitro*. By employing a serum shock protocol, the cycling of claudin-5 could be re-established in brain ECs. RNAi-based suppression of BMAL-1 attenuated this cycling of claudin-5 and impaired barrier integrity as assessed by reductions in TEER as well as increased paracellular permeability of a monolayer of brain ECs to a 40 kDa FITC-dextran compound. These data suggest that paracellular permeability at the BBB is dynamically regulated through the day and that targeting therapies across the BBB at certain times of the day may improve brain penetration and therapeutic response.

6.1 The blood-brain barrier: Gateway to neuropsychiatric disorders

Although dysfunction of the BBB is a hallmark of numerous traumas and neurodegenerative disorders, it remains unclear whether a dysfunctional BBB plays a harmful role promoting disease or if it is a clinical manifestation of disease progression. In the context of neuropsychiatric disorders, several studies have identified structural and functional impairments of the microvasculature and surrounding NVU including reduced capillary diameter, reduced CBF, downregulation of astrocyte markers, microglial activation, up-regulation of pro-permeability factors such as VEGF and MMP-9 and up-regulation of markers involved in the transport of lymphocytes to the CNS such as the selectins and cell adhesion molecules. Up until now however, a direct analysis of CNS EC-specific genes involved in the regulation of the BBB has never been investigated regarding dysfunction specifically in neuropsychiatric disorders as well as the symptomatology of neuropsychiatric conditions. A role for the BBB, and more specifically, claudin-5, in schizophrenia has been demonstrated. It is possible that a balance may exist whereby the CNS tolerates enhanced permeability of the microvasculature, however, prolonged permeability may cause a shift in homeostasis in the neural microenvironment that can manifest as neurophysiological impairments and

behavioural disorders. A recent study examining the effects of BBB disruption on hippocampal neurophysiology in a rodent stroke model revealed BBB dysfunction preceding hippocampal seizures and suggests that this is due to abnormal synaptic plasticity, astrocytic activation, network excitability and reduced GABAergic inhibition (Lippmann et al., 2017). Gamma aminobutyric acid (GABA) interneurons are essential in the normal brain to counteract excitatory glutamatergic activity with changes in GABAergic function reported to contribute to the pathogenesis of epilepsy (Campbell et al., 2015). With evidence of the emerging role of astrocytes in regulating synaptic plasticity (De Pitta et al., 2016) as well as their key role in regulating potassium concentrations (Coulter and Steinhäuser, 2015), localised BBB dysfunction resulting in astrocytic activation observed in the claudin-5 knockdown mouse described herein may impair local neural networks resulting in network hyperactivation and seizures. The studies detailed in this thesis clearly show that microvascular permeability produced by targeted suppression of claudin-5 at the BBB induces dramatic behavioural impairments in mice. However, further studies are required to determine the influence of BBB permeability on neuronal function. Schizophrenia is a neurodevelopmental disorder that typically manifests in the late 2nd and 3rd decades of life. How does a disrupted BBB influence disease progression? Future studies involving these mice could examine the influence of age-related changes in cognitive function. Does post-natal suppression of claudin-5 exacerbate behavioural abnormalities? Similarly, does a disrupted BBB in the aged brain exacerbate age-related disorders?

Disruption of the BBB is often a double-edged sword. On one hand, numerous preclinical models have shown the therapeutic potential of modulation of TJ proteins, in particular, claudin-5 and occludin siRNAs, in the treatment of cerebral oedema and Alzheimer's disease as well as for improving drug delivery to the brain for the treatment of glioblastoma brain tumours and to the eye for the treatment of degenerative retinopathies (Campbell et al., 2012, Campbell et al., 2009, Keaney et al., 2015). Indeed, a therapeutic approach has been devised based on modulation of the BBB. Numerous studies have documented the use of focused ultrasound (FUS) coupled with circulating microbubbles to reversibly open the BBB to enhance delivery of therapeutic agents to the brain. FUS employs low-frequency ultrasound waves to precise neuronal regions to specifically increase BBB permeability by widening TJs (Sheikov et al., 2004). The potential of FUS has previously been reported where dopamine D(4) receptor-targeting antibodies could

cross the BBB following FUS. Also, I.V injection of anti- Aβ antibodies can be delivered across the BBB following FUS which was shown to significantly reduce Aβ plaques 4 days post treatment in a transgenic mouse model of Alzheimer's disease (Kinoshita et al., 2006). However, the long-term consequences of modulation of the BBB, even for short durations, is largely unknown. The work presented in this thesis demonstrates that modulation of BBB permeability can have profound impacts on animal behaviour and induce psychosis-like symptoms in mice.

In summary, these studies highlight the crucial role of claudin-5 in maintaining BBB integrity and show that disruption of the BBB can produce numerous behavioural and cognitive symptoms typical of those observed in psychiatric patients. While previous studies on the role of the microvasculature and BBB in schizophrenia have highlighted several abnormalities indicative of BBB dysfunction, there are numerous limitations to these studies including confounding factors of post-mortem histopathological examination of brain tissue including post-mortem interval, fixative and fixation time. Additionally, several of the markers of BBB dysfunction including measurements of serum S100β, MMP-9 and albumin don't factor in other biological processes that could elicit these responses such as proliferation or degradation of astrocytes. Thirdly, the lack of EC-specific models of BBB disruption have limited the assessment of BBB disruption on behavioural outcomes in animals. This thesis aimed to address these problems by targeting suppression of claudin-5 in distinct neuronal regions and mapping the behavioural consequences of localised BBB permeability on cognition and memory. Additionally, the knockdown model developed during these studies will be an invaluable tool for studying CNS disorders. In conclusion, this work has examined various aspects of BBB biology and schizophrenia pathology and proposes that dysfunctional TJ complexes at the BBB may explain certain aspects of neuropsychiatric disorders and targeting therapies to restore BBB function could represent a novel means in treating schizophrenia and other mental disorders.

References

1960. MENTAL DISORDERS IN URBAN AREAS. AN ECOLOGICAL STUDY OF SCHIZOPHRENIA AND OTHER PSYCHOSES. *American Journal of Public Health and the Nations Health,* 50**,** 1455-1455.

2014. Biological insights from 108 schizophrenia-associated genetic loci. *Nature,* 511**,** 421-7.

2016. *Schizophrenia* [Online]. World Health Organisation. Available: http://www.who.int/mediacentre/factsheets/fs397/en/ [Accessed 2018].

ABBOTT, N. J., HUGHES, C. C., REVEST, P. A. & GREENWOOD, J. 1992. Development and characterisation of a rat brain capillary endothelial culture: towards an in vitro blood-brain barrier. *J Cell Sci,* 103 (Pt 1)**,** 23-37.

ABBOTT, N. J., PATABENDIGE, A. A., DOLMAN, D. E., YUSOF, S. R. & BEGLEY, D. J. 2010. Structure and function of the blood-brain barrier. *Neurobiol Dis,* 37**,** 13-25.

ABBOTT, N. J., RONNBACK, L. & HANSSON, E. 2006. Astrocyte-endothelial interactions at the blood-brain barrier. *Nat Rev Neurosci,* 7**,** 41-53.

ABOUL-FOTOUH, S. & ELGAYAR, N. 2013. Atypical antipsychotics such as risperidone, but not paliperidone, worsen vascular endothelial function via upregulation of adhesion molecules VCAM-1, ICAM-1, and E-selectin in diabetic rats. *Can J Physiol Pharmacol,* 91**,** 1119-26.

ABRAHAMSON, E. E. & MOORE, R. Y. 2001. Suprachiasmatic nucleus in the mouse: retinal innervation, intrinsic organization and efferent projections. *Brain Res,* 916**,** 172-91.

ADACHI, M., INOKO, A., HATA, M., FURUSE, K., UMEDA, K., ITOH, M. & TSUKITA, S. 2006. Normal establishment of epithelial tight junctions in mice and cultured cells lacking expression of ZO-3, a tight-junction MAGUK protein. *Mol Cell Biol,* 26**,** 9003-15.

AGUZZI, A., BARRES, B. A. & BENNETT, M. L. 2013. Microglia: scapegoat, saboteur, or something else? *Science,* 339**,** 156-61.

AHISHALI, B., KAYA, M., ORHAN, N., ARICAN, N., EKIZOGLU, O., ELMAS, I., KUCUK, M., KEMIKLER, G., KALAYCI, R. & GURSES, C. 2010. Effects of levetiracetam on blood-brain barrier disturbances following hyperthermia-induced seizures in rats with cortical dysplasia. *Life Sci,* 87**,** 609-19.

ALLEN, N. C., BAGADE, S., MCQUEEN, M. B., IOANNIDIS, J. P., KAVVOURA, F. K., KHOURY, M. J., TANZI, R. E. & BERTRAM, L. 2008. Systematic meta-analyses and field synopsis of genetic association studies in schizophrenia: the SzGene database. *Nat Genet,* 40**,** 827-34.

ALVAREZ, J. I., DODELET-DEVILLERS, A., KEBIR, H., IFERGAN, I., FABRE, P. J., TEROUZ, S., SABBAGH, M., WOSIK, K., BOURBONNIERE, L., BERNARD, M., VAN HORSSEN, J., DE VRIES, H. E., CHARRON, F. & PRAT, A. 2011. The Hedgehog pathway promotes blood-brain barrier integrity and CNS immune quiescence. *Science,* 334**,** 1727-31.

ANDREASEN, N. C., CALARGE, C. A. & O'LEARY, D. S. 2008. Theory of mind and schizophrenia: a positron emission tomography study of medication-free patients. *Schizophr Bull,* 34**,** 708-19.

ANDREONE, B. J., CHOW, B. W., TATA, A., LACOSTE, B., BEN-ZVI, A., BULLOCK, K., DEIK, A. A., GINTY, D. D., CLISH, C. B. & GU, C. 2017. Blood-Brain Barrier Permeability Is Regulated by Lipid Transport-Dependent Suppression of Caveolae-Mediated Transcytosis. *Neuron,* 94**,** 581-594.e5.

ARINAMI, T. 2006. Analyses of the associations between the genes of 22q11 deletion syndrome and schizophrenia. *J Hum Genet,* 51**,** 1037-45.

ARMULIK, A., GENOVE, G., MAE, M., NISANCIOGLU, M. H., WALLGARD, E., NIAUDET, C., HE, L., NORLIN, J., LINDBLOM, P., STRITTMATTER, K., JOHANSSON, B. R. & BETSHOLTZ, C. 2010. Pericytes regulate the blood-brain barrier. *Nature,* 468**,** 557-61.

AURRAND-LIONS, M., LAMAGNA, C., DANGERFIELD, J. P., WANG, S., HERRERA, P., NOURSHARGH, S. & IMHOF, B. A. 2005. Junctional adhesion molecule-C regulates the early influx of leukocytes into tissues during inflammation. *J Immunol,* 174**,** 6406-15.

BACHILLER, D., KLINGENSMITH, J., SHNEYDER, N., TRAN, U., ANDERSON, R., ROSSANT, J. & DE ROBERTIS, E. M. 2003. The role of chordin/Bmp signals in mammalian pharyngeal development and DiGeorge syndrome. *Development,* 130**,** 3567-78.

BAILEY, K. R. & CRAWLEY, J. N. 2009. Frontiers in Neuroscience

Anxiety-Related Behaviors in Mice. *In:* BUCCAFUSCO, J. J. (ed.) *Methods of Behavior Analysis in Neuroscience.* Boca Raton (FL): CRC Press/Taylor & Francis

Taylor & Francis Group, LLC.

BALABANOV, R., WASHINGTON, R., WAGNEROVA, J. & DORE-DUFFY, P. 1996. CNS microvascular pericytes express macrophage-like function, cell surface integrin alpha M, and macrophage marker ED-2. *Microvasc Res,* 52**,** 127-42.

BALDA, M. S., WHITNEY, J. A., FLORES, C., GONZALEZ, S., CEREIJIDO, M. & MATTER, K. 1996. Functional dissociation of paracellular permeability and transepithelial electrical resistance and disruption of the apical-basolateral intramembrane diffusion barrier by expression of a mutant tight junction membrane protein. *J Cell Biol,* 134**,** 1031-49.

BALLABH, P., BRAUN, A. & NEDERGAARD, M. 2004. Anatomic analysis of blood vessels in germinal matrix, cerebral cortex, and white matter in developing infants. *Pediatr Res,* 56**,** 117-24.

BALSALOBRE, A., DAMIOLA, F. & SCHIBLER, U. 1998. A serum shock induces circadian gene expression in mammalian tissue culture cells. *Cell,* 93**,** 929-37.

BANDOPADHYAY, R., ORTE, C., LAWRENSON, J. G., REID, A. R., DE SILVA, S. & ALLT, G. 2001. Contractile proteins in pericytes at the blood-brain and blood-retinal barriers. *J Neurocytol,* 30**,** 35-44.

BANKS, W. A., KASTIN, A. J. & EHRENSING, C. A. 1998. Diurnal uptake of circulating interleukin-1alpha by brain, spinal cord, testis and muscle. *Neuroimmunomodulation,* 5**,** 36-41.

BARKER, G. R., BIRD, F., ALEXANDER, V. & WARBURTON, E. C. 2007. Recognition memory for objects, place, and temporal order: a disconnection analysis of the role of the medial prefrontal cortex and perirhinal cortex. *J Neurosci,* 27**,** 2948-57.

BAZZONI, G., MARTINEZ-ESTRADA, O. M., ORSENIGO, F., CORDENONSI, M., CITI, S. & DEJANA, E. 2000. Interaction of junctional adhesion molecule with the tight junction components ZO-1, cingulin, and occludin. *J Biol Chem,* 275**,** 20520-6.

BECHTER, K., REIBER, H., HERZOG, S., FUCHS, D., TUMANI, H. & MAXEINER, H. G. 2010. Cerebrospinal fluid analysis in affective and schizophrenic spectrum

disorders: identification of subgroups with immune responses and blood-CSF barrier dysfunction. *J Psychiatr Res,* 44**,** 321-30.
BELL, R. D., WINKLER, E. A., SAGARE, A. P., SINGH, I., LARUE, B., DEANE, R. & ZLOKOVIC, B. V. 2010. Pericytes control key neurovascular functions and neuronal phenotype in the adult brain and during brain aging. *Neuron,* 68**,** 409-27.
BEN-ZVI, A., LACOSTE, B., KUR, E., ANDREONE, B. J., MAYSHAR, Y., YAN, H. & GU, C. 2014. Mfsd2a is critical for the formation and function of the blood-brain barrier. *Nature,* 509**,** 507-11.
BIRON, K. E., DICKSTEIN, D. L., GOPAUL, R. & JEFFERIES, W. A. 2011. Amyloid triggers extensive cerebral angiogenesis causing blood brain barrier permeability and hypervascularity in Alzheimer's disease. *PLoS One,* 6**,** e23789.
BLASIG, I. E., BELLMANN, C., CORDING, J., DEL VECCHIO, G., ZWANZIGER, D., HUBER, O. & HASELOFF, R. F. 2011. Occludin protein family: oxidative stress and reducing conditions. *Antioxid Redox Signal,* 15**,** 1195-219.
BLASIG, I. E., WINKLER, L., LASSOWSKI, B., MUELLER, S. L., ZULEGER, N., KRAUSE, E., KRAUSE, G., GAST, K., KOLBE, M. & PIONTEK, J. 2006. On the self-association potential of transmembrane tight junction proteins. *Cell Mol Life Sci,* 63**,** 505-14.
BOULDIN, T. W. & KRIGMAN, M. R. 1975. Differential permeability of cerebral capillary and choroid plexus to lanthanum ion. *Brain Res,* 99**,** 444-8.
BRADFIELD, P. F., NOURSHARGH, S., AURRAND-LIONS, M. & IMHOF, B. A. 2007. JAM family and related proteins in leukocyte migration (Vestweber series). *Arterioscler Thromb Vasc Biol,* 27**,** 2104-12.
BRADY, A. M. 2016. The Neonatal Ventral Hippocampal Lesion (NVHL) Rodent Model of Schizophrenia. *Curr Protoc Neurosci,* 77**,** 9.55.1-9.55.17.
BRIGHTMAN, M. W. & REESE, T. S. 1969. Junctions between intimately apposed cell membranes in the vertebrate brain. *J Cell Biol,* 40**,** 648-77.
BRZOZOWSKA, N. I., SMITH, K. L., ZHOU, C., WATERS, P. M., CAVALCANTE, L. M., ABELEV, S. V., KULIGOWSKI, M., CLARKE, D. J., TODD, S. M. & ARNOLD, J. C. 2017. Genetic deletion of P-glycoprotein alters stress responsivity and increases depression-like behavior, social withdrawal and microglial activation in the hippocampus of female mice. *Brain Behav Immun,* 65**,** 251-261.
BUHR, E. D. & TAKAHASHI, J. S. 2013. Molecular components of the mammalian circadian clock. *Handbook of experimental pharmacology***,** 3-27.
BUSSE, M., KUNSCHMANN, R., DOBROWOLNY, H., HOFFMANN, J., BOGERTS, B., STEINER, J., FRODL, T. & BUSSE, S. 2017. Dysfunction of the blood-cerebrospinal fluid-barrier and N-methyl-D-aspartate glutamate receptor antibodies in dementias. *Eur Arch Psychiatry Clin Neurosci*.
BUTT, A. M., JONES, H. C. & ABBOTT, N. J. 1990. Electrical resistance across the blood-brain barrier in anaesthetized rats: a developmental study. *J Physiol,* 429**,** 47-62.
CALDWELL, C. B. & GOTTESMAN, II 1990. Schizophrenics kill themselves too: a review of risk factors for suicide. *Schizophr Bull,* 16**,** 571-89.
CAMPBELL, M., HANRAHAN, F., GOBBO, O. L., KELLY, M. E., KIANG, A. S., HUMPHRIES, M. M., NGUYEN, A. T., OZAKI, E., KEANEY, J., BLAU, C. W., KERSKENS, C. M., CAHALAN, S. D., CALLANAN, J. J., WALLACE, E., GRANT, G. A., DOHERTY, C. P. & HUMPHRIES, P. 2012. Targeted

suppression of claudin-5 decreases cerebral oedema and improves cognitive outcome following traumatic brain injury. *Nat Commun,* 3**,** 849.
CAMPBELL, M., HUMPHRIES, M. M., KIANG, A. S., NGUYEN, A. T., GOBBO, O. L., TAM, L. C., SUZUKI, M., HANRAHAN, F., OZAKI, E., FARRAR, G. J., KENNA, P. F. & HUMPHRIES, P. 2011. Systemic low-molecular weight drug delivery to pre-selected neuronal regions. *EMBO Mol Med,* 3**,** 235-45.
CAMPBELL, M., KIANG, A. S., KENNA, P. F., KERSKENS, C., BLAU, C., O'DWYER, L., TIVNAN, A., KELLY, J. A., BRANKIN, B., FARRAR, G. J. & HUMPHRIES, P. 2008. RNAi-mediated reversible opening of the blood-brain barrier. *J Gene Med,* 10**,** 930-47.
CAMPBELL, M., NGUYEN, A. T., KIANG, A. S., TAM, L. C., GOBBO, O. L., KERSKENS, C., NI DHUBHGHAILL, S., HUMPHRIES, M. M., FARRAR, G. J., KENNA, P. F. & HUMPHRIES, P. 2009. An experimental platform for systemic drug delivery to the retina. *Proc Natl Acad Sci U S A,* 106**,** 17817-22.
CAMPBELL, S. L., ROBEL, S., CUDDAPAH, V. A., ROBERT, S., BUCKINGHAM, S. C., KAHLE, K. T. & SONTHEIMER, H. 2015. GABAergic disinhibition and impaired KCC2 cotransporter activity underlie tumor-associated epilepsy. *Glia,* 63**,** 23-36.
CAN, A., DAO, D. T., ARAD, M., TERRILLION, C. E., PIANTADOSI, S. C. & GOULD, T. D. 2012. The mouse forced swim test. *J Vis Exp***,** e3638.
CANNON, M., JONES, P. B. & MURRAY, R. M. 2002a. Obstetric complications and schizophrenia: historical and meta-analytic review. *Am J Psychiatry,* 159**,** 1080-92.
CANNON, T. D., THOMPSON, P. M., VAN ERP, T. G., TOGA, A. W., POUTANEN, V. P., HUTTUNEN, M., LONNQVIST, J., STANDERSKJOLD-NORDENSTAM, C. G., NARR, K. L., KHALEDY, M., ZOUMALAN, C. I., DAIL, R. & KAPRIO, J. 2002b. Cortex mapping reveals regionally specific patterns of genetic and disease-specific gray-matter deficits in twins discordant for schizophrenia. *Proc Natl Acad Sci U S A,* 99**,** 3228-33.
CANTOR-GRAAE, E. & SELTEN, J. P. 2005. Schizophrenia and migration: a meta-analysis and review. *Am J Psychiatry,* 162**,** 12-24.
CARMEL, M., ZARCHI, O., MICHAELOVSKY, E., FRISCH, A., PATYA, M., GREEN, T., GOTHELF, D. & WEIZMAN, A. 2014. Association of COMT and PRODH gene variants with intelligence quotient (IQ) and executive functions in 22q11.2DS subjects. *J Psychiatr Res,* 56**,** 28-35.
CARMELIET, P., FERREIRA, V., BREIER, G., POLLEFEYT, S., KIECKENS, L., GERTSENSTEIN, M., FAHRIG, M., VANDENHOECK, A., HARPAL, K., EBERHARDT, C., DECLERCQ, C., PAWLING, J., MOONS, L., COLLEN, D., RISAU, W. & NAGY, A. 1996. Abnormal blood vessel development and lethality in embryos lacking a single VEGF allele. *Nature,* 380**,** 435-9.
CASTLE, D. J. & MURRAY, R. M. 1991. The neurodevelopmental basis of sex differences in schizophrenia. *Psychol Med,* 21**,** 565-75.
CECCHELLI, R., BEREZOWSKI, V., LUNDQUIST, S., CULOT, M., RENFTEL, M., DEHOUCK, M. P. & FENART, L. 2007. Modelling of the blood-brain barrier in drug discovery and development. *Nat Rev Drug Discov,* 6**,** 650-61.
CHANG, W. H., LIN, S. K., LANE, H. Y., HU, W. H., JANN, M. W. & LIN, H. N. 1997. Clozapine dosages and plasma drug concentrations. *J Formos Med Assoc,* 96**,** 599-605.
CHAPMAN, D. L., GARVEY, N., HANCOCK, S., ALEXIOU, M., AGULNIK, S. I., GIBSON-BROWN, J. J., CEBRA-THOMAS, J., BOLLAG, R. J., SILVER, L.

M. & PAPAIOANNOU, V. E. 1996. Expression of the T-box family genes, Tbx1-Tbx5, during early mouse development. *Dev Dyn,* 206**,** 379-90.
CHEN, C. K., LIN, S. K., SHAM, P. C., BALL, D., LOH, E. W., HSIAO, C. C., CHIANG, Y. L., REE, S. C., LEE, C. H. & MURRAY, R. M. 2003. Pre-morbid characteristics and co-morbidity of methamphetamine users with and without psychosis. *Psychol Med,* 33**,** 1407-14.
CHEN, J., LUO, Y., HUI, H., CAI, T., HUANG, H., YANG, F., FENG, J., ZHANG, J. & YAN, X. 2017. CD146 coordinates brain endothelial cell-pericyte communication for blood-brain barrier development. *Proc Natl Acad Sci U S A.*
CHEN, Z. L., YAO, Y., NORRIS, E. H., KRUYER, A., JNO-CHARLES, O., AKHMEROV, A. & STRICKLAND, S. 2013. Ablation of astrocytic laminin impairs vascular smooth muscle cell function and leads to hemorrhagic stroke. *J Cell Biol,* 202**,** 381-95.
CHEUNG, E. N., GEORGE, S. R., COSTAIN, G. A., ANDRADE, D. M., CHOW, E. W., SILVERSIDES, C. K. & BASSETT, A. S. 2014. Prevalence of hypocalcaemia and its associated features in 22q11.2 deletion syndrome. *Clin Endocrinol (Oxf),* 81**,** 190-6.
CHODOBSKI, A., ZINK, B. J. & SZMYDYNGER-CHODOBSKA, J. 2011. Blood-brain barrier pathophysiology in traumatic brain injury. *Translational stroke research,* 2**,** 492-516.
CHONG, H. Y., TEOH, S. L., WU, D. B.-C., KOTIRUM, S., CHIOU, C.-F. & CHAIYAKUNAPRUK, N. 2016. Global economic burden of schizophrenia: a systematic review. *Neuropsychiatric Disease and Treatment,* 12**,** 357-373.
CITI, S., AMOROSI, A., FRANCONI, F., GIOTTI, A. & ZAMPI, G. 1991. Cingulin, a specific protein component of tight junctions, is expressed in normal and neoplastic human epithelial tissues. *Am J Pathol,* 138**,** 781-9.
CITI, S., PASCHOUD, S., PULIMENO, P., TIMOLATI, F., DE ROBERTIS, F., JOND, L. & GUILLEMOT, L. 2009. The tight junction protein cingulin regulates gene expression and RhoA signaling. *Ann N Y Acad Sci,* 1165**,** 88-98.
CORDENONSI, M., D'ATRI, F., HAMMAR, E., PARRY, D. A., KENDRICK-JONES, J., SHORE, D. & CITI, S. 1999. Cingulin contains globular and coiled-coil domains and interacts with ZO-1, ZO-2, ZO-3, and myosin. *J Cell Biol,* 147**,** 1569-82.
CORTES-CANTELI, M., MATTEI, L., RICHARDS, A. T., NORRIS, E. H. & STRICKLAND, S. 2015. Fibrin deposited in the Alzheimer's disease brain promotes neuronal degeneration. *Neurobiol Aging,* 36**,** 608-17.
COULTER, D. A. & STEINHÄUSER, C. 2015. Role of Astrocytes in Epilepsy. *Cold Spring Harbor perspectives in medicine,* 5**,** a022434-a022434.
CREESE, I., BURT, D. R. & SNYDER, S. H. 1976. Dopamine receptor binding predicts clinical and pharmacological potencies of antischizophrenic drugs. *Science,* 192**,** 481-3.
CRUSIO, W. E., SCHWEGLER, H. & BRUST, I. 1993. Covariations between hippocampal mossy fibres and working and reference memory in spatial and non-spatial radial maze tasks in mice. *Eur J Neurosci,* 5**,** 1413-20.
CUMMINS, P. M. 2012. Occludin: one protein, many forms. *Mol Cell Biol,* 32**,** 242-50.
D'MELLO, C. & SWAIN, M. G. 2014. Liver-brain interactions in inflammatory liver diseases: implications for fatigue and mood disorders. *Brain Behav Immun,* 35**,** 9-20.

DANEMAN, R., AGALLIU, D., ZHOU, L., KUHNERT, F., KUO, C. J. & BARRES, B. A. 2009. Wnt/beta-catenin signaling is required for CNS, but not non-CNS, angiogenesis. *Proc Natl Acad Sci U S A,* 106**,** 641-6.
DANEMAN, R., ZHOU, L., AGALLIU, D., CAHOY, J. D., KAUSHAL, A. & BARRES, B. A. 2010a. The mouse blood-brain barrier transcriptome: a new resource for understanding the development and function of brain endothelial cells. *PLoS One,* 5**,** e13741.
DANEMAN, R., ZHOU, L., KEBEDE, A. A. & BARRES, B. A. 2010b. Pericytes are required for blood-brain barrier integrity during embryogenesis. *Nature,* 468**,** 562-6.
DAS, A. T., TENENBAUM, L. & BERKHOUT, B. 2016. Tet-On Systems For Doxycycline-inducible Gene Expression. *Curr Gene Ther,* 16**,** 156-67.
DAVALOS, D., GRUTZENDLER, J., YANG, G., KIM, J. V., ZUO, Y., JUNG, S., LITTMAN, D. R., DUSTIN, M. L. & GAN, W. B. 2005. ATP mediates rapid microglial response to local brain injury in vivo. *Nat Neurosci,* 8**,** 752-8.
DE GIORGIS, V. & VEGGIOTTI, P. 2013. GLUT1 deficiency syndrome 2013: current state of the art. *Seizure,* 22**,** 803-11.
DE JONG, F. J., VERNOOIJ, M. W., IKRAM, M. K., IKRAM, M. A., HOFMAN, A., KRESTIN, G. P., VAN DER LUGT, A., DE JONG, P. T. & BRETELER, M. M. 2008. Arteriolar oxygen saturation, cerebral blood flow, and retinal vessel diameters. The Rotterdam Study. *Ophthalmology,* 115**,** 887-92.
DE KONING, M. B., VAN DUIN, E. D., BOOT, E., BLOEMEN, O. J., BAKKER, J. A., ABEL, K. M. & VAN AMELSVOORT, T. A. 2015. PRODH rs450046 and proline x COMT Val(1)(5)(8) Met interaction effects on intelligence and startle in adults with 22q11 deletion syndrome. *Psychopharmacology (Berl),* 232**,** 3111-22.
DE PITTA, M., BRUNEL, N. & VOLTERRA, A. 2016. Astrocytes: Orchestrating synaptic plasticity? *Neuroscience,* 323**,** 43-61.
DE ROSSI, P., HARDE, E., DUPUIS, J. P., MARTIN, L., CHOUNLAMOUNTRI, N., BARDIN, M., WATRIN, C., BENETOLLO, C., PERNET-GALLAY, K., LUHMANN, H. J., HONNORAT, J., MALLERET, G., GROC, L., ACKER-PALMER, A., SALIN, P. A. & MEISSIREL, C. 2016. A critical role for VEGF and VEGFR2 in NMDA receptor synaptic function and fear-related behavior. *Mol Psychiatry,* 21**,** 1768-1780.
DEACON, R. M. 2013. Measuring motor coordination in mice. *J Vis Exp***,** e2609.
DEACON, R. M. & RAWLINS, J. N. 2006. T-maze alternation in the rodent. *Nat Protoc,* 1**,** 7-12.
DECZKOWSKA, A., BARUCH, K. & SCHWARTZ, M. 2016. Type I/II Interferon Balance in the Regulation of Brain Physiology and Pathology. *Trends Immunol,* 37**,** 181-192.
DEJANA, E., ORSENIGO, F. & LAMPUGNANI, M. G. 2008. The role of adherens junctions and VE-cadherin in the control of vascular permeability. *J Cell Sci,* 121**,** 2115-22.
DICKINS, R. A., MCJUNKIN, K., HERNANDO, E., PREMSRIRUT, P. K., KRIZHANOVSKY, V., BURGESS, D. J., KIM, S. Y., CORDON-CARDO, C., ZENDER, L., HANNON, G. J. & LOWE, S. W. 2007. Tissue-specific and reversible RNA interference in transgenic mice. *Nat Genet,* 39**,** 914-21.
DIDRIKSEN, M., FEJGIN, K., NILSSON, S. R., BIRKNOW, M. R., GRAYTON, H. M., LARSEN, P. H., LAURIDSEN, J. B., NIELSEN, V., CELADA, P., SANTANA, N., KALLUNKI, P., CHRISTENSEN, K. V., WERGE, T. M.,

STENSBOL, T. B., EGEBJERG, J., GASTAMBIDE, F., ARTIGAS, F., BASTLUND, J. F. & NIELSEN, J. 2017. Persistent gating deficit and increased sensitivity to NMDA receptor antagonism after puberty in a new mouse model of the human 22q11.2 microdeletion syndrome: a study in male mice. *J Psychiatry Neurosci,* 42**,** 48-58.

DOMENICI, E., WILLE, D. R., TOZZI, F., PROKOPENKO, I., MILLER, S., MCKEOWN, A., BRITTAIN, C., RUJESCU, D., GIEGLING, I., TURCK, C. W., HOLSBOER, F., BULLMORE, E. T., MIDDLETON, L., MERLO-PICH, E., ALEXANDER, R. C. & MUGLIA, P. 2010. Plasma protein biomarkers for depression and schizophrenia by multi analyte profiling of case-control collections. *PLoS One,* 5**,** e9166.

DRUCKER-COLIN, R., AGUILAR-ROBLERO, R., GARCIA-HERNANDEZ, F., FERNANDEZ-CANCINO, F. & BERMUDEZ RATTONI, F. 1984. Fetal suprachiasmatic nucleus transplants: diurnal rhythm recovery of lesioned rats. *Brain Res,* 311**,** 353-7.

EBNET, K., SCHULZ, C. U., MEYER ZU BRICKWEDDE, M. K., PENDL, G. G. & VESTWEBER, D. 2000. Junctional adhesion molecule interacts with the PDZ domain-containing proteins AF-6 and ZO-1. *J Biol Chem,* 275**,** 27979-88.

ECKEL-MAHAN, K. & SASSONE-CORSI, P. 2013. Metabolism and the circadian clock converge. *Physiol Rev,* 93**,** 107-35.

EDELMANN, L., PANDITA, R. K. & MORROW, B. E. 1999. Low-copy repeats mediate the common 3-Mb deletion in patients with velo-cardio-facial syndrome. *Am J Hum Genet,* 64**,** 1076-86.

ELMORSY, E., ELZALABANY, L. M., ELSHEIKHA, H. M. & SMITH, P. A. 2014. Adverse effects of antipsychotics on micro-vascular endothelial cells of the human blood-brain barrier. *Brain Res,* 1583**,** 255-68.

ELMORSY, E. & SMITH, P. A. 2015. Bioenergetic disruption of human micro-vascular endothelial cells by antipsychotics. *Biochem Biophys Res Commun,* 460**,** 857-62.

ENOMOTO, T., NODA, Y. & NABESHIMA, T. 2007. Phencyclidine and genetic animal models of schizophrenia developed in relation to the glutamate hypothesis. *Methods Find Exp Clin Pharmacol,* 29**,** 291-301.

ESPOSITO, P., GHEORGHE, D., KANDERE, K., PANG, X., CONNOLLY, R., JACOBSON, S. & THEOHARIDES, T. C. 2001. Acute stress increases permeability of the blood-brain-barrier through activation of brain mast cells. *Brain Res,* 888**,** 117-127.

FANNING, A. S., JAMESON, B. J., JESAITIS, L. A. & ANDERSON, J. M. 1998. The tight junction protein ZO-1 establishes a link between the transmembrane protein occludin and the actin cytoskeleton. *J Biol Chem,* 273**,** 29745-53.

FANNING, A. S., LITTLE, B. P., RAHNER, C., UTEPBERGENOV, D., WALTHER, Z. & ANDERSON, J. M. 2007. The unique-5 and -6 motifs of ZO-1 regulate tight junction strand localization and scaffolding properties. *Mol Biol Cell,* 18**,** 721-31.

FANTIN, A., VIEIRA, J. M., GESTRI, G., DENTI, L., SCHWARZ, Q., PRYKHOZHIJ, S., PERI, F., WILSON, S. W. & RUHRBERG, C. 2010. Tissue macrophages act as cellular chaperones for vascular anastomosis downstream of VEGF-mediated endothelial tip cell induction. *Blood,* 116**,** 829-40.

FARDE, L., NORDSTROM, A. L., WIESEL, F. A., PAULI, S., HALLDIN, C. & SEDVALL, G. 1992. Positron emission tomographic analysis of central D1 and D2 dopamine receptor occupancy in patients treated with classical neuroleptics

and clozapine. Relation to extrapyramidal side effects. *Arch Gen Psychiatry,* 49**,** 538-44.
FEARON, P., KIRKBRIDE, J. B., MORGAN, C., DAZZAN, P., MORGAN, K., LLOYD, T., HUTCHINSON, G., TARRANT, J., FUNG, W. L., HOLLOWAY, J., MALLETT, R., HARRISON, G., LEFF, J., JONES, P. B. & MURRAY, R. M. 2006. Incidence of schizophrenia and other psychoses in ethnic minority groups: results from the MRC AESOP Study. *Psychol Med,* 36**,** 1541-50.
FEDER, A., NESTLER, E. J. & CHARNEY, D. S. 2009. Psychobiology and molecular genetics of resilience. *Nat Rev Neurosci,* 10**,** 446-57.
FEDER, N. 1971. Microperoxidase. An ultrastructural tracer of low molecular weight. *J Cell Biol,* 51**,** 339-43.
FERGUSSON, D. M., HORWOOD, L. J. & SWAIN-CAMPBELL, N. R. 2003. Cannabis dependence and psychotic symptoms in young people. *Psychol Med,* 33**,** 15-21.
FIORENTINO, M., SAPONE, A., SENGER, S., CAMHI, S. S., KADZIELSKI, S. M., BUIE, T. M., KELLY, D. L., CASCELLA, N. & FASANO, A. 2016. Blood–brain barrier and intestinal epithelial barrier alterations in autism spectrum disorders. *Molecular Autism,* 7**,** 49.
FORBES, B. J., BINENBAUM, G., EDMOND, J. C., DELARATO, N., MCDONALD-MCGINN, D. M. & ZACKAI, E. H. 2007. Ocular findings in the chromosome 22q11.2 deletion syndrome. *J aapos,* 11**,** 179-82.
FRANK, D. U., FOTHERINGHAM, L. K., BREWER, J. A., MUGLIA, L. J., TRISTANI-FIROUZI, M., CAPECCHI, M. R. & MOON, A. M. 2002. An Fgf8 mouse mutant phenocopies human 22q11 deletion syndrome. *Development,* 129**,** 4591-603.
FREEMAN, H. 1994. Schizophrenia and city residence. *Br J Psychiatry Suppl***,** 39-50.
FRIEDMAN, A. 2011. Blood-brain barrier dysfunction, status epilepticus, seizures and epilepsy: a puzzle of a chicken and egg? *Epilepsia,* 52**,** 19-20.
FULZELE, S. & PILLAI, A. 2009. Decreased VEGF mRNA expression in the dorsolateral prefrontal cortex of schizophrenia subjects. *Schizophr Res,* 115**,** 372-3.
FURUSE, M., FUJIMOTO, K., SATO, N., HIRASE, T., TSUKITA, S. & TSUKITA, S. 1996. Overexpression of occludin, a tight junction-associated integral membrane protein, induces the formation of intracellular multilamellar bodies bearing tight junction-like structures. *J Cell Sci,* 109 (Pt 2)**,** 429-35.
FURUSE, M., HATA, M., FURUSE, K., YOSHIDA, Y., HARATAKE, A., SUGITANI, Y., NODA, T., KUBO, A. & TSUKITA, S. 2002. Claudin-based tight junctions are crucial for the mammalian epidermal barrier: a lesson from claudin-1-deficient mice. *J Cell Biol,* 156**,** 1099-111.
FURUSE, M., HIRASE, T., ITOH, M., NAGAFUCHI, A., YONEMURA, S., TSUKITA, S. & TSUKITA, S. 1993. Occludin: a novel integral membrane protein localizing at tight junctions. *J Cell Biol,* 123**,** 1777-88.
FURUSE, M., SASAKI, H. & TSUKITA, S. 1999. Manner of interaction of heterogeneous claudin species within and between tight junction strands. *J Cell Biol,* 147**,** 891-903.
FUSAR-POLI, P., KEMPTON, M. J. & ROSENHECK, R. A. 2013. Efficacy and safety of second-generation long-acting injections in schizophrenia: a meta-analysis of randomized-controlled trials. *Int Clin Psychopharmacol,* 28**,** 57-66.

GAEBEL, W. 1997. Towards the improvement of compliance: the significance of psycho-education and new antipsychotic drugs. *Int Clin Psychopharmacol,* 12 Suppl 1**,** S37-42.
GARDNER, D. M., BALDESSARINI, R. J. & WARAICH, P. 2005. Modern antipsychotic drugs: a critical overview. *Cmaj,* 172**,** 1703-11.
GAUTAM, J., ZHANG, X. & YAO, Y. 2016. The role of pericytic laminin in blood brain barrier integrity maintenance. *Sci Rep,* 6**,** 36450.
GEKAKIS, N., STAKNIS, D., NGUYEN, H. B., DAVIS, F. C., WILSBACHER, L. D., KING, D. P., TAKAHASHI, J. S. & WEITZ, C. J. 1998. Role of the CLOCK protein in the mammalian circadian mechanism. *Science,* 280**,** 1564-9.
GEYER, M. A., KREBS-THOMSON, K., BRAFF, D. L. & SWERDLOW, N. R. 2001. Pharmacological studies of prepulse inhibition models of sensorimotor gating deficits in schizophrenia: a decade in review. *Psychopharmacology (Berl),* 156**,** 117-54.
GINHOUX, F., GRETER, M., LEBOEUF, M., NANDI, S., SEE, P., GOKHAN, S., MEHLER, M. F., CONWAY, S. J., NG, L. G., STANLEY, E. R., SAMOKHVALOV, I. M. & MERAD, M. 2010. Fate mapping analysis reveals that adult microglia derive from primitive macrophages. *Science,* 330**,** 841-5.
GOGOS, J. A., MORGAN, M., LUINE, V., SANTHA, M., OGAWA, S., PFAFF, D. & KARAYIORGOU, M. 1998. Catechol-O-methyltransferase-deficient mice exhibit sexually dimorphic changes in catecholamine levels and behavior. *Proc Natl Acad Sci U S A,* 95**,** 9991-6.
GOMEZ-GONZALEZ, B., HURTADO-ALVARADO, G., ESQUEDA-LEON, E., SANTANA-MIRANDA, R., ROJAS-ZAMORANO, J. A. & VELAZQUEZ-MOCTEZUMA, J. 2013. REM sleep loss and recovery regulates blood-brain barrier function. *Curr Neurovasc Res,* 10**,** 197-207.
GOTTESMAN, I. 1991. *Schizophrenia Genesis: The Origins of Madness,* New York, WH Freeman.
GOW, A., DAVIES, C., SOUTHWOOD, C. M., FROLENKOV, G., CHRUSTOWSKI, M., NG, L., YAMAUCHI, D., MARCUS, D. C. & KACHAR, B. 2004. Deafness in Claudin 11-null mice reveals the critical contribution of basal cell tight junctions to stria vascularis function. *J Neurosci,* 24**,** 7051-62.
GOW, A., SOUTHWOOD, C. M., LI, J. S., PARIALI, M., RIORDAN, G. P., BRODIE, S. E., DANIAS, J., BRONSTEIN, J. M., KACHAR, B. & LAZZARINI, R. A. 1999. CNS myelin and sertoli cell tight junction strands are absent in Osp/claudin-11 null mice. *Cell,* 99**,** 649-59.
GREENE, C. & CAMPBELL, M. 2016. Tight junction modulation of the blood brain barrier: CNS delivery of small molecules. *Tissue Barriers,* 4**,** e1138017.
GRIFFIN, E. A., JR., STAKNIS, D. & WEITZ, C. J. 1999. Light-independent role of CRY1 and CRY2 in the mammalian circadian clock. *Science,* 286**,** 768-71.
GUILLAUMOND, F., DARDENTE, H., GIGUERE, V. & CERMAKIAN, N. 2005. Differential control of Bmal1 circadian transcription by REV-ERB and ROR nuclear receptors. *J Biol Rhythms,* 20**,** 391-403.
GUILLEMOT, L. & CITI, S. 2006. Cingulin regulates claudin-2 expression and cell proliferation through the small GTPase RhoA. *Mol Biol Cell,* 17**,** 3569-77.
GUNA, A., BUTCHER, N. J. & BASSETT, A. S. 2015. Comparative mapping of the 22q11.2 deletion region and the potential of simple model organisms. *J Neurodev Disord,* 7**,** 18.
GUO, T., MCDONALD-MCGINN, D., BLONSKA, A., SHANSKE, A., BASSETT, A. S., CHOW, E., BOWSER, M., SHERIDAN, M., BEEMER, F., DEVRIENDT,

K., SWILLEN, A., BRECKPOT, J., DIGILIO, M. C., MARINO, B., DALLAPICCOLA, B., CARPENTER, C., ZHENG, X., JOHNSON, J., CHUNG, J., HIGGINS, A. M., PHILIP, N., SIMON, T. J., COLEMAN, K., HEINE-SUNER, D., ROSELL, J., KATES, W., DEVOTO, M., GOLDMUNTZ, E., ZACKAI, E., WANG, T., SHPRINTZEN, R., EMANUEL, B. & MORROW, B. 2011. Genotype and cardiovascular phenotype correlations with TBX1 in 1,022 velo-cardio-facial/DiGeorge/22q11.2 deletion syndrome patients. *Hum Mutat,* 32**,** 1278-89.

GURSES, C., EKIZOGLU, O., ORHAN, N., USTEK, D., ARICAN, N., AHISHALI, B., ELMAS, I., KUCUK, M., BILGIC, B., KEMIKLER, G., KALAYCI, R., KARADENIZ, A. & KAYA, M. 2009. Levetiracetam decreases the seizure activity and blood-brain barrier permeability in pentylenetetrazole-kindled rats with cortical dysplasia. *Brain Res,* 1281**,** 71-83.

HALL, C. N., REYNELL, C., GESSLEIN, B., HAMILTON, N. B., MISHRA, A., SUTHERLAND, B. A., O'FARRELL, F. M., BUCHAN, A. M., LAURITZEN, M. & ATTWELL, D. 2014. Capillary pericytes regulate cerebral blood flow in health and disease. *Nature,* 508**,** 55-60.

HAMMOND, R. S., TULL, L. E. & STACKMAN, R. W. 2004. On the delay-dependent involvement of the hippocampus in object recognition memory. *Neurobiol Learn Mem,* 82**,** 26-34.

HANSEN, S. D., KWIATKOWSKI, A. V., OUYANG, C. Y., LIU, H., POKUTTA, S., WATKINS, S. C., VOLKMANN, N., HANEIN, D., WEIS, W. I., MULLINS, R. D. & NELSON, W. J. 2013. alphaE-catenin actin-binding domain alters actin filament conformation and regulates binding of nucleation and disassembly factors. *Mol Biol Cell,* 24**,** 3710-20.

HARRIS, L. W., WAYLAND, M., LAN, M., RYAN, M., GIGER, T., LOCKSTONE, H., WUETHRICH, I., MIMMACK, M., WANG, L., KOTTER, M., CRADDOCK, R. & BAHN, S. 2008. The cerebral microvasculature in schizophrenia: a laser capture microdissection study. *PLoS One,* 3**,** e3964.

HARTSOCK, A. & NELSON, W. J. 2008. Adherens and tight junctions: structure, function and connections to the actin cytoskeleton. *Biochim Biophys Acta,* 1778**,** 660-9.

HARTZ, A. M., BAUER, B., SOLDNER, E. L., WOLF, A., BOY, S., BACKHAUS, R., MIHALJEVIC, I., BOGDAHN, U., KLUNEMANN, H. H., SCHUIERER, G. & SCHLACHETZKI, F. 2012. Amyloid-beta contributes to blood-brain barrier leakage in transgenic human amyloid precursor protein mice and in humans with cerebral amyloid angiopathy. *Stroke,* 43**,** 514-23.

HAWKINS, B. T. & DAVIS, T. P. 2005. The blood-brain barrier/neurovascular unit in health and disease. *Pharmacol Rev,* 57**,** 173-85.

HE, J., HSUCHOU, H., HE, Y., KASTIN, A. J., WANG, Y. & PAN, W. 2014. Sleep restriction impairs blood-brain barrier function. *J Neurosci,* 34**,** 14697-706.

HELLSTROM, M., KALEN, M., LINDAHL, P., ABRAMSSON, A. & BETSHOLTZ, C. 1999. Role of PDGF-B and PDGFR-beta in recruitment of vascular smooth muscle cells and pericytes during embryonic blood vessel formation in the mouse. *Development,* 126**,** 3047-55.

HERMAN, S. B., GUO, T., MCGINN, D. M., BLONSKA, A., SHANSKE, A. L., BASSETT, A. S., CHOW, E. W., BOWSER, M., SHERIDAN, M., BEEMER, F., DEVRIENDT, K., SWILLEN, A., BRECKPOT, J., DIGILIO, M. C., MARINO, B., DALLAPICCOLA, B., CARPENTER, C., ZHENG, X., JOHNSON, J., CHUNG, J., HIGGINS, A. M., PHILIP, N., SIMON, T.,

COLEMAN, K., HEINE-SUNER, D., ROSELL, J., KATES, W., DEVOTO, M., ZACKAI, E., WANG, T., SHPRINTZEN, R., EMANUEL, B. S. & MORROW, B. E. 2012. Overt cleft palate phenotype and TBX1 genotype correlations in velo-cardio-facial/DiGeorge/22q11.2 deletion syndrome patients. *Am J Med Genet A,* 158a**,** 2781-7.

HINO, T., YOKOTA, T., ITO, S., NISHINA, K., KANG, Y. S., MORI, S., HORI, S., KANDA, T., TERASAKI, T. & MIZUSAWA, H. 2006. In vivo delivery of small interfering RNA targeting brain capillary endothelial cells. *Biochem Biophys Res Commun,* 340**,** 263-7.

HITTI, F. L. & SIEGELBAUM, S. A. 2014. The hippocampal CA2 region is essential for social memory. *Nature,* 508**,** 88-92.

HLADKY, S. B. & BARRAND, M. A. 2014. Mechanisms of fluid movement into, through and out of the brain: evaluation of the evidence. *Fluids Barriers CNS,* 11**,** 26.

HLADKY, S. B. & BARRAND, M. A. 2016. Fluid and ion transfer across the blood-brain and blood-cerebrospinal fluid barriers; a comparative account of mechanisms and roles. *Fluids Barriers CNS,* 13**,** 19.

HOANG, U., STEWART, R. & GOLDACRE, M. J. 2011. Mortality after hospital discharge for people with schizophrenia or bipolar disorder: retrospective study of linked English hospital episode statistics, 1999-2006. *Bmj,* 343**,** d5422.

HOLTER, K. E., KEHLET, B., DEVOR, A., SEJNOWSKI, T. J., DALE, A. M., OMHOLT, S. W., OTTERSEN, O. P., NAGELHUS, E. A., MARDAL, K.-A. & PETTERSEN, K. H. 2017. Interstitial solute transport in 3D reconstructed neuropil occurs by diffusion rather than bulk flow. *Proceedings of the National Academy of Sciences of the United States of America,* 114**,** 9894-9899.

HUA, J., BRANDT, A. S., LEE, S., BLAIR, N. I. S., WU, Y., LUI, S., PATEL, J., FARIA, A. V., LIM, I. A. L., UNSCHULD, P. G., PEKAR, J. J., VAN ZIJL, P. C. M., ROSS, C. A. & MARGOLIS, R. L. 2017. Abnormal Grey Matter Arteriolar Cerebral Blood Volume in Schizophrenia Measured With 3D Inflow-Based Vascular-Space-Occupancy MRI at 7T. *Schizophr Bull,* 43**,** 620-632.

HUANG, Y. H., BAO, Y., PENG, W., GOLDBERG, M., LOVE, K., BUMCROT, D. A., COLE, G., LANGER, R., ANDERSON, D. G. & SAWICKI, J. A. 2009. Claudin-3 gene silencing with siRNA suppresses ovarian tumor growth and metastasis. *Proc Natl Acad Sci U S A,* 106**,** 3426-30.

HUDSON, N., POWNER, M. B., SARKER, M. H., BURGOYNE, T., CAMPBELL, M., OCKRIM, Z. K., MARTINELLI, R., FUTTER, C. E., GRANT, M. B., FRASER, P. A., SHIMA, D. T., GREENWOOD, J. & TUROWSKI, P. 2014. Differential apicobasal VEGF signaling at vascular blood-neural barriers. *Dev Cell,* 30**,** 541-52.

HWANG, Y., KIM, J., SHIN, J. Y., KIM, J. I., SEO, J. S., WEBSTER, M. J., LEE, D. & KIM, S. 2013. Gene expression profiling by mRNA sequencing reveals increased expression of immune/inflammation-related genes in the hippocampus of individuals with schizophrenia. *Transl Psychiatry,* 3**,** e321.

IKENOUCHI, J., FURUSE, M., FURUSE, K., SASAKI, H., TSUKITA, S. & TSUKITA, S. 2005. Tricellulin constitutes a novel barrier at tricellular contacts of epithelial cells. *J Cell Biol,* 171**,** 939-45.

ILIFF, J. J., WANG, M., LIAO, Y., PLOGG, B. A., PENG, W., GUNDERSEN, G. A., BENVENISTE, H., VATES, G. E., DEANE, R., GOLDMAN, S. A., NAGELHUS, E. A. & NEDERGAARD, M. 2012. A paravascular pathway

facilitates CSF flow through the brain parenchyma and the clearance of interstitial solutes, including amyloid beta. *Sci Transl Med,* 4**,** 147ra111.
ITOH, K., ISHIHARA, Y., KOMORI, R., NOCHI, H., TANIGUCHI, R., CHIBA, Y., UENO, M., TAKATA-TSUJI, F., DOHGU, S. & KATAOKA, Y. 2016. Levetiracetam treatment influences blood-brain barrier failure associated with angiogenesis and inflammatory responses in the acute phase of epileptogenesis in post-status epilepticus mice. *Brain Res,* 1652**,** 1-13.
ITOH, M., FURUSE, M., MORITA, K., KUBOTA, K., SAITOU, M. & TSUKITA, S. 1999. Direct binding of three tight junction-associated MAGUKs, ZO-1, ZO-2, and ZO-3, with the COOH termini of claudins. *J Cell Biol,* 147**,** 1351-63.
ITOH, M., SASAKI, H., FURUSE, M., OZAKI, H., KITA, T. & TSUKITA, S. 2001. Junctional adhesion molecule (JAM) binds to PAR-3: a possible mechanism for the recruitment of PAR-3 to tight junctions. *J Cell Biol,* 154**,** 491-7.
IWATA, Y., SUZUKI, K., NAKAMURA, K., MATSUZAKI, H., SEKINE, Y., TSUCHIYA, K. J., SUGIHARA, G., KAWAI, M., MINABE, Y., TAKEI, N. & MORI, N. 2007. Increased levels of serum soluble L-selectin in unmedicated patients with schizophrenia. *Schizophr Res,* 89**,** 154-60.
JEROME, L. A. & PAPAIOANNOU, V. E. 2001. DiGeorge syndrome phenotype in mice mutant for the T-box gene, Tbx1. *Nat Genet,* 27**,** 286-91.
JIAO, X., HE, P., LI, Y., FAN, Z., SI, M., XIE, Q., CHANG, X. & HUANG, D. 2015. The Role of Circulating Tight Junction Proteins in Evaluating Blood Brain Barrier Disruption following Intracranial Hemorrhage. *Dis Markers,* 2015**,** 860120.
JOHNSON, A. W., JAARO-PELED, H., SHAHANI, N., SEDLAK, T. W., ZOUBOVSKY, S., BURRUSS, D., EMILIANI, F., SAWA, A. & GALLAGHER, M. 2013. Cognitive and motivational deficits together with prefrontal oxidative stress in a mouse model for neuropsychiatric illness. *Proc Natl Acad Sci U S A,* 110**,** 12462-7.
KAHN, R. S., SOMMER, I. E., MURRAY, R. M., MEYER-LINDENBERG, A., WEINBERGER, D. R., CANNON, T. D., O'DONOVAN, M., CORRELL, C. U., KANE, J. M., VAN OS, J. & INSEL, T. R. 2015. Schizophrenia. *Nat Rev Dis Primers,* 1**,** 15067.
KAIDANOVICH-BEILIN, O., LIPINA, T., VUKOBRADOVIC, I., RODER, J. & WOODGETT, J. R. 2011. Assessment of social interaction behaviors. *J Vis Exp*.
KANOSKI, S. E., ZHANG, Y., ZHENG, W. & DAVIDSON, T. L. 2010. The effects of a high-energy diet on hippocampal function and blood-brain barrier integrity in the rat. *J Alzheimers Dis,* 21**,** 207-19.
KAO, A., MARIANI, J., MCDONALD-MCGINN, D. M., MAISENBACHER, M. K., BROOKS-KAYAL, A. R., ZACKAI, E. H. & LYNCH, D. R. 2004. Increased prevalence of unprovoked seizures in patients with a 22q11.2 deletion. *Am J Med Genet A,* 129a**,** 29-34.
KAPUR, S., ZIPURSKY, R., JONES, C., REMINGTON, G. & HOULE, S. 2000. Relationship between dopamine D(2) occupancy, clinical response, and side effects: a double-blind PET study of first-episode schizophrenia. *Am J Psychiatry,* 157**,** 514-20.
KATSEL, P., ROUSSOS, P., PLETNIKOV, M. & HAROUTUNIAN, V. 2017. Microvascular anomaly conditions in psychiatric disease. Schizophrenia - angiogenesis connection. *Neurosci Biobehav Rev,* 77**,** 327-339.
KATSUNO, T., UMEDA, K., MATSUI, T., HATA, M., TAMURA, A., ITOH, M., TAKEUCHI, K., FUJIMORI, T., NABESHIMA, Y., NODA, T., TSUKITA, S.

& TSUKITA, S. 2008. Deficiency of zonula occludens-1 causes embryonic lethal phenotype associated with defected yolk sac angiogenesis and apoptosis of embryonic cells. *Mol Biol Cell,* 19**,** 2465-75.
KEANEY, J., WALSH, D. M., O'MALLEY, T., HUDSON, N., CROSBIE, D. E., LOFTUS, T., SHEEHAN, F., MCDAID, J., HUMPHRIES, M. M., CALLANAN, J. J., BRETT, F. M., FARRELL, M. A., HUMPHRIES, P. & CAMPBELL, M. 2015. Autoregulated paracellular clearance of amyloid-beta across the blood-brain barrier. *Sci Adv,* 1**,** e1500472.
KELLY, B. D., O'CALLAGHAN, E., WADDINGTON, J. L., FEENEY, L., BROWNE, S., SCULLY, P. J., CLARKE, M., QUINN, J. F., MCTIGUE, O., MORGAN, M. G., KINSELLA, A. & LARKIN, C. 2010. Schizophrenia and the city: A review of literature and prospective study of psychosis and urbanicity in Ireland. *Schizophr Res,* 116**,** 75-89.
KIEHL, T. R., CHOW, E. W., MIKULIS, D. J., GEORGE, S. R. & BASSETT, A. S. 2009. Neuropathologic features in adults with 22q11.2 deletion syndrome. *Cereb Cortex,* 19**,** 153-64.
KIM, S., HWANG, Y., LEE, D. & WEBSTER, M. J. 2016. Transcriptome sequencing of the choroid plexus in schizophrenia. *Transl Psychiatry,* 6**,** e964.
KINOSHITA, M., MCDANNOLD, N., JOLESZ, F. A. & HYNYNEN, K. 2006. Targeted delivery of antibodies through the blood-brain barrier by MRI-guided focused ultrasound. *Biochem Biophys Res Commun,* 340**,** 1085-90.
KIRKBRIDE, J. B., FEARON, P., MORGAN, C., DAZZAN, P., MORGAN, K., TARRANT, J., LLOYD, T., HOLLOWAY, J., HUTCHINSON, G., LEFF, J. P., MALLETT, R. M., HARRISON, G. L., MURRAY, R. M. & JONES, P. B. 2006. Heterogeneity in incidence rates of schizophrenia and other psychotic syndromes: findings from the 3-center AeSOP study. *Arch Gen Psychiatry,* 63**,** 250-8.
KOMADA, M., TAKAO, K. & MIYAKAWA, T. 2008. Elevated plus maze for mice. *J Vis Exp*.
KONDRATOVA, A. A. & KONDRATOV, R. V. 2012. The circadian clock and pathology of the ageing brain. *Nat Rev Neurosci,* 13**,** 325-35.
KRAUSE, G., WINKLER, L., MUELLER, S. L., HASELOFF, R. F., PIONTEK, J. & BLASIG, I. E. 2008. Structure and function of claudins. *Biochim Biophys Acta,* 1778**,** 631-45.
KRAUSE, G., WINKLER, L., PIEHL, C., BLASIG, I., PIONTEK, J. & MULLER, S. L. 2009. Structure and function of extracellular claudin domains. *Ann N Y Acad Sci,* 1165**,** 34-43.
KRISTENSSON, K. & OLSSON, Y. 1973. Accumulation of protein tracers in pericytes of the central nervous system following systemic injection in immature mice. *Acta Neurol Scand,* 49**,** 189-94.
KUMARI, V., FANNON, D., GEYER, M. A., PREMKUMAR, P., ANTONOVA, E., SIMMONS, A. & KUIPERS, E. 2008. Cortical grey matter volume and sensorimotor gating in schizophrenia. *Cortex,* 44**,** 1206-14.
KUME, K., ZYLKA, M. J., SRIRAM, S., SHEARMAN, L. P., WEAVER, D. R., JIN, X., MAYWOOD, E. S., HASTINGS, M. H. & REPPERT, S. M. 1999. mCRY1 and mCRY2 are essential components of the negative limb of the circadian clock feedback loop. *Cell,* 98**,** 193-205.
KVAJO, M., MCKELLAR, H., ARGUELLO, P. A., DREW, L. J., MOORE, H., MACDERMOTT, A. B., KARAYIORGOU, M. & GOGOS, J. A. 2008. A mutation in mouse Disc1 that models a schizophrenia risk allele leads to specific

alterations in neuronal architecture and cognition. *Proc Natl Acad Sci U S A,* 105**,** 7076-81.
LALLY, J., AJNAKINA, O., DI FORTI, M., TROTTA, A., DEMJAHA, A., KOLLIAKOU, A., MONDELLI, V., REIS MARQUES, T., PARIANTE, C., DAZZAN, P., SHERGIL, S. S., HOWES, O. D., DAVID, A. S., MACCABE, J. H., GAUGHRAN, F. & MURRAY, R. M. 2016. Two distinct patterns of treatment resistance: clinical predictors of treatment resistance in first-episode schizophrenia spectrum psychoses. *Psychol Med,* 46**,** 3231-3240.
LARA, D. R., GAMA, C. S., BELMONTE-DE-ABREU, P., PORTELA, L. V., GONCALVES, C. A., FONSECA, M., HAUCK, S. & SOUZA, D. O. 2001. Increased serum S100B protein in schizophrenia: a study in medication-free patients. *J Psychiatr Res,* 35**,** 11-4.
LEBLEU, V. S., MACDONALD, B. & KALLURI, R. 2007. Structure and function of basement membranes. *Exp Biol Med (Maywood),* 232**,** 1121-9.
LEE, S. W., KIM, W. J., CHOI, Y. K., SONG, H. S., SON, M. J., GELMAN, I. H., KIM, Y. J. & KIM, K. W. 2003. SSeCKS regulates angiogenesis and tight junction formation in blood-brain barrier. *Nat Med,* 9**,** 900-6.
LEGER, M., QUIEDEVILLE, A., BOUET, V., HAELEWYN, B., BOULOUARD, M., SCHUMANN-BARD, P. & FRERET, T. 2013. Object recognition test in mice. *Nat Protoc,* 8**,** 2531-7.
LIDDELOW, S. A. 2011. Fluids and barriers of the CNS: a historical viewpoint. *Fluids and Barriers of the CNS,* 8**,** 2-2.
LIDDLE, P. F., FRISTON, K. J., FRITH, C. D., HIRSCH, S. R., JONES, T. & FRACKOWIAK, R. S. 1992. Patterns of cerebral blood flow in schizophrenia. *Br J Psychiatry,* 160**,** 179-86.
LIEBERMAN, J. A. 1993. Prediction of outcome in first-episode schizophrenia. *J Clin Psychiatry,* 54 Suppl**,** 13-7.
LIEBNER, S., CORADA, M., BANGSOW, T., BABBAGE, J., TADDEI, A., CZUPALLA, C. J., REIS, M., FELICI, A., WOLBURG, H., FRUTTIGER, M., TAKETO, M. M., VON MELCHNER, H., PLATE, K. H., GERHARDT, H. & DEJANA, E. 2008. Wnt/beta-catenin signaling controls development of the blood-brain barrier. *J Cell Biol,* 183**,** 409-17.
LIEBNER, S., KNIESEL, U., KALBACHER, H. & WOLBURG, H. 2000. Correlation of tight junction morphology with the expression of tight junction proteins in blood-brain barrier endothelial cells. *Eur J Cell Biol,* 79**,** 707-17.
LIN, J. H. & YAMAZAKI, M. 2003. Role of P-glycoprotein in pharmacokinetics: clinical implications. *Clin Pharmacokinet,* 42**,** 59-98.
LINDAHL, P., JOHANSSON, B. R., LEVEEN, P. & BETSHOLTZ, C. 1997. Pericyte loss and microaneurysm formation in PDGF-B-deficient mice. *Science,* 277**,** 242-5.
LINDSAY, E. A., BOTTA, A., JURECIC, V., CARATTINI-RIVERA, S., CHEAH, Y. C., ROSENBLATT, H. M., BRADLEY, A. & BALDINI, A. 1999. Congenital heart disease in mice deficient for the DiGeorge syndrome region. *Nature,* 401**,** 379-83.
LIPPMANN, K., KAMINTSKY, L., KIM, S. Y., LUBLINSKY, S., PRAGER, O., NICHTWEISS, J. F., SALAR, S., KAUFER, D., HEINEMANN, U. & FRIEDMAN, A. 2017. Epileptiform activity and spreading depolarization in the blood-brain barrier-disrupted peri-infarct hippocampus are associated with impaired GABAergic inhibition and synaptic plasticity. *J Cereb Blood Flow Metab,* 37**,** 1803-1819.

LIPPOLDT, A., KNIESEL, U., LIEBNER, S., KALBACHER, H., KIRSCH, T., WOLBURG, H. & HALLER, H. 2000. Structural alterations of tight junctions are associated with loss of polarity in stroke-prone spontaneously hypertensive rat blood-brain barrier endothelial cells. *Brain Res,* 885**,** 251-61.

LIU, H., HEATH, S. C., SOBIN, C., ROOS, J. L., GALKE, B. L., BLUNDELL, M. L., LENANE, M., ROBERTSON, B., WIJSMAN, E. M., RAPOPORT, J. L., GOGOS, J. A. & KARAYIORGOU, M. 2002. Genetic variation at the 22q11 PRODH2/DGCR6 locus presents an unusual pattern and increases susceptibility to schizophrenia. *Proc Natl Acad Sci U S A,* 99**,** 3717-22.

LIU, X., DREFFS, A., DÍAZ-CORÁNGUEZ, M., RUNKLE, E. A., GARDNER, T. W., CHIODO, V. A., HAUSWIRTH, W. W. & ANTONETTI, D. A. 2016. Occludin S490 Phosphorylation Regulates Vascular Endothelial Growth Factor–Induced Retinal Neovascularization. *The American Journal of Pathology,* 186**,** 2486-2499.

LONGDEN, T. A., DABERTRAND, F., KOIDE, M., GONZALES, A. L., TYKOCKI, N. R., BRAYDEN, J. E., HILL-EUBANKS, D. & NELSON, M. T. 2017. Capillary K+-sensing initiates retrograde hyperpolarization to increase local cerebral blood flow. *Nat Neurosci,* 20**,** 717-726.

LUDEWIG, K., GEYER, M. A. & VOLLENWEIDER, F. X. 2003. Deficits in prepulse inhibition and habituation in never-medicated, first-episode schizophrenia. *Biol Psychiatry,* 54**,** 121-8.

LUI, J., CASTELLI, L. M., PIZZINGA, M., SIMPSON, C. E., HOYLE, N. P., BAILEY, K. L., CAMPBELL, S. G. & ASHE, M. P. 2014. Granules harboring translationally active mRNAs provide a platform for P-body formation following stress. *Cell Rep,* 9**,** 944-54.

MACDONALD, B. T., TAMAI, K. & HE, X. 2009. Wnt/beta-catenin signaling: components, mechanisms, and diseases. *Dev Cell,* 17**,** 9-26.

MACKEPRANG, T., KRISTIANSEN, K. T. & GLENTHOJ, B. Y. 2002. Effects of antipsychotics on prepulse inhibition of the startle response in drug-naive schizophrenic patients. *Biol Psychiatry,* 52**,** 863-73.

MARCO, S. & SKAPER, S. D. 2006. Amyloid beta-peptide1-42 alters tight junction protein distribution and expression in brain microvessel endothelial cells. *Neurosci Lett,* 401**,** 219-24.

MARTIN-PADURA, I., LOSTAGLIO, S., SCHNEEMANN, M., WILLIAMS, L., ROMANO, M., FRUSCELLA, P., PANZERI, C., STOPPACCIARO, A., RUCO, L., VILLA, A., SIMMONS, D. & DEJANA, E. 1998. Junctional adhesion molecule, a novel member of the immunoglobulin superfamily that distributes at intercellular junctions and modulates monocyte transmigration. *J Cell Biol,* 142**,** 117-27.

MASOPUST, J., MALY, R., ANDRYS, C., VALIS, M., BAZANT, J. & HOSAK, L. 2011. Markers of thrombogenesis are activated in unmedicated patients with acute psychosis: a matched case control study. *BMC Psychiatry,* 11**,** 2.

MAURICE, T., HIRAMATSU, M., ITOH, J., KAMEYAMA, T., HASEGAWA, T. & NABESHIMA, T. 1994. Behavioral evidence for a modulating role of sigma ligands in memory processes. I. Attenuation of dizocilpine (MK-801)-induced amnesia. *Brain Res,* 647**,** 44-56.

MAYNARD, T. M., GOPALAKRISHNA, D., MEECHAN, D. W., PARONETT, E. M., NEWBERN, J. M. & LAMANTIA, A. S. 2013. 22q11 Gene dosage establishes an adaptive range for sonic hedgehog and retinoic acid signaling during early development. *Hum Mol Genet,* 22**,** 300-12.

MCCULLUMSMITH, R. E., O'DONOVAN, S. M., DRUMMOND, J. B., BENESH, F. S., SIMMONS, M., ROBERTS, R., LAURIAT, T., HAROUTUNIAN, V. & MEADOR-WOODRUFF, J. H. 2016. Cell-specific abnormalities of glutamate transporters in schizophrenia: sick astrocytes and compensating relay neurons? *Mol Psychiatry,* 21**,** 823-30.

MCDONALD-MCGINN, D. M., SULLIVAN, K. E., MARINO, B., PHILIP, N., SWILLEN, A., VORSTMAN, J. A., ZACKAI, E. H., EMANUEL, B. S., VERMEESCH, J. R., MORROW, B. E., SCAMBLER, P. J. & BASSETT, A. S. 2015. 22q11.2 deletion syndrome. *Nat Rev Dis Primers,* 1**,** 15071.

MCGRATH, J., SAHA, S., CHANT, D. & WELHAM, J. 2008. Schizophrenia: a concise overview of incidence, prevalence, and mortality. *Epidemiol Rev,* 30**,** 67-76.

MCNEIL, E., CAPALDO, C. T. & MACARA, I. G. 2006. Zonula occludens-1 function in the assembly of tight junctions in Madin-Darby canine kidney epithelial cells. *Mol Biol Cell,* 17**,** 1922-32.

MEIER, M. H., SHALEV, I., MOFFITT, T. E., KAPUR, S., KEEFE, R. S., WONG, T. Y., BELSKY, D. W., HARRINGTON, H., HOGAN, S., HOUTS, R., CASPI, A. & POULTON, R. 2013. Microvascular abnormality in schizophrenia as shown by retinal imaging. *Am J Psychiatry,* 170**,** 1451-9.

MEIJER, J. H. & SCHWARTZ, W. J. 2003. In search of the pathways for light-induced pacemaker resetting in the suprachiasmatic nucleus. *J Biol Rhythms,* 18**,** 235-49.

MENARD, C., PFAU, M. L., HODES, G. E., KANA, V., WANG, V. X., BOUCHARD, S., TAKAHASHI, A., FLANIGAN, M. E., ALEYASIN, H., LECLAIR, K. B., JANSSEN, W. G., LABONTE, B., PARISE, E. M., LORSCH, Z. S., GOLDEN, S. A., HESHMATI, M., TAMMINGA, C., TURECKI, G., CAMPBELL, M., FAYAD, Z. A., TANG, C. Y., MERAD, M. & RUSSO, S. J. 2017. Social stress induces neurovascular pathology promoting depression. *Nat Neurosci,* 20**,** 1752-1760.

MERRITT, K., EGERTON, A., KEMPTON, M. J., TAYLOR, M. J. & MCGUIRE, P. K. 2016. Nature of Glutamate Alterations in Schizophrenia: A Meta-analysis of Proton Magnetic Resonance Spectroscopy Studies. *JAMA Psychiatry,* 73**,** 665-74.

MERSCHER, S., FUNKE, B., EPSTEIN, J. A., HEYER, J., PUECH, A., LU, M. M., XAVIER, R. J., DEMAY, M. B., RUSSELL, R. G., FACTOR, S., TOKOOYA, K., JORE, B. S., LOPEZ, M., PANDITA, R. K., LIA, M., CARRION, D., XU, H., SCHORLE, H., KOBLER, J. B., SCAMBLER, P., WYNSHAW-BORIS, A., SKOULTCHI, A. I., MORROW, B. E. & KUCHERLAPATI, R. 2001. TBX1 is responsible for cardiovascular defects in velo-cardio-facial/DiGeorge syndrome. *Cell,* 104**,** 619-29.

MILLER, D. D. 2004. Atypical antipsychotics: sleep, sedation, and efficacy. *Prim Care Companion J Clin Psychiatry,* 6**,** 3-7.

MILSTED, A., BARNA, B. P., RANSOHOFF, R. M., BROSNIHAN, K. B. & FERRARIO, C. M. 1990. Astrocyte cultures derived from human brain tissue express angiotensinogen mRNA. *Proc Natl Acad Sci U S A,* 87**,** 5720-3.

MIZEE, M. R., WOOLDRIK, D., LAKEMAN, K. A., VAN HET HOF, B., DREXHAGE, J. A., GEERTS, D., BUGIANI, M., ARONICA, E., MEBIUS, R. E., PRAT, A., DE VRIES, H. E. & REIJERKERK, A. 2013. Retinoic acid induces blood-brain barrier development. *J Neurosci,* 33**,** 1660-71.

MOGHADDAM, B. & JAVITT, D. 2012. From revolution to evolution: the glutamate hypothesis of schizophrenia and its implication for treatment. *Neuropsychopharmacology,* 37**,** 4-15.
MOORE, M. J. 2005. From birth to death: the complex lives of eukaryotic mRNAs. *Science,* 309**,** 1514-8.
MORGAN, L., SHAH, B., RIVERS, L. E., BARDEN, L., GROOM, A. J., CHUNG, R., HIGAZI, D., DESMOND, H., SMITH, T. & STADDON, J. M. 2007. Inflammation and dephosphorylation of the tight junction protein occludin in an experimental model of multiple sclerosis. *Neuroscience,* 147**,** 664-73.
MORITA, K., FURUSE, M., FUJIMOTO, K. & TSUKITA, S. 1999. Claudin multigene family encoding four-transmembrane domain protein components of tight junction strands. *Proc Natl Acad Sci U S A,* 96**,** 511-6.
MURAKAMI, T., FELINSKI, E. A. & ANTONETTI, D. A. 2009. Occludin phosphorylation and ubiquitination regulate tight junction trafficking and vascular endothelial growth factor-induced permeability. *J Biol Chem,* 284**,** 21036-46.
MURPHY, K. C. 2002. Schizophrenia and velo-cardio-facial syndrome. *Lancet,* 359**,** 426-30.
MUSIEK, E. S., XIONG, D. D. & HOLTZMAN, D. M. 2015. Sleep, circadian rhythms, and the pathogenesis of Alzheimer disease. *Exp Mol Med,* 47**,** e148.
NAJJAR, S., PAHLAJANI, S., DE SANCTIS, V., STERN, J. N. H., NAJJAR, A. & CHONG, D. 2017. Neurovascular Unit Dysfunction and Blood-Brain Barrier Hyperpermeability Contribute to Schizophrenia Neurobiology: A Theoretical Integration of Clinical and Experimental Evidence. *Front Psychiatry,* 8**,** 83.
NAJJAR, S., PEARLMAN, D. M., ALPER, K., NAJJAR, A. & DEVINSKY, O. 2013. Neuroinflammation and psychiatric illness. *J Neuroinflammation,* 10**,** 43.
NAKAZATO, R., KAWABE, K., YAMADA, D., IKENO, S., MIEDA, M., SHIMBA, S., HINOI, E., YONEDA, Y. & TAKARADA, T. 2017. Disruption of Bmal1 impairs blood-brain barrier integrity via pericyte dysfunction. *J Neurosci*.
NGUYEN, L. N., MA, D., SHUI, G., WONG, P., CAZENAVE-GASSIOT, A., ZHANG, X., WENK, M. R., GOH, E. L. & SILVER, D. L. 2014. Mfsd2a is a transporter for the essential omega-3 fatty acid docosahexaenoic acid. *Nature,* 509**,** 503-6.
NIITSU, T., ISHIMA, T., YOSHIDA, T., HASHIMOTO, T., MATSUZAWA, D., SHIRAYAMA, Y., NAKAZATO, M., SHIMIZU, E., HASHIMOTO, K. & IYO, M. 2014. A positive correlation between serum levels of mature brain-derived neurotrophic factor and negative symptoms in schizophrenia. *Psychiatry Res,* 215**,** 268-73.
NIMMERJAHN, A., KIRCHHOFF, F. & HELMCHEN, F. 2005. Resting microglial cells are highly dynamic surveillants of brain parenchyma in vivo. *Science,* 308**,** 1314-8.
NISHIURA, K., ICHIKAWA-TOMIKAWA, N., SUGIMOTO, K., KUNII, Y., KASHIWAGI, K., TANAKA, M., YOKOYAMA, Y., HINO, M., SUGINO, T., YABE, H., TAKAHASHI, H., KAKITA, A., IMURA, T. & CHIBA, H. 2017. PKA activation and endothelial claudin-5 breakdown in the schizophrenic prefrontal cortex. *Oncotarget,* 8**,** 93382-93391.
NITTA, T., HATA, M., GOTOH, S., SEO, Y., SASAKI, H., HASHIMOTO, N., FURUSE, M. & TSUKITA, S. 2003. Size-selective loosening of the blood-brain barrier in claudin-5-deficient mice. *J Cell Biol,* 161**,** 653-60.

NOEL, A. C., PELLUARD, F., DELEZOIDE, A. L., DEVISME, L., LOEUILLET, L., LEROY, B., MARTIN, A., BOUVIER, R., LAQUERRIERE, A., JEANNE-PASQUIER, C., BESSIERES-GRATTAGLIANO, B., MECHLER, C., ALANIO, E., LEROY, C. & GAILLARD, D. 2014. Fetal phenotype associated with the 22q11 deletion. *Am J Med Genet A,* 164a**,** 2724-31.

OBERMEIER, B., DANEMAN, R. & RANSOHOFF, R. M. 2013. Development, maintenance and disruption of the blood-brain barrier. *Nat Med,* 19**,** 1584-96.

OMIDINIA, E., MASHAYEKHI MAZAR, F., SHAHAMATI, P., KIANMEHR, A. & SHAHBAZ MOHAMMADI, H. 2014. Polymorphism of the CLDN5 gene and Schizophrenia in an Iranian Population. *Iran J Public Health,* 43**,** 79-83.

PACCHIONI, A. M., GABRIELE, A., DONOVAN, J. L., DEVANE, C. L. & SEE, R. E. 2010. P-glycoprotein inhibition potentiates the behavioural and neurochemical actions of risperidone in rats. *Int J Neuropsychopharmacol,* 13**,** 1067-77.

PAN, W., CORNELISSEN, G., HALBERG, F. & KASTIN, A. J. 2002. Selected contribution: circadian rhythm of tumor necrosis factor-alpha uptake into mouse spinal cord. *J Appl Physiol (1985),* 92**,** 1357-62; discussion 1356.

PAN, W. & KASTIN, A. J. 2001. Diurnal variation of leptin entry from blood to brain involving partial saturation of the transport system. *Life Sci,* 68**,** 2705-14.

PAOLICELLI, R. C., BOLASCO, G., PAGANI, F., MAGGI, L., SCIANNI, M., PANZANELLI, P., GIUSTETTO, M., FERREIRA, T. A., GUIDUCCI, E., DUMAS, L., RAGOZZINO, D. & GROSS, C. T. 2011. Synaptic pruning by microglia is necessary for normal brain development. *Science,* 333**,** 1456-8.

PARDRIDGE, W. M. 2005. The blood-brain barrier: bottleneck in brain drug development. *NeuroRx,* 2**,** 3-14.

PARDRIDGE, W. M. 2009. Alzheimer's disease drug development and the problem of the blood-brain barrier. *Alzheimers Dement,* 5**,** 427-32.

PATTON, N., ASLAM, T., MACGILLIVRAY, T., PATTIE, A., DEARY, I. J. & DHILLON, B. 2005. Retinal vascular image analysis as a potential screening tool for cerebrovascular disease: a rationale based on homology between cerebral and retinal microvasculatures. *Journal of Anatomy,* 206**,** 319-348.

PEDERSEN, C. B. & MORTENSEN, P. B. 2001. Evidence of a dose-response relationship between urbanicity during upbringing and schizophrenia risk. *Arch Gen Psychiatry,* 58**,** 1039-46.

PEPPIATT, C. M., HOWARTH, C., MOBBS, P. & ATTWELL, D. 2006. Bidirectional control of CNS capillary diameter by pericytes. *Nature,* 443**,** 700-4.

PERALA, J., SUVISAARI, J., SAARNI, S. I., KUOPPASALMI, K., ISOMETSA, E., PIRKOLA, S., PARTONEN, T., TUULIO-HENRIKSSON, A., HINTIKKA, J., KIESEPPA, T., HARKANEN, T., KOSKINEN, S. & LONNQVIST, J. 2007. Lifetime prevalence of psychotic and bipolar I disorders in a general population. *Arch Gen Psychiatry,* 64**,** 19-28.

PERRIERE, N., DEMEUSE, P., GARCIA, E., REGINA, A., DEBRAY, M., ANDREUX, J. P., COUVREUR, P., SCHERRMANN, J. M., TEMSAMANI, J., COURAUD, P. O., DELI, M. A. & ROUX, F. 2005. Puromycin-based purification of rat brain capillary endothelial cell cultures. Effect on the expression of blood-brain barrier-specific properties. *J Neurochem,* 93**,** 279-89.

PERUZZO, D., RAMBALDELLI, G., BERTOLDO, A., BELLANI, M., CERINI, R., SILVIA, M., POZZI MUCELLI, R., TANSELLA, M. & BRAMBILLA, P. 2011. The impact of schizophrenia on frontal perfusion parameters: a DSC-MRI study. *J Neural Transm (Vienna),* 118**,** 563-70.

PILLAI, A., HOWELL, K. R., AHMED, A. O., WEINBERG, D., ALLEN, K. M., BRUGGEMANN, J., LENROOT, R., LIU, D., GALLETLY, C., WEICKERT, C. S. & WEICKERT, T. W. 2016. Association of serum VEGF levels with prefrontal cortex volume in schizophrenia. *Mol Psychiatry,* 21**,** 686-92.

PIONTEK, J., WINKLER, L., WOLBURG, H., MULLER, S. L., ZULEGER, N., PIEHL, C., WIESNER, B., KRAUSE, G. & BLASIG, I. E. 2008. Formation of tight junction: determinants of homophilic interaction between classic claudins. *Faseb j,* 22**,** 146-58.

POLLAK, T. A., DRNDARSKI, S., STONE, J. M., DAVID, A. S., MCGUIRE, P. & ABBOTT, N. J. 2017. The blood-brain barrier in psychosis. *Lancet Psychiatry*.

POWELL, S. B. & GEYER, M. A. 2002. Developmental markers of psychiatric disorders as identified by sensorimotor gating. *Neurotox Res,* 4**,** 489-502.

POWELL, S. B., ZHOU, X. & GEYER, M. A. 2009. Prepulse Inhibition and Genetic Mouse Models of Schizophrenia. *Behavioural brain research,* 204**,** 282-294.

PREMSRIRUT, P. K., DOW, L. E., KIM, S. Y., CAMIOLO, M., MALONE, C. D., MIETHING, C., SCUOPPO, C., ZUBER, J., DICKINS, R. A., KOGAN, S. C., SHROYER, K. R., SORDELLA, R., HANNON, G. J. & LOWE, S. W. 2011. A rapid and scalable system for studying gene function in mice using conditional RNA interference. *Cell,* 145**,** 145-58.

PULVER, A. E. 2000. Search for schizophrenia susceptibility genes. *Biol Psychiatry,* 47**,** 221-30.

RAAB, S., BECK, H., GAUMANN, A., YUCE, A., GERBER, H. P., PLATE, K., HAMMES, H. P., FERRARA, N. & BREIER, G. 2004. Impaired brain angiogenesis and neuronal apoptosis induced by conditional homozygous inactivation of vascular endothelial growth factor. *Thromb Haemost,* 91**,** 595-605.

RADOEVA, P. D., COMAN, I. L., SALAZAR, C. A., GENTILE, K. L., HIGGINS, A. M., MIDDLETON, F. A., ANTSHEL, K. M., FREMONT, W., SHPRINTZEN, R. J., MORROW, B. E. & KATES, W. R. 2014. Association between autism spectrum disorder in individuals with velocardiofacial (22q11.2 deletion) syndrome and PRODH and COMT genotypes. *Psychiatr Genet,* 24**,** 269-72.

RAICHLE, M. E. & GUSNARD, D. A. 2002. Appraising the brain's energy budget. *Proc Natl Acad Sci U S A,* 99**,** 10237-9.

RALPH, M. R., FOSTER, R. G., DAVIS, F. C. & MENAKER, M. 1990. Transplanted suprachiasmatic nucleus determines circadian period. *Science,* 247**,** 975-8.

RAO, M. L., HIEMKE, C., GRASMADER, K. & BAUMANN, P. 2001. [Olanzapine: pharmacology, pharmacokinetics and therapeutic drug monitoring]. *Fortschr Neurol Psychiatr,* 69**,** 510-7.

REES, E., KIROV, G., SANDERS, A., WALTERS, J. T., CHAMBERT, K. D., SHI, J., SZATKIEWICZ, J., O'DUSHLAINE, C., RICHARDS, A. L., GREEN, E. K., JONES, I., DAVIES, G., LEGGE, S. E., MORAN, J. L., PATO, C., PATO, M., GENOVESE, G., LEVINSON, D., DUAN, J., MOY, W., GORING, H. H., MORRIS, D., CORMICAN, P., KENDLER, K. S., O'NEILL, F. A., RILEY, B., GILL, M., CORVIN, A., CRADDOCK, N., SKLAR, P., HULTMAN, C., SULLIVAN, P. F., GEJMAN, P. V., MCCARROLL, S. A., O'DONOVAN, M. C. & OWEN, M. J. 2014. Evidence that duplications of 22q11.2 protect against schizophrenia. *Mol Psychiatry,* 19**,** 37-40.

REESE, T. S. & KARNOVSKY, M. J. 1967. Fine structural localization of a blood-brain barrier to exogenous peroxidase. *J Cell Biol,* 34**,** 207-17.

RIVERA-CALIMLIM, L., NASRALLAH, H., STRAUSS, J. & LASAGNA, L. 1976. Clinical response and plasma levels: effect of dose, dosage schedules, and drug interactions on plasma chlorpromazine levels. *Am J Psychiatry,* 133**,** 646-52.

ROCH, C., LEROY, C., NEHLIG, A. & NAMER, I. J. 2002. Magnetic resonance imaging in the study of the lithium-pilocarpine model of temporal lobe epilepsy in adult rats. *Epilepsia,* 43**,** 325-35.

ROH, J. H., HUANG, Y., BERO, A. W., KASTEN, T., STEWART, F. R., BATEMAN, R. J. & HOLTZMAN, D. M. 2012. Disruption of the sleep-wake cycle and diurnal fluctuation of beta-amyloid in mice with Alzheimer's disease pathology. *Sci Transl Med,* 4**,** 150ra122.

ROSSI, J. J. 2011. Inducible and reversible breaching of the blood brain barrier by RNAi. *EMBO Molecular Medicine,* 3**,** 186-188.

ROSZKOWSKI, M. & BOHACEK, J. 2016. Stress does not increase blood-brain barrier permeability in mice. *J Cereb Blood Flow Metab,* 36**,** 1304-15.

ROTHERMUNDT, M., FALKAI, P., PONATH, G., ABEL, S., BURKLE, H., DIEDRICH, M., HETZEL, G., PETERS, M., SIEGMUND, A., PEDERSEN, A., MAIER, W., SCHRAMM, J., SUSLOW, T., OHRMANN, P. & AROLT, V. 2004a. Glial cell dysfunction in schizophrenia indicated by increased S100B in the CSF. *Mol Psychiatry,* 9**,** 897-9.

ROTHERMUNDT, M., MISSLER, U., AROLT, V., PETERS, M., LEADBEATER, J., WIESMANN, M., RUDOLF, S., WANDINGER, K. P. & KIRCHNER, H. 2001. Increased S100B blood levels in unmedicated and treated schizophrenic patients are correlated with negative symptomatology. *Mol Psychiatry,* 6**,** 445-9.

ROTHERMUNDT, M., PONATH, G., GLASER, T., HETZEL, G. & AROLT, V. 2004b. S100B serum levels and long-term improvement of negative symptoms in patients with schizophrenia. *Neuropsychopharmacology,* 29**,** 1004-11.

RYU, J. K. & MCLARNON, J. G. 2009. A leaky blood-brain barrier, fibrinogen infiltration and microglial reactivity in inflamed Alzheimer's disease brain. *J Cell Mol Med,* 13**,** 2911-25.

SAITOU, M., FUJIMOTO, K., DOI, Y., ITOH, M., FUJIMOTO, T., FURUSE, M., TAKANO, H., NODA, T. & TSUKITA, S. 1998. Occludin-deficient embryonic stem cells can differentiate into polarized epithelial cells bearing tight junctions. *J Cell Biol,* 141**,** 397-408.

SAITOU, M., FURUSE, M., SASAKI, H., SCHULZKE, J. D., FROMM, M., TAKANO, H., NODA, T. & TSUKITA, S. 2000. Complex phenotype of mice lacking occludin, a component of tight junction strands. *Mol Biol Cell,* 11**,** 4131-42.

SANDOVAL, K. E. & WITT, K. A. 2008. Blood-brain barrier tight junction permeability and ischemic stroke. *Neurobiol Dis,* 32**,** 200-19.

SANTHA, P., VESZELKA, S., HOYK, Z., MESZAROS, M., WALTER, F. R., TOTH, A. E., KISS, L., KINCSES, A., OLAH, Z., SEPRENYI, G., RAKHELY, G., DER, A., PAKASKI, M., KALMAN, J., KITTEL, A. & DELI, M. A. 2015. Restraint Stress-Induced Morphological Changes at the Blood-Brain Barrier in Adult Rats. *Front Mol Neurosci,* 8**,** 88.

SAUNDERS, N. R., LIDDELOW, S. A. & DZIEGIELEWSKA, K. M. 2012. Barrier mechanisms in the developing brain. *Front Pharmacol,* 3**,** 46.

SAVOLAINEN, H., MEERLO, P., ELSINGA, P. H., WINDHORST, A. D., DIERCKX, R. A., COLABUFO, N. A., VAN WAARDE, A. & LUURTSEMA, G. 2016. P-glycoprotein Function in the Rodent Brain Displays a Daily Rhythm, a Quantitative In Vivo PET Study. *Aaps j,* 18**,** 1524-1531.

SAVVIDIS, C. & KOUTSILIERIS, M. 2012. Circadian rhythm disruption in cancer biology. *Mol Med,* 18**,** 1249-60.
SCHACHTRUP, C., LU, P., JONES, L. L., LEE, J. K., LU, J., SACHS, B. D., ZHENG, B. & AKASSOGLOU, K. 2007. Fibrinogen inhibits neurite outgrowth via beta 3 integrin-mediated phosphorylation of the EGF receptor. *Proc Natl Acad Sci U S A,* 104**,** 11814-9.
SCHINKEL, A. H., SMIT, J. J., VAN TELLINGEN, O., BEIJNEN, J. H., WAGENAAR, E., VAN DEEMTER, L., MOL, C. A., VAN DER VALK, M. A., ROBANUS-MAANDAG, E. C., TE RIELE, H. P. & ET AL. 1994. Disruption of the mouse mdr1a P-glycoprotein gene leads to a deficiency in the blood-brain barrier and to increased sensitivity to drugs. *Cell,* 77**,** 491-502.
SCHLAGETER, K. E., MOLNAR, P., LAPIN, G. D. & GROOTHUIS, D. R. 1999. Microvessel organization and structure in experimental brain tumors: microvessel populations with distinctive structural and functional properties. *Microvasc Res,* 58**,** 312-28.
SCHNEIDER, M., DEBBANE, M., BASSETT, A. S., CHOW, E. W., FUNG, W. L., VAN DEN BREE, M., OWEN, M., MURPHY, K. C., NIARCHOU, M., KATES, W. R., ANTSHEL, K. M., FREMONT, W., MCDONALD-MCGINN, D. M., GUR, R. E., ZACKAI, E. H., VORSTMAN, J., DUIJFF, S. N., KLAASSEN, P. W., SWILLEN, A., GOTHELF, D., GREEN, T., WEIZMAN, A., VAN AMELSVOORT, T., EVERS, L., BOOT, E., SHASHI, V., HOOPER, S. R., BEARDEN, C. E., JALBRZIKOWSKI, M., ARMANDO, M., VICARI, S., MURPHY, D. G., OUSLEY, O., CAMPBELL, L. E., SIMON, T. J. & ELIEZ, S. 2014. Psychiatric disorders from childhood to adulthood in 22q11.2 deletion syndrome: results from the International Consortium on Brain and Behavior in 22q11.2 Deletion Syndrome. *Am J Psychiatry,* 171**,** 627-39.
SCHROETER, M. L., ABDUL-KHALIQ, H., FRUHAUF, S., HOHNE, R., SCHICK, G., DIEFENBACHER, A. & BLASIG, I. E. 2003. Serum S100B is increased during early treatment with antipsychotics and in deficit schizophrenia. *Schizophr Res,* 62**,** 231-6.
SCHROETER, M. L., ABDUL-KHALIQ, H., KREBS, M., DIEFENBACHER, A. & BLASIG, I. E. 2008. Serum markers support disease-specific glial pathology in major depression. *J Affect Disord,* 111**,** 271-80.
SEEMAN, P. 1987. Dopamine receptors and the dopamine hypothesis of schizophrenia. *Synapse,* 1**,** 133-52.
SEIBLER, J., KLEINRIDDERS, A., KUTER-LUKS, B., NIEHAVES, S., BRUNING, J. C. & SCHWENK, F. 2007. Reversible gene knockdown in mice using a tight, inducible shRNA expression system. *Nucleic Acids Res,* 35**,** e54.
SEIFFERT, E., DREIER, J. P., IVENS, S., BECHMANN, I., TOMKINS, O., HEINEMANN, U. & FRIEDMAN, A. 2004. Lasting blood-brain barrier disruption induces epileptic focus in the rat somatosensory cortex. *J Neurosci,* 24**,** 7829-36.
SEKAR, A., BIALAS, A. R., DE RIVERA, H., DAVIS, A., HAMMOND, T. R., KAMITAKI, N., TOOLEY, K., PRESUMEY, J., BAUM, M., VAN DOREN, V., GENOVESE, G., ROSE, S. A., HANDSAKER, R. E., DALY, M. J., CARROLL, M. C., STEVENS, B. & MCCARROLL, S. A. 2016. Schizophrenia risk from complex variation of complement component 4. *Nature,* 530**,** 177-83.
SHAIKH, T. H., KURAHASHI, H., SAITTA, S. C., O'HARE, A. M., HU, P., ROE, B. A., DRISCOLL, D. A., MCDONALD-MCGINN, D. M., ZACKAI, E. H., BUDARF, M. L. & EMANUEL, B. S. 2000. Chromosome 22-specific low copy

repeats and the 22q11.2 deletion syndrome: genomic organization and deletion endpoint analysis. *Hum Mol Genet,* 9**,** 489-501.
SHALABY, F., ROSSANT, J., YAMAGUCHI, T. P., GERTSENSTEIN, M., WU, X. F., BREITMAN, M. L. & SCHUH, A. C. 1995. Failure of blood-island formation and vasculogenesis in Flk-1-deficient mice. *Nature,* 376**,** 62-6.
SHALEV, H., SERLIN, Y. & FRIEDMAN, A. 2009. Breaching the blood-brain barrier as a gate to psychiatric disorder. *Cardiovasc Psychiatry Neurol,* 2009**,** 278531.
SHARMA, H. S. & DEY, P. K. 1981. Impairment of blood-brain barrier (BBB) in rat by immobilization stress: role of serotonin (5-HT). *Indian J Physiol Pharmacol,* 25**,** 111-22.
SHEIKOV, N., MCDANNOLD, N., VYKHODTSEVA, N., JOLESZ, F. & HYNYNEN, K. 2004. Cellular mechanisms of the blood-brain barrier opening induced by ultrasound in presence of microbubbles. *Ultrasound Med Biol,* 30**,** 979-89.
SHENTON, M. E., KIKINIS, R., JOLESZ, F. A., POLLAK, S. D., LEMAY, M., WIBLE, C. G., HOKAMA, H., MARTIN, J., METCALF, D., COLEMAN, M. & ET AL. 1992. Abnormalities of the left temporal lobe and thought disorder in schizophrenia. A quantitative magnetic resonance imaging study. *N Engl J Med,* 327**,** 604-12.
SHI, J., GERSHON, E. S. & LIU, C. 2008. Genetic associations with schizophrenia: meta-analyses of 12 candidate genes. *Schizophr Res,* 104**,** 96-107.
SINGH-CURRY, V. & HUSAIN, M. 2009. The functional role of the inferior parietal lobe in the dorsal and ventral stream dichotomy. *Neuropsychologia,* 47**,** 1434-1448.
SINKA, L., KOVARI, E., SANTOS, M., HERRMANN, F. R., GOLD, G., HOF, P. R., BOURAS, C. & GIANNAKOPOULOS, P. 2012. Microvascular changes in late-life schizophrenia and mood disorders: stereological assessment of capillary diameters in anterior cingulate cortex. *Neuropathol Appl Neurobiol,* 38**,** 696-709.
SMITH, A. J., YAO, X., DIX, J. A., JIN, B. J. & VERKMAN, A. S. 2017. Test of the 'glymphatic' hypothesis demonstrates diffusive and aquaporin-4-independent solute transport in rodent brain parenchyma. *Elife,* 6.
STEINER, J., SCHILTZ, K., WALTER, M., WUNDERLICH, M. T., KEILHOFF, G., BRISCH, R., BIELAU, H., BERNSTEIN, H. G., BOGERTS, B., SCHROETER, M. L. & WESTPHAL, S. 2010a. S100B serum levels are closely correlated with body mass index: an important caveat in neuropsychiatric research. *Psychoneuroendocrinology,* 35**,** 321-4.
STEINER, O., COISNE, C., CECCHELLI, R., BOSCACCI, R., DEUTSCH, U., ENGELHARDT, B. & LYCK, R. 2010b. Differential roles for endothelial ICAM-1, ICAM-2, and VCAM-1 in shear-resistant T cell arrest, polarization, and directed crawling on blood-brain barrier endothelium. *J Immunol,* 185**,** 4846-55.
STENMAN, J. M., RAJAGOPAL, J., CARROLL, T. J., ISHIBASHI, M., MCMAHON, J. & MCMAHON, A. P. 2008. Canonical Wnt signaling regulates organ-specific assembly and differentiation of CNS vasculature. *Science,* 322**,** 1247-50.
STEPHAN, F. K. & ZUCKER, I. 1972. Circadian rhythms in drinking behavior and locomotor activity of rats are eliminated by hypothalamic lesions. *Proc Natl Acad Sci U S A,* 69**,** 1583-6.

STEWART, P. A. & WILEY, M. J. 1981. Developing nervous tissue induces formation of blood-brain barrier characteristics in invading endothelial cells: a study using quail--chick transplantation chimeras. *Dev Biol,* 84**,** 183-92.
STILO, S. A. & MURRAY, R. M. 2010. The epidemiology of schizophrenia: replacing dogma with knowledge. *Dialogues Clin Neurosci,* 12**,** 305-15.
SUN, Z. Y., WEI, J., XIE, L., SHEN, Y., LIU, S. Z., JU, G. Z., SHI, J. P., YU, Y. Q., ZHANG, X., XU, Q. & HEMMINGS, G. P. 2004. The CLDN5 locus may be involved in the vulnerability to schizophrenia. *Eur Psychiatry,* 19**,** 354-7.
SWEENEY, M. D., SAGARE, A. P. & ZLOKOVIC, B. V. 2018. Blood-brain barrier breakdown in Alzheimer disease and other neurodegenerative disorders. *Nat Rev Neurol*.
TADDEI, A., GIAMPIETRO, C., CONTI, A., ORSENIGO, F., BREVIARIO, F., PIRAZZOLI, V., POTENTE, M., DALY, C., DIMMELER, S. & DEJANA, E. 2008. Endothelial adherens junctions control tight junctions by VE-cadherin-mediated upregulation of claudin-5. *Nat Cell Biol,* 10**,** 923-34.
TAKEICHI, M. 2014. Dynamic contacts: rearranging adherens junctions to drive epithelial remodelling. *Nat Rev Mol Cell Biol,* 15**,** 397-410.
TAKESHITA, Y. & RANSOHOFF, R. M. 2012. Inflammatory cell trafficking across the blood-brain barrier: chemokine regulation and in vitro models. *Immunol Rev,* 248**,** 228-39.
THOERINGER, C. K., WULTSCH, T., SHAHBAZIAN, A., PAINSIPP, E. & HOLZER, P. 2007. Multidrug-resistance gene 1-type p-glycoprotein (MDR1 p-gp) inhibition by tariquidar impacts on neuroendocrine and behavioral processing of stress. *Psychoneuroendocrinology,* 32**,** 1028-40.
TOKUDA, S., HIGASHI, T. & FURUSE, M. 2014. ZO-1 knockout by TALEN-mediated gene targeting in MDCK cells: involvement of ZO-1 in the regulation of cytoskeleton and cell shape. *PLoS One,* 9**,** e104994.
TORNAVACA, O., CHIA, M., DUFTON, N., ALMAGRO, L. O., CONWAY, D. E., RANDI, A. M., SCHWARTZ, M. A., MATTER, K. & BALDA, M. S. 2015. ZO-1 controls endothelial adherens junctions, cell-cell tension, angiogenesis, and barrier formation. *J Cell Biol,* 208**,** 821-38.
TORREY, E. F. 2007. Schizophrenia and the inferior parietal lobule. *Schizophr Res,* 97**,** 215-25.
TSUKITA, S., FURUSE, M. & ITOH, M. 2001. Multifunctional strands in tight junctions. *Nat Rev Mol Cell Biol,* 2**,** 285-93.
UDRISTOIU, I., MARINESCU, I., PIRLOG, M. C., MILITARU, F., UDRISTOIU, T., MARINESCU, D. & MUTICA, M. 2016. The microvascular alterations in frontal cortex during treatment with antipsychotics: a post-mortem study. *Rom J Morphol Embryol,* 57**,** 501-6.
UEDA, H. R., HAYASHI, S., CHEN, W., SANO, M., MACHIDA, M., SHIGEYOSHI, Y., IINO, M. & HASHIMOTO, S. 2005. System-level identification of transcriptional circuits underlying mammalian circadian clocks. *Nat Genet,* 37**,** 187-92.
URANOVA, N., ZIMINA, I., VIKHREVA, O., RACHMANOVA, V., KLINTSOVA, A. & ORLOVSKAYA, D. 2013. Reduced Capillary Density in the Prefrontal Cortex in Schizophrenia. *American Journal of Medical Sciences and Medicine,* 1**,** 45-51.
URANOVA, N. A., ZIMINA, I. S., VIKHREVA, O. V., KRUKOV, N. O., RACHMANOVA, V. I. & ORLOVSKAYA, D. D. 2010. Ultrastructural damage

of capillaries in the neocortex in schizophrenia. *World J Biol Psychiatry,* 11**,** 567-78.
VAN HORN, J. D. & MCMANUS, I. C. 1992. Ventricular enlargement in schizophrenia. A meta-analysis of studies of the ventricle:brain ratio (VBR). *Br J Psychiatry,* 160**,** 687-97.
VAN MEER, G. & SIMONS, K. 1986. The function of tight junctions in maintaining differences in lipid composition between the apical and the basolateral cell surface domains of MDCK cells. *Embo j,* 5**,** 1455-64.
VAN NOORT, M., MEELDIJK, J., VAN DER ZEE, R., DESTREE, O. & CLEVERS, H. 2002. Wnt signaling controls the phosphorylation status of beta-catenin. *J Biol Chem,* 277**,** 17901-5.
VAN OS, J., BAK, M., HANSSEN, M., BIJL, R. V., DE GRAAF, R. & VERDOUX, H. 2002. Cannabis use and psychosis: a longitudinal population-based study. *Am J Epidemiol,* 156**,** 319-27.
VAN PUTTEN, T., MARDER, S. R., MINTZ, J. & POLAND, R. E. 1992. Haloperidol plasma levels and clinical response: a therapeutic window relationship. *Am J Psychiatry,* 149**,** 500-5.
VAN VLIET, E. A., DA COSTA ARAUJO, S., REDEKER, S., VAN SCHAIK, R., ARONICA, E. & GORTER, J. A. 2007. Blood-brain barrier leakage may lead to progression of temporal lobe epilepsy. *Brain,* 130**,** 521-34.
VAZANA, U., VEKSLER, R., PELL, G. S., PRAGER, O., FASSLER, M., CHASSIDIM, Y., ROTH, Y., SHAHAR, H., ZANGEN, A., RACCAH, R., ONESTI, E., CECCANTI, M., COLONNESE, C., SANTORO, A., SALVATI, M., D'ELIA, A., NUCCIARELLI, V., INGHILLERI, M. & FRIEDMAN, A. 2016. Glutamate-Mediated Blood-Brain Barrier Opening: Implications for Neuroprotection and Drug Delivery. *J Neurosci,* 36**,** 7727-39.
VERMOT, J., NIEDERREITHER, K., GARNIER, J. M., CHAMBON, P. & DOLLE, P. 2003. Decreased embryonic retinoic acid synthesis results in a DiGeorge syndrome phenotype in newborn mice. *Proc Natl Acad Sci U S A,* 100**,** 1763-8.
VERREY, F., CLOSS, E. I., WAGNER, C. A., PALACIN, M., ENDOU, H. & KANAI, Y. 2004. CATs and HATs: the SLC7 family of amino acid transporters. *Pflugers Arch,* 447**,** 532-42.
VOGEL, F. 1991. Schizophrenia genesis: The origins of madness. *American Journal of Human Genetics,* 48**,** 1218-1218.
VOSTRIKOV, V., ORLOVSKAYA, D. & URANOVA, N. 2008. Deficit of pericapillary oligodendrocytes in the prefrontal cortex in schizophrenia. *World J Biol Psychiatry,* 9**,** 34-42.
WANG, C. S., YANG, Y. K., CHEN, M., CHIU, N. T., YEH, T. L. & LEE, I. H. 2003. Negative symptoms and regional cerebral blood flow in patients with schizophrenia: a single photon emission computed tomography study. *Kaohsiung J Med Sci,* 19**,** 464-9.
WEBER, C., FRAEMOHS, L. & DEJANA, E. 2007. The role of junctional adhesion molecules in vascular inflammation. *Nat Rev Immunol,* 7**,** 467-77.
WEBSTER, M. J., KNABLE, M. B., JOHNSTON-WILSON, N., NAGATA, K., INAGAKI, M. & YOLKEN, R. H. 2001. Immunohistochemical localization of phosphorylated glial fibrillary acidic protein in the prefrontal cortex and hippocampus from patients with schizophrenia, bipolar disorder, and depression. *Brain Behav Immun,* 15**,** 388-400.

WEBSTER, M. J., O'GRADY, J., KLEINMAN, J. E. & WEICKERT, C. S. 2005. Glial fibrillary acidic protein mRNA levels in the cingulate cortex of individuals with depression, bipolar disorder and schizophrenia. *Neuroscience,* 133**,** 453-61.

WEI, J. & HEMMINGS, G. P. 2005a. Gene, gut and schizophrenia: the meeting point for the gene-environment interaction in developing schizophrenia. *Med Hypotheses,* 64**,** 547-52.

WEI, J. & HEMMINGS, G. P. 2005b. A study of the combined effect of the CLDN5 locus and the genes for the phospholipid metabolism pathway in schizophrenia. *Prostaglandins Leukot Essent Fatty Acids,* 73**,** 441-5.

WEISER, M., KNOBLER, H. Y., NOY, S. & KAPLAN, Z. 2002. Clinical characteristics of adolescents later hospitalized for schizophrenia. *Am J Med Genet,* 114**,** 949-55.

WEISS, N., MILLER, F., CAZAUBON, S. & COURAUD, P. O. 2009. The blood-brain barrier in brain homeostasis and neurological diseases. *Biochim Biophys Acta,* 1788**,** 842-57.

WELSH, D. K., TAKAHASHI, J. S. & KAY, S. A. 2010. Suprachiasmatic Nucleus: Cell Autonomy and Network Properties. *Annual review of physiology,* 72**,** 551-577.

WEN, H., WATRY, D. D., MARCONDES, M. C. & FOX, H. S. 2004. Selective decrease in paracellular conductance of tight junctions: role of the first extracellular domain of claudin-5. *Mol Cell Biol,* 24**,** 8408-17.

WIESMANN, M., WANDINGER, K. P., MISSLER, U., ECKHOFF, D., ROTHERMUNDT, M., AROLT, V. & KIRCHNER, H. 1999. Elevated plasma levels of S-100b protein in schizophrenic patients. *Biol Psychiatry,* 45**,** 1508-11.

WILLIAMS, N. M. 2011. Molecular mechanisms in 22q11 deletion syndrome. *Schizophr Bull,* 37**,** 882-9.

WILSON, S. & ARGYROPOULOS, S. 2012. Sleep in schizophrenia: time for closer attention. *Br J Psychiatry,* 200**,** 273-4.

WINKLER, E. A., BELL, R. D. & ZLOKOVIC, B. V. 2011. Central nervous system pericytes in health and disease. *Nat Neurosci,* 14**,** 1398-405.

WINKLER, E. A., NISHIDA, Y., SAGARE, A. P., REGE, S. V., BELL, R. D., PERLMUTTER, D., SENGILLO, J. D., HILLMAN, S., KONG, P., NELSON, A. R., SULLIVAN, J. S., ZHAO, Z., MEISELMAN, H. J., WENBY, R. B., SOTO, J., ABEL, E. D., MAKSHANOFF, J., ZUNIGA, E., DE VIVO, D. C. & ZLOKOVIC, B. V. 2015. GLUT1 reductions exacerbate Alzheimer's disease vasculo-neuronal dysfunction and degeneration. *Nat Neurosci,* 18**,** 521-30.

WINTERS, B. D., FORWOOD, S. E., COWELL, R. A., SAKSIDA, L. M. & BUSSEY, T. J. 2004. Double dissociation between the effects of peri-postrhinal cortex and hippocampal lesions on tests of object recognition and spatial memory: heterogeneity of function within the temporal lobe. *J Neurosci,* 24**,** 5901-8.

WOLBURG, H. & LIPPOLDT, A. 2002. Tight junctions of the blood-brain barrier: development, composition and regulation. *Vascul Pharmacol,* 38**,** 323-37.

WOLKING, S., SCHAEFFELER, E., LERCHE, H., SCHWAB, M. & NIES, A. T. 2015. Impact of Genetic Polymorphisms of ABCB1 (MDR1, P-Glycoprotein) on Drug Disposition and Potential Clinical Implications: Update of the Literature. *Clin Pharmacokinet,* 54**,** 709-35.

WU, N., ZHANG, X., JIN, S., LIU, S., JU, G., WANG, Z., LIU, L., YE, L. & WEI, J. 2010. A weak association of the CLDN5 locus with schizophrenia in Chinese case-control samples. *Psychiatry Res,* 178**,** 223.

XIE, L., KANG, H., XU, Q., CHEN, M. J., LIAO, Y., THIYAGARAJAN, M., O'DONNELL, J., CHRISTENSEN, D. J., NICHOLSON, C., ILIFF, J. J., TAKANO, T., DEANE, R. & NEDERGAARD, M. 2013. Sleep drives metabolite clearance from the adult brain. *Science,* 342**,** 373-7.

XU, J., KAUSALYA, P. J., PHUA, D. C., ALI, S. M., HOSSAIN, Z. & HUNZIKER, W. 2008. Early embryonic lethality of mice lacking ZO-2, but Not ZO-3, reveals critical and nonredundant roles for individual zonula occludens proteins in mammalian development. *Mol Cell Biol,* 28**,** 1669-78.

YALCIN, I., AKSU, F. & BELZUNG, C. 2005. Effects of desipramine and tramadol in a chronic mild stress model in mice are altered by yohimbine but not by pindolol. *Eur J Pharmacol,* 514**,** 165-74.

YAMAMORI, H., HASHIMOTO, R., ISHIMA, T., KISHI, F., YASUDA, Y., OHI, K., FUJIMOTO, M., UMEDA-YANO, S., ITO, A., HASHIMOTO, K. & TAKEDA, M. 2013. Plasma levels of mature brain-derived neurotrophic factor (BDNF) and matrix metalloproteinase-9 (MMP-9) in treatment-resistant schizophrenia treated with clozapine. *Neurosci Lett,* 556**,** 37-41.

YE, L., SUN, Z., XIE, L., LIU, S., JU, G., SHI, J., YU, Y., ZHANG, X., WEI, J., XU, Q. & SHEN, Y. 2005. Further study of a genetic association between the CLDN5 locus and schizophrenia. *Schizophr Res,* 75**,** 139-41.

YEGNANARAYAN, R., MAHESH, S. D. & SANGLE, S. 2006. Chronotherapeutic dose schedule of phenytoin and carbamazepine in epileptic patients. *Chronobiol Int,* 23**,** 1035-46.

YOUNG, J. W., POWELL, S. B., RISBROUGH, V., MARSTON, H. M. & GEYER, M. A. 2009. Using the MATRICS to guide development of a preclinical cognitive test battery for research in schizophrenia. *Pharmacol Ther,* 122**,** 150-202.

ZHANG, B., GUAN, F., CHEN, G., LIN, H., ZHANG, T., FENG, J., LI, L. & FU, D. 2015. Common variants in SLC1A2 and schizophrenia: Association and cognitive function in patients with schizophrenia and healthy individuals. *Schizophr Res,* 169**,** 128-134.

ZHANG, R., LAHENS, N. F., BALLANCE, H. I., HUGHES, M. E. & HOGENESCH, J. B. 2014. A circadian gene expression atlas in mammals: implications for biology and medicine. *Proc Natl Acad Sci U S A,* 111**,** 16219-24.

ZHAO, J., HE, X., LIU, Z. & YANG, D. 2006. The effects of clozapine on cognitive function and regional cerebral blood flow in the negative symptom profile schizophrenia. *Int J Psychiatry Med,* 36**,** 171-81.

ZHU, J. C., SI, M. Y., LI, Y. Z., CHEN, H. Z., FAN, Z. C., XIE, Q. D. & JIAO, X. Y. 2017. Circulating tight junction proteins mirror blood-brain barrier integrity in leukaemia central nervous system metastasis. *Hematol Oncol,* 35**,** 365-373.

ZLOKOVIC, B. V. 2008. The blood-brain barrier in health and chronic neurodegenerative disorders. *Neuron,* 57**,** 178-201.

Appendix:

Materials

Buffers and reagents for general procedures

Sigma-Aldrich: Acetic acid, chloroform, isoamyl alcohol, isopentane, 2-propanol, ethanol, hydrochloric acid (HCL), β-mercaptoethanol, methanol, phenol, ethylenediaminetetraacetic acid (EDTA), Triton X-100, sodium dodecyl sulphate (SDS), ammonium persulfate (APS), N, N, N', N'-tetramethylethylenediamine (TEMED), bis-acrylamide, Ponceau S, agarose, sucrose, sodium deoxycholate, tri-sodium citrate dihydrate, Nonidet P-40, bovine serum albumin (BSA), trizma hydrochloride (Tris-HCL), glycine, sodium chloride, polyethylene glycol (PEG), Tween-20.

Materials and reagents for tissue culture

Corning: Costar™ Transwell™ permeable supports

Gibco: Trypsin-EDTA, sterile phosphate buffer saline (PBS), N-2-hydroxyethylpiperazine-N-2-ethane sulfonic acid (HEPES) buffer

Life Technologies: Dulbecco's modified Eagle Medium (DMEM) GlutaMAX™ with 1 mM Sodium Pyruvate, Hank's Balanced Salt Solution (HBSS), Gibco™ Opti-MEM 1 Reduced Serum media

Lonza: Endothelial Cell Basal Medium-2 (EBM-2) supplemented with 4% FBS, Hydrocortisone, Recombinant Human Fibroblast Growth Factor-B, Recombinant Human VEGF, Insulin-like Growth Factor-1, Ascorbic Acid, Recombinant Human Epidermal Growth Factor and Gentamicin/amphotericin B-1000 according to manufacturer's instructions (Endothelial Cell Growth Medium-2, (EGM-2 MV))

Promega: CellTiter 96 Aqueous One Solution Cell Proliferation Assay

Roche: Collagenase/Dispase

Sarstedt: Plastic tissue culture ware

Sigma-Aldrich: Fetal bovine serum (FBS), Glutamine, Puromycin, Non-essential amino acids, Hydrocortisone, Fibronectin, Collagen IV, Penicillin-Streptomycin (P/S), Dimethyl sulfoxide (DMSO), DNase I, Tosyllysine Chloromethyl Ketone Hydrochloride (TLCK), Trypan Blue Solution, Dispase 1, Dextran (MW: 70,000 Da), FITC-Dextran 4 kDa, 40 kDa, 70 kDa, Doxycycline

Thermo Scientific: Nunc™ Lab-Tek™ II Chamber Slide™ System

Materials and reagents for protein study

Advansta: WesternBright™ ECL Western blotting detection kit

FUJIFILM: Super RX FUJI Medical X-ray Film

Millipore: Polyvinyl Difluoride (PVDF) membrane, Collagen Type 1 Rat Tail

New England Biolabs: Prestained Protein Loading Marker Broad Range (11-190 kDa)

Roche: Complete Mini-Protease Inhibitor Cocktail

Sigma-Aldrich: Kodak GBx Developer and Replenisher, Kodak GBx Fixer and Replenisher

Thermo Scientific: Bicinchoninic Acid (BCA) Protein Assay Reagent, 5X Lane Marker Reducing Sample Buffer, Pierce ECL Western Blotting Substrate, Restore™ Western Blotting Stripping Buffer

Antibodies

Abcam: β-actin, Occludin, Axin-2, Sox-17, LC3, CD68, PDGFRβ, Goat anti-rabbit IgG Cy3, Goat anti-rabbit IgG Cy2, Goat anti-mouse IgG Alexa Fluor 488, rabbit anti-human IgG Cy3

Cell Signaling Technology: Phospho-ERK (Tr202/Tyr204), ERK, Phospho-AKT (Ser473), AKT, GAPDH

DAKO: Rabbit anti-human Fibrinogen

Invitrogen: Claudin-5, ZO-1, Tricellulin, Occludin

Novacastra: CD163

Santa Cruz Biotech: Claudin-5 (A-12)

Sigma-Aldrich: LC3, ATG5, ATG7, Beclin-1, p62, GFAP, anti-rabbit HRP-conjugated secondary antibody

Recombinant Proteins, Small Molecule Inducers and Inhibitors

Merck: 3-Methyladenine, MG-132

Santa-Cruz: Wortmannin, Rapamycin

Sigma-Aldrich: Chlorpromazine Hydrochloride, Lithium Chloride, Valproic Acid Sodium Salt, Haloperidol, Carbamazepine, Olanzapine, Clozapine, Clonidine Hydrochloride Mission MicroRNA HSA-Mir-125a-3p, Mission MicroRNA HSA-Mir-3934, Mission Synthetic microRNA inhibitor

Materials and reagents for RNA and DNA study

Ambion: Nuclease free (NF) H_2O

Applied Biosystems: High Capacity cDNA Reverse Transcription Kit

Dharmicon: Claudin-5 siRNAs, ARNTL siRNA, siRNA buffer

Invitrogen: RNase Away

Life Technologies: Lipofectamine® 2000

New England BioLabs: Proteinase K, dNTPs, 100 base pair Ladder

Omega: E.Z.N.A Total RNA Kit 1

Polyplus: *In vivo*-JetPEI

Sigma-Aldrich: Ethidium bromide

Thermo Scientific: Silencer™ Negative Control No.1 siRNA

Materials and reagents used for histology and vascular casts

Flow Tech Inc.: Microfil CP-101 MV-130

Molecular Probes: Griffonia-simplicifolia-isolectin-Alexa 568

Polysciencecs: Aqua PolyMount

Sigma-Aldrich: Paraformaldehyde (PFA), Formalin, Xylene, Methyl Salicylate, Normal Goat Serum (NGS), Streptavidin-Cy3

Thermo Scientific: Poly-lysine Adhesion Slides, EZ-Link Sulfo-NHS-Biotin

VWR: Cover Glass

Anaesthetics and reagents used for animal procedures

- Ketamine
- Xylazine (Domitor)
- Anti-Sedan

Buffer recipes

- 10% APS: 0.1 g APS, 1 ml dH_2O
- 1X RIPA Lysis Buffer: 50 mM Tris-Cl (pH 8.0), 0.1% NP-40, 150 mM NaCl, 0.1% SDS, 0.5% sodium deoxycholate and 1 complete mini-protease inhibitor cocktail tablet (1 tablet/10 ml)
- 1X Protein Lysis Buffer: 62.5 mM Tris-Cl, 2% SDS, 10 mM DTT, 100 ml dH_2O (pH 7.4)
- 10X Running Buffer: 250 mM Tris, 1.92 mM Glycine, 0.1% SDS, 1000 mL dH_2O (pH 8.6)

- 1.5 M Tris: 18.165 g Tris, 100 ml dH_2O (pH 8.8)
- 0.5 M Tris: 6.05 g Tris, 100 ml dH_2O (pH 6.8)
- 10% SDS: 10 g SDS, 100 ml dH_2O (pH 7.2)
- Transfer Buffer: 3.03 g Tris, 14.42 g Glycine, 200 ml Methanol, 800 ml dH_2O (pH 8.3)
- 10X Tris Buffered Saline (TBS): 60.5 g Tris, 87.66 g NaCl, 1000 ml dH_2O (pH 7.4)
- 10 mM Sodium Citrate Buffer: 2.94 g Tri-sodium Citrate, 1000 ml dH_2O, 0.5 ml Tween 20 (pH 6.0)
- 10X TAE Buffer: 400 mM Tris-Acetate and 10 mM EDTA (pH 8.3)
- 10X Tail Lysis Buffer: 50 ml 1 M Tris-Cl (pH 8.0), 50 ml 0.5 M EDTA (pH 8.0), 20 ml 5 M NaCl, 100 ml 10% SDS, 780 ml dH_2O